UNIVERSITY OF LIVERPOOL

Stem cell adhesome: Deciphering the role of distinct integrin-signalling networks in regulating stem cell behaviour

Thesis submitted in accordance with the requirements of the University of Liverpool for the degree of Doctor in Philosophy by Adams George

March 2022

Abstract

Pluripotent stem cells are characterized by their capacity for self-renewal and differentiation, playing a critical role in the maintenance and regeneration of tissues. The composition, organization, and topology of the extracellular matrix (ECM) within the tissue microenvironment, collectively known as the niche regulates stem cell fate. Integrins are heterodimeric receptors that interact with extracellular matrix proteins, forming a mechanical link between the ECM and the actin cytoskeleton. The dimensionality, chemistry, topography, and elasticity of the microenvironment can be tuned to modulate gene expression and stem cell fate. These force-induced changes in gene expression and stem cell fate are mediated by dynamic regulation of signalling, adaptor and cytoskeletal proteins, nuclear morphology and chromatin organization in response to mechanical stress. This study aimed to characterise the integrin heterodimers and integrin-dependent signalling networks recruited on the ECM ligands vitronectin and fibronectin, and two self-assembling nano-engineered polymers that serve as stem cell substrates that promote self-renewal, ZTFN and ZT910

Immunofluorescence imaging demonstrated that iPSCs plated on vitronectin fibronectin, ZTFN and ZT910 recruited αVβ5, α5β1, αVβ1 and α5β1 respectively to integrin-associated adhesion complexes. The distinct integrin heterodimers recruited on vitronectin, fibronectin, ZTFN and ZT910 were confirmed using adhesion complex enrichment and integrin inhibition assays. Traction force microscopy of iPSCs plated on hydrogels of different rigidities (5kPa to 70-100 kPa) demonstrated that vitronectin fibronectin, ZTFN and ZT910 induced differential force transmission on soft and stiff, but not intermediate rigidity matrices. Suggesting that the different integrin heterodimers possess distinct biophysical properties that are tuneable in a rigidity-dependent manner. To determine how the mechanical properties of different integrin heterodimers influence stem cell behaviour, nuclear morphology, chromatin organisation and YAP localisation, iPSCs were plated on substrate-coated hydrogels of different rigidities. Under these conditions, iPSCs demonstrated no difference in nuclear morphology or YAP localisation but exhibited significant changes in substrate and rigidity-dependent chromatin organisation suggesting that distinct biophysical properties integrin-dependent gene regulation.

Adhesion complex enrichment was employed to isolate and characterise for the first-time integrin adhesion complexes recruited by iPSC on vitronectin, fibronectin, ZTFN and ZT910. The αVβ5-VIT, α5β1-FN, αVβ1-ZTFN and α5β1-ZT910 adhesomes exhibited broad convergence when comparing the α5-mediated adhesomes (fibronectin and ZT910) and αV-mediated adhesomes (vitronectin and ZTFN). Bioinformatic analysis of α5β1-IACs and αVβ5-IACs recruited on fibronectin and vitronectin respectively revealed enrichment of gene ontology terms containing Focal Adhesion and Metabolism proteins. Integrative analysis revealed that SLC3A2 may play a potential role in regulating both integrin mechanosignalling and metabolism. Immunofluorescence imaging demonstrated that SLC3A2 localises to α5-mediated adhesions, but not αV-mediated adhesions, suggesting that SLC3A2 may modulate mechanosignalling and metabolism in an α5β1-heterodimer specific manner. Traction force microscopy revealed that SLC3A2 knockdown did not affect force transmission of iPSCs plated on vitronectin or fibronectin. However, treatment of iPSCs with SLC3A2 siRNA alone or in combination SLC3A2 light chain inhibitor LAT1 significantly reduced overall intracellular ATP

levels, demonstrating a putative impact on cellular energetics and metabolism. Analysis of the SLC3A2-LAT1 cryo-EM structure enabled the identification of SLC3A2-LAT1 regulatory domains and constructs were generated to target different structural domains of the SLC3A2-LAT1 complex. These constructs will allow dissection of the relative contribution of SLC3A2-integrin-binding to SLC3A2-LAT1-mediated amino acid transport, in force transduction, metabolic reprogramming and transcriptional regulation. Together, these advances contribute to our understanding of the mechanisms by which integrin-ECM engagement regulates global cellular processes in stem cells but will likely also have relevance in somatic cell biology and disease.

Acknowledgements

Thank you to my supervisors Mark Morgan and Trish Murray for firstly giving me the fantastic opportunity to work on this project in their labs. Secondly, I am truly grateful for their unwavering support and guidance throughout my PhD. Thank you to all members of the Trish and Morgan lab past and present: namely Christopher Hill, Kurtis John Hegarty, Theano Kyriakou, Katarzyna Wolanska, Horacio Maldonado, Emily Cubitt, Dan Newman, Joanna Thomas and Heather Swift.

Over the last four years, I experienced a rollercoaster of emotions, and faced numerous ups and downs, but through it all, I am grateful for the support of my Dad, Mum and Sister who continued to encourage and motivate me to strive for the best. I would like to extend my heartfelt thanks to the members of Liverpool Prayer Fellowship for their persistent prayers. I am thankful to my wife Nissy for her continuous encouragement.

Thank you to the BBSRC for generously supporting my PhD and academic development over the last four years.

I thank God for everything.

Contents

List of Figures

List of Tables

Abbreviations

AAA	ATPases Associated with diverse cellular Activities
ACN	Acetonitrile
ADAMTS	A Disintegrin and Metalloproteinase with Thrombospondin motifs
ADP	Additional macrodomain-containing proteins
AEBSF	4-benzenesulfonyl fluoride hydrochloride
AHNAK	Desmoyokin
AKT	Ak strain transforming
AMPK	AMP-activated protein kinase
ANOVA	Analysis of variance
APES	(3-Aminopropyl)triethoxysilane
APS	Ammonium persulfate
ATP	Adenosine triphosphate
AU	adenylate-uridylate
BAF	Barrier-to-autointegration factor
BAK	Bcl-2 homologous antagonist/killer
BCA	Bicinchoninic acid assay
BIOID	Proximity-dependent biotin identification
BSA	Bovine Serum Albumin
CAS	Crk associated substrate
CCT	Chaperonin-containing tailless complex polypeptide 1
CH	Calponin Homology
CTRL	Control
DAPI	4’,6-diamidino-2-phenylindole
DNA	Deoxyribonucleic acid

DTBP	Di-tert-butyl peroxide
DTT	Dithiothreitol
ECM	Extracellular Matrix
EGFR	Epidermal growth factor receptor
EHS	Engelbreth-Holm-Swarm
ERK	Extracellular signal-regulated kinases
ERM	Ezrin, Radixin and Moesin
ESC	Embryonic Stem Cells
FA	Focal adhesion
FAK	Focal adhesion kinase
FBS	Foetal Bovine Serum
FERM	4.1 protein, Ezrin, Radixin and Moesin
FGA	Fibrinogen A
FGB	Fibrinogen B
FGG	Fibrinogen G
FIJI	Fiji Is Just ImageJ
FN	Fibronectin
FRET	Förster resonance energy transfer
GAG	Glycosaminoglycan
GAP	GTPase-activating proteins
GAPDH	Glyceraldehyde-3-phosphate dehydrogenase
GEF	Guanine nucleotide exchange factors
GO	Gene ontology
GRD	GAP-related domain
GTP	Nucleotide guanosine triphosphate

HEPES	4-(2-hydroxyethyl)-1-piperazineethanesulfonic acid
HIF	Hypoxia Inducible Factor
HNRNPD	Heterogeneous Nuclear Ribonucleoprotein D
IA	Iodoacetamide
IAC	Integrin Adhesion Complex
IF	Immunofluorescence
IGFIR	Insulin-like growth factor 1 receptor
ILK	Integrin Linked Kinase
IQGAP	IQ-motif containing Ras GTPase-activating-like protein
KASH	Klarsicht, ANC-1, Syne Homology
KHSRP	KH-Type Splicing Regulatory Protein
LATS	Large tumor suppressor kinase
LBR	Lamin B Receptor
LIM	Lin-11, Isl-1 and Mec-3
LINC	Linker of nucleoskeleton and cytoskeleton
MAPK	Mitogen-activated protein kinase
MES	2-(N-morpholino)ethanesulfonic
MMP	Matrix metalloproteinases
MS	Mass Spectrometry
MST	Mammalian Sterile20-like
mTOR	Mammalian target of rapamycin
NADPH	nicotinamide adenine dinucleotide phosphate
NMII	Non-muscle myosin II
NSAF	normalized spectral abundance factor
OXPHOS	Oxidative Phosphorylation

PAGE	Polyacrylamide gel electrophoresis
PBS	Phosphate buffered saline
PBST	Phosphate buffered saline with tween-20
PDGF	Platelet-Derived Growth Factor
PDMS	Polydimethylsiloxane
PEP	Phosphoenolpyruvic acid
PGA	Phosphoglycerate
PINA	Protein Interaction Network Analysis
PINCH	Particularly interesting new cysteine-histidine-rich protein
PTB	Phosphotyrosine-binding domain
RIAM	Rap1 GTP–interacting adaptor molecule
RIPA	Mammalian target of rapamycin
RNA	Ribonucleic acid
ROCK	Rho-associated kinase
ROI	Region of interest
RPE	Retinal Pigment Epithelium
RPM	Revolutions per minute
SDS	Sodium dodecyl sulfate
SHANK	SH3 and multiple ankyrin repeat domains
SHARPIN	SHANK associated RH domain interactor
siRNA	SH3 and multiple ankyrin repeat domains
TAZ	Transcriptional coactivator with PDZ-binding motif
TCA	tricarboxylic
TCL	Total cell lysate
TEMED	Tetramethylethylenediamine

TER ATPase	Transitional endoplasmic reticulum ATPase
TFM	Traction Force Microscopy
TIF	Telomerase-induced fibroblasts
TKT	Transketolase
UPLC	Ultra Performance Liquid Chromatography
UV	Ultraviolet
VASP	Vasodilator-stimulated phosphoprotein
VCP	Valosin-containing protein
YAP	Yes-associated protein

1. INTRODUCTION

1.1. Pluripotent stem cells

Pluripotent stem cells (PSCs) are defined by two main characteristics; firstly, their ability to self-renew indefinitely, generating daughter cells that preserve the same properties as the progenitor cells, and secondly, their ability to differentiate into specialized cell types. The pluripotent stem cell family includes embryonic stem cells (ESCs) and induced pluripotent stem cells (iPSCs) (Fortier, 2005). ESCs and iPSCs have the potential to give rise to cells from the three germ layers (ectoderm, mesoderm, and endoderm) (Fortier, 2005, Thomson et al., 2011). For the first time in 1981, ESCs were isolated from the inner cell mass of mouse blastocysts (Evans and Kaufman, 1981, Martin, 1981). More than a decade later, human ESCs were isolated and established as a cell line by the seminal work carried out by James Thomson's group (Thomson et al., 1998). This ability of pluripotent ESCs to differentiate into any somatic or germ cell lineage opened avenues to further understand developmental biology and explore avenues for cellular therapies for neurogenerative diseases, ocular diseases, and diabetes (Aly, 2020).

Despite its enormous promise, the use of ESCs in research can be viewed by some people to be both ethically and politically controversial. However, in 2006, Yamanaka's group generated a group of iPSC lines following retroviral induction of 24 candidate genes in mouse fibroblasts. Further analysis revealed that a minimum of four transcriptional factors (Klf4, Oct3/4, c-Myc, and Sox2) were sufficient to reprogram somatic cells to possess a pluripotent phenotype (Takahashi and Yamanaka, 2006). The following year, the group was successful in reprogramming human dermal fibroblasts into human iPSCs through the induction of these four genes (Takahashi et al., 2007a). Following Yamanaka's work, several labs have

successfully generated iPSCs from multiple cell types including keratinocytes, neural stem cells, melanocytes, lymphocytes, and hepatocytes (Li et al., 2014). The generation of iPSCs bypassed the ethical concern raised by the use and destruction of embryos (Aly, 2020). Furthermore, the use of allogenic donor cells reduced the risk of immune rejection.

Following Yamanaka's work, the first phase 1 iPSCs clinical trial was conducted in Japan in September 2014 at the RIKEN Center of Developmental Biology. Skin fibroblasts from two patients suffering from advanced age-related macular degeneration (AMD) were differentiated into retinal pigment epithelial (RPE) cells and transplanted as a sheet under the retina (Mandai et al., 2017). Following one-year post-transplantation, there was no improvement in the patient's vision. However, in a separate study, adipose tissue-derived stem cells intravitreally injected in AMD patients led to rapid loss of vision (Kuriyan et al., 2017). Thus, despite having tremendous clinical potential, the use of iPSCs in translational therapy has a long way to go and highlights the need for urgent development of improved iPSCs-based cell therapies.

1.2. Extracellular matrix

Stem cell identity is dynamically maintained by regulatory networks that are influenced by the complex microenvironment that stem cells exist within, termed the stem cell niche (Ellis and Tanentzapf, 2010). The components of this microenvironment provide crucial biochemical and structural signals that regulate stem cell behaviour and stem cell fate (Wang et al., 2015, Ellis and Tanentzapf, 2010). The stem cell niche plays a protective role in guarding stem cells from an oncogenic conversion and damage potentiated by extracellular stimuli, while also ensuring maintenance of quiescence and low metabolic activity (Watt and Huck, 2013). One essential component of the niche is the extracellular matrix (ECM). The ECM is the

dynamic, non-cellular component of the niche modulating the production, degradation, and remodelling of its components both directly and indirectly, ultimately supporting tissue function and repair (Watt and Huck, 2013, Gattazzo et al., 2014). ECM is fundamentally composed of proteins, polysaccharides and water (Frantz et al., 2010). The composition and topology of the ECM is unique to each tissue and is generated through the dynamic integration of biochemical and biophysical cues between several cellular components including fibroblasts, endothelial cells and epithelial cells (Frantz et al., 2010).

Understanding the biochemistry of the native ECM is difficult due to its insoluble and highly-crosslinked nature (Hynes and Naba, 2012). However, the availability of the mouse Engelbreth-Holm-Swarm (EHS) tumour model system paved the way for the discovery of different ECM proteins that make up the basement membrane (Hynes and Naba, 2012). A combination of both proteomics and *in silico* bioinformatic approaches defined a list of "core" ECM proteins called matrisome (Naba et al., 2012). This core matrisome comprised approximately 300 proteins and whose major components included proteoglycans and fibrillar proteins (Yue, 2014). Proteoglycans and fibrillar proteins form the two main classes of macromolecules found in the ECM (Schaefer and Schaefer, 2010). Proteoglycans are biological molecules that contain glycosaminoglycan (GAG) chains that are covalently linked to a specific protein core (except for hyaluronic acid) (Iozzo and Schaefer, 2015). Proteoglycans can be classified according to their GAG composition, localization, and core protein, and can be classified into three main families: modular proteoglycans, small leucine-rich proteoglycans, and cell-surface proteoglycans (Schaefer and Schaefer, 2010). Modular proteoglycans (perlecan, agrin and collagen type XVIII) present in the basement membrane and the pericellular environment modulate cell adhesion migration and proliferation (Iozzo

and Schaefer, 2015). Small leucine-rich proteoglycans are involved in crosstalk with growth factor receptors such as epidermal growth factor receptor (EGFR) and insulin-like growth factor 1 receptor (IGFIR), where upon binding mediate activation and regulation of multiple signalling pathways (Frantz et al., 2010). Cell-surface proteoglycans such as syndecans and glypicans act as co-receptors, presenting ligands to complementary signalling receptors (Frantz et al., 2010). Fibrillar ECM proteins include fibronectin, collagen, elastin, vitronectin (Wang et al., 2015). Collagen is the most abundant fibrous protein and the primary structural element in the extracellular matrix (Rozario and DeSimone, 2010). Collagen forms a triple helical structure whose fibril organization, density, and distribution vary and is dependent on tissue type, and the magnitude and direction of force experienced by tissue (Rozario and DeSimone, 2010). Collagen associates with elastin, and these fibres act as a buffer system for tissues that experience frequent biomechanical stretches (Frantz et al., 2010). Fibronectin is another fibrillar protein that plays an important role in the organisation of the interstitial ECM and mediates cell adhesion and function.

Components of the ECM can act as a reservoir by both binding and releasing growth factors thereby regulating growth factor receptor-dependent activity (Schultz and Wysocki, 2009). Proteoglycans comprise a core protein covalently attached to highly anionic glycosaminoglycans (Yanagishita, 1993). The negatively charged glycosaminoglycan chains can sequester water, divalent cations, and a variety of macromolecules supporting structural integrity that regulate both biochemical and biomechanical phenotypes (Yanagishita, 1993). GAG chains maintain growth factors proximal to their receptors contributing to the establishment of local gradients of soluble growth factors, which play an important role in development (Kim et al., 2011). For example, vascular endothelial growth factors (VEGFs) and

fibroblast growth factors (FGFs) bind to heparan sulfate proteoglycans (HSPGs) but can be cleaved and released as a soluble growth factor by the enzyme heparinase (Kim et al., 2011). In some cases, growth factors do not need to be released in a soluble form. FGFs bind heparan sulfate and act as a cofactor which is presented as a complex by HSPGs to regulate signalling (Kim et al., 2011).

The composition, organization and topology of ECM proteins vary greatly between tissues but are specific to each tissue microenvironment. For example, in the brain, the ECM is significantly softer in comparison to the ECM in the bone (Engler et al., 2006). Subsequently, a compliant matrix promotes neuronal cell growth, survival, and differentiation, whereas a stiff matrix promotes osteoblast survival, growth, and differentiation (Engler et al., 2006). ECM is transiently remodelled in response to both biochemical and biomechanical extracellular stimuli and thereby regulating a variety of cell behaviour. For example, to maintain the structural stability of bones and cartilages, a stable external loading is vital. Reduction in mechanical loading in bones results in decreased mineral density and bone remodelling leading to osteoporosis (Handorf et al., 2015). Similarly, dysregulation of collagen crosslinking leads to a loss in proteoglycan content and thereby degeneration of cartilage (Kinnunen et al., 2012). The remodelling of ECM is principally modulated by two families of metalloproteinases; matrix metalloproteinase (MMP) and A Disintegrin and Metalloproteinase with Thrombospondin motifs (ADAMTs). Dynamic remodelling of the ECM confers distinct biomechanical properties such as dimensionality, chemistry, rigidity, and topography contribute to tissue-specific developmental behaviours including cell division, differentiation, migration, and polarity (Reilly and Engler, 2010, Frantz et al., 2010).

1.3. Integrins

1.3.1. Integrin family and structure

Cells interact with ECM proteins through a family of cell surface receptors called Integrins (Barczyk et al., 2010). Unlike other cell surface receptors such as cadherins and growth factor receptors which are primarily involved in biochemical signalling, integrins, function primarily as a link between the cell and ECM. Thus, integrin-ligand engagement permits the transduction of dynamic biochemical and physical cues from the matrix and subsequently regulates cellular functions including proliferation, differentiation, and survival (Wang et al., 2015). Integrins are heterodimeric transmembrane receptors comprising non-covalently associated α- and β-subunits. All metazoans express at least one β and two α integrin subunits, with no homologs found in prokaryotes, plants, or fungi. In mammals, there are 18 α and 8 β subunits that together form 24 heterodimers (Wang et al., 2015). Post-translational modification and alternative splicing of α and β subunit mRNAs further diversify the integrin family. However, in mammals' integrin expression is limited dependent on cell type. For example, α4β1 and α6β4 integrins are largely found in leukocytes, whereas integrin heterodimers such as α5β1 and αVβ3 are ubiquitously expressed (Bachmann et al., 2019). The combination of α and β subunits determines ligand binding specificity. Integrins can be classed into four matrix-binding classes: RGD (Arginine, Glycine, and Aspartate) -binding integrins (α5β1, αVβ1, αVβ3, αVβ5, αVβ6, αVβ8, and αIIbβ3), collagen-binding integrins (α1β1, α2β1, α3β1, α10β1, and α11β1), laminin-binding integrins (α1β1, α2β1, α3β1, α6β1 and α6β4) and leukocyte integrins (αLβ2, αMβ2, αXβ2, and αDβ2) (Barczyk et al., 2010) (Figure 1.1).

The α and β subunits that comprise the integrin heterodimers are constructed from numerous domains connected by flexible linkers (Campbell and Humphries, 2011). The α and β subunits contain around 1000 and 750 amino acids respectively, with each subunit containing a large extracellular domain, a transmembrane-spanning helix that is connected to a cytoplasmic tail (Campbell and Humphries, 2011). The α-subunit consists of a seven-bladed β- propeller region, a thigh, and two calf domains. Each structural domain plays a key role in the function of the overall integrin heterodimer function (Campbell and Humphries, 2011). The β-propeller domain contains a binding site for Ca^{2+} ions that have been shown to modulate ligand binding. 9 of the 18 integrins alpha subunit contain an α-I domain that is directly involved in ligand binding (Campbell and Humphries, 2011). The β-subunit consists of seven domains and contains a similar I-like domain found in the α-subunit that participates in ligand binding (Campbell and Humphries, 2011). This I-domain in the β-subunit contains a metal ion-dependent adhesion site that binds to cations: Mg^{2+}, Ca^{2+}, and Mn^{2+}. The structure of both the α and β subunits contributes to their binding specificity to ligands (Campbell and Humphries, 2011). RGD motif binds at a boundary between the α and β subunits, where the Arginine residue encompasses a β-propeller domain in the α subunit and the Aspartate domain linking to the A-domain in the β-subunit (Campbell and Humphries, 2011). The promiscuous nature of the RGD motif to bind multiple integrin heterodimers reflects the variation in the structure and affinity of the α and β binding pockets in the different integrin heterodimers (Campbell and Humphries, 2011). The integrin cytoplasmic tail is less than 100 amino acids in length except for the β4 subunit. Both the α and β subunits share a divergent homology except for a GFFKR motif present in the cytoplasmic tail of the α-subunit that is critical for its association with the cytoplasmic tail of the β subunit (Campbell and Humphries, 2011).

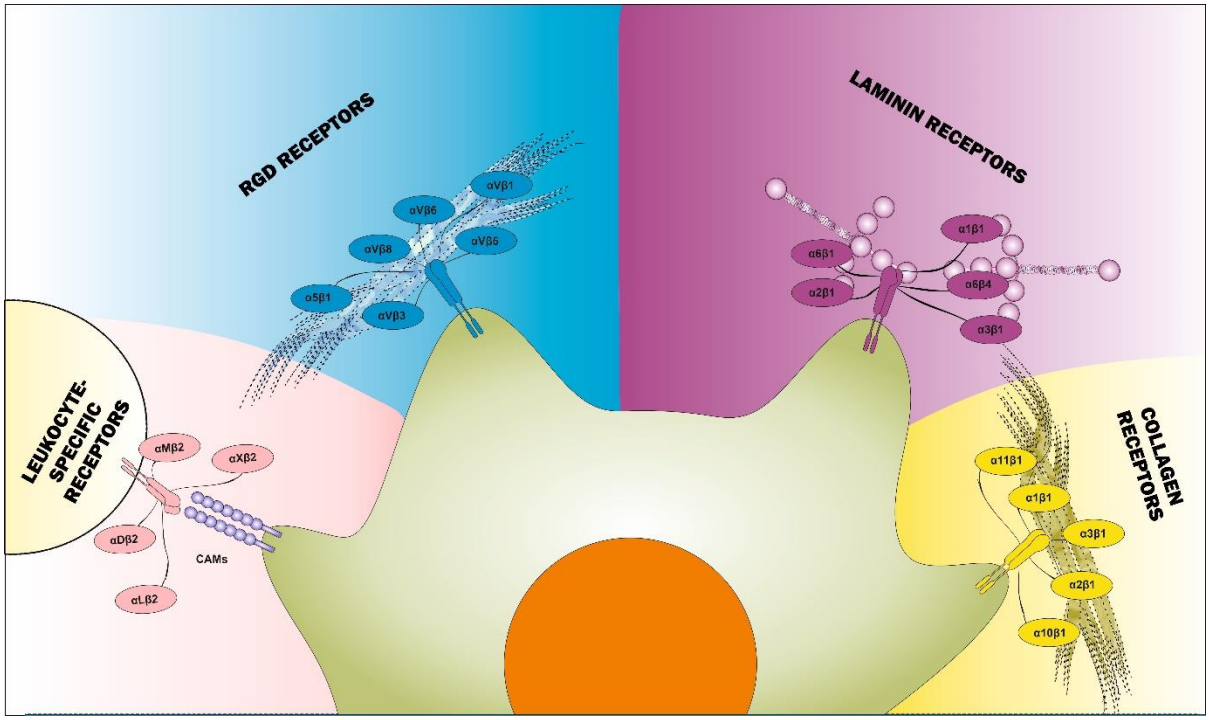

Figure 1.1: The integrin receptor family. Heterodimers are formed by integrin α- and β-subunits (Hynes, 2002). Integrin families are coloured based on ligand-binding specificity, namely; Leukocyte-specific receptors, RGD receptors, Laminin receptors and Collagen receptors. (Humphries et al., 2006).

1.3.2. Integrin function and regulation

Integrins function by integrating both intracellular and extracellular signals to regulate various cellular processes. Integrins transduce signals bidirectionally (Hu and Luo, 2013, Springer and Dustin, 2012). When integrin transduces signals from the extracellular matrix intracellularly, it is termed outside-in signalling (Hu and Luo, 2013). By contrast, when integrins transduce signals intracellularly towards the ECM, it is termed inside-out signalling. In both scenarios, the conformational changes in the structure of the integrin heterodimers play a critical role in integrin-mediated bidirectional signalling (Hu and Luo, 2013).

Integrins adopt distinct structural conformations that possess different ligand affinities that modulate the activation state of integrins (Sun et al., 2019, Springer and Dustin, 2012, Nishida et al., 2006, Xiao et al., 2004). When integrins adopt a bent-closed and extended-closed conformation, the extracellular domains of the α and β subunits bend inwards and the transmembrane regions of both subunits remain associated with the ligand-binding site closed (Sun et al., 2019, Springer and Dustin, 2012). In contrast, when the integrins adopt an extended-open conformation, α and β subunits dissociate with the hybrid domain which correlates with the re-arrangement of the metal-ion dependent adhesion site and opening of the ligand-binding site (Sun et al., 2019). Although the extended-closed conformation shows low-affinity integrin-ligand interaction, the extended-open conformation is primarily associated with high-affinity integrin-ligand interaction (Sun et al., 2019). Therefore, integrin activation is associated with a transition from the bent-closed/extended-closed integrin conformation to the extended-open integrin conformation (Luo and Springer, 2006).

Integrin engagement of extracellular matrix proteins promotes the recruitment of downstream proteins that can be classed into two major groups: namely scaffolding proteins

and signalling/regulatory proteins (Wolfenson et al., 2013). Scaffolding molecules include cytoskeletal and adaptor proteins and signalling/regulatory molecules include GTPases, kinases, proteases, and phosphatases (Wolfenson et al., 2013). Dissecting focal adhesion structures vertically using interferometric photoactivated localization microscopy reveals a hierarchical layer of proteins beginning with an integrin signalling module at the plasma membrane, followed by a force transduction module and an actin regulatory module (Monteiro et al., 2018, Kanchanawong et al., 2010, Stubb et al., 2019) (Figure 1.2). Among the proteins within these three layers, the presence of talin and kindlin is necessary for integrin activation (Theodosiou et al., 2016).

Talin a cytoskeletal protein, when inactive, exists in an auto-inhibitory conformation (Sun et al., 2019). However, Rap1 GTPase and its effector RIAM (Rap1-GTP-interacting adapter molecule) have been shown to bind and activate talin following chemokine signalling in leukocytes (Sun et al., 2019). Conformation changes of talin then mediate its binding to the NPXY motif on the cytoplasmic tail of β integrins through its phosphotyrosine-binding motif and its binding to actin through its actin-binding rod domain at the C-terminus (Sun et al., 2019). On the other hand, kindlin functions as an adaptor protein that recruits several signalling proteins including paxillin, Arp 2/3 complex, and the integrin-linked pseudo kinase PINCH (Böttcher et al., 2017). Furthermore, this multi-subunit complex has been shown to activate FAK, RAC1 and Arp 2/3 complex to mediate cell spreading (Böttcher et al., 2017). Thus, talin and kindlin integrate integrins with the actomyosin machinery to mediate bidirectional force transmission and stabilize focal adhesion through the regulation of actin polymerization respectively (Sun et al., 2019).

The activation of integrins is tightly regulated by several proteins. Some proteins that comprise the PTB domain function as a competitive inhibitor of talin binding to the β integrin cytoplasmic tail (Chen et al., 2019). For example, Docking protein 1 (DOK1) interacts with the β3 integrin through its PTB domain (Oxley et al., 2008). This interaction with the β3 cytoplasmic tail impedes integrin activation (Oxley et al., 2008). Similarly, filamins bind to the integrin cytoplasmic domain and inhibit integrin activation (Truong et al., 2015). The filamin binding site overlaps with the talin binding site on the β integrin cytoplasmic tail and because of the higher filamin affinity blocks talin-induced activation (Truong et al., 2015). Integrin inactivators such as the ezrin, radixin and moesin (ERM) family of proteins function by sequestering integrins, preventing integrin reactivation and facilitating adhesion disassembly. Furthermore, the FERM domain can bind to the cytoplasmic tail of β1 integrins outcompeting talin binding (Vitorino et al., 2015). By contrast, SHANK-associated RH domain-interacting protein (SHARPIN) associates with cytoplasmic tails of integrin α subunits with mammary-derived growth inhibitor to maintain integrins at a low-affinity conformation (Rantala et al., 2011).

1.3.3. Integrin Trafficking

A characteristic feature of most integrin receptors is their ability to bind a wide variety of ECM proteins. Heterogeneity of integrin heterodimer engagement to ECM proteins can lead to variation in integrin adhesome composition and downstream heterodimer-specific signalling pathways. αvβ3 and α5β1 expressing epithelial cells demonstrate morphological and signalling differences reflecting the recruitment of specific integrin heterodimers (Danen et al., 2005). For example, αvβ3 expressing epithelial cells have low RhoA activity, which is associated with the formation of broad lamellipodia, whereas α5β1 expressing cells form

robust actin stress fibres associated with high RhoA activity (Danen et al., 2005). αvβ3 expressing epithelial cells are unable to organise fibronectin into fibrils compared to α5β1 expressing cells, however, expression of dominant active RhoA in αvβ3 expressing epithelial cells can partially rescue this phenotype (Danen et al., 2002, Huveneers et al., 2008). In addition to differential integrin heterodimer-specific modulation of RhoA activity, integrin heterodimeric-specific relationships with serine/threonine kinases regulate integrin localisation. Protein kinase C (PKC) α and ε isoforms regulate the trafficking of integrin β1 either directly or in complex with RACK1 (Ng et al., 1999). By contrast, integrin β3 interacts solely with PKC β isoform to regulate cell migration (Buensuceso et al., 2005). These studies suggest that β1 and β3 integrins are connected to similar, but distinct pathways eliciting distinct cellular phenotypes.

Another mode of integrin regulation is mediated by the availability of integrins at the plasma membrane (Bridgewater et al., 2012). Integrin trafficking plays an essential role in regulating cell adhesion, spreading and migration by modulating focal adhesion disassembly, ECM turnover and localised redistribution of integrins to new adhesion sites (Caswell et al., 2009). Integrins are internalized via a clathrin-independent and clathrin-dependent endocytosis (Bridgewater et al., 2012). The recruitment of endocytic regulators to integrins represents the primary mechanism that regulates integrin endocytosis (Bridgewater et al., 2012). For example, protein kinase C alpha (PKCα) co-localises with beta1 integrin to promote the internalisation of integrin β1 in a caveolin-dependent manner (Ng et al., 1999, Shi and Sottile, 2008). Integrins that are internalised are either trafficked to early endosomes for recycling or degradation. Although α5β1 integrin engagement of the fibronectin ligand can be trafficked to degradation in late endosomes, the majority of integrins are recycled back to the plasma

membrane (Bridgewater et al., 2012). For example, integrin heterodimer αVβ3 internalised by micropinocytosis following platelet-derived growth factor (PDGF) stimulation is recycled through endosomal compartments and redistributed to newly formed focal adhesions (Gu et al., 2011).

Internalised integrins can be either recycled back to the plasma membrane or re-routed for degradation to lysosomes. The decision to degrade internalised integrin heterodimers is mediated by ubiquitination. For example, the cytoplasmic tail of α5 Integrins is multi-ubiquitinated following engagement to fibronectin, directing fibronectin-α5β1 complexes to lysosomes (Lobert et al., 2010). Four integrin recycling pathways have been described: ARF6 pathway, Rab4-dependent short-loop, Rab11-dependent long-loop and tubular actin-dependent recycling (Arjonen et al., 2012). The majority of integrins are recycled through a slow 'long loop' or fast 'short loop' pathway. The fast 'short loop' pathway is regulated by Rab4 and Rab 35 and mediates the recycling of cargo from early endosomes (Arjonen et al., 2012). αVβ3 is recycled to the plasma membrane following autophosphorylation of PKD1 in response to growth factor stimulation in a Rab4-dependent manner (di Blasio et al., 2010). This recycling of αVβ3 is important in regulating directional migration in cells. In contrast, the slow 'long-loop' pathway is regulated by Rab11 and Arf6 and mediates the recycling of cargo to the perinuclear recycling compartments from early endosomes (Powelka et al., 2004). For example, Rab21 binds to the cytoplasmic tails of integrin α subunits and promotes their internalisation through early endosomes into perinuclear recycling compartments (Mai et al., 2011). Here, RASA1 displaces Rab21, releasing integrin-containing vesicles from perinuclear recycling compartments to the plasma membrane (Mai et al., 2011).

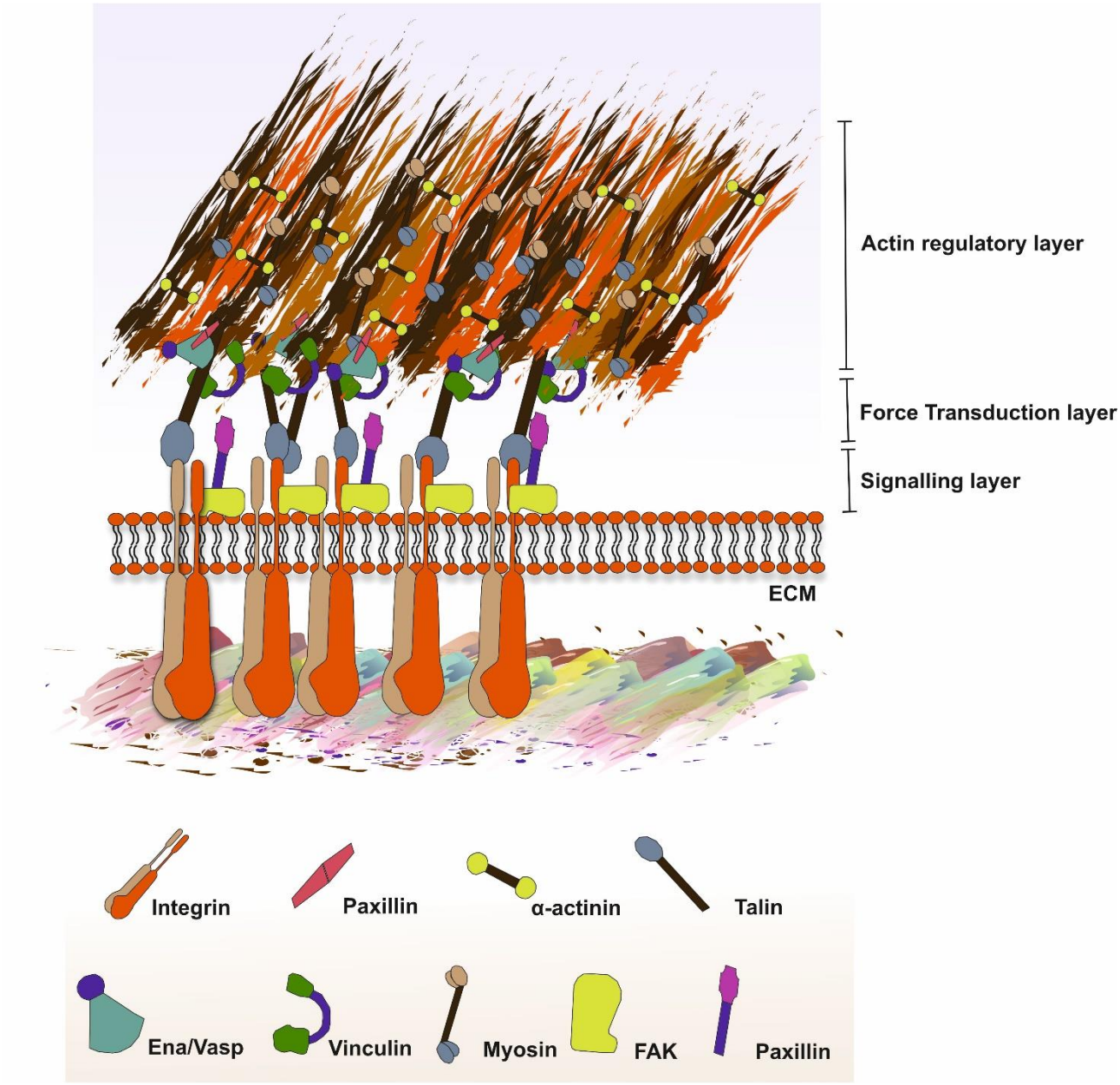

Figure 1.2: Schematic model of IAC architecture. IACs are composed of core structural and signalling protein modules for the receptor/matrix-binding, intracellular signalling, force transduction layer and actin linkage.

1.3.4. The integrin adhesome

Due to the specificity of integrin-ligand engagements, the integrin adhesion complexes (IACs) composition, component stoichiometry, and downstream signalling responses (i.e. proliferation, differentiation, and survival) are highly dependent on the type of integrin and ligand engagement (Byron et al., 2010). During the process of adhesion and cell spreading, cells exhibit several different IAC structures such as nascent adhesions, focal adhesions, and fibrillar adhesions (Humphries et al., 2015). Nascent adhesions are short-lived adhesions that mature into focal adhesions (Geiger and Yamada, 2011). Focal adhesions are distributed focally along the cell periphery and are observed as long flat and asymmetric stripes at the end of actin stress fibres and form via integrin-ligand engagement on rigid surfaces (Byron et al., 2010, Jones et al., 2015). In contrast, fibrillar adhesions are located towards the centre of cells and are associated primarily with fibronectin and α5β1 engagement (Pankov et al., 2000). As these adhesion structures mature, the multi-molecular complexes recruited to the cytoplasmic region of the cell-ECM matrix increases in size and complexity, reinforcing the ECM-integrin complex to the actin cytoskeleton.

When integrins bind to ECM proteins, integrin clustering is accompanied by the recruitment of downstream signalling, adaptor, and cytoskeletal proteins (Winograd-Katz et al., 2014). The families of proteins recruited play diverse roles in matrix remodelling, cell signalling, migration, and invasion (Winograd-Katz et al., 2014). The underlying protein networks associated with integrin adhesion complexes are known as the 'integrin adhesome' (Humphries et al., 2009). *in silico* characterization of these IACs has revealed a network composed of over 232 components known as the 'literature curated integrin adhesome' (Winograd-Katz et al., 2014, Horton et al., 2016, Winograd-Katz et al., 2009, Geiger and Zaidel-

Bar, 2012, Geiger and Yamada, 2011). These components were divided mainly into intrinsic components of the adhesome comprising proteins that reside at the adhesion site and transient components, that transiently associate with the adhesion (Winograd-Katz et al., 2014). Some of the adhesion molecules within these families include scaffolding proteins that function to physically link the integrin to the actin cytoskeleton, and other molecules function to mediate or regulate adhesion-dependent signalling (Winograd-Katz et al., 2014).

Approaches to isolate integrin adhesion complexes (IACs) using adhesion complex enrichment approaches and mass-spectrometric analysis have been performed in multiple cell types including mouse embryonic fibroblasts (MEFs), human foreskin fibroblasts (HFFs), and mouse kidney fibroblasts (MKFs) under a range of conditions (Byron et al., 2010, Horton et al., 2016, Horton et al., 2015, Jones et al., 2015). An experimentally defined integrin meta-adhesome was generated from the analysis of multiple mass spectrometry proteomics induced by the different cell types plated on the ligand fibronectin. The consolidation of these multiple IAC datasets identified 2412 proteins (Horton et al., 2015). Comparative analysis of datasets identified variations in IAC composition that suggests that these differences are cell-type, negative-control, and isolation-method dependent (Horton et al., 2015). Most components within IACs were identified to be chaperones, adaptor proteins, and actin regulators, with a lower abundance of kinases, GTPases, phosphatases, adhesion receptors and channels in comparison (Horton et al., 2015). Based on this, a consensus integrin adhesome was identified containing core set of 60 IAC components broadly belonging to four signalling axes; (1) α-actinin and zyxin family members, (2) vinculin and talin, (3) focal adhesion kinase and paxillin and (4) kindlin and integrin-linked kinase interactions (Horton et al., 2015). The cooperation and regulation of components within these modules generate mechanical forces that are

transmitted bi-directionally, inducing dynamic spatial and temporal changes in the ECM and intracellular components downstream and consequently regulating cell behaviour (Harburger and Calderwood, 2009, Geiger and Yamada, 2011).

1.4. Mechanosensation and Mechanotransduction

Mechanosensation is the process by which cells sense dynamic mechanical stimuli and mechanotransduction, is the transduction of these stimuli into biochemical signals (Ingber, 2003). Regulation and manipulation of cell behaviour by modulating mechanical stimuli is an emerging and evolving field in cell biology. *In vivo*, cells are continuously subjected to mechanical stimuli in the form of shear stress, stretching, and compression that regulate cell division, adhesion, homeostasis, proliferation, and differentiation (Eyckmans et al., 2011, Yashiro et al., 2007, Edmondson et al., 2014). For example, in development, the effect of shear stress on endothelial cells is responsible for vascular network formation and variations in osmotic pressure can inhibit cell proliferation (Schwartz et al., 2018). Forces in cells originate primarily from actin polymerization and actomyosin-dependent contraction of the cytoskeleton, which are transmitted through components within IACs to the ECM (Elosegui-Artola et al., 2018).

The dynamic interplay of force transmission and transduction between the actin cytoskeleton, components of the IACs, and the ECM is described as the 'molecular clutch' (Elosegui-Artola et al., 2018, Mitchison and Kirschner, 1988). The fundamental components of this clutch system are myosin, actin filaments, adaptor proteins, integrins, and the ECM (Schiller et al., 2013, Elosegui-Artola et al., 2014b, Carisey et al., 2013). Additionally, there are direct interactions that link cytoskeleton and integrin, including α-actinin, filamin, kindlin, tensin, and talin; and indirect interactions, including vinculin, focal adhesion kinase (FAK), and

paxillin (Elosegui-Artola et al., 2018). Here the clutch is defined as adaptor protein-integrin complexes. Cells continuously undergo actin polymerization, with myosin freely contracting actin filaments, but initially unbound to ligands in the ECM (Theriot and Mitchison, 1991). This drives a constant flow of actin from the cell edge (Elosegui-Artola et al., 2018, Lin and Forscher, 1995). However, with time, ligand engagement and therefore clutch engagement with components within the ECM continues at a given binding rate. This engaged clutch system leads to increased integrin clustering, concentrating multiple ECM-integrin-cytoskeleton linkages at defined points at the cell-matrix interface, and greatly increasing local adhesion strength (Elosegui-Artola et al., 2016). Once these links are established, the force generated from myosin-mediated actin contraction pulls on the substrate distributing and maintaining force bi-directionally among the engaged clutches (Elosegui-Artola et al., 2018). Once engaged, clutches can behave dynamically in one of two ways. Firstly, when clutch unbinding rates (rate of disengagement of the ECM-integrin-adaptors-actin) become faster than the binding rate (rate of engagement of the ECM-integrin-adaptors-actin), a feature called slip bonds, the number of engaged clutches decreases, and overall force transmission is reduced (Chan and Odde, 2008). This type of behaviour observed in neuronal growth cones is known as frictional slippage and a biphasic relationship between the loading rate and force transmission is observed, where force initially increases and then decreases (Chan and Odde, 2008, Wang et al., 2021a). However, in other systems, there is a monotonic increase in loading rate and force transmission, a feature called catch bonds (Elosegui-Artola et al., 2018). Such behaviour is observed when cells form focal adhesions which stabilize engaged molecular clutches and maintain force transmission, preventing frictional slippage (Elosegui-Artola et al., 2018, Chan and Odde, 2008).

Integrins and their downstream adaptor and cytoskeletal proteins recruited to IACs enable cells to sense, adapt and respond to changes in mechanical stimuli in their microenvironment. Transduction of forces across the ECM and actin cytoskeleton is dependent on mechanosensitive components within IACs. Proteins within IACs can respond to mechanical cues either with a change in protein binding affinities or with a conformational change in protein structure (Janoštiak et al., 2014b). This mechanism of force transduction is independent of biochemical signals, where these proteins act as both a direct and indirect mechanical link for the bi-directional transmission of extracellular forces across the cell-ECM matrix (Janoštiak et al., 2014b). These changes can lead to modulation in enzymatic activity and function regulating mechanochemical signalling pathways downstream that regulate proliferation, survival, differentiation, and migration (Janoštiak et al., 2014b). These mechanosensitive components can be characterized into primary mechanosensors, which undergo force-dependent conformational changes upon mechanical stress, or secondary mechanosensors, whose activity is regulated by force-dependent activation of primary mechanosensors (Janoštiak et al., 2014b). These components include:

1.4.1. Primary Mechanosensors

1.4.1.1. Talin and Vinculin

Talin is a cytoskeletal protein highly enriched at cell adhesion sites that directly interacts with integrins and actin cytoskeleton (Critchley and Gingras, 2008). In the absence of ligand engagement, talin is autoinhibited preventing interaction between actin and integrins. However, upon ligand engagement, talin is localized to the membrane and mediates integrin binding and activation at the N-terminus and binding to F-actin at the C-terminus (Critchley and Gingras, 2008, Das et al., 2014, Roberts and Critchley, 2009). Talin, subjected to

actomyosin forces in vivo, displayed substantial dynamic and transient structural changes of stretching and relaxation (Margadant et al., 2011). This suggests that, depending on the cellular context, talin undergoes stochastic stick-slip cycles by regulating the transduction of mechanical forces during adhesion and migration. For example, force transduction across the actin–talin–integrin–fibronectin clutch is regulated by a dynamic clutch mechanism (Elosegui-Artola et al., 2016). In this system, force transduction in the absence of talin and/or below a stiffness threshold reveals a biphasic relationship between loading rate and force transmission (Elosegui-Artola et al., 2016). However, in the presence of talin and/or above the stiffness threshold, a monotonic relationship between loading rate and force transmission is observed (Elosegui-Artola et al., 2016). This experiment highlighted the important role talin plays as a primary intermediary of force transmission. It suggests that below the stiffness threshold, talin experiences low forces and exists in the autoinhibited form undergoing stochastic stick-slip cycles represented by the biphasic relationship between loading rate and force transmission. However, above the threshold, talin unfolds, establishing the actin–talin–integrin–fibronectin clutch resulting in the monotonic relationship between loading rate and force transmission. The mechanosensitive nature of talin is confined in the rod domain, whereupon integrin and actin-binding, force transmission leads to a conformational change and increases the length of talin by 140nm exposing five vinculin binding sites (Roberts and Critchley, 2009, del Rio et al., 2009, Humphries et al., 2007). Furthermore, this binding of vinculin enables maturation from an early nascent non-load bearing IAC to a fully load-bearing mechanical linkage between ECM and cytoskeleton (Atherton et al., 2015). This unfolding establishes vinculin: talin complexes. The interaction between talin, vinculin, and actin is critical for the maturation of transient nascent adhesions into focal adhesion, thereby strengthening cell-matrix adhesion (Atherton et al., 2016, Bays and DeMali, 2017a).

Disruption of this interaction leads to impairment in force transduction, cell morphology, motility, stiffness, and adhesion (Carisey and Ballestrem, 2011, Thievessen et al., 2015).

1.4.1.2. Zyxin and p130Cas

Zyxin is a mechanosensitive LIM-domain containing protein that regulates actin polymerization in response to mechanical forces (Lele et al., 2006). The LIM-binding domain of zyxin promotes protein-protein interactions with binding partners including α-actinin and Ena/VASP, forming a scaffold at focal adhesions (Lele et al., 2006). Studies have shown that zyxin is recruited to focal adhesion in a force-dependent manner, such that the removal of forces results in reduced zyxin binding and increased zyxin unbinding rate (Lele et al., 2006). At IACs, zyxin regulates actin assembly, polymerization, and organization by recruiting Ena/VASP, and stabilizing adhesion sites. However, the introduction of cyclic stretch mobilized zyxin from focal adhesion to actin filaments, resulting in the thickening of stress fibres (Lele et al., 2006). Furthermore, mislocalization of zyxin impedes cell spreading and migration (Drees et al., 1999). This shows the importance of zyxin, upon induction of mechanical stress in an integrin-dependent manner, to reinforce stress fibres and stabilize adhesion sites, by active re-localization and actin reorganization. Similarly, p130Cas (CAS – Crk associated substrate) is a ubiquitously expressed adaptor protein, which at resting state is localized in the cytoplasm, where it exists in an auto-inhibited form (Janoštiak et al., 2014b, Donato et al., 2010, Lu et al., 2013). However, upon integrin engagement and force transmission, the CAS substrate domain unfolds exposing cryptic tyrosine residues and is phosphorylated (Lu et al., 2013, Janoštiak et al., 2011). This leads to the subsequent recruitment of signalling molecules such as FAK, vinculin, and DOCK180 that trigger downstream signalling pathways that regulate cell proliferation and survival (Lu et al., 2013,

Janoštiak et al., 2011). Interaction of vinculin with p130Cas is necessary for stretch-mediated activation of p130Cas, such that in the absence of vinculin there is increased focal adhesion turnover, migration, decreased focal adhesion size, cell stiffness, and traction (Janoštiak et al., 2014a). Furthermore, following uniform and biaxial cell stretching showed a stretch-dependent increase in phosphorylation of Cas, resulting in Rap 1 activation (Sawada et al., 2006). These data highlight the role of both zyxin and p130Cas as both a mechanosensor, where their activity is dependent upon force-mediated activation of talin and vinculin; and a mechanotransducer, where their activation regulates signalling pathways that modulate cellular behaviour.

1.4.2. Secondary Mechanosensors

1.4.2.1. YAP/TAZ

YAP/TAZ are transcriptional co-activators linked to the Hippo signalling pathway that regulates cell proliferation, differentiation, and survival (Piccolo et al., 2014, Low et al., 2014). The hippo signalling pathway is composed of two kinases MST and LATS that become active in response to stimuli, phosphorylating YAP and TAZ. At specific serine residues (Piccolo et al., 2014, Low et al., 2014). This phosphorylation localizes YAP/TAZ in the cytoplasm. Inhibition of LATS phosphorylation prevents YAP/TAZ phosphorylation, promoting YAP/TAZ translocation into the nucleus (Piccolo et al., 2014, Low et al., 2014). Once in the nucleus, YAP/TAZ binds TEA domain family members (TEAD) driving transcription and translation of proteins that regulate cell proliferation, differentiation, and survival (Piccolo et al., 2014, Low et al., 2014). In addition to the biochemical regulation of YAP/TAZ activity, they have also been identified as key mechanotransducers modulating their activity in response to mechanical cues (Dupont, 2016, Mohri et al., 2017, Dupont et al., 2011). Cells that are allowed to spread and stretch

over ECM through the formation of F-actin stress fibres promote YAP/TAZ activation and nuclear shuttling regulating cell behaviour (Halder et al., 2012). However, when the ECM is manipulated such that cells cannot spread and therefore form a round and compact morphology without robust stress fibre formation or contact-inhibited, YAP/TAZ is excluded from the nucleus, transcriptional regulation is disabled and cells undergo differentiation and apoptosis (Halder et al., 2012). The subcellular localization of YAP/TAZ is regulated by a stiffness threshold and the presence of talin (Elosegui-Artola et al., 2017b). MEFs plated on fibronectin-coated polyacrylamide gels of a range of rigidities showed the presence of a rigidity threshold of 5kPa, below which YAP translocation into the nucleus was inhibited (Elosegui-Artola et al., 2017b). However, there was no significant difference in YAP nuclear-to-cytoplasmic ratio in talin-knockdown cells which are unable to develop mature F-actin stress fibres (Elosegui-Artola et al., 2017b). The role of YAP/TAZ in sensing changes in substrate stiffness is dependent on the actin cytoskeleton such that treating cells with Blebbistatin (inhibitor of non-muscle myosin II), Latrunculin A (inhibitor of actin polymerization) results in loss of actin cytoskeletal integrity leading to cytoplasmic localization of YAP (Elosegui-Artola et al., 2017b). Epidermal stem cell fate has been demonstrated to be regulated by YAP/TAZ regulation in response to mechanical cues (Totaro et al., 2017). YAP/TAZ inhibition of epidermal stem cells plated on soft substrates activated the Notch signalling pathway leading to differentiation and the loss of stem cell characteristics (Totaro et al., 2017). These data highlight how changes in mechanical cues at the cell surface modulate nuclear morphology to mediate changes in stem cell fate (Dupont, 2016, Dupont et al., 2011, Halder et al., 2012, Piccolo et al., 2014).

1.5. Nuclear Mechanotransduction

Mechanical cues originating from the extracellular matrix regulate numerous cellular processes. Maniotis and his colleagues were the first group that demonstrated that external forces could deform the nucleus, hypothesizing a potential role of indirect regulation of force on gene expression (Maniotis et al., 1997). For such a mechanotransduction mechanism to exist, the forces that originate at the cell surface must be transmitted and translated downstream to the nucleus. Over the past decade, multiple dynamic components have been identified that both, directly and indirectly, link the nucleus to the ECM, cooperatively regulating the mechanical and biological nature of the nucleus and gene expression respectively (Cho et al., 2017, Fedorchak et al., 2014, Gruenbaum et al., 2005, Hu et al., 2017, Miroshnikova et al., 2017, Nava et al., 2020). The nucleus of eukaryotic cells is highly dynamic and well-organized, enabling efficient accessibility for DNA-dependent processes such as replication, transcription, and repair (Zhang et al., 2017). The nucleus is encapsulated by a double lipid membrane that is composed of the inner and outer nuclear membrane and comprises function-specific compartments including, euchromatin and heterochromatin domains, compartmentalized multiprotein complexes, nuclear bodies, and nuclear pores (Zhang et al., 2017). These compartments are spatially and temporally regulated by intrinsic and extrinsic factors, a critical determinant of genome function.

The Linker of Nucleoskeleton and Cytoskeleton (LINC) complex comprising multiple protein components is primarily involved in physically tethering the nucleus to the cytoskeleton (Rothballer et al., 2013, Crisp et al., 2006). The main protein components of the LINC complex include nesprin, sun, and emerin. Nesprin proteins form the cytoplasmic face of the LINC complex possessing a Calponin Homology (CH) domain at the N-terminus that binds to actin

filaments with high affinity (Rothballer et al., 2013, Crisp et al., 2006). The C-terminus of nesprin is present in the inner nuclear membrane and comprises the KASH domain. The KASH domains bind to Sun protein that spans the nuclear envelope, interacting with the lamin A/C network (Rothballer et al., 2013, Crisp et al., 2006). This membrane-spanning interaction allows for exogenous force transmission from the actin cytoskeleton to the nuclear lamina (Crisp et al., 2006). Emerin, an actin-capping protein forms complexes with α- and β-catenin and components of the LINC complex, enabling binding to and polymerization of actin filaments (Berk et al., 2013). Underlying the inner nuclear membrane is the nuclear lamina that is composed of lamin type A/C and B proteins that form thick filamentous meshwork, providing structural integrity to the nucleus (Turgay et al., 2017, Swift et al., 2013). Lamins A/C possess a viscoelastic nature and provide the nucleus with its mechanical strength and their expression correlates with tissue stiffness, such that cells on a stiff substrate require more lamin A/C networks to maintain nuclear integrity (Turgay et al., 2017, Swift et al., 2013).

In addition to proteins that regulate the integrity of the nucleus, proteins such as Lap2α, Lamin-B Receptor (LBR), Heterochromatin Protein 1 (HP1) and BAF modulate chromatin organization (Gruenbaum et al., 2005). In most cells, transcriptionally silent heterochromatin is lost from the nuclear periphery upon knockdown of lamin leading to gene silencing-mediated changes in cell phenotype (Kalverda et al., 2008). This can be mediated by a direct and indirect loss of chromatin binding proteins to lamins. One such protein is LBR which is an integral membrane protein that through its association with B-type lamins binds double-stranded DNA, HP1, histone H3–H4 tetramers, and chromatin-associated protein HA95 (Duband-Goulet and Courvalin, 2000, Ye and Worman, 1996). Mutations of the LBR protein led to aberrant chromatin organization and decreased lobulation (Hoffmann et al., 2002). HP1

is a chromatin-binding protein that directly binds methylated K9 residue of histone H3 (H3K9me), a characteristic marker for repressed regions of chromatin that promotes chromatin condensation and inter-chromatin contacts (Eskeland et al., 2007). LAP2α are type II membrane proteins that bind type-A lamin in the nucleoplasm mediating the interaction between lamins and transcriptional factor binding sites on promoters (Dorner et al., 2007, Vlcek et al., 1999). Furthermore, LAP2α also complexes with chromatin by interacting with Barrier-to-Autointegration Factor (BAF) which binds to double-stranded DNA non-specifically, tethering it at the nuclear periphery (Zheng et al., 2000).

There is increasing evidence that the structure and function of these interconnected proteins directly modulate nuclear architecture and transcriptional regulation in response to force at the cell surface (Fedorchak et al., 2014). For example, in fibroblasts and cardiomyocytes, mechanical stimuli in form of cyclic strain promote the activation of mechanosensitive genes Egr-1 and Iex-1 (Banerjee et al., 2014). However, following the knockdown of nuclear proteins lamin A/C, nesprins 1/2, and emerin, the expression of Egr-1 and Iex-1 is significantly reduced, despite hyperactivation of MAPK signalling (Lammerding et al., 2004, Lammerding et al., 2005). The propagation of mechanical forces across the cytoplasm occurs at a faster rate (30m/s) than biochemical signals, suggesting that changes in chromatin reorganization and transcriptional regulation may result directly from mechanical cues (Wang et al., 2009a). For example, the application of small transient forces on the surface of cells using a magnetic tweezer in HeLa cells resulted in a rapid decrease in anisotropy in fluorescently-labelled histones, symbolic of chromatin condensation (Guilluy et al., 2014). The effect of this force is reversible, as force alleviation leads to transformation to the original conformation. To confound the effects of biochemical effects originating from the cytoplasm, studies have

employed the use of isolated nuclei to determine the direct effects of nuclear mechanosensing. For example, isolated nuclei adjusted their stiffness in response to force by recruiting lamin A/C to the LINC complex through Src-dependent phosphorylation of emerin, thereby strengthening the nuclear-cytoskeletal link (Guilluy et al., 2014).

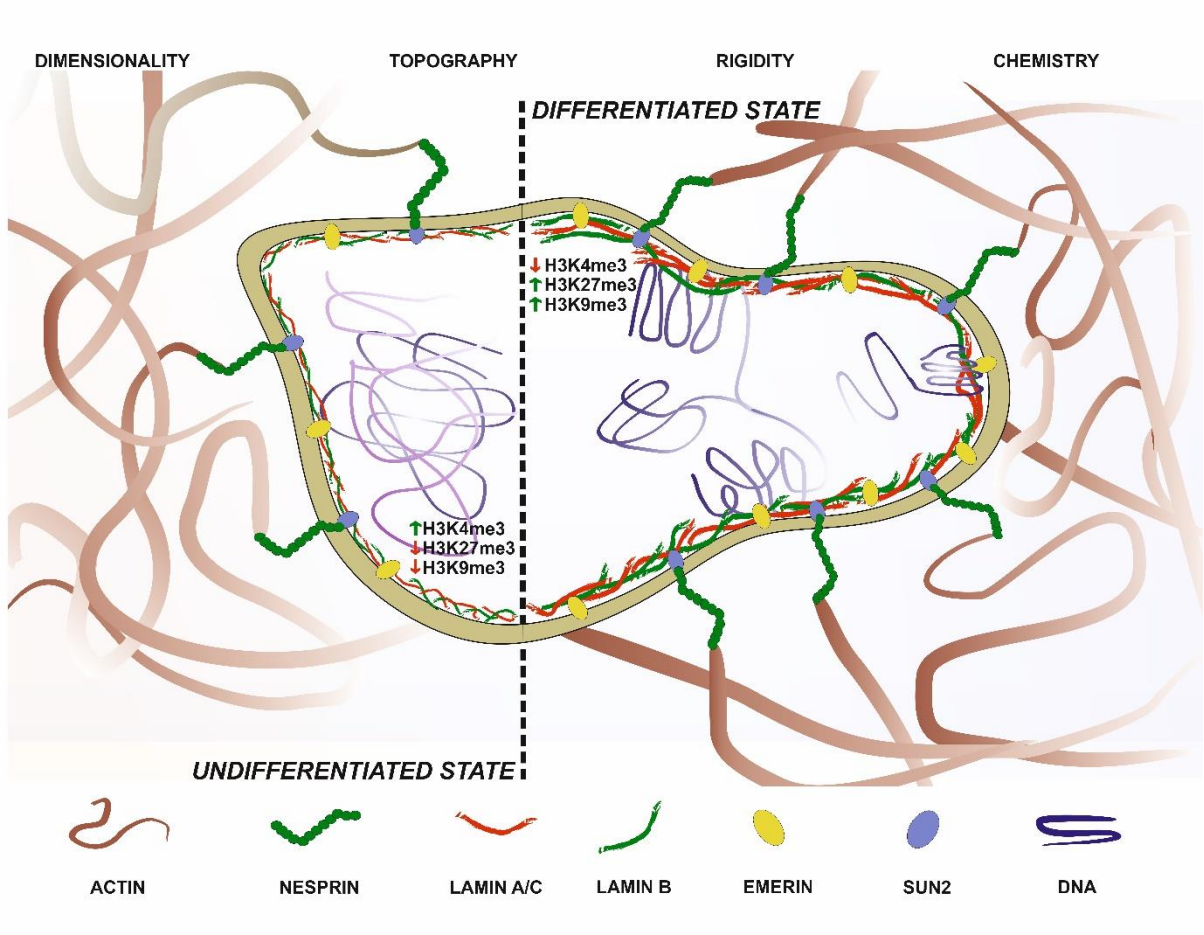

Figure 1.3: Schematic model of the nuclear morphology of pluripotent cells in an undifferentiated and differentiated state. Model conveys histone methylation states and the LINC complex (Linker of Nucleoskeleton and Cytoskeleton) comprising multiple protein components primarily involved in physically tethering the nucleus to the cytoskeleton.

1.5.1. Stem cells and Nuclear mechanotransduction

PSCs possess distinct nuclear characteristics such as a permissive chromatin structure and distinct histone modifications that are pertinent to the pluripotent genotype that distinguishes them from differentiated cells (Mattout and Meshorer, 2010, Meshorer and Misteli, 2006, Dixon et al., 2015, Gaspar-Maia et al., 2011). The nucleus of naïve hESCs is physically plastic and stiffens six-fold during differentiation (Pajerowski et al., 2007). This plastic nature of the nucleus is a consequence of low lamin A/C concentration at the nuclear periphery, which acts as the major contributor to nuclear mechanical strength (Pajerowski et al., 2007). Furthermore, during differentiation, lamin A/C expression is activated, increasing lamin A/C concentration at the nuclear periphery and contributing to the increase in nuclear stiffness (Pajerowski et al., 2007).

In the nucleus, chromatin adopts two conformations: heterochromatin, which is more condensed chromatin that is enriched in regions where genes are inactive or silent, and euchromatin, which takes an "open" conformation is localized in regions of high gene activity (Pajerowski et al., 2007, Penagos-Puig and Furlan-Magaril, 2020). Electron spectroscopic imaging has demonstrated that chromatin in pluripotent cells has been shown to exist in an open conformation and highly dynamic association with chromatin proteins reflecting their phenotypical and genotypical plasticity (Park et al., 2004) (Figure 1.3). In contrast, chromatin in differentiated cells shows a more condensed morphology (Park et al., 2004) (Figure 1.3).

Both euchromatin and heterochromatin can be defined molecularly by the presence of specific post-translational modification (Mattout and Meshorer, 2010). These modifications include methylation, acetylation, sumoylation, ubiquitination, and ribosylation which directly affect the structure of chromatin (Mattout and Meshorer, 2010). The open conformation of

chromatin in pluripotent stem cells is associated with epigenetic markers that are indicative of active transcription such as histones H3K4me3, H3K27me3, and acetylation of histones H3 and H4 (Lee et al., 2004, Bártová et al., 2008, Krejcí et al., 2009) (Figure 1.3). However, during differentiation, there is an increased presence of several repressive and heterochromatin markers such as H3K9me2, H3K9me3, and HP1α (Lee et al., 2004, Bártová et al., 2008, Krejcí et al., 2009). In addition, gene-rich chromosomes are positioned at the centre of the nucleus (chromosome 19), in contrast to gene-poor chromosomes (chromosome 18), which is localized at the nuclear periphery (Pradhan et al., 2018). Chromosomes 18 and 19 in adenocarinoma cells plated on soft matrices mis-localized further into the nuclear interior (Pradhan et al., 2018). Remarkably, when the cells were transferred back to stiffer matrices, chromosome 18 re-localised to the nuclear periphery, whereas chromosome 19 remained unperturbed at the centre of the nucleus (Pradhan et al., 2018). In ESCs, Nanog which is located in the chromosome arm 12p is localised at the nuclear centre in comparison to differentiated cells (Wiblin et al., 2005). These observations demonstrate that pluripotent stem cells possess distinct nuclear organisation that correlates with pluripotency and modulating mechanical properties of the ECM can dynamically influence chromatin reorganisation.

1.6. Stem cell metabolism

Pluripotent stem cells are also characterised by distinct metabolic profiles. Metabolic pathways in pluripotent stem cells can adapt to balance intracellular metabolic needs and external metabolic restrictions. Recent progress in the metabolomics field has shown that in addition to growth factor regulation, various metabolic pathways play an important role in the regulation of stem cell fate (Burgess et al., 2014). Energy consumption from mammalian

cells relies on both mitochondrial oxidative phosphorylation (OXPHOS) and glycolysis (Zheng, 2012). The first organisms that originated on earth relied on glycolysis as the primary energy source in the absence of oxygen (Zheng, 2012). However, as the concentration of atmospheric oxygen increased, cells evolved to use OXPHOS as the primary source of energy, which generates more ATP per metabolite than glycolysis (Burgess et al., 2014, Zheng, 2012). Energy production and therefore ATP production is directly proportional to the energy demands in the cell. Although mammalian cells rely on both glycolysis and OXPHOS, the degree to which each pathway contributes to total ATP yield is dependent on cell type and microenvironment (Burgess et al., 2014).

Hyperproliferative cells such as cancer cells show dependence on glycolysis even in an environment where oxygen is not a limiting factor (Vander Heiden et al., 2009, Tanosaki et al., 2021). This observation initially described by Warburg and known as the Warburg effect is advantageous as it generates sufficient metabolite yield, such as lipids, nucleotides, and nonessential amino acids to support rapidly proliferating cells (Vander Heiden et al., 2009). This phenomenon was later observed in both human and mouse PSCs. Embryonic stem cells characteristically possess a short G1 phase and divide rapidly (Coronado et al., 2013). Consistent with reliance on the Warburg effect, embryonic stem cells exhibit a high rate of lactate production through the glycolytic pathway and minimal OXPHOS compared to cardiomyocytes (Tanosaki et al., 2021). Reprogramming of somatic cells into iPSCs showed a radical transition of cells from an oxidative state to a glycolytic state (Tanosaki et al., 2021). This transition was supported when examining expression profiles of iPSCs and somatic cells, which showed upregulation of hexokinase 2 (a glycolytic gene) and downregulation of pyruvate dehydrogenase, which reduces pyruvate entry into the tricarboxylic (TCA) cycle in

undifferentiated iPSCs (Tanosaki et al., 2021). These results suggest that undifferentiated pluripotent stem cells characteristically have a higher rate of glycolysis in comparison to differentiated cells. The higher rate of glycolysis in pluripotent stem cells is functionally critical for maintaining a pluripotent state. For example, inhibition of glycolysis in embryonic stem cells inhibits the cell cycle and induces apoptosis (Salti et al., 2021). Furthermore, inhibition of glycolysis inhibits reprogramming of fibroblasts into iPSCs (Salti et al., 2021). The preference of pluripotent stem cells for glycolysis in comparison to OXPHOS has been proposed to be because of the presence of immature mitochondria in PSCs with reduced transcription of components of the electron transport chain (Prigione et al., 2010).

1.6.1. Integrins and metabolism

Integrin activity is regulated by several mechanisms that modulate integrin signalling, trafficking, transcription, and degradation (Ata and Antonescu, 2017). In cancer, changes in metabolic signals have been shown to regulate the transcription of specific integrin heterodimers. In hypoxic environments, tumour cells promote the activation of transcription factor HIF1α, which acts as an O_2 sensor that mediates increased transcription of genes including GLUT1 and other glycolytic enzymes to facilitate survival (Ata and Antonescu, 2017). The introduction of a hypoxic environment in colon cancer cells showed a significant increase in the expression of cell adhesion molecules such as syndecan-4 and integrin α5 (Koike et al., 2004). Similarly, in ovarian cancer αVβ3 overexpression has been linked to a systemic metabolic regulator thyroid hormone, independent of RGD binding. These data suggest that integrin transcription is regulated by metabolic cues (Shinderman-Maman et al., 2016).

The localization of proteins at the cell surface is tightly regulated by endocytosis. AMPK, a key metabolic sensor has been reported to mediate the transport of many proteins to the cell

surface including the integrin β1 subunit into intracellular compartments upon activation (Ross et al., 2015, Georgiadou and Ivaska, 2017b, Georgiadou et al., 2017). Furthermore, there is evidence that the availability of amino acids regulates the internalization and recycling of ligand-engaged α5β1 in an Arf4-dependent manner (Rainero et al., 2015). Nutrient depletion and/or mTORC1 knockdown promoted the endocytosis of α5β1 heterodimer from adhesions (Rainero et al., 2015, Georgiadou and Ivaska, 2017a). These results convey how different regulatory mechanisms that mediate the activation of metabolic sensors AMPK and mTOR can modulate cell migration by regulating integrin recycling (Georgiadou et al., 2017).

Prolonged nutrient deprivation can induce cellular autophagy through the formation of an autophagosome that encapsulates and fuses proteins and organelles to lysosomes. This process mediates the release of metabolic intermediates that enable cells to survive during nutrient deprivation. ULK1 (Unc-51-like autophagy activating kinase) activity is regulated by both AMPK and mTORC1-mediated phosphorylation. Autophagy is induced upon AMPK-dependent phosphorylation of ULK1, whereas mTORC1-mediated phosphorylation of ULK1 at a different site inhibits autophagy (Tuloup-Minguez et al., 2013). Induction of autophagy promoted integrin β1 translocation into autophagosomes and following lysosomal fusion it was degraded (Tuloup-Minguez et al., 2013). However, inhibition of autophagy by ATG7 (E1-like ligase) knockdown significantly increased cell migration which corresponded with reduced integrin β1 internalisation and degradation (Tuloup-Minguez et al., 2013). The overall regulation of integrin trafficking, transcription and degradation by changes in metabolic signals play an important in modulating downstream integrin signalling. For example, the addition of cobalt chloride ($CoCl_2$) to smooth muscle cells reduced cell adhesion and migration, that corresponded with decreased FAK phosphorylation in a HIF1α-dependent

manner (Corley et al., 2005). Similarly, the addition of metformin, an AMPK activator in carcinoma cells impaired cell growth and corresponded with reduced Integrin-linked kinase (ILK) expression (Hahn et al., 2014).

Equally, integrin activity regulates cell metabolism through several mechanisms that modulate the activation of specific signalling pathways and the physical association of cell surface proteins that regulate the transport of metabolites (Ata and Antonescu, 2017). Detachment of cells from ECM has been shown to reduce the uptake of glucose, which corresponded to reduced ATP levels (Schafer et al., 2009). This loss was rescued following integrin-mediated cell re-engagement to the matrix. These results convey the importance of integrins integrating downstream signalling including the PI3K-AKT pathway to regulate glucose metabolism (Schafer et al., 2009).

Monocarboxylate transporters belong to a family of proton symporters that mediate the transport of pyruvate and lactate across the plasma membrane and play an essential role in the maintenance of homeostasis (Pinheiro et al., 2012). MCT4 (monocarboxylase transporter 4), a lactate transporter has been shown to interact with integrin β1. MCT4 knockdown was associated with reduced cell migration and an increase in focal adhesion size (Gallagher et al., 2009).

Integrin β1 is also associated with a heterodimeric protein called CD98 that comprises a heavy chain that interacts with β1, and a light chain that mediates the transport of amino acids across the plasma membrane (Ata and Antonescu, 2017). The light chain of CD98 includes LAT1 and LAT2 (L-Type Amino Acid Transporter 1 and 2) and mediates the intracellular transport of essential neutral amino acids including leucine, isoleucine, valine, and arginine, in exchange for extracellular efflux of glutamine (Nicklin et al., 2009). The uptake of essential

amino acid L-glutamine has shown to be a rate-limiting step that regulates the activity of mTOR kinase that modulates cell growth, protein translation, and autophagy in a CD98/LAT1 dependent manner (Nicklin et al., 2009). This two-step amino acid regulation of mTORC1 activity is mediated firstly by the increased intracellular transport of L-glutamine by SLC1A5. CD98/LAT1 complex removes L-glutamine as an efflux substrate to regulate the influx of leucine which mediates the activation of mTORC1, by blocking the inhibitory effect of the protein sestrin 2 (Chen et al., 2021) (Nicklin et al., 2009). The CD98 heavy chain upon association with integrin β1 mediates the clustering of integrins and downstream signalling proteins including FAK and PI3K. However, knockdown of CD98 heavy chain contributes to disruption of integrin-dependent cell spreading and migration (Feral et al., 2005). These results suggest that cells can regulate the transport of metabolites in an integrin-dependent manner to regulate cellular homeostasis.

1.7. Thesis Aims

The primary aim of this thesis was to characterize the integrins and integrin-dependent signalling networks recruited on four defined substrates: vitronectin, fibronectin ZTFN, and ZT910. Traction force microscopy was employed to investigate if the distinct integrin heterodimers recruited on the four defined substrates possessed distinct biochemical and biophysical properties. To investigate the effect of distinct integrin properties on the regulation of cell behaviour; nuclear morphology, chromatin organization and YAP localization were assessed. Isolation and proteomic analysis of vitronectin-, fibronectin-, ZTFN and ZT910 IACs enabled the characterisation of integrin and integrin-dependent signalling networks. Combinatorial and integrative network analysis identified SLC3A2 as a putative

node that may integrate stem cell signalling and metabolism in an integrin-dependent manner.

2. MATERIAL AND METHODS

2.1. Antibodies

2.1.1. Immunoblotting antibodies

Immunoblotting antibodies were diluted in either 5% BSA, 1X Casein solution (#B6429, Sigma) or 5% non-fat dry milk (Marvel) in PBST (PBS-1% tween). Alexa fluor secondary antibodies were conjugated with either 680 and 790 fluorophores (Invitrogen) diluted to 1:5000 in the same primary antibody buffer.

Table 1: List of immunoblotting primary antibodies. The table provides detail of the primary antibody clone, host species, supplier, catalogue number, dilution factor used, and the buffer solution the primary/secondary antibodies were diluted in.

Primary Antibody	Clone	Host Species	Supplier	Catalogue Number	Dilution	Buffer
AKT		Rabbit	Cell Signalling Technology	#9272	1/1000	1% Casein
Anti-CD71		Mouse	ThermoFisher	#13-6890	1/1000	5% BSA
BAK	D4E4	Rabbit	Cell Signalling Technology	#12105	1/1000	5% BSA
E-cadherin		Mouse	R&D systems	#MAB18381	1/1000	5% BSA
GAPDH		Mouse	ABCAM	ab9484	1/2000	5% BSA
Integrin α5		Rabbit	Cell Signalling Technology	#4705	1/1000	5% BSA
Integrin αV	EPR16800	Rabbit	Cell Signalling Technology	ab179475	1/1000	5% BSA
Integrin β1		Rabbit	Cell Signalling Technology	#9699	1/1000	5% BSA
Integrin β3	D7X3P	Rabbit	Cell Signalling Technology	#13166	1/1000	5% BSA
Integrin β5		Rabbit	Cell Signalling Technology	#4708	1/1000	5% milk
mTOR		Rabbit	Cell Signalling Technology	2972S	1/1000	1% Casein
Paxillin		Rabbit	BD Transduction laboratories	#610051	1/1000	5% BSA

Phospho-AKT (Ser473)		Rabbit	Cell Signalling Technology	#4060	1/1000	1% Casein
Phospho-S6 Ribosomal Protein (Ser235/236)		Rabbit	Cell Signalling Technology	#4858	1/1000	1% Casein
S6		Rabbit	Cell Signalling Technology	#2217	1/1000	1% Casein
SLC3A2		Rabbit	ProteinTech	15193-1-AP	1/1000	1% Casein
Tubulin	DM1A	Mouse	Sigma Aldrich	T9026	1/2000	5% BSA
Vinculin	hVIN-1	Mouse	ABCAM	ab11194	1/1000	5% BSA

2.1.2. Immunofluorescence

Table 2: List of immunofluorescence primary antibodies. The table provides detail of the primary antibody clone, host species, supplier, catalogue number, primary and secondary antibody dilution factor used, and the buffer solution the primary/secondary antibodies were diluted in.

Primary Antibody	Clone	Host Species	Supplier	Catalogue Number	Primary antibody dilution	Secondary antibody dilution
SLC3A2		Rabbit	ProteinTech	15193-1-AP	1/250	1/400
Integrin α5	mab11	Rat	Hybridoma		1/250	1/400
Integrin αV	L230	Mouse	Hybridoma		1/250	1/400
Integrin β1	mab13	Rat	Hybridoma		1/250	1/400
Integrin β3	D7X3P	Rabbit	Cell Signalling Technology	#13166	1/250	1/400
Integrin β5		Rabbit	Cell Signalling Technology	#4708	1/250	1/400
Vinculin	hVIN-1	Mouse	ABCAM	ab11194	1/250	1/400

2.2. Immunoblotting

2.2.1. Sample Preparation

Cells ready for lysis were placed on ice and washed once in ice-cold PBS-. Cells were lysed in a RIPA lysis buffer (25 mM Tris-HCl pH 7.6, 150 mM NaCl, 1% NP-40, 1% sodium deoxycholate, 0.1% SDS) supplemented with 25µg/µl leupeptin, 25 µg/µl apoprotein, 50µg/uL AEBSF), and cells were scraped off and transferred to an Eppendorf tube. Total cell lysate solutions were centrifuged at 14700 x g for 30 minutes at 4°C. Supernatants were harvested and stored at –20°C until electrophoresis was run.

Sample protein concentration was measured using the Pierce BCA Protein Assay Kit (ThermoFisher) following manufacturers' instructions. Samples were diluted at 1:75 for the assay, and all samples and standard curve samples were made in triplicates. Sample absorbance was measured at 562 nm on the FLUOstar Omega Microplate Reader. 5x SDS sample reducing buffer (0.25 M Tris-HCl pH 6.8, 0.5 M DTT, 10 % SDS, 50 % Glycerol and 0.5 % bromphenol blue) was added to samples for a final 1x concentration. Samples were heated at 95°C for 5 minutes to denature the protein.

2.2.2. Electrophoresis

Samples from either total cell lysates or 2D integrin adhesion complex isolation preparations were run on polyacrylamide gel electrophoresis (PAGE), in either a 10-well 1.5mm gel, 15-well 1.5mm gel or a 12-well 1.0mm 4 – 12% Novex NuPAGE gradient gel (Invitrogen), in Novex® Mini-cell XCell SureLock™ Electrophoresis tanks (Invitrogen). A constant of 100 V was used to resolve the samples. Novex NuPAGE MES-SDS running buffer (Invitrogen) was used. Sample protein concentrations for total cell lysates were typically loaded at 15µg. Care was taken to ensure equal amounts of protein were loaded for each sample electrophoresed on

the same gel. Precision Plus Protein All Blue Prestained Protein Standards (Bio-Rad) was used as the molecular weight marker.

2.2.3. Transfer and Detection of Proteins

Proteins were transferred using the semi-dry Trans-Blot Turbo Transfer System (BioRad) onto immunoblotting nitrocellulose membrane (pore size 0.2µm) in 1X transfer buffer. Proteins were transferred at 25V and 2.5A for 10-12 minutes (time varied according to the molecular weight of proteins to be assessed).

Membranes were incubated in the appropriate blocking buffer corresponding to the primary antibody used (5% BSA in PBST, 5% non-fat dry milk in PBST, or 1 x casein), for half an hour at room temperature on a rocker. Membranes were incubated with primary antibody solution overnight at 4°C on a rocker.

Membranes were washed three times in PBST for five minutes on a shaker, before incubation with the secondary antibody (Alexa fluor 680 or 790 conjugated, Molecular Probes Invitrogen) diluted to 1:5000 in the corresponding blocking solution that was used. Membranes were washed again in PBST as before, then visualized on the LI-COR Odyssey imaging system. Band pixel intensities were quantified using the Image Studio Version 3.1 software.

2.3. Immunofluorescence

Cells were fixed with 4% (w/v) paraformaldehyde for 10 minutes at room temperature, then washed three times in PBS-. Cells were then permeabilized for 10 minutes with 0.1% (v/v) Triton X-100 at room temperature followed by three washes with PBS-. Primary antibody incubations were overnight at 4°C, with antibodies diluted 1/250 in 0.5% BSA and 0.5% Triton. The secondary antibodies were diluted at 1/400 in PBS- for 2 hours at room temperature in

the dark. Samples were then washed thrice in PBS- and before being mounted using DAKO fluorescent medium (Sigma). Samples were imaged using the Laser Scanning Microscope Airyscan using a 63x/1.4 oil objective. Image analyses were performed using Image-J FIJI.

2.4. Cell culture

iPSCs and ESCs were maintained in Complete mTesR Plus (Stem Cell Technologies) at 37°C, 5% CO_2. MSCs were maintained in Dulbecco's Modified Eagle's Medium (DMEM), supplemented with 10% (v/v) fetal bovine serum (FBS) (Gibco). For iPSCs, cells were detached from the culture flask using incubation with Gentle Cell Dissociation Reagent (Stem Cell Technologies) for 3 minutes at room temperature. Following removal of the dissociation reagent, cell colonies were gently scraped in mTesR plus. Cell suspensions were re-plated in appropriate cell concentrations. For MSCs, cells were detached as single cells following incubation with 1x Trypsin-EDTA solution (GIBCO) at 37°C. 1x Trypsin-EDTA solution was neutralised in DMEM with 10% FBS. Following centrifugation at 1500rpm for 5 minutes, MSC pellets were then resuspended in an appropriate volume of DMEM with 10% FBS and re-plated in appropriate cell concentrations.

2.5. Cryopreservation

iPSCs were detached from the culture flask using Gentle Cell Dissociation reagent (Stem Cell Technologies) for 3 minutes at room temperature. Following removal of the dissociation reagent, cell colonies were gently scraped in mTesR plus and centrifuged at 1500RPM for 3 minutes. Cell pellets were re-suspended in either STEMdiff freezing medium or CryoStor (Stem Cell Technologies). Cell suspensions in cryovials were frozen in Mr Frosty freezing container at -80°C before being transferred to liquid nitrogen for long-term storage.

2.6. Adhesion Complex Enrichment

The protocol for isolating integrin adhesion complexes from a 2D substrate is based on the published protocol with some outlined stem cell line-specific modifications (Jones et al., 2015). Non-tissue culture 10cm^2 dishes were coated with vitronectin, fibronectin, ZTFN, ZT910 and/or ECAD overnight at 4°C on a rocker. Dishes were then washed twice in PBS-, before blocking in 10mg/mL heat-inactivated BSA for 30 minutes at room temperature. Plates were then washed twice in PBS- and then 4 ml of mTesR plus were added to the plates and incubated at 37°C and 5% CO_2. Cells were harvested as single cells using Accutase (Stem Cell Technologies) and centrifuged at 1500rpm for 4 minutes. Cell pellets were then re-suspended in mTesR plus and cells were seeded at 5 x 10^6 per plate and allowed to adhere for 4 hours at 37°C and 5% CO_2.

Cells were cross-linked with the cell-permeable crosslinker DTBP (dimethyl 3,3'-dithiobispropionimidate, Thermo Fisher) constituted in mTesR plus. For initial adhesion complex enrichment experiments (Chapter 1 experiments), cells were incubated in 3mM DTBP for 30 minutes. However, following optimization experiments, DTBP concentration was increased to 6mM for 3 minutes (Chapter 4). Due to mass spectrometry equipment issues and delays, the proteomic dataset has been integrated from three repeats, where the first experiment was performed using 3mM DTBP for 30 minutes and the remaining two experiments were performed using 6mM DTBP for 3 minutes. Plates are incubated at 37°C to permit cross-linking. Cells were then washed twice in ice-cold PBS- and incubated with 20 mM pH 8.0 Tris for 5 minutes at room temperature to quench the crosslinker activity. Plates were then washed twice in ice-cold PBS- and transferred to ice packs. Before sonication, cells were incubated with cold extraction buffer (20 mM NH_4OH, 0.5% (v/v) Triton X-100 in PBS- for 5

minutes. Cells were sonicated submerged in extraction buffer, using the SONICS Vibra cell™ sonicator for 30 seconds at 20% amplitude. Following sonication, plates were washed two times in cold extraction buffer, and two times in cold PBS-. All PBS- was completely removed from the plate and the plates were stood up to completely dry. The cross-linked integrin adhesion complexes were harvested by scraping in a 2x reducing sample buffer. Harvested material was collected in an Eppendorf and incubated at 95°C for 5 minutes. 10% of the sample was then immunoblotted to assess the quality of the integrin adhesion complex experiment, with the remaining sample processed for mass spectrometry.

2.7. Cell Attachment Assays

Non-tissue cultured 96-well plates (Greiner) were coated with vitronectin (5µg/mL), fibronectin (10µg/mL), ZTFN (10µg/mL) and ZT910 (10µg/mL) in PBS+ overnight at 4°C. Furthermore, wells were coated with poly-L-lysine (10µg/mL) in PBS+ as a control for 100% attachment. All wells (excluding poly-L-lysine) were then washed with PBS- twice before blocking at room temperature with heat-inactivated BSA (10mg/mL) for 30 min. Following this, the wells were washed with PBS- twice before the addition of cells. iPSCs were dissociated into single cells with Accutase and resuspended in mTesR plus at 50,000 cells/100µL. 100µL of the cell suspension was transferred to the 96-well plates and incubated for 2hrs, 4hrs, and 6hrs at 37°C/5% CO_2. At the specific timepoints, plates were washed (excluding poly-L-lysine wells) with PBS- twice and fixed with 5% glutaraldehyde for 20 minutes at room temperature. The plates were washed two times with PBS- and once with H_2O. The plates were then stained for 1hr in 0.1% crystal violet solution. The plates were washed three times in H_2O before being allowed to dry at room temperature overnight. Once

the plates were completely dry, 100µL of 10% acetic acid was added to each well to enable solubilization of crystal violet. Absorbance was measured at 595nm using FLUOstar Omega.

2.8. Integrin Inhibitory Assays

Table 3: List of integrin inhibitory antibodies/inhibitors. The table provides detail of the primary antibody clone, host species, supplier, catalogue number and final antibody/inhibitor concentration used.

Primary Antibody/Inhibitors	Clone	Host Species	Supplier	Catalogue Number	Final antibody/inhibitor concentration
Integrin α5	mab11	Rat	Hybridoma		10µg/µL
Integrin αV	L230	Mouse	Hybridoma		10µg/µL
Integrin β1	mab13	Rat	Hybridoma		10µg/µL
Integrin αVβ5	P1F6	Mouse	Millipore	MAB1961Z	10µg/µL
C8 (αVβ1 inhibitor)	C8 inhibitor was kindly donated by Dean Sheppard				10µM

Non-tissue cultured 96-well plates (Greiner) were coated with vitronectin (5µg/mL), fibronectin (10µg/mL), ZTFN (10µg/mL) and ZT910 (10µg/mL) in PBS+ overnight at 4°C. Furthermore, wells were coated with poly-L-lysine (10µg/mL) in PBS+ to control for 100% attachment. All wells (excluding poly-L-lysine) were then washed with PBS- twice before blocking at room temperature with heat-inactivated BSA (10mg/mL) for 30 min. Following this, the wells were washed with PBS- twice before the addition of cells. iPSCs were dissociated into single cells with Accutase and resuspended in mTesR plus HEPES at 100,000 cells/100µL. The cells were then treated with appropriate antibodies and small molecules to inhibit integrin function; Mab 11 (α5), Mab 13 (β1), L230 (αV), C8 (αVβ1), and αVβ5. 100µL of this cell suspension was transferred to the 96-well plates and incubated for 4hrs at 37 °C/5% CO_2. After 4hrs, plates were washed (excluding poly-L-lysine wells) with PBS- twice, fixed with 5% glutaraldehyde for 20 minutes at room temperature, before being washed two times with

PBS- and once with H_2O. The plates were then stained for 1hr in 0.1% crystal violet solution. The plates were washed three times in H_2O before being allowed to dry at room temperature overnight. Once the plates were completely dry, 100µL of 10% acetic acid was added to each well to enable solubilization of crystal violet. Absorbance was measured at 595nm using FLUOstar Omega.

2.9. Traction Force Microscopy (TFM)

2.9.1. Reagents and Consumables

Table 4: List of TFM experimental reagents and consumables.

Reagents	Supplier	Catalog Number
0.1 M Sodium Hydroxide (NaOH)	Fisher	10396240
0.5% Glutaraldehyde in water	Sigma	G6257
10% Ammonium Persufate in water	Sigma	A 3678
35 mm Dish | No. 1.5 Coverslip | 14 mm Glass Diameter | Uncoated	MatTek	P35G-1.5-14-C
50mM HEPES pH 8.5	Sigma	H0887
APES ((3-Aminopropyl) trimethoxysilane)	Sigma	281778
Circular Cover Slips No.1 Dia 13mm (100)	Appleton Woods	MS002
FluoSpheres™ yellow-green, fluorescent (505/515)	ThermoFisher	F8811
ProtoGel (30% Solution at 37.5:1 Ratio)	Geneflow	A2-0072
Rain-X repellent	Halfords	108282
Sulfo-SANPAH	ThermoFisher	22589
TEMED	Sigma	T9281

2.9.2. Preparation Of Amino-Silanated Glass-Bottomed Dishes

Glass-bottomed Mattek were incubated for 5 minutes in 250µL 0.1M NaOH at room temperature. Following aspiration of NaOH, the dishes were treated with 200µL APES for 3 minutes. The APES was then neutralized using 2mLs of PBS- for 2 minutes. Mattek dishes were then washed thoroughly in milliQ water. The dishes were allowed to dry under the fume hood before addition and incubation with 400µL of 0.5% glutaraldehyde solution for 30 minutes.

The dishes were then washed thoroughly with milliQ water in a beaker twice, before being allowed to dry in the fume hood overnight. Once dry, the dishes were incubated in 70% ethanol for 2-3 hours. The dishes were then air-dried in the fumehood and stored at 4°C.

2.9.3. Preparation of coverslips

13mm round glass coverslips were incubated in 50 mL RainX repellent and agitated in the rotator for 2-3 hours. The coverslips were then washed thoroughly three times in milliQ water before incubation at 55°C to dry before use.

2.9.4. Polyacrylamide gel preparation + ECM coating

To obtain the expected stiffness (kPa), stock solutions were prepared from mixtures of acrylamide, PBS, APS, TEMED and fluorospheres according to Table 4. Before the addition of APS and TEMED, the stock solution was vortexed for 1 minute and then degassed in a vacuum for 15 minutes. APS and TEMED were then added to the stock solution and mixed gently to avoid air bubbles. 6µL of this mixture was added to the amino-silanated glass-bottomed dish. Pre-treated coverslips were then gently placed on the mixture before the dish was tapped on a solid surface to ensure the mixture covered the glass-bottomed dish. The dish was then turned upside down and incubated at room temperature for 30 minutes. Once the gel has polymerized, the glass coverslip was removed using forceps. The gels were washed twice in PBS-. To coat the gels with ECM protein, the gels were incubated in 150µl of 0.2mg/mL sulfo-SANPAH, before being placed under 185-254nm UV light source for 20 minutes. The gels were then rinsed with HEPES to remove excess sulfo-SANPAH. ECM proteins were diluted in HEPES to the appropriate concentration and incubated at 4°C overnight. The gels were then washed twice with 1mL of sterile PBS- and sterilized under ultraviolet light in a tissue-culture hood for 20 minutes before use.

Table 5: Rigidities used for Traction force microscopy experiments. The table contains the volumes of protogel, fluorospheres, APS, and TEMED solutions to achieve the appropriate rigidities.

Condition	Expected stiffness (kPa)	Protogel (µl)	PBS (1x) (µl)	Flurospheres (µl)	APS (10%) (µl)	TEMED (µl)	Final volume (µl)
5%	5	83.3	391.7	20	5	0.5	500.5
9%	10-15	150	325	20	5	0.5	500.5
21%	70-100	350	125	20	5	0.5	500.5

2.9.5. Image acquisition

Images were obtained in conditions with and without the cells. The images without the cells were taken following the removal of cells from polyacrylamide gels using a 1% SDS solution. For each set (before vs after), 21 images were obtained typically separated by a distance of 0.5µm in the Z-plane using 3i Spinning Disk Confocal Microscope. Both sets of images correspond to the top of the gel, the point of contact between the cell-extracellular matrix. Furthermore, it is important to image a single cell within the field of view to avoid interference of bead displacement of beads as a result of cells within proximity.

2.9.6. TFM analysis

Traction force analysis was carried out as described using image-J macros that were developed by the Cytomorpho Lab (Martiel et al., 2015). The two macros are called: *GenerateParameterFile.ijm* and *AlignCropPIVForce.ijm.* The first macro aims to list the specific experimental conditions (number of beads and young modulus of gel) which is exported as a

text file that contains all the required parameters for force analysis. Following the generation of the parameter file, the second macro was employed to translate bead displacement and young modulus of the gel into force magnitude.

2.10. YAP localisation

Subcellular localization of YAP protein was quantified following plating of single-celled iPSCs on polyacrylamide gels of different rigidities. The cells were then immunostained for YAP as per the immunofluorescence protocol described above. The nuclear-to-cytoplasmic YAP ratio was calculated manually. For each condition, a single region of interest (ROI) square was placed in the nucleus and cytoplasm. ROIs were always selected using the DAPI channel of IF images to avoid bias. The nuclear ROI fluorescence intensity was divided by the cytoplasmic ROI fluorescence intensity to derive the nuclear-to-cytoplasmic ratio. This method of quantification is based on the relative ratio of nuclear to cytoplasmic intensities and therefore does not consider the cell shape. Therefore, this method of quantification is less sensitive, because when a cell is rounded, the concentration of YAP proteins is higher per area compared to a cell that is more spread.

2.11. Nuclear and Chromatin parameters (NucleusJ)

Nuclear and chromatin parameters were quantified following plating of single-celled iPSCs on polyacrylamide gels of different rigidities. The cells were then immunostained for DAPI as per the immunofluorescence protocol described above. For each experiment, the whole nucleus was imaged at 0.2µm in the z-plane using Airyscan Laser Scanning Microscope 800/900. NucleusJ, an image-J plugin was then employed to quantify up to 15 nuclear and chromocenter parameters (Poulet et al., 2015). The nuclear parameters included nuclear volume, surface area, sphericity, flatness, and elongation. The chromocenter parameters

included the number of chromocenters, mean volume of chromocenters per nucleus, the total volume of chromocenter per nucleus, mean distance of chromocenters border to the nuclear periphery, the mean distance of chromocenter barycenter to the nuclear periphery, total chromocenter intensity / nuclear intensity, and total chromocenter volume / nuclear volume. Both 2D and 3D nuclear and chromocenter parameters were derived from the NucleusJ plugin as described in the supplementary website available at: https://imagejdocu.tudor.lu/doku.php?id=plugin:stacks:nuclear_analysis_plugin:start.

Briefly, the first step of NucleusJ analysis begins with nuclear segmentation using an Otsu threshold. The second automated step computes intensity contrasts in the 3D DAPI image using a watershed algorithm. Chromocenters are then extracted by manual thresholding. 2D and 3D parameters of both nucleus morphology and chromocenter organisation are extracted from both segmentation steps and exported as an excel file for analysis.

2.12. Mass Spectrometry

2.12.1. Protein Gel preparation

Integrin adhesion complex samples were resolved by polyacrylamide gel electrophoresis (PAGE), in a 10-well 1.5 mm 4 – 12% gradient Novex NuPAGE gels (Invitrogen), in the Novex Mini-cell XCell SureLock Electrophoresis tanks (Invitrogen). A constant 100V was used to resolve the samples in Novex® NuPAGE™ MES-SDS running buffer (Invitrogen) until they migrated halfway down the gel. Instant Blue™ (Expedion) protein stain was used to stain the protein in the gels for 30 minutes at room temperature on a rocker. Gels were then de-stained with three 30-minute washes in MilliQ water, on the rocker.

1mm^3 sized gel bands were excised with sterile scalpel blades on a clean tile and transferred into a single well of a 96-well perforated plate (Glygen Corp). 150µL of MilliQ water was then added to each well, before storing in MilliQ water overnight at 4°C. MilliQ water was removed by centrifugation at 1500 RPM for 2 minutes Gel pieces were then destained by repeated 30-minute incubations in 100µl 50% (v/v) (ACN) / 50% (v/v) NH_4HCO_3 until the gel pieces in each well were completely destained and transparent.

2.12.2. Peptide digestion

Two five-minute incubations of 50 µl 100% ACN were used to dehydrate the gels at room temperature. ACN was removed using a vacuum centrifuge (program: V-HV, Eppendorf speed vac). The gel pieces were dried by vacuum centrifugation for 30 minutes. The gels were then incubated in 50 µl in 10 mM Dithiothreitol (DTT) for one hour at 56°C, to reduce the proteins. DTT was removed by centrifugation and proteins in the gel were alkylated with 50µL 55 mM Iodoacetamide (IA) for 45 minutes at room temperature, in the dark. IA was removed by centrifugation. Gel pieces were washed and dehydrated 50µl 25 mM NH_4HCO_3 twice for 10 minutes followed by incubation with 50µL ACN for 5 minutes respectively at room temperature. The plate was centrifuged, and the supernatant was disposed of each time. Gel pieces were dried using a vacuum centrifuge for 20 minutes (program: V-HV). Following the last wash, a 96-well collection plate (microplate u-shaped well bottom, Thermo Scientific) was placed under the perforated plate for peptide elution and collection. The gel pieces were then incubated in 1.25 ng/µL trypsin gold (Promega) in 25 mM NH_4HCO_3 at 4°C for 45 minutes, before incubation overnight at 37°C for protein digestion.

2.12.3. Peptide extraction

Following overnight tryptic protein digestion, the gel pieces were incubated in 50 µl 99.8% (v/v) ACN/ and 0.2% (v/v) formic acid (FA) for 30 minutes at room temperature following centrifugation of overnight trypsin solution. The plates were centrifuged to collect the first 50 µl of eluted peptides. This was followed by incubating gel pieces with 50 µl 50% (v/v) ACN and 0.1% (v/v) FA for 30 minutes at room temperature to extract additional peptides. A total of 150µL of collected peptide solution was then dried using a vacuum centrifuge (program: V-AQ) for 2.5 hours. Dried peptides were then re-suspended in 20 µl 5% (v/v) ACN in 0.1% FA and transferred into glass screw neck vials (Waters) for analysis on the mass spectrometer. 4µL of each gel digest was injected onto a Nanoacquity™ (Waters) Ultra Performance Liquid Chromatography (UPLC) column, coupled to an LTQ-Orbitrap XL (Thermo Fisher) equipped with a nanoelectrospray source (Proxeon). Samples were separated on a 1 – 85% ACN gradient, 0.300 µl/min flow rate, with an 80-minute retention time. Dynamic exclusion was enabled for a repeat count of 1 for a duration of 30.00 s. MS spectra were acquired by the LTQ-Orbitrap at a resolution of 30,000 and MS/MS was performed on the top 12 most intense ions in the LTQ ion trap.

2.12.4. Proteomic analysis

Raw mass spectrometry data were converted into peak lists and searched against a reviewed H. Sapiens UniProt database (dated: 071215) containing 149,633 sequences using Mascot Daemon (version 2.3.2) software. Cysteine carbamidomethylation (C) was set as a fixed modification, whereas oxidation (M, K, P), and phosphorylation (S, T, Y) were considered variable modifications. Scaffold (version 4) was used to process and statistically evaluate proteins identified in Mascot daemon. The exported protein list from Scaffold was analyzed

using R (v.3.9.2). R packages used: corrplot. Data were imported into Cytoscape (v3.9.2) for visualization of protein-protein interactions mapped using the Protein Interaction Network Analysis (PINA) interactome database.

2.13. siRNA knockdown of SLC3A2

All-Stars siRNA negative control oligonucleotide was obtained from Qiagen (Stock: 20 µM, siRNA ID: SI03650318) and siRNA SLC3A2 oligonucleotide was obtained from Thermofisher (Stock: 40 µM, siRNA ID: s12943) and used at a concentration of 1µM. iPSCs were transfected with Lonza 4D Nucleofector® Kit (Lonza) using the P3 program, per the manufacturer's instructions. iPSCs were transfected as single cells. To obtain optimal cell survival, the cells were initially grown in two T175 flasks. Once the cells reached 70-80% confluence, the first siRNA control and siRNA SLC3A2 nucleofection was carried out. Following nucleofection, the cells were plated on vitronectin-coated T175 flasks in mTesR plus with ROCK inhibitor. After 48 hours, a second siRNA control and siRNA SLC3A2 nucleofection was carried out on single iPSCs. Following the second nucleofection iPSCs were seeded on two T75 flasks for 48 hours in mTesR plus (ROCK inhibitor was added for the first 24 hours).

2.14. CellTitre-Glo assay

Tissue-cultured 96-well plates (Greiner) were coated with vitronectin (5µg/mL) or fibronectin (10µg/mL) in PBS+ overnight at 4°C. Following overnight incubation, wells were washed with PBS- twice, before blocking at room temperature with heat-inactivated BSA (10mg/mL) for 30 min. Following this, the wells were washed with PBS- twice before the addition of cells. iPSCs were dissociated into single cells with Accutase and resuspended in mTesR plus and plated at 30,000 cells/100µL cells per well in mTesR Plus Complete Medium at 37 °C and 5% CO_2 for 4 hours. siRNA CTRL and siRNA CD98 knockdown cells were plated on vitronectin and

fibronectin, with and without LAT1 (JPH303) inhibition. Cells plated on vitronectin and fibronectin were treated with 10µM Oligomycin to inhibit ATP synthase activity. Following 4-hour incubation, 100 µl of reconstituted Cell TiterGlo™ (Promega) reagent was added to the cells. The plate was shaken for 2 min at room temperature on a circular-moving shaker at 250 rpm to induce cell lysis while covered with aluminium foil. The plate was incubated at room temperature for a further 10 min before luminescence was read on a FLUOstar Omega Microplate Reader.

2.15. Seahorse Assay

The Seahorse XF96 Analyzer enables quantitative measure of oxygen consumption rate (OCR) and extracellular acidification rate (ECAR). OCR corresponds to the rate of oxygen concentration in the assay medium and is an indicator of mitochondrial respiration. ECAR corresponds to the proton concentration in the assay medium and is an indicator of the rate of glycolysis. iPSC siRNA control and iPSC siRNA SLC3A2 were seeded into the Seahorse XF96 Cell Culture Microplates (Agilent) at the cell density of 50,000 cells/well for 4 hours. Following 4-hour incubation, the cells were washed once and incubated in XF Seahorse Base Medium (40mL) containing mTesR supplement (10mLs). The XF Seahorse Base Medium was prepared following manufacturer's instruction (Agilent). For both siRNA control and siRNA SLC3A2 conditions, OCR and ECAR readings were taken over time under basal conditions and after the addition of mitochondrial inhibitors (1 µM oligomycin, 2 µM FCCP and 1 µM rotenone).

Following seahorse assay experiment, seahorse assay medium was removed and 200µL of Pierce BCA Protein solution and incubated for 30 minutes. Sample absorbance was measured at 562 nm on the FLUOstar Omega Microplate Reader. The data obtained from seahorse experiment was normalised to the BCA absorbance values in each well.

2.16. Statistics

All statistical analyses were performed using GraphPad Prism 9 software. Statistical tests were performed by using either parametric and non-parametric ANOVA (one way or two ways) or Unpaired t-test, with appropriate post-hoc test indicated in the figure legends.

3. RECRUITMENT OF DISTINCT INTEGRIN HETERODIMERS ON DIFFERENT RGD-SUBSTRATES

3.1. Introduction

Cells primarily attach to ECM by recognising and binding to specific ECM proteins through the integrin family of adhesion receptors. The integrins family is composed of 18 α and 8 β subunits that together assemble into 24 distinct integrin heterodimers. The different integrin heterodimers each have specific ECM binding partners and this specificity is attributed to the extracellular domains of α and β subunits. Pluripotent human embryonic stem cells (hESCs) have been reported to express a limited subset of integrins. Microarray data demonstrated above-background levels of mRNA expression integrins α3, α5, α6, α7, αV, β1 and β5 in both hESCs and iPSCs (Rowland et al., 2010). Structural studies of integrin heterodimers have revealed that two β1 integrins (α5β1 and α8β1), five αV integrins (αVβ1, αVβ3, αVβ5, αVβ6 and αVβ8) and αIIbβ3 can promote cell adhesion through engagement with the RGD-motif. Human ESC lines have been reported to express high levels of integrin protein subunits α5, α6, αV, β1, and β5 (Prowse et al., 2011). α5β1 and αVβ1 have been reported to engage fibronectin, αVβ5 and αVβ1 have been reported to engage vitronectin(Rowland et al., 2010). For this study, the aim was to determine how distinct heterodimers recruited on RGD-substrates modulate stem cell behaviour. To this end, RGD peptide-containing substrates vitronectin, fibronectin, ZTFN and ZT910 were employed.

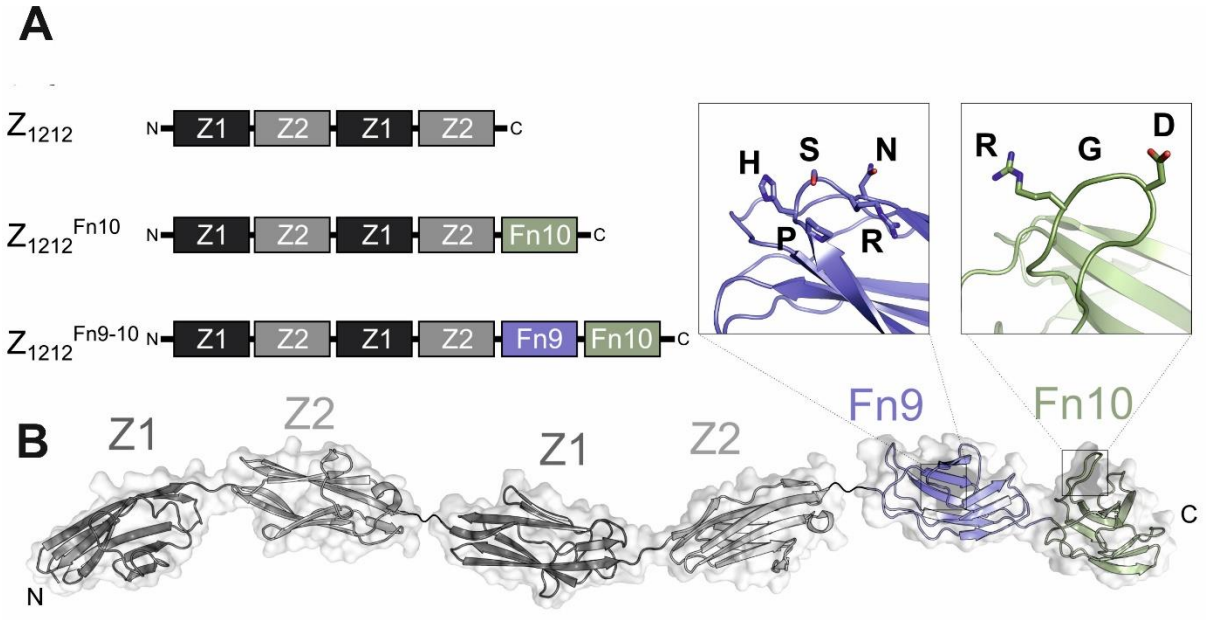

Figure 3.1: Schematic model of the ZT substrates. (a) Z_{1212} represents the building block of the ZT substrates, with the Z_{1212}^{Fn10} and Z_{1212}^{Fn9-10} representing the ZTFN and ZT910 substrates respectively. (b) Schematic representative structure of the ZT910 substrate containing the PHSRN and RGD motif.

ZTFN and ZT910 were generated from the protein polymer ZT to create self-assembling recombinant substrates for the long-term culture of pluripotent stem cells (Hill et al., 2019) (Figure 3.1). The principal ZT polymer is formed from the fusion of the protein telethonin with two N-terminal immunoglobulin domains of titin, Z1Z2, which is found naturally in human sarcomeres (Hill et al., 2019). The telethonin joins two antiparallel Z1Z2 doublet which is linked to another Z1Z2 doublet using a GETTQ linker sequence Z1Z2-Z1Z2 tandem repeat (Hill et al., 2019). The GETTQ linker at the C-terminus of the Z2 monomer results in spontaneous self-propagative self-assembly of the Z1Z2-telethonin polymer (Hill et al., 2019). ZT components can be readily functionalised with active protein moieties (Hill et al., 2019). The functional and scaffolding properties of the ZT polymer were exploited to create a substrate enabling the successful culture of human pluripotent stem cells (Hill et al., 2019). In

fibronectin, the small RGD peptide found in the Fn10 domain is essential for integrin-binding that mediates cell adhesion and migration (Kalaskar et al., 2013) (Figure 3.1). Although it has been shown that hESCs do not adhere to mimetic RGD peptides, fibronectin fragments that contain the Fn10 domain were shown to promote hESC attachment and supported self-renewal in culture (Kalaskar et al., 2013). Consequently, the ZTFN substrate was engineered to contain the RGD-containing Fn10 domain of fibronectin, and therefore did not comprise the short amino acid sequence Pro-His-Ser-Arg-Asn (PHSRN) present in the Fn9 domain, essential in enhancing cell-adhesive function (Aota et al., 1994) (Figure 3.1). Subsequently, the ZT910 substrate has been designed to contain the Fn9 and Fn10 domains of fibronectin.

Integrins are the primary site of force transmission across the plasma membrane at sites of cell-ECM interaction (Martino et al., 2018). The engagement of integrins to the ECM leads to the formation of multi-protein complexes at the cell-matrix interface called IACs (Martino et al., 2018). The multi-layered complex structure of focal adhesions acts not only as a signalling hub but as a mechanical conduit transmitting dynamic changes in ECM composition and mechanics, resulting in the modulation of biochemical signals in a process called mechanotransduction (Martino et al., 2018). Different ECM proteins such as fibronectin, laminin, vitronectin and collagen are specifically recognised by distinct integrin heterodimers (Humphries et al., 2006). For example, vitronectin has been shown to recruit both α5β1 and αVβ5, fibronectin specifically recruits α5β1 and αVβ3 and, laminins recruit α3β1, α2β1, α6β1 and α6β4 and collagens recruit both α1β1, α10β1 and α2β1 in a cell-dependent manner (Humphries et al., 2006). There is also evidence that differential recruitment of integrins is also translated to changes in downstream integrin-dependent signalling (Danen et al., 2000). NIH-3T3 cells plated on fibronectin, collagen, laminin and poly-L-lysine (non-integrin binding

substrate) and assessed for the ability of the cells to enter Rb-dependent S phase entry showed that only cells on fibronectin successfully entered S phase (Danen et al., 2000). Furthermore, analysis of RhoA showed significant induction of active RhoA in cells plated on fibronectin, with active RhoA barely detectable on collagen, laminin and polylysine (Danen et al., 2000).

In this chapter, integrin heterodimers recruited on vitronectin, fibronectin, ZTFN and ZT910 were characterised. Traction force microscopy was employed to assess if the integrin heterodimers recruited on the defined substrates possess distinct mechano-transducing properties. Integrins and their downstream adaptor and cytoskeletal proteins recruited to IACs enable cells to sense, adapt and respond to changes in mechanical stimuli in their microenvironment. Variation in ECM mechanical cues can lead to modulation in nuclear translocation of transcriptional co-activators, changes in enzymatic activity and function regulating mechanochemical signalling pathways downstream that regulate proliferation, survival, differentiation, and migration (Janoštiak et al., 2014b). Furthermore, multiple components of the LINC complex have been identified that both, directly and indirectly, link the nucleus to the ECM, cooperatively regulating the mechanical and biological nature of the nucleus and gene expression respectively (Cho et al., 2017, Fedorchak et al., 2014, Gruenbaum et al., 2005, Hu et al., 2017, Miroshnikova et al., 2017, Nava et al., 2020). To evaluate the effect of distinct integrin heterodimer mechanical properties on stem cell phenotype, the localisation of YAP, a mechanosensitive transcriptional co-activator, and nuclear morphology and chromatin organisation were assessed.

3.2. Results

3.2.1. Characterisation Of Integrin Expression

For this study, an appropriate pluripotent stem cell line for studying the role of RGD-binding integrins had to be established. The substrates used in this study namely, vitronectin, fibronectin, ZTFN and ZT910 possess the RGD-motif. Therefore, the expression of various integrins with RGD-binding capabilities was assessed in an induced pluripotent stem cell line and two embryonic stem cell lines (RC17 and H9). Mesenchymal stromal cells (MSCs) were used as a control for a non-pluripotent stem cell line, with telomerase-induced foreskin fibroblasts (TIFs) as a positive control for RGD-binding integrin subunits. The iPSC line used was derived from $CD34^{+}$ cord blood that is integrated with seven pluripotency-inducing factors (SOX2, OCT4, KLF4, MYC, NANOG, LIN28, and SV40L T antigen).

The total expression of RGD-binding integrin subunits α5, αV, β3 and β5 were evaluated in iPSCs, H9 and RC17. Specific integrin subunits (α8, β8, β6 and αIIbβ3) were excluded from the assessment due to evidence from the literature of their lack of expression in pluripotent stem cells (Rowland et al., 2010). Total expression of RGD-binding integrins and focal adhesion protein vinculin were assessed by immunoblotting. All cell lines were positive for α5, αV, β5 and vinculin expression (Figure 3.2). However, all three pluripotent cell lines were negative for β3 by contrast to the MSCs (Figure 3.2). These results suggest that all three pluripotent stem cell lines positively express RGD-binding integrin subunits.

3.2.2. Cell attachment assay

Unlike MSCs, pluripotent stem cells characteristically exist in compact colonies with defined edges. These colonies are maintained by E-cadherin mediated cell-cell contact (Soncin and Ward, 2011). To characterise the effect of integrin-dependent functions, it was necessary to

assess cellular processes in single cells to exclude the effect of E-cadherin-mediated signalling Therefore, pluripotent stem cells (iPSC, RC17 and H9) were treated with Accutase, a cell detachment solution comprised of collagenolytic and proteolytic enzymes to generate single cells and their levels of optimal attachment were determined following engagement to vitronectin, fibronectin, ZTFN and ZT910 at 2-, 4- and 6-hour incubations (Figure 3.3). Due to the sensitivity of single pluripotent stem cells, this assay aimed to determine the timepoint for optimal cell attachment for immunofluorescence imaging and to maximise the collection of IACs from downstream adhesion complex enrichment and proteomics experiments. All three cell lines plated on vitronectin, fibronectin and ZT910 displayed >30-40% attachment in all cell lines at two and four incubation (Figure 3.3). iPSCs displayed a substantial reduction in cell attachment following a six-hour incubation compared to both two and four-hour incubations. All three cell lines plated on ZTFN displayed a greater than 70% less cell attachment compared to vitronectin, fibronectin and ZT910 (Figure 3.3). Although there wasn't a significant difference between cell attachment between 2 and 4 hours for all cell lines, except for the RC17 cell line when plated on ZTFN and considering the >70% less cell attachment on the ZTFN substrate in all cell lines, it was determined that 4 hours to be the optimal timepoint for maximal cell survival and attachment.

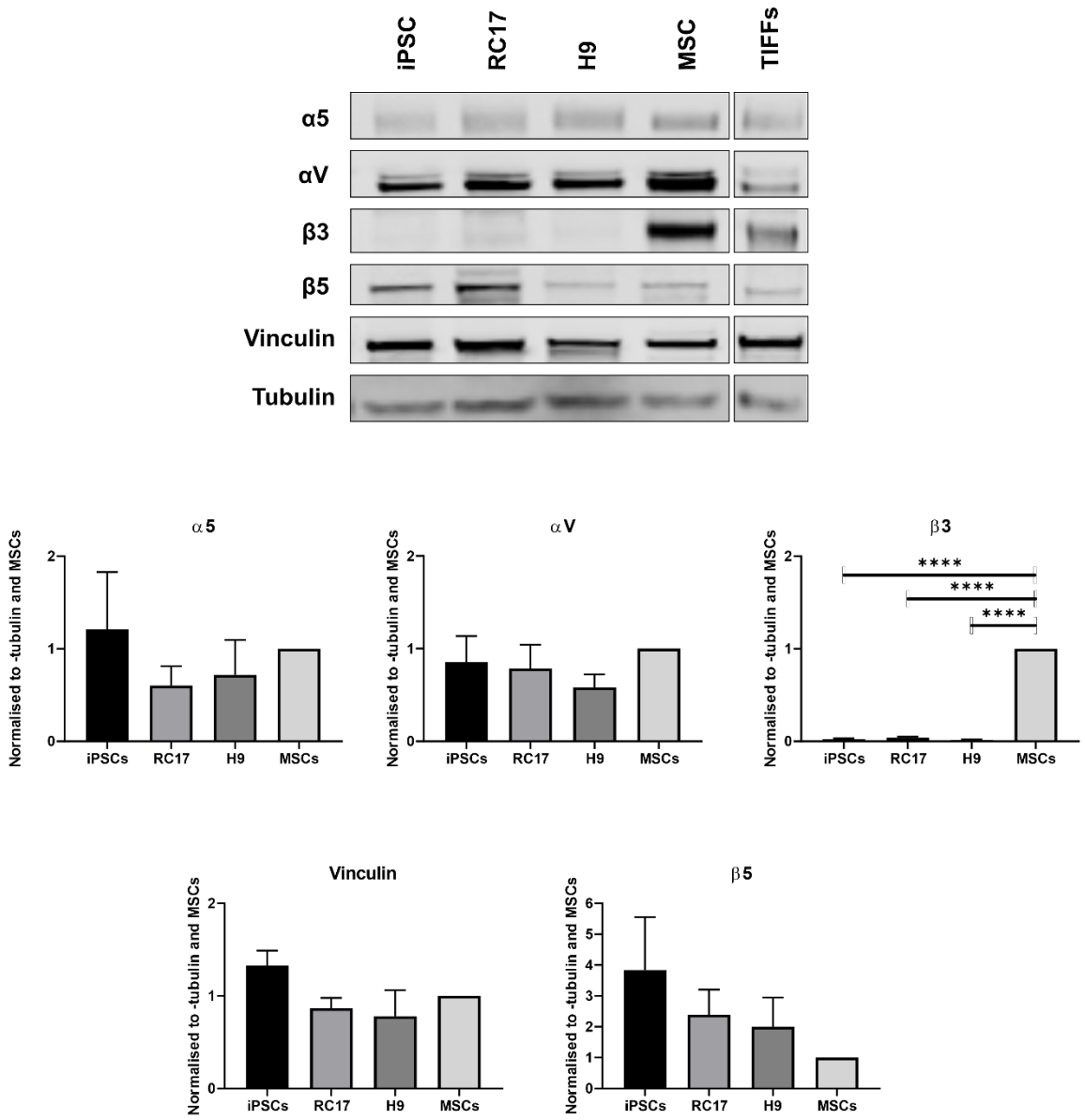

Figure 3.2: Characterisation of RGD-binding integrin expression in stem cell lines. Integrin and vinculin expression in a panel of cell lines. Immunoblotting of integrin subunits (α5, αV, β3 and β5) and vinculin protein expression levels in Human Induced Pluripotent Stem cells (iPSCs, N=3), Human Embryonic Stem Cells (RC17 and H9, N=2), Mesenchymal Stromal Cells (MSCs, N=2) and TIF (positive control) total cell lysates. Protein expression was normalised to α-tubulin and MSCs. Data shown as mean ± SEM are representative of three independent experiments: One-way ANOVA with Tukey's post-hoc test **** $p<0.0001$.

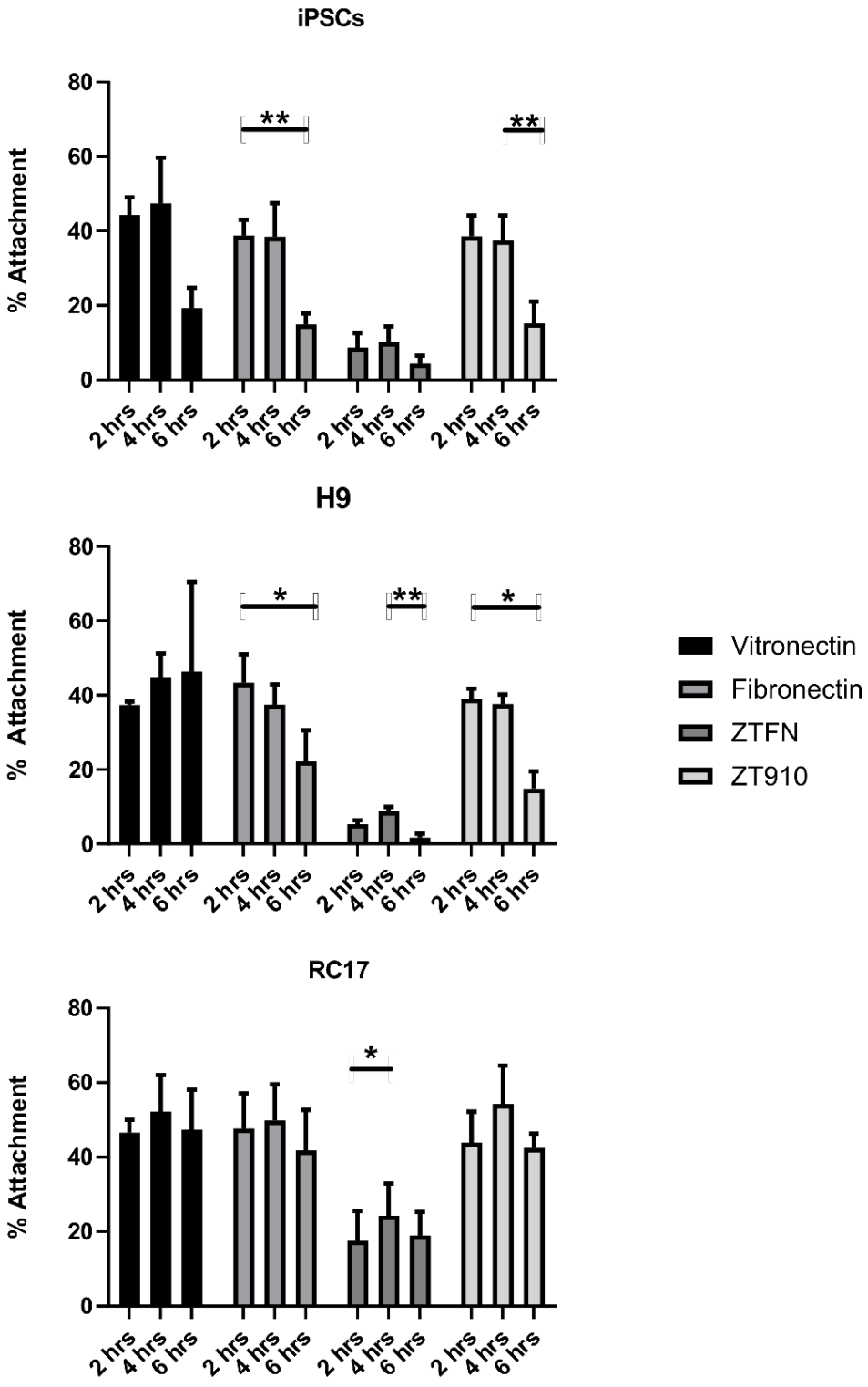

Figure 3.3: Pluripotent stem cells display optimal cell attachment at 4 hours. iPSC, H9 and RC17 were plated on vitronectin (5µg/mL), fibronectin (10µg/mL), ZTFN (10µg/mL) and ZT910 (10µg/mL) for 2,4 and 6 hours, respectively. Data shown as mean ± SEM are representative of three independent experiments: Two-way ANOVA with Tukey's post-hoc test * $p<0.05$ and ** $p<0.01$.

3.2.3. Characterisation of integrin heterodimers recruited to IACs

Next, we sought to determine which RGD-binding integrin heterodimers were principally recruited and mediated integrin-mediated adhesion by iPSCs, H9 and RC17 on vitronectin, fibronectin, ZTFN and ZT910 (Figure 3.4, 3.5 and 3.6). Therefore, immunofluorescence imaging of all three cell lines plated for 4 hours on vitronectin, fibronectin, ZTFN and ZT910 were performed, with cells stained for RGD-binding integrin subunits and focal adhesion protein vinculin (Figure 3.4, 3.5 and 3.6).

All three cell lines plated on vitronectin displayed robust focal adhesion structure formation as evidenced by the localisation of vinculin at the end of actin stress fibres (Figures 3.4, 3.5 and 3.6). iPSCs and RC17 cells plated on vitronectin displayed αV and β5 localisation at IACs (Figures 3.4 and 3.6). However, H9 cells plated on vitronectin displayed only αV localisation at focal adhesion structures (Figure 3.5). iPSCs plated on vitronectin also displayed increased β1 localisation at focal adhesions (Figure 3.4). By contrast, both H9 and RC17 cells displayed an increased level of α5 and β1 recruitment to IACs (Figures 3.5 and 3.6). These observations suggest that both αVβ5 and a β1-associated integrin heterodimer are localised at IACs in iPSC on vitronectin, with α5β1 integrin recruitment to vitronectin-dependent adhesions in H9 and RC17 cells.

Unlike vitronectin, all three cell lines plated on fibronectin and ZT910 displayed substantial recruitment of α5 and β1 localisation at IACs (Figures 3.4, 3.5 and 3.6). Furthermore, iPSCs on fibronectin also display recruitment of αV subunit (Figure 3.4). These observations suggest that both α5β1 and an αV-associated integrin heterodimer are recruited to IACs in iPSCs but not H9 and RC17 cells on fibronectin and ZT910 (Figures 3.4, 3.5 and 3.6). IPSCs and H9 plated on ZTFN displayed recruitment of αV and β1 subunit to IACs (Figures 3.4 and 3.5).

Furthermore, iPSCs and H9 cells plated on vitronectin also displayed increased β1 localisation at focal adhesions However, only iPSC and H9 cell lines displayed recruitment of the β1 subunit to IACs (Figures 3.4 and 3.5). These observations suggest that iPSCs and H9 principally recruit αVβ1 heterodimer to ZTFN-dependent adhesions. The recruitment of multiple integrins subunits and/or heterodimers at focal adhesion suggest a potential functional role of the primary and secondary integrins recruited to IACs.

3.2.4. Integrin inhibitory assays

Due to the presence of multiple integrin subunits localising to IACs, integrin inhibitory attachment assays were employed to determine the primary integrin heterodimer mediating engagement on vitronectin, fibronectin, ZTFN and ZT910 (Figure 3.7). For this and the subsequent downstream validation and functional experiments, the iPSC line was chosen as the primary model of study due to a more robust pattern of integrin subunit recruitment to IACs and increased cell maintenance issues associated with culturing H9 and RC17 cell lines. The attachment of iPSCs was measured in conditions enabling inhibition of single integrin-subunits, pairs of integrin subunits and specific heterodimers using function-blocking anti-integrin antibodies and small molecule inhibitors.

Immunofluorescence of iPSCs suggested that αVβ5 and a β1-associated integrin heterodimer are recruited to IACs in cells to vitronectin (Figure 3.7A). Inhibition of α5 and β1 individually and in a combinatorial fashion to target the α5β1 and other β1-containing heterodimers did not significantly affect iPSC attachment, suggesting iPSC does not use α5β1 or any other β1-containing heterodimers to engage vitronectin (Figure 3.7A). Furthermore, αVβ1-inhibiting small molecule C8 did not significantly affect attachment (Figure 3.7A). However, inhibition of the αV subunit alone or the αVβ5 heterodimer significantly suppressed attachment to basal

levels. Moreover, the reduction in adhesion achieved by antibody-mediated inhibition of αV was not enhanced by co-incubation reagents blocking other integrin subunits (i.e. αV + β1, α5 + αV, αV + C8) (Figure 3.7A). These data demonstrate that αVβ5 is the primary integrin heterodimer that promotes attachment to vitronectin in iPSCs.

Immunofluorescence of iPSCs suggested that α5β1 and an αV-containing integrin heterodimer are recruited to IACs in cells on fibronectin and ZT910 (Figure 3.7B and 3.7D). Inhibition of α5 and β1 individually and in a combinatorial fashion to target the α5β1 heterodimer and other β1-containing heterodimers significantly suppressed attachment to basal levels (Figure 3.7B and 3.7D). Moreover, the reduction in adhesion achieved by antibody-mediated inhibition of α5 was not enhanced by co-incubation reagents blocking other integrin subunits (i.e. αVβ5, αV and αV + C8) (Figure 3.7B and 3.7D). These data demonstrate that α5β1 is the primary integrin heterodimer that promotes attachment to fibronectin and ZT910.

Immunofluorescence of iPSCs suggested that αVβ1 is recruited to IACs in cells on ZTFN (Figure 3.7C). Inhibition of αV and β1 subunit both individually and in combination, alongside small molecule inhibitor C8 significantly suppressed attachment to basal levels (Figure 3.7C). However, inhibition of the α5 subunit did not significantly affect attachment. Surprisingly, inhibition of the αVβ5 heterodimer significantly reduced cell attachment (Figure 3.7C). However, combinatorial inhibition of αV and β1 subunits, and combinatorial inhibition of αV with c8 significantly suppressed attachment compared to αVβ5 heterodimer inhibition (Figure 3.7C). These data demonstrate that αVβ1 is the primary integrin heterodimer that promotes attachment to ZTFN.

Integrating immunofluorescence and integrin inhibitory attachment assay data from all three cell lines suggests that the primary integrin heterodimers recruited on vitronectin, fibronectin, ZTFN and ZT910 are αVβ5, α5β1, αVβ1 and α5β1 respectively.

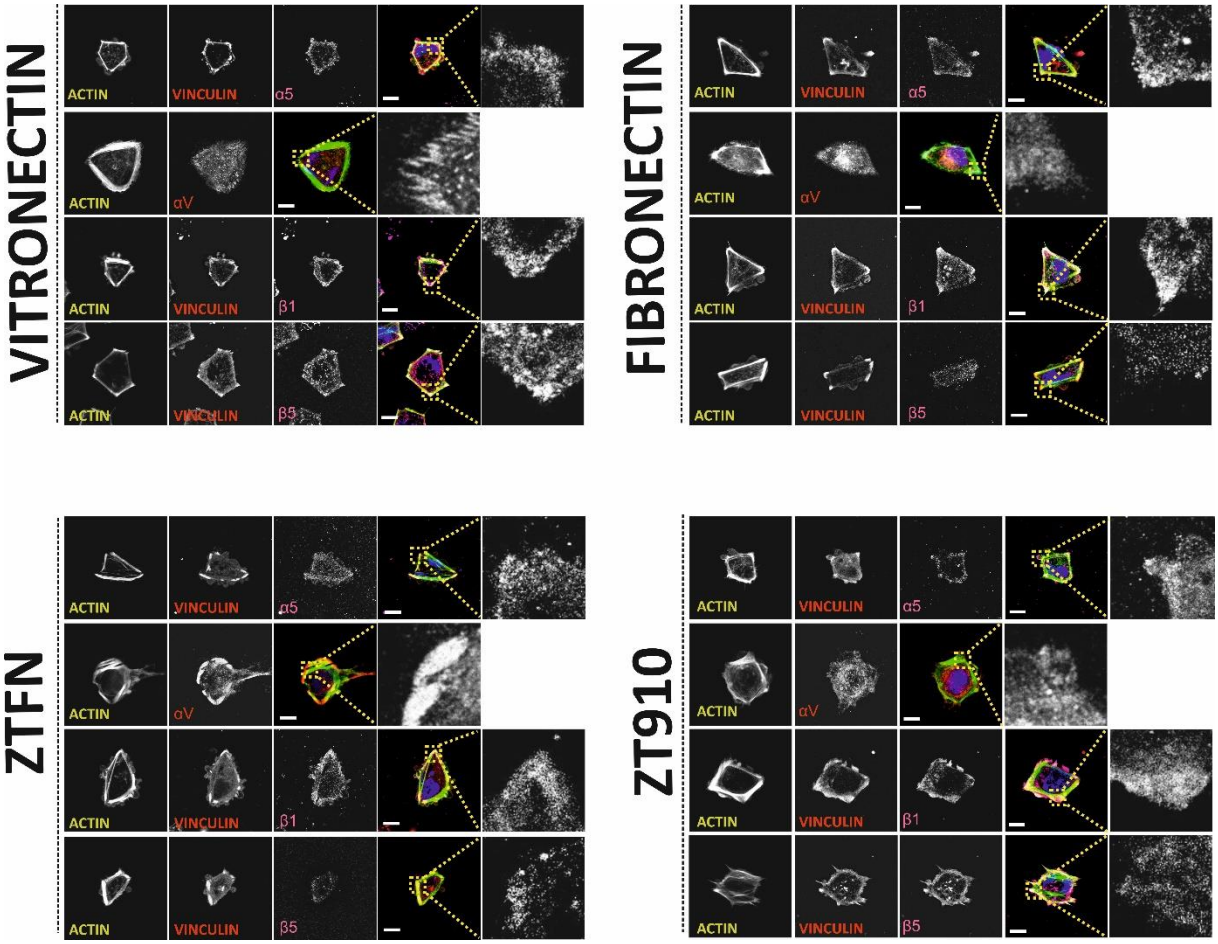

Figure 3.4: iPSCs display distinct integrin heterodimer recruitment to IACs on vitronectin, fibronectin, ZTFN and ZT910. iPSCs were plated on vitronectin (5µg/mL), fibronectin (10µg/mL), ZTFN (10µg/mL) and ZT910 (10µg/mL) for 4 hours and probed for RGD-binding integrin subunits and focal adhesion protein vinculin. Each row contains zoomed-in images of the respective integrin α and β subunits. N=5. Scale: 10µm

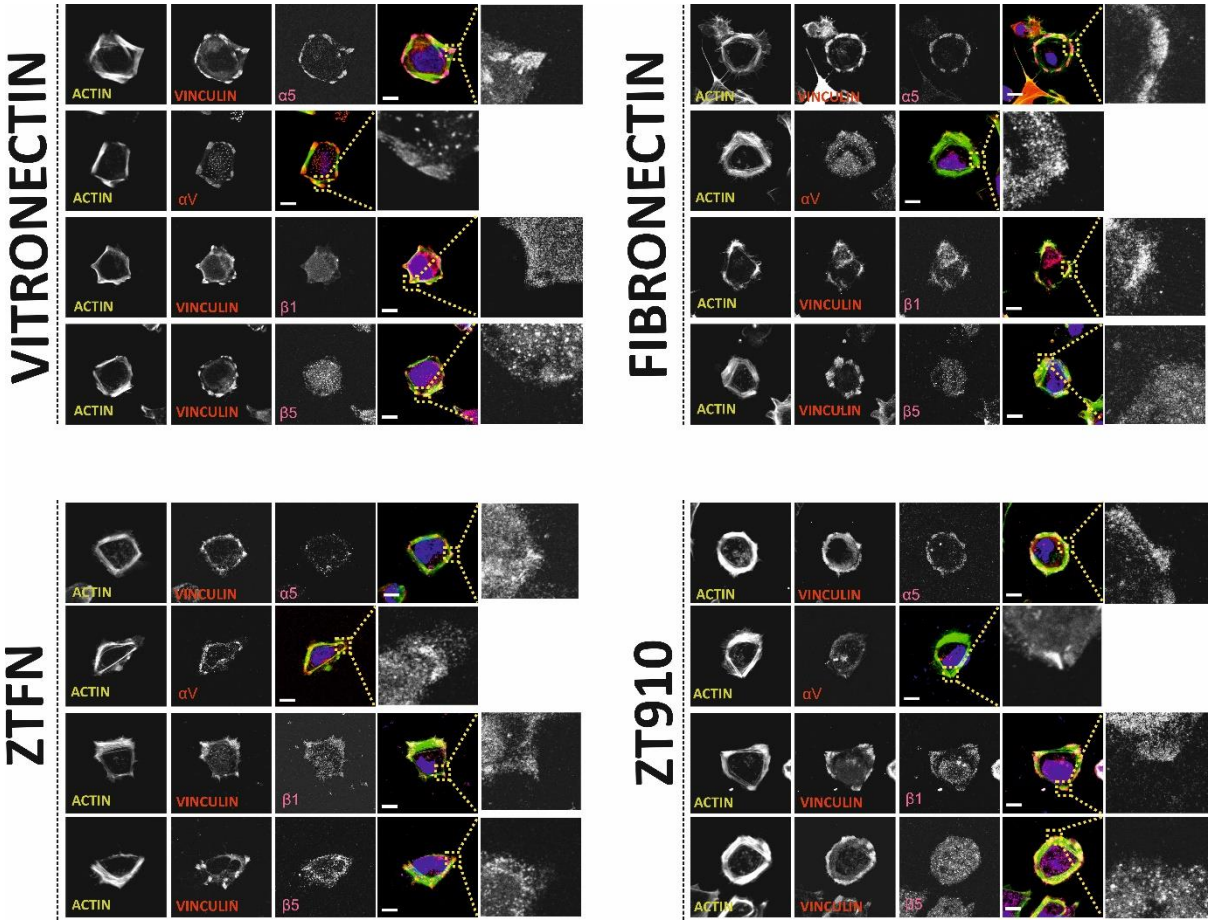

Figure 3.5: H9 display distinct integrin heterodimer recruitment to IACs on vitronectin, fibronectin, ZTFN and ZT910. H9 was plated on vitronectin (5µg/mL), fibronectin (10µg/mL), ZTFN (10µg/mL) and ZT910 (10µg/mL) for 4 hours and probed for RGD-binding integrin subunits and focal adhesion protein vinculin. Each row contains zoomed-in images of the respective integrin α and β subunits. N=5. Scale: 10µm

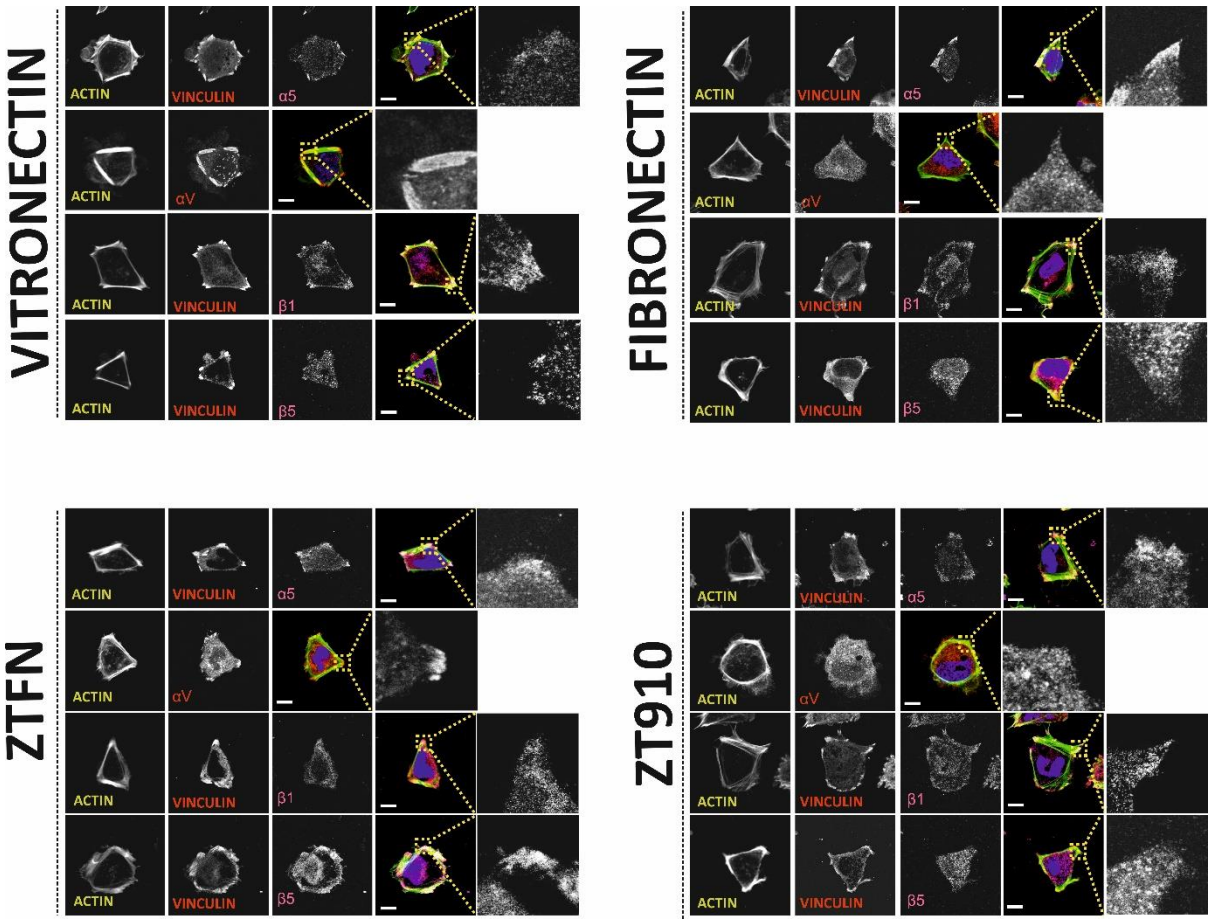

Figure 3.6: RC17 display distinct integrin heterodimer recruitment to IACs on vitronectin, fibronectin, ZTFN and ZT910. RC17 was plated on vitronectin (5µg/mL), fibronectin (10µg/mL), ZTFN (10µg/mL) and ZT910 (10µg/mL) for 4 hours and probed for RGD-binding integrin subunits and focal adhesion protein vinculin. Each row contains zoomed-in images of the respective integrin α and β subunits. N=5. Scale: 10µm

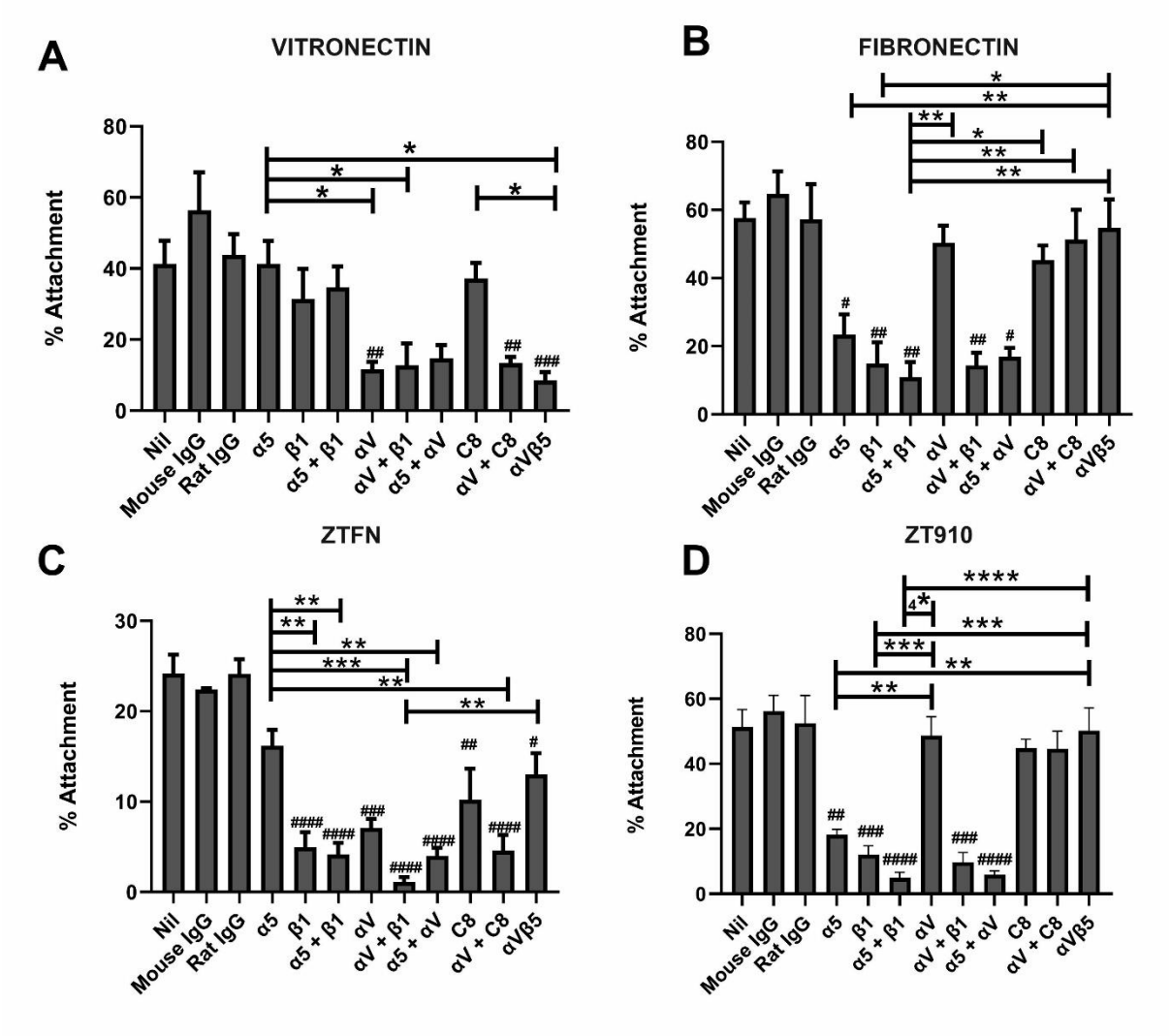

Figure 3.7: Integrin inhibitory attachment assay displays distinct integrin heterodimer recruitment to IACs on vitronectin, fibronectin, ZTFN and ZT910. iPSCs were plated on defined substrates (vitronectin, fibronectin, ZTFN and ZT910) after 4 hours. Cells were treated with appropriate antibodies and small molecules to inhibit integrin function; Mab 11 (α5), Mab 13 (β1), L230 (αV), C8 (αVβ1) and αVβ5 (P1F6). One-way ANOVA with Tukey's post-hoc test was applied. Statistically significant differences between IgG controls are represented by # ($p<0.05$), ## ($p<0.01$), ### ($p<0.001$) and #### ($p<0.00001$). Statistically significant differences between integrin-blocking conditions were represented by * ($p<0.05$), ** ($p<0.01$), *** ($p<0.001$) and **** ($p<0.00001$). Data shown as mean ± SEM of three independent experiments, One-way ANOVA with Tukey's post-hoc test.

3.2.5. Traction Force Microscopy

As iPSCs differentially recruit integrin heterodimers upon engagement on vitronectin, fibronectin, ZTFN and ZT910, and different integrin heterodimers exhibit different biophysical and biomechanical properties, we sought to determine whether iPSC engagement of the different substrates modulates mechanical force transduction (Elosegui-Artola et al., 2014a, Kechagia et al., 2019). Initially, traction force microscopy was employed to determine if the different integrins recruited possessed intrinsically distinct biophysical properties. The traction force of iPSCs was measured on vitronectin, fibronectin, ZTFN and ZT910 at rigidities 5kPa, 10-15 kPa and 70-100kPa. Here 5kPa represents a soft rigidity, 10-15 kPa (medium rigidity) and 70-100kPa stiff rigidity. Beads on soft hydrogel display a large displacement of beads and this displacement decreases as the rigidity increases (Figure 3.8A). Analysis of bead displacement using an image-j plugin (as described in the Methods) showed that as the gel rigidity increases from 5kPa, 10-15kPa and 70-100kPa, the force magnitude of iPSCs increased proportionally and significantly on vitronectin, fibronectin, ZTFN and ZT910 (Figure 3.8B). This suggests that as the rigidity of the substrate-coated gel increases, the force exerted by iPSCs increases proportionally.

Next, the force magnitude of cells engaging the different substrates (vitronectin, fibronectin, ZTFN and ZT910) were compared at each rigidity; 5kPa, 10-15kPa and 70-100kPa (Figure 3.8C). At 5kPa, cells on fibronectin transmit force significantly greater in comparison to vitronectin and ZTFN (Figure 3.8C). Interestingly, even though iPSCs plated on fibronectin and ZT910 both engage α5β1, fibronectin transmits force significantly greater to ZT910 (Figure 3.8C). Although significantly greater force transmission was observed in iPSCs plated on fibronectin in comparison to the other substrates at low rigidity (5kPa), iPSCs on high rigidity substrates

(70-100kPa), exhibited comparable force transmission on both vitronectin and fibronectin (Figure 3.8C). On a high rigidity (70-100kPa) iPSCs on vitronectin transmits significantly greater force compared to ZTFN, and iPSCs plated on ZTFN transmit significantly greater force compared to ZT910. (Figure 3.8C). However, cells on low rigidity fibronectin transmit significantly greater force compared to ZTFN at high rigidities (70-100kPa) (Figure 3.8C). Surprisingly, at the 10-15 kPa, no significant difference in force transmission between the four substrates (Figure 3.8C). The significant shift in force transmission of iPSCs plated on vitronectin, fibronectin, ZTFN and ZT910 at soft (5kPa) and stiff (70-100 kPa) rigidities suggest that integrin heterodimers recruited on the four substrates possess intrinsically distinct biophysical properties that are tunable in a rigidity-dependent manner.

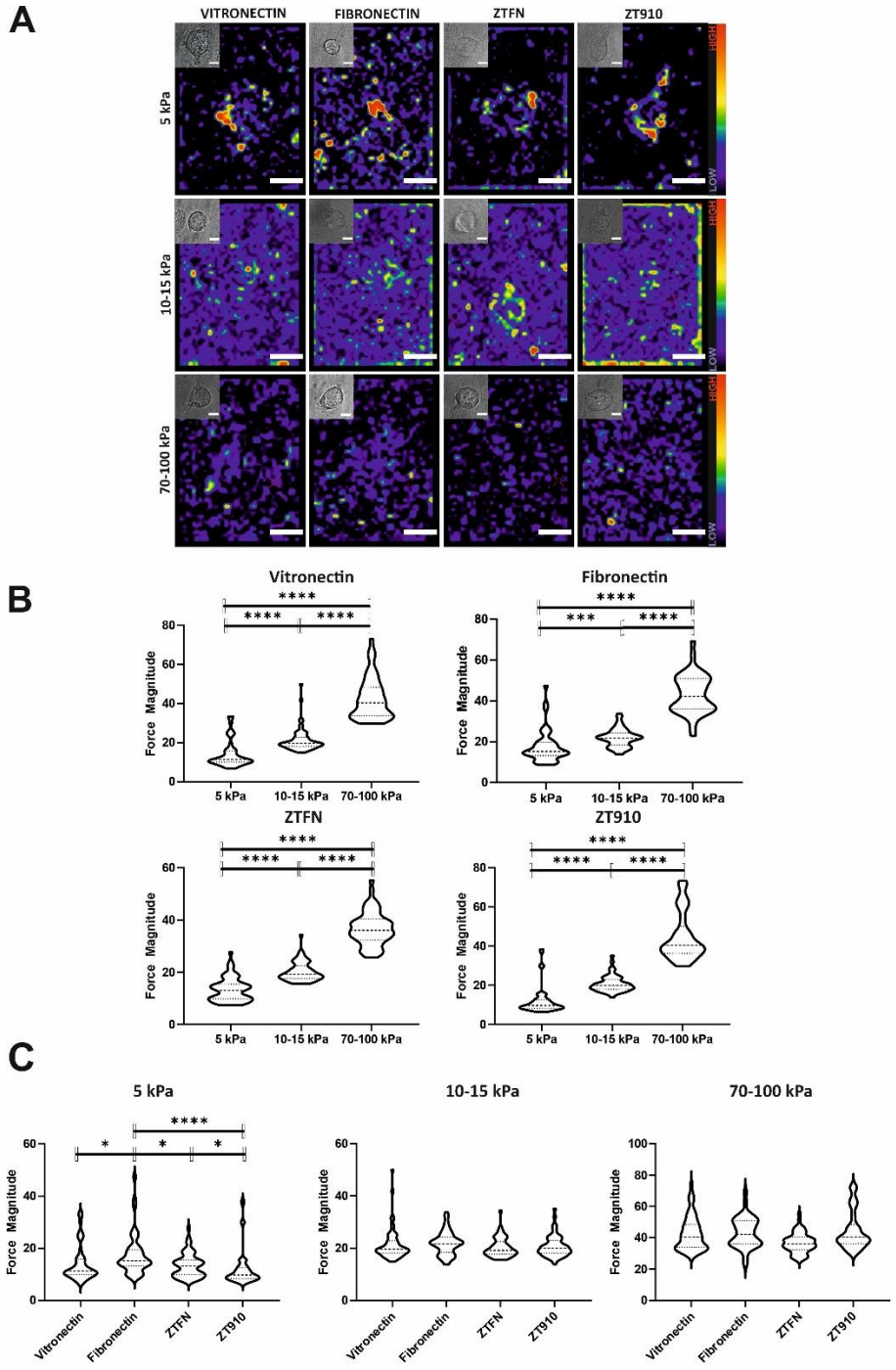

Figure 3.8: **iPSCs display distinct biophysical properties.** iPSCs plated on vitronectin, fibronectin, ZTFN and ZT910 for 4 hours. The cells were plated on three different rigidities ranging from soft to stiff rigidity: 5kPa, 10-15 kPa and 70-100 kPa. (A) Qualitative representation of flurosphere (bead) displacement of iPSCs at different rigidities on vitronectin, fibronectin, ZTFN and ZT910. (B) Quantitative representation of force magnitude of iPSCs at different rigidities on vitronectin, fibronectin, ZTFN and ZT910, and TIFs at different rigidities on fibronectin. (C) Quantitative representation comparing force magnitude of iPSCs plated on vitronectin, fibronectin, ZTFN and ZT910 at a single rigidity. Data shown are of three independent experiments. Violin plots represent median, upper and lower quartiles. Kruskal-Wallis with Dunn's post-hoc test, n=45-58 * $p<0.05$, **** $p<0.0001$.

3.2.6. Cell area

The ability of cells to sense and respond to mechanical stimuli is called mechanotransduction. Cells adapt and respond to differences in substrate rigidity by modulating the area and composition of IACs, cell area, actin cytoskeleton organisation and transmission of traction force (Doss et al., 2020). Since integrin heterodimers recruited on the four substrates displayed intrinsically distinct biophysical properties, cell spread area was assessed to determine if the differences in force transmission translated to changes in cell area. A TIF cell line was used as a control. As the rigidities increased from 5kPa, 10-15 kPa and 70-100kPa, there was no significant difference in cell area for iPSCs plated on all four substrates (Figure 3.9A and 3.9B). However, TIF displayed a significant difference in cell area 5kPa vs 10-15kPa vs 70-100kPa (Figure 3.9A and 3.9B). The expectation was that iPSCs plated on the four substrates would follow the same trend as the traction force microscopy dataset, where an increase in cell rigidity would translate to an increase in cell spread area (Figure 3.8B). At 5kPa, iPSCs plated on vitronectin showed a significantly larger spread area in comparison to ZTFN and ZT910, an observation that was also made at 70-100kPa (Figure 3.9C). Additionally, at 70-100kPa iPSCs plated on fibronectin displayed significantly greater cell area compared to ZT910 (Figure 3.9C). However, at 10-15kPa a shift in the iPSC area was observed, where iPSCs plated on fibronectin displayed significantly greater cell spread area in comparison to iPSCs plated on vitronectin, ZTFN and ZT910 (Figure 3.9C). These data suggest that iPSCs displayed substrate/integrin heterodimer-specific changes in cell area.

3.2.7. Effect of distinct mechanical properties of integrins on stem cell behaviour

Variation in ECM mechanical cues can modulate nuclear morphology by opening nuclear pores mediating nuclear translocation of transcriptional co-activators such as YAP (Elosegui-

Artola et al., 2017b). Furthermore, multiple components of the LINC complex have been identified that both, directly and indirectly, link the nucleus to the ECM, cooperatively regulating the biological nature of the nucleus and chromatin morphology and organisation, thereby regulating gene expression (Cho et al., 2017, Fedorchak et al., 2014, Gruenbaum et al., 2005, Hu et al., 2017, Miroshnikova et al., 2017, Nava et al., 2020). To examine if the distinct biophysical properties of the integrin heterodimers recruited on vitronectin, fibronectin, ZTFN and ZT910 functionally modulated stem cell behaviour, the localisation of YAP and organisation of chromatin were assessed.

3.2.8. YAP localisation

The localisation of YAP was assessed to determine if the differences in force transmission translated to changes in YAP localisation between the nucleus and the cytoplasm. As the rigidities increased from 5kPa, 10-15 kPa and 70-100kPa, there was no significant difference in YAP localisation for iPSCs plated on all four substrates, except on vitronectin 10-15kPa vs 70-100kPa (Figure 3.10A and 3.10B). Furthermore, no difference was observed in YAP localisation when comparing substrates at 5kPa, 10-15kPa and 70-100kPa (Figure 3.10C). These results suggest that even though integrin heterodimers recruited upon iPSC attachment on vitronectin, fibronectin, ZTFN and ZT910 possess intrinsically distinct biophysical properties, their differential recruitment at soft and stiff rigidities does not affect the localisation of YAP.

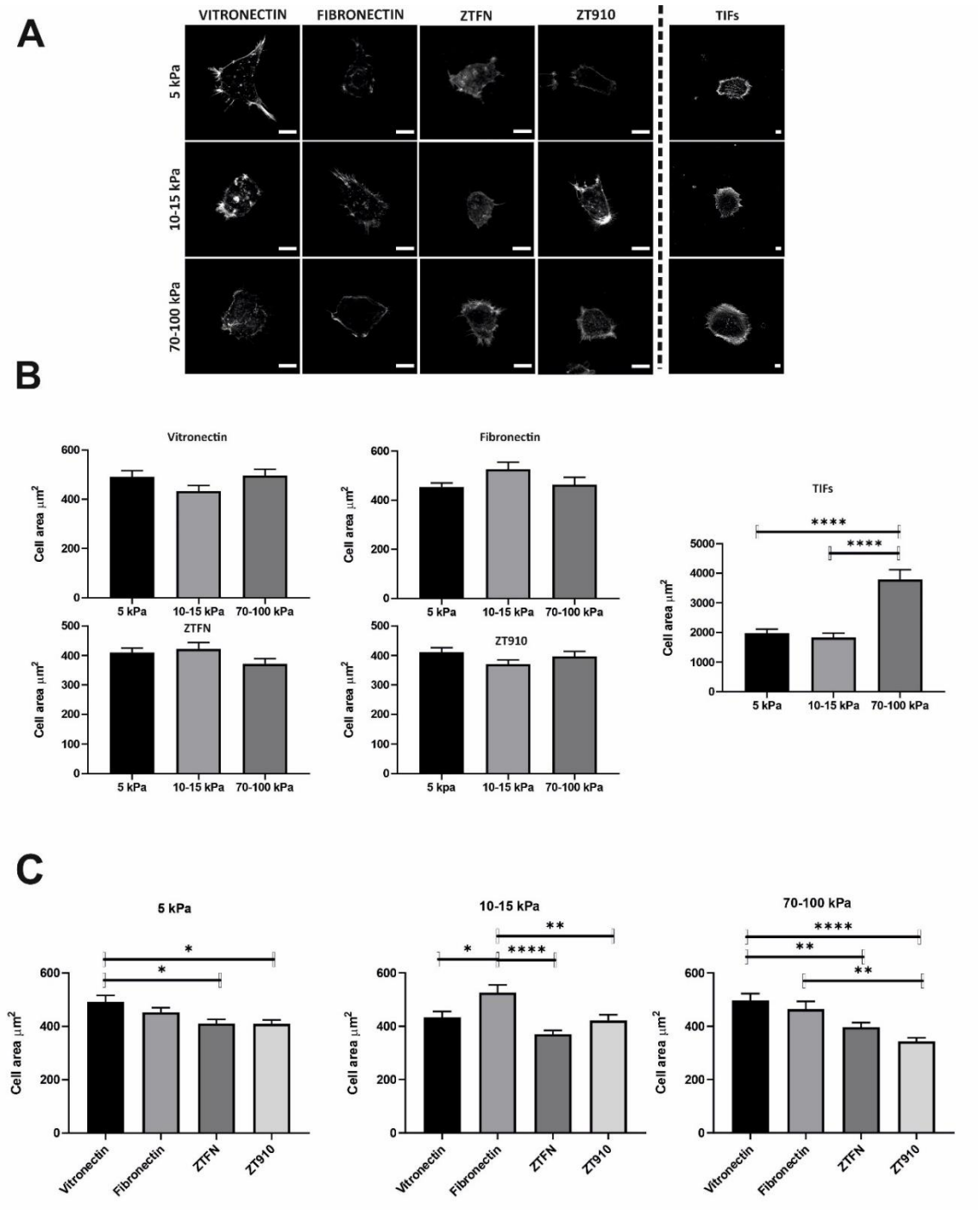

Figure 3.9: iPSCs display substrate-specific differences in cell area. iPSCs plated on vitronectin (5µg/mL), fibronectin (10µg/mL), ZTFN (10µg/mL) and ZT910 (10µg/mL), with TIFs plated on fibronectin (10µg/mL) for 4 hours. The cells were plated on three different rigidities ranging from soft to stiff rigidity; 5kPa, 10-15 kPa and 70-100 kPa. (A) Qualitative representation of spread area of iPSCs at different rigidities. (B) Quantitative representation of cell area of iPSCs at different rigidities on vitronectin, fibronectin, ZTFN and ZT910, and TIFs at different rigidities on fibronectin. (C) Quantitative representation comparing spread area of iPSCs plated on vitronectin, fibronectin, ZTFN and ZT910 at a single rigidity. Data shown as mean ± SEM of three independent experiments: One-way ANOVA with Tukey's post-hoc test, n=55-59 * $p<0.05$, ** $p<0.01$, **** $p<0.0001$.

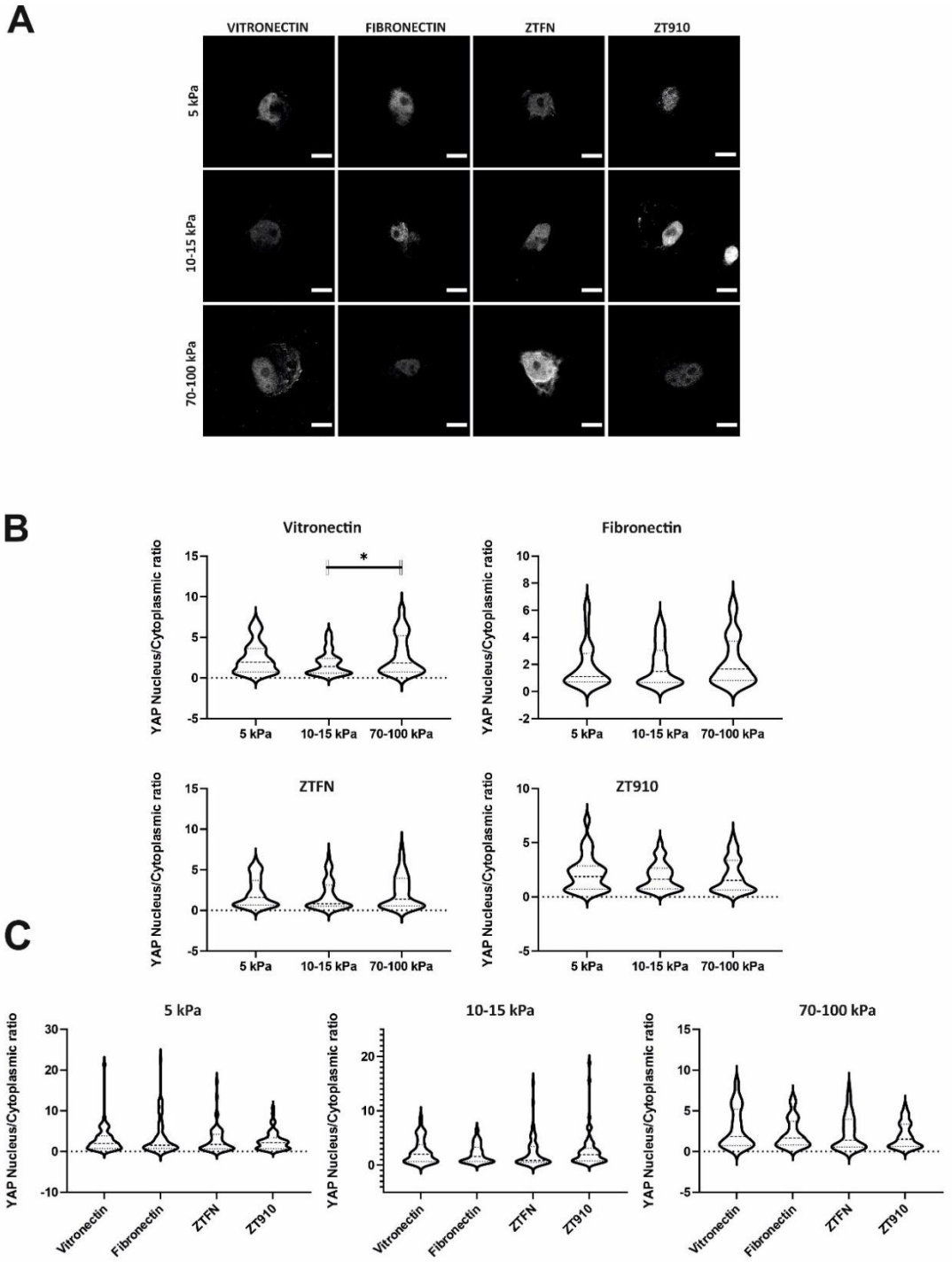

Figure 3.10: **iPSCs display no substrate-specific differences in YAP localisation.** iPSCs were plated on three different rigidities ranging from soft to stiff rigidity; 5kPa, 10-15 kPa and 70-100 kPa. (A) Qualitative representation of YAP localisation of iPSCs at different rigidities on vitronectin, fibronectin, ZTFN and ZT910. (B) Quantitative representation of YAP localisation of iPSCs at different rigidities on vitronectin, fibronectin, ZTFN and ZT910. (C) Quantitative representation comparing YAP localisation of iPSCs plated on vitronectin, fibronectin, ZTFN and ZT910 at a single rigidity. Data shown from five independent experiments. Violin plots represent median, upper and lower quartiles. One-way ANOVA with Tukey's post-hoc test, n=58-65 * $p<0.05$.

3.2.9. Nuclear Morphology and Chromatin Organisation

NucleusJ, an image-j plugin was employed to determine if the differences in force transmission translated to changes in nuclear and chromatin morphology and organisation. NucleusJ implements 3D image processing and analysis to measure nuclear morphology by quantifying nuclear flatness, elongation, sphericity and surface area, and measure chromatin morphology by quantifying the number of chromocenters, mean volume of chromocenters, the intensity of heterochromatin fraction and distance of chromocenters to the nuclear periphery (Figure 3.11).

Analysis of nuclear volume, flatness, elongation and surface area of iPSCs plated on vitronectin, fibronectin, ZTFN and ZT910 at rigidities 5kPa, 10-15 kPa and 70-100kPa revealed no significant differences in nuclear volume, elongation, flatness, sphericity and surface area. However, iPSCs plated on ZTFN displayed a significant reduction in nuclear volume at 10-15kPa compared to the other rigidities (Figure 3.11A). iPSCs plated on vitronectin, fibronectin, ZTFN and ZT910 displayed changes in chromocenter organisation in relation to the nuclear periphery in a rigidity-dependent manner (Figure 3.11B). As the substrate rigidity increased from 5kPa to 10-15kPa and 70-100kPa, the chromocenter border to nuclear border distance increased on vitronectin, fibronectin and ZT910 (Figure 3.11B). However, on ZTFN, as substrate rigidity increased from 5kPa and 10-15kPa, the chromocenter border to nuclear border distance and the barycentre to nuclear border distance decreases (Figure 3.11B). As the substrate rigidity increased from 5kPa to 10-15kPa and 70-100kPa, the barycentre to nuclear border distance increased on fibronectin and ZT910, however, no difference was observed on iPSCs plated on vitronectin (Figure 3.11B).

When examining chromocenter organisation of vitronectin, fibronectin, ZTFN and ZT910 at rigidities 5kPa, 10-15 kPa and 70-100kPa at individual rigidities, substrate-specific differences were observed (Figure 3.11C). At 5kPa, the distance from the barycentre to the nuclear border was significantly greater in iPSCs plated on ZTFN compared to cells plated on fibronectin and ZT910 (Figure 3.11C). Additionally, the distance from the barycentre border to the nuclear border was significantly greater on vitronectin compared to fibronectin (Figure 3.11C). Similarly, the distance from the barycentre border to the nuclear border was significantly greater in iPSCs plated on ZTFN compared to cells plated on fibronectin and vitronectin (Figure 3.11C).

As the rigidity increased from soft (5kPa) to stiff (70-100kPa), a change in chromocenter organisation was observed where both the distance from the chromocenter's barycentre to the nuclear border and the distance from the chromocenter's barycentre border to nuclear border of iPSCs plated on ZT910 was significantly greater compared to cells plated on fibronectin (Figure 3.11C). No significant differences were observed when comparing nuclear volume, elongation, flatness, sphericity, surface area and the number and volume of chromocenters between the substrates (Appendix: Supplementary Figure 1). These results suggest iPSC attachment on vitronectin, fibronectin, ZTFN and ZT910 produce significant integrin-specific changes in chromocenter organisation in a rigidity-dependent manner, potentially modulating transcriptional silencing of genes that influence various stem cell behaviours.

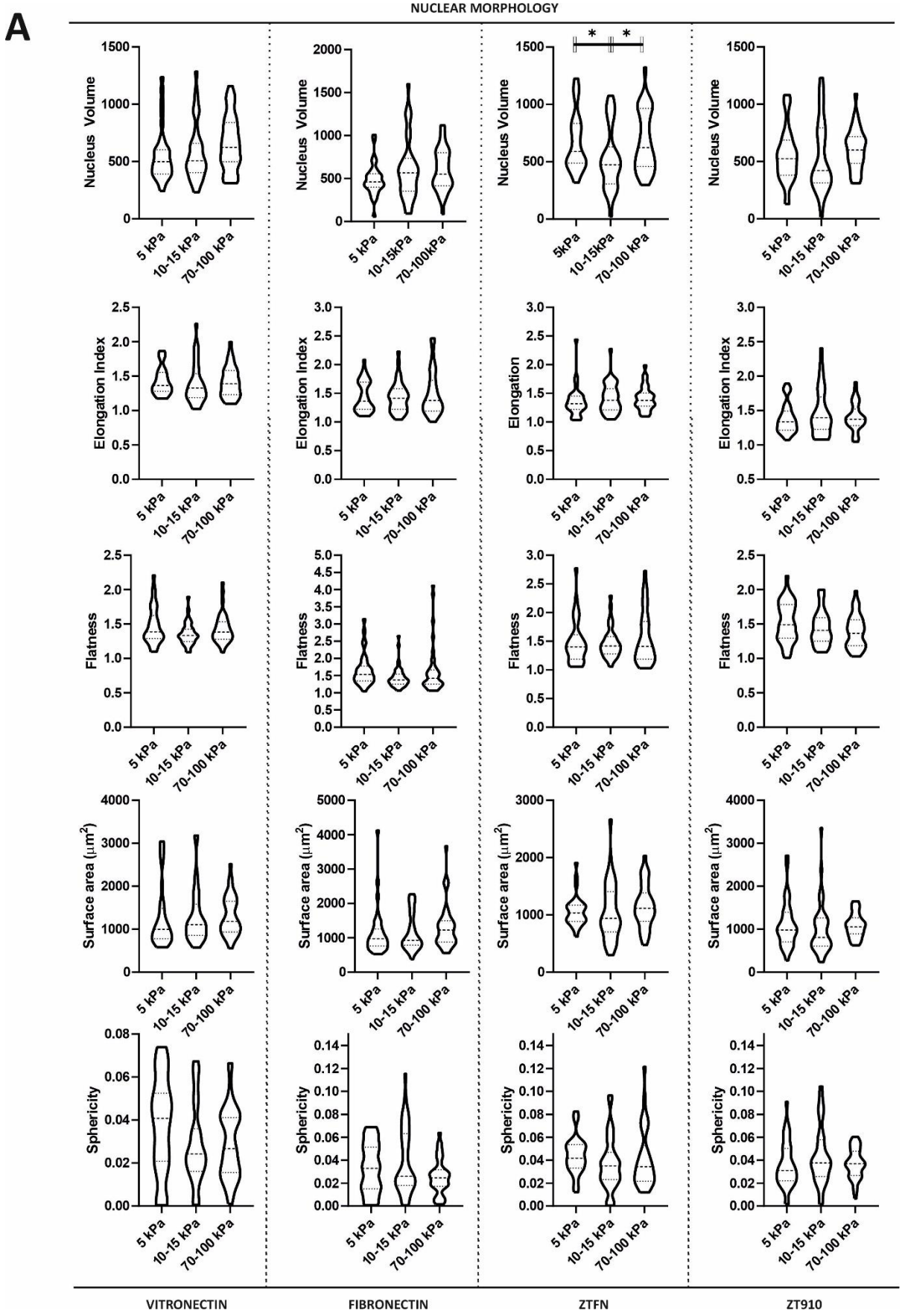
A
NUCLEAR MORPHOLOGY
Nucleus Volume
Elongation Index
Elongation
Flatness
Surface area (μm²)
Sphericity
5 kPa
10-15 kPa
70-100 kPa
5kPa
10-15kPa
70-100kPa
*
*
VITRONECTIN
FIBRONECTIN
ZTFN
ZT910

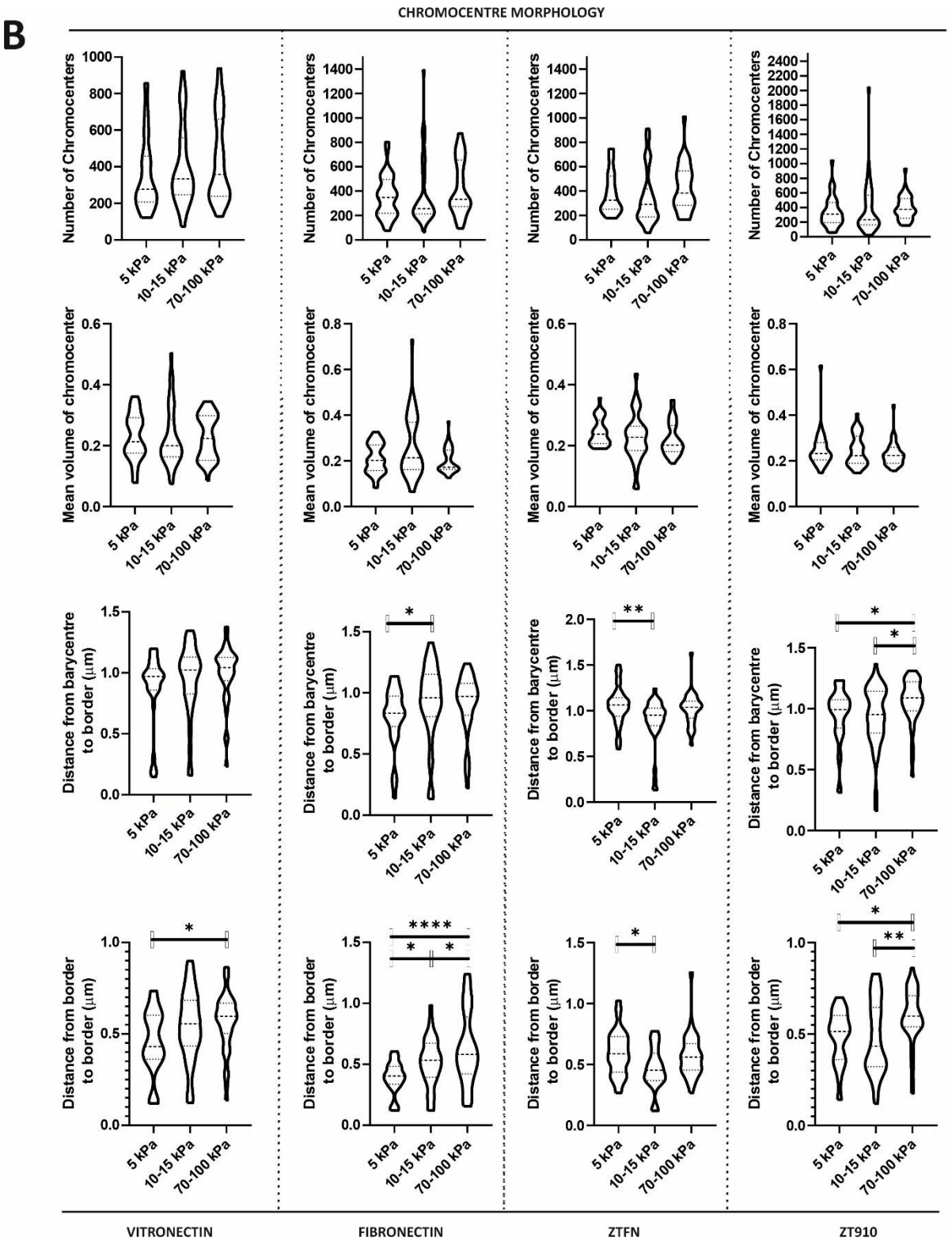
B
CHROMOCENTRE MORPHOLOGY
Number of Chromocenters
Mean volume of chromocenter
Distance from barycentre to border (µm)
Distance from border to border (µm)
5 kPa
10-15 kPa
70-100 kPa
VITRONECTIN
FIBRONECTIN
ZTFN
ZT910

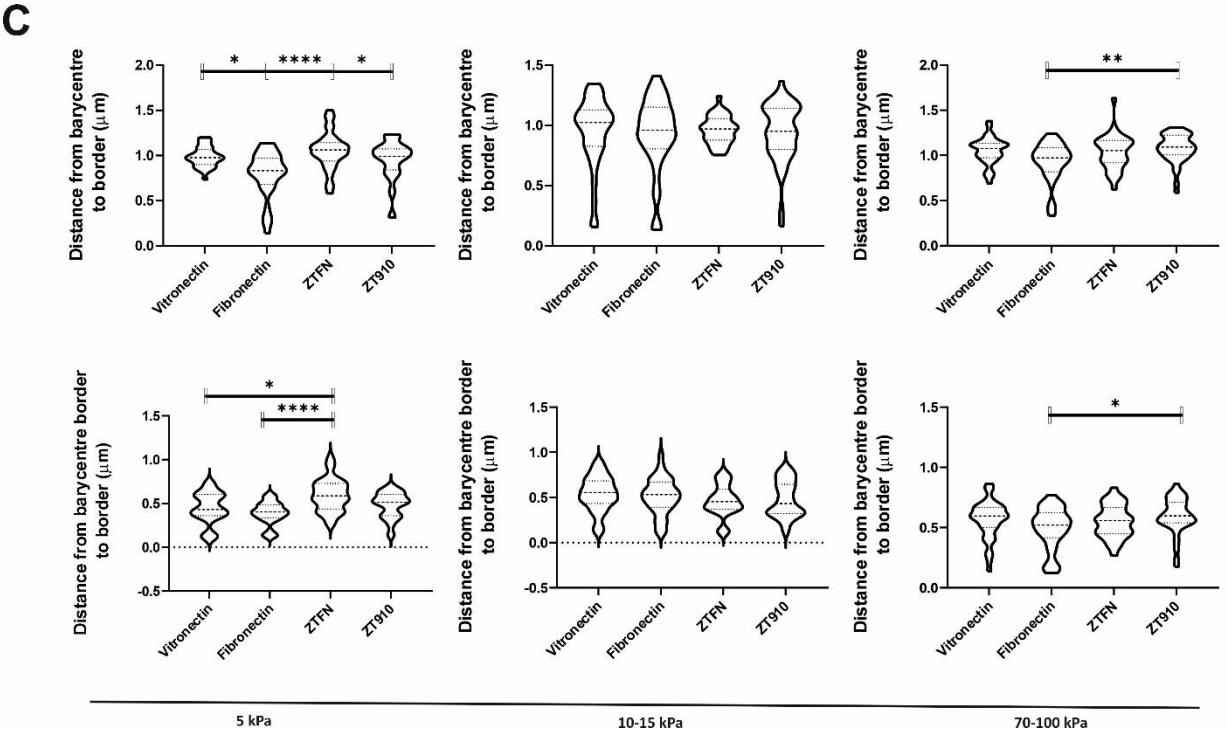

Figure 3.11: **iPSCs display substrate/integrin heterodimer-specific changes in chromatin organisation.** iPSCs plated on vitronectin (5μg/mL), fibronectin (10μg/mL), ZTFN (10μg/mL) and ZT910 (10μg/mL) for 4 hours. The cells were plated on three different rigidities ranging from soft to stiff rigidity: 5kPa, 10-15 kPa and 70-100 kPa respectively. (A) Quantitative profile of nuclear morphology including circularity, elongation index, flatness index, sphericity, and surface area. (B) Quantitative profile of chromocentre morphology including the number of chromocenter, mean volume of chromocentres, distance from barycentre to border and distance from barycentre border to border. (C) Nuclear and chromocentre morphology were determined by image-J plugin NucleusJ. Data shown from three independent experiments. Violin plots represent median, upper and lower quartiles. Kruskal-Wallis test with Dunn's post-hoc test, n=45-58 * $p<0.05$, ** $p<0.01$, **** $p<0.0001$.

3.3. Discussion

In this chapter, the recruitment of integrin heterodimers on iPSCs was investigated on vitronectin, fibronectin, ZTFN and ZT910. Immunofluorescence imaging in conjunction with integrin inhibitory attachment assay demonstrated that the primary integrin heterodimers recruited on vitronectin, fibronectin, ZTFN and ZT910 were αVβ5, α5β1, αVβ1 and α5β1 respectively. Traction force microscopy revealed that integrin heterodimers recruited on the four substrates possess intrinsically distinct biophysical properties that are tunable in a rigidity-dependent manner. YAP localisation, nuclear morphology and chromatin organisation were assessed to determine if the different properties of integrin heterodimers differentially modulated stem cell behaviour. The distinct properties of integrin heterodimers significantly affected chromatin organisation but had no effect on YAP localisation and nuclear morphology.

Pluripotent stem cells from all three cell lines (iPSC, H9 and RC17) showed <50% cell attachment on vitronectin, fibronectin, ZTFN and ZT910. This reduction in cell survival and attachment can be explained by cell-matrix/cell-colony detachment-mediated anoikis (Wang et al., 2009b). The use of the selective Rho-associated kinase (ROCK) inhibitor (Y-27632) has been shown to improve cell survival by reducing dissociation-associated apoptosis (Wang et al., 2009b). However, since the downstream experiments focused on defining substrate-specific integrin adhesion complexes, and because components recruited to IACs such as GTPase RhoA and its downstream effector ROCK play a principal role in adhesion dynamics and integrin-mediated force transduction, ROCK inhibitor was not used for these experiments. Cells on ZTFN displayed a substantial reduction in survival and attachment compared to vitronectin, fibronectin and ZT910. These data demonstrate the negative effect

of the absent PHSRN domain on iPSC attachment on the ZTFN substrate in comparison to the PHSRN domain containing ZT910 substrate, which showed markedly greater levels of attachment.

Experimental immunofluorescence, adhesion complex enrichment and integrin inhibitory attachment assay suggest iPSCs recruit distinct integrin heterodimers to engage αVβ5-VIT, α5β1-FN, αVβ1-ZTFN and α5β1-ZT910 respectively. The recruitment of different integrin heterodimers to RGD motif-containing substrates is dependent on the presentation and conformation of the RGD motif (Kapp et al., 2017). For example, an extended conformation of the positively charged arginine and the carboxyl group of aspartate that maintains a distance of 0.7-0.9nm within the RGD-motif preferentially binds αIIbβ3 (Kapp et al., 2017) (Pfaff et al., 1994). However, if the conformation of the RGD-binding motif presented is more bent, cells preferentially engage ligands using αvβ3 and α5β1 (Kapp et al., 2017). Although vitronectin, fibronectin, ZTFN and ZT910 possess the RGD motif, the distinct recruitment and engagement of RGD-binding integrin heterodimers point to differences in RGD-motif presentation and conformation.

Traction force microscopy revealed the integrin heterodimers recruited on vitronectin, fibronectin, ZTFN and ZT910 possessed distinct biophysical properties. An increase in substrate rigidity from soft, medium and stiff rigidity led to a proportional increase in force magnitude on all four substrates. This observation might be expected because the molecular clutch model predicts a monotonically increasing relationship between force and rigidity due to the formation of focal adhesions (Elosegui-Artola et al., 2018). Furthermore, the study of actin rheology on soft and stiff substrates reveals a transition of actin from a low-ordered and low-tension state to a highly-order state with increased cell traction force (Gupta et al., 2015).

However, the differences in the way that cells apply force on different substrates, following the engagement of different integrins, would not be predicted based on these studies alone. The Rho family of GTPases RhoA, Rac1 and Cdc42 are key regulators of actin cytoskeletal organisation. RhoA modulates myosin II activity to influence intracellular force generation (Chrzanowska-Wodnicka and Burridge, 1996). For example, even though α5β1 and αVβ3 demonstrate similar levels of adhesion on fibronectin, cells show integrin-specific behaviour. For example, α5β1-mediated adhesions to fibronectin promote cells to display a more contractile and fibroblastic morphology compared to αVβ3-mediated adhesion on fibronectin. This difference has been attributed to the high and low RhoA activity in α5β1 and αVβ3-mediated adhesions respectively (Danen et al., 2002, Humphries et al., 2015). Cells on fibronectin that engage different integrin heterodimers (α5β1 and αVβ6) displayed an ability to differentially adapt force generation and level of integrin recruitment to soft and stiff rigidities (Elosegui-Artola et al., 2014b). Proteomic analysis of IACs that are formed on vitronectin, fibronectin, ZTFN and ZT910 will enable the characterisation of downstream signalling proteins and how differential recruitment of these proteins may influence integrin heterodimer-specific force transmission.

Unexpectedly, the proportional increase in force magnitude as rigidity increases does not translate to a proportional increase in cell area as observed on the TIF cell line. A similar observation was revealed on hESCs plated on flexible polydimethylsiloxane (PDMS) showed no difference in cell surface area with increasing substrate rigidities (Eroshenko et al., 2013). However, analysis of hMSC spread area on polyacrylamide gels of different rigidities ranging from 1kPa to 70GPa suggests the existence of a threshold rigidity beyond which there is no change in cell area (Tee et al., 2011). Here, the cell area plateaued at a substrate rigidity of

20kPa. Based on this observation, a substrate rigidity of 5kPa may potentially be above the rigidity threshold and explains why the increase in substrate rigidity does not translate to a proportional increase in cell spread area (Tee et al., 2011). However, significant differences were observed when comparing changes in cell spread area between vitronectin, fibronectin, ZTFN and ZT910 within each rigidity. These differences in cell area are likely a result of changes in downstream integrin signalling following recruitment of distinct integrin heterodimers upon engagement to vitronectin, fibronectin, ZTFN and ZT910. Human squamous carcinoma cells (HSCCs) plated on collagen-1 showed significantly lower spreading compared to cells plated on laminin-5 (Zhou and Kramer, 2005). Subsequent analysis showed that distinct integrin heterodimers recruited on collagen 1 (α2β1) and laminin-5 (α3β1) produces unique patterns of active Rho, Rac and cdc42 GTPases (Zhou and Kramer, 2005). The differences in cell spread area as the rigidity increases can be explained by force-dependent conformational changes of signalling/adaptor proteins (Moore et al., 2010). These observations suggests both integrin-dependent and rigidity-dependent modulation of downstream signalling event that regulate cell spread area.

Similarly, as substrate rigidity increases, no difference in YAP localisation was observed in iPSCs when plated on vitronectin, fibronectin, ZTFN and ZT910. Numerous studies have shown a rigidity-dependent translocation of YAP between the cytoplasm and the nucleus, with increasing substrate rigidity associated with an increased translocation of YAP into the nucleus (Dupont, 2016, Dupont et al., 2011, Elosegui-Artola et al., 2017a, Guo and Zhao, 2013a, Halder et al., 2012, Lee et al., 2019a, Low et al., 2014, Mohri et al., 2017, Nukuda et al., 2015). Furthermore, cells with increased YAP nuclear localisation display increased cell area. Since iPSCs plated on vitronectin, fibronectin, ZTFN and ZT910 displayed no changes in

cell area with increasing substrate rigidity, these results suggest that a substrate rigidity of 5kPa maybe above the rigidity threshold and explains potentially why the increase in substrate rigidity not only prevents a proportional increase in cell spread area but also changes in nuclear YAP localisation. Interestingly, YAP nuclear localisation has been shown to be differentially regulated by rigidity-dependent integrin-engaging substrates laminin and collagen (Lee et al., 2019a). Epithelial cell line plated on collagen-coated 2kPa polyacrylamide gels displayed greater YAP nuclear localisation compared to laminin-rich Matrigel-coated 2kPa polyacrylamide gels (Lee et al., 2019a). These results suggest the regulation of YAP nuclear localisation is integrin substrate-dependent, and independent of rigidity. However, these rigidities were over a smaller range between 0.1 and 2kPa, significantly lower than the rigidities used in this study. It is also important to consider the possible integrative effects of integrin-dependent signalling and mechanical effects that influence YAP nuclear translocation (Guo and Zhao, 2013b). For example, YAP activity is also regulated by the Hippo signalling pathway and interacts with components of other signalling pathways, which serve a role in mechanotransduction (Guo and Zhao, 2013b). The inhibition of rigidity-dependent YAP nuclear translocation as rigidity increases suggests a potential integrative effects of signalling and mechanical in regulating YAP activity.

The role of rigidity on nuclear and chromatin morphology and organisation was evaluated using an innovative image-J plugin called NucleusJ. Analysis of nuclear volume, flatness, elongation and surface area of iPSCs plated on vitronectin, fibronectin, ZTFN and ZT910 at rigidities 5kPa, 10-15 kPa and 70-100kPa revealed no significant differences in nuclear volume, elongation, flatness, sphericity and surface area. This was surprising as previous work has shown the nucleus exhibiting a rounded morphology in soft substrates and possessing a

more flattened morphology on stiffer substrates (Stephens et al., 2018). Interestingly, rigidity-dependent re-organisation of chromocenters was observed when iPSCs were plated on vitronectin, fibronectin, ZTFN and ZT910. The distribution of histone marks within the nucleus regulates gene expression (Pradhan et al., 2018). Active histone marks such as H3/H4 lysine acetylation and H3K4me3 are associated with transcriptional activation, whereas inactive histone marks such as H3K9me2/3 and H3K27me3 are primarily associated with transcriptional repression and typically localised at the nuclear periphery (Pradhan et al., 2018). The spatial organisation of inactive histone marks and chromosome territories show remarkable emerin mediated rigidity-dependent reversible localisation from the nuclear periphery to the nuclear interior between soft and stiff rigidities (Pradhan et al., 2018). In addition, human ESCs that undergo differentiation exhibited centromere redistribution at the nuclear periphery, with inactive H3K27-trimethylated X chromosome localising at the nuclear periphery compared to pluripotent hESCs (Bártová et al., 2008). Furthermore, the presence of substrate-specific differences in chromatin organisation suggests an integrin-specific regulation of chromatin morphology.

This chapter highlights how distinct integrin heterodimers recruited on vitronectin, fibronectin, ZTFN and ZT910 possess distinct biophysical/biomechanical properties that differentially regulate cell area, YAP localisation, nuclear morphology, and chromatin organisation. The subsequent use of the term biophysical or biomechanical properties of integrins takes into context the integrative effects of both the biochemical and biophysical nature of integrin and integrin-dependent downstream signalling. In an attempt to understand the mechanisms that modulate these differences in stem cell phenotype,

proteomic analysis of IACs formed on vitronectin, fibronectin, ZTFN and ZT910 were next analysed.

4. PLURIPOTENT STEM CELL ADHESOME

4.1. Introduction

Cell interaction with the extracellular microenvironment is primarily mediated by integrins. Integrin-dependent engagement of ECM proteins promotes the recruitment of downstream proteins that can be classed into two major groups: scaffolding proteins and signalling/regulatory proteins (Wolfenson et al., 2013). Scaffolding molecules include cytoskeletal and adaptor proteins and signalling/regulatory molecules include GTPases, kinases, phosphatases and proteases (Wolfenson et al., 2013). When cells initially engage ligands, they form nascent adhesions near the leading edge of the plasma membrane called lamellipodia (Vicente-Manzanares and Horwitz, 2011). Characterisation of nascent adhesion has revealed the presence of traditional adhesion proteins including integrins, talin and vinculin, and signalling proteins including focal adhesion kinase (FAK) and p130Cas (CRK-associated substrate) (Chastney et al., 2021). Nascent adhesions mature to form focal complexes. Like nascent adhesions, focal complexes are transient and further mature into larger, more elongated stable focal adhesions, characterised by the presence of zyxin which is absent in less mature adhesions (Wolfenson et al., 2013). Fibrillar adhesions found mostly in fibroblasts where they are associated with fibronectin fibrils represent the endpoint of adhesion maturation. Although some of the molecular constituents in these adhesions are the same, they differ in their localisation, distribution, size and dependence on non-muscle myosin 2 (NMII) (Wolfenson et al., 2013). Dynamic assembly, disassembly and maturation of adhesions are tightly regulated by the recruitment of signalling proteins that primarily include the small GTPases RhoA, Rac1 and cdc42 that modulate actin polymerisation and crosslinking (Wolfenson et al., 2013).

Atomic force microscopy of focal adhesions reveals a tightly organised complex network of integrin and cytoplasmic signalling and adaptor proteins that form a <200nm plaque (Franz and Müller, 2005). Super-resolution deconstruction of focal adhesion structures within the Z-plane suggest that focal adhesion proteins localise into three hierarchical functional layers that span ~40nm from the plasma membrane: an integrin signalling layer (consisting of integrins, paxillin and focal adhesion kinase), a force transduction later (consisting of talin and vinculin) and a actin regulatory layer (consisting of actin, zyxin, VASP and α-actinin) (Kanchanawong et al., 2010). To further understand the complexity of adhesion signalling, protocols have been developed to isolate and characterise adhesion signalling networks in an unbiased manner. Proteomic analysis and downstream validation of isolated IACs have enabled the identification of proteins previously recognised to be canonical IAC proteins and novel proteins not previously isolated or identified (Byron et al., 2011, Byron et al., 2010, Chastney et al., 2021, Geiger and Yamada, 2011, Horton et al., 2016, Humphries et al., 2009, Humphries et al., 2015, Jones et al., 2015).

Several IAC isolation methods have been developed which involve cell attachment to either ligand-coated microbeads or ECM-coated on a 2D tissue culture dish (Jones et al., 2015). The ligand-coated microbead isolation of IAC involves the incubation of cells in suspension with ECM ligand or antibody-coated magnetic micro-beads. Following the formation and stabilisation of adhesions, the cell body is removed by sonication and beads with bound adhesion complexes were separated (Jones et al., 2015, Humphries et al., 2009, Byron et al., 2011). The bead-IAC complex is then eluted for immunoblotting or mass spectrometric analysis. Although this technique was simple and fast, there were several issues that led to the establishment of the alternative protocol (Jones et al., 2015, Byron et al., 2011, Schiller et

al., 2013). For example, certain canonical IAC components were not detected and some cell types such as primary human fibroblasts and mouse embryonic fibroblasts engulfed the microbeads when incubated at 37°C (Jones et al., 2015). Thus, an alternative approach was developed that involves the attachment of cells to ligand-coated dishes for a sufficient time to form IACs (Jones et al., 2015) (Figure 4.1). The addition of a cell-permeable crosslinker DTBP promotes the crosslinking of intramolecular interactions before the removal of cell bodies by sonication or hydrodynamic force resulting in enrichment of IAC components at the basal membrane cells proximal to the cell-matrix interface (Figure 4.1). Enriched IACs crosslinked to the dish are then collected by scrapping for immunoblot or mass spectrometry analysis (Jones et al., 2015) (Figure 4.1). Before the development of unbiased methods to characterise IACs, individual components of the adhesome were identified through conventional candidate-driven cell biological experiments, often involving pharmacological or genetic perturbation. These initial studies led to the generation of the 'literature-curated adhesome', which estimated the presence of more than 200 proteins in the network (Winograd-Katz et al., 2014). However, the emergence of novel isolation techniques combined with mass spectrometry analysis has revealed a larger, complex and dynamic network of proteins within the adhesome (Horton et al., 2015). Integration of seven proteomic datasets of enriched IACs was used to identify the consensus adhesome (proteins identified in ≥ 5 of the seven datasets) and meta (proteins identified in ≥ 5 of the seven datasets) adhesome (Horton et al., 2015). These datasets were derived from multiple cell types that were plated on the ligand fibronectin against a negative-control ligand. 60 proteins were identified to belong to the consensus adhesome, which represented the core set of IAC components, and 2412 proteins were identified that belong to the non-canonical variable meta-adhesome (Horton et al., 2015).

Mass spectrometry-based proteomics datasets derived from the isolation of IACs are variable and dependent on the cell type, ECM ligand and integrin heterodimers recruited. The definition of the consensus and meta-adhesome were derived from somatic cells plated on fibronectin. To date, there has been no such characterisation of the pluripotent stem cell adhesome. Using super-resolution microscopy, the architecture of the cornerstone focal adhesion formed by human iPSCs on vitronectin showed focal adhesion proteins that were organised in functional layers similar to the classical focal adhesions (Stubb et al., 2019). However, β5 integrin was localised in ring-like clusters at the edge of adhesions, in contrast to the homogeneously distributed αV and β1 integrins (Stubb et al., 2019). In this chapter, the αVβ5-VIT, α5β1-FN, αVβ1-ZTFN and α5β1-ZT910 IACs were isolated and characterised through proteomic and bioinformatic analyses to gain insight into the distinct integrin adhesomes.

The previous chapter highlighted how distinct integrin heterodimers recruited on vitronectin, fibronectin, ZTFN and ZT910 possess distinct properties that differentially regulate cell area, YAP localisation, nuclear morphology, and chromatin organisation. In this chapter, proteomic analysis of IACs isolated from iPSCs plated on vitronectin, fibronectin, ZTFN and ZT910 was performed to elucidate the precise mechanisms that modulate these differences in iPSCs.

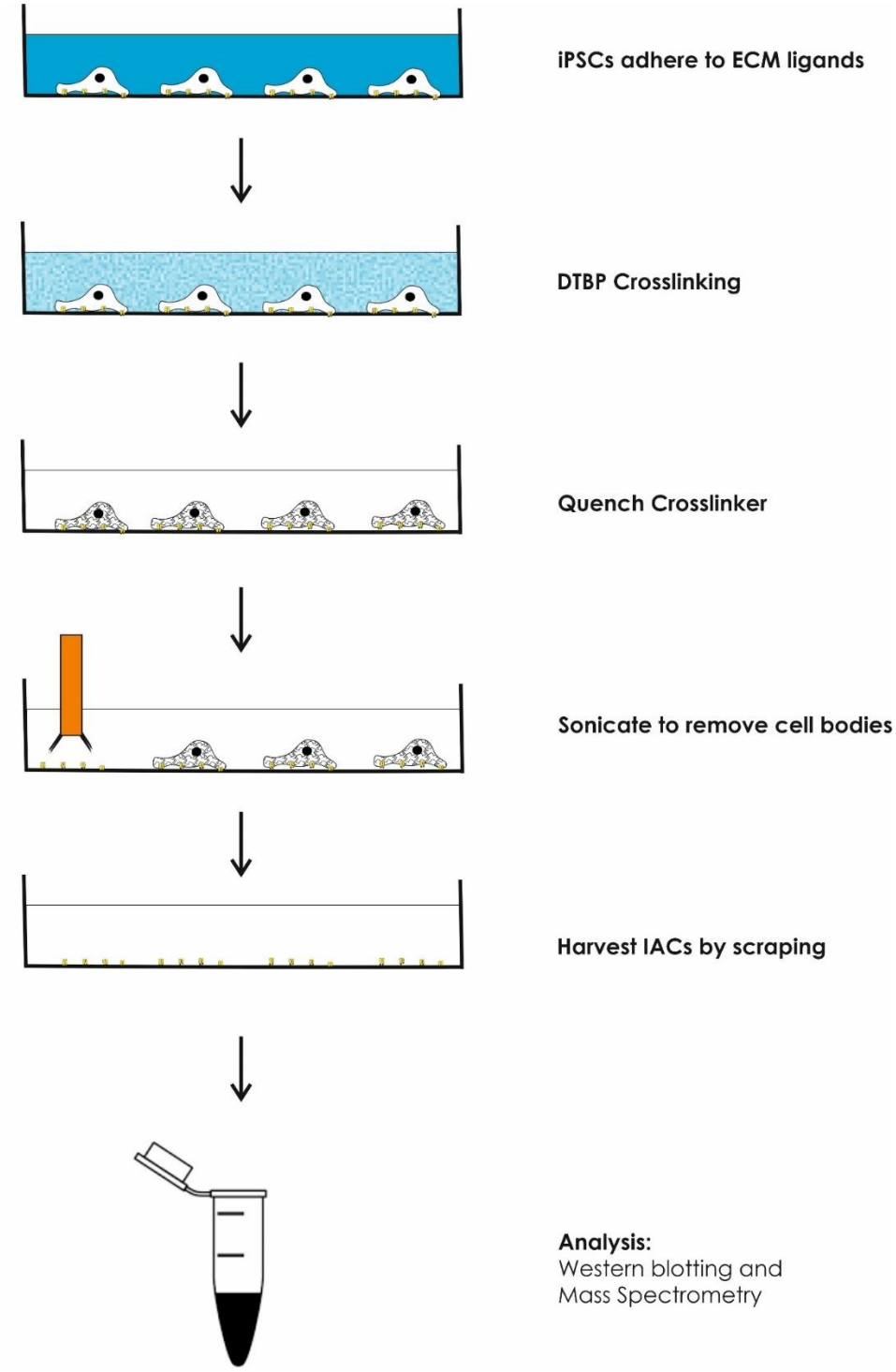

Figure 4.1: Schematic of IAC isolation. iPSCs adhere and spread on ligand-coated plates. The addition of cell-permeable crosslinker DTBP promotes crosslinking of IAC complexes to the dish. This is followed by quenching and the addition of extraction buffer to the cells. iPSC bodies are removed by sonication leaving behind IACs, which are then harvested by scraping. Samples can be analysed by immunoblotting or mass spectrometry.

4.2. Results

4.2.1. Isolation of integrin substrate-specific adhesome

4.2.1.1. Optimisation of IAC enrichment conditions

To characterise integrin-dependent signalling networks, integrin adhesion complex enrichment was employed to obtain IACs recruited on vitronectin, fibronectin, ZTFN and ZT910 (Figure 4.2A). Initially, poly-L-Lysine was used as a negative control, as this was shown to adhere without engaging integrin heterodimers (Jones et al., 2015) (Figure 4.2A). Total cell lysates from TIFs were used as a negative control for immunoblotting.

IAC enrichment revealed that vitronectin-associated IACs were αV, β5 and vinculin (Figure 4.2A). While, fibronectin, ZT910 and ZTFN-associated IACs also exhibited recruitment of αV, these levels were substantially lower than on vitronectin (Figure 4.2A). Moreover, β5 enrichment was only observed on vitronectin (Figure 4.2A). These results confirm our observation from both immunofluorescence and integrin inhibitory experiments about the dominant role of αVβ5 during binding to vitronectin. integrin α5 enrichment was observed on both fibronectin and ZT910 -associated IACs, with reduced enrichment observed on vitronectin, ZTFN and poly-L-Lysine (Figure 4.2A). Although both immunofluorescence and integrin inhibitory experiments suggested ZTFN primarily recruited αVβ1, ZTFN-associated IACs did not show the same level of enrichment that was observed on vitronectin (Figure 4.2A). No expression and enrichment of β6 were observed in the TCL and IAC enrichment samples of any substrates, suggesting that β6 is not expressed in these cells (Figure 4.2A). However, in this experiment, poly-L-Lysine was determined to be an inadequate negative control due to reduced cell attachment in comparison to the other substrates as evidenced by low levels of protein detected in total cell lysates. In addition, evidence from parallel

experiments performed by Heather Swift, another PhD student in the lab performing IAC enrichment analysis in natural killer cells, suggested that poly-L-Lysine attracts proteins that are released from cells during the addition of extraction buffer and sonication, resulting in very high levels of cytoplasmic protein contamination in IAC enrichment samples on these substrates. For this reason, multiple negative control candidates were examined.

A monoclonal antibody (OKT9) that binds to transferrin receptor 1 (CD71) on the cell surface was used as a candidate (Figure 4.2B). Adhesion complex enrichment was carried out with iPSCs plated on vitronectin and OKT9-coated non-tissue cultured dishes (Figure 4.2B). iPSCs primarily used transferrin receptors to adhere to OKT9 as demonstrated by the enrichment of transferrin receptors (Figure 4.2B). However, anti-CD71 associated IACs also displayed αV- and α5- enrichment, although this enrichment was significantly lower as compared to vitronectin-associated IACs (Figure 4.2B). These results suggest that when IPSCs are plated on anti-CD71, recruit αV and α5 subunits to transferrin receptor-dependent complexes or are contaminants in these samples. Therefore, anti-CD71 was determined to be an inadequate negative control due to the recruitment of integrin receptors in cell attachment.

Cadherins are a large family of adhesion molecules that play a key role in mediating cell-cell adhesion (Soncin and Ward, 2011). E-cadherin is the primary cadherin that is expressed in human PSCs and mediates colony formation and adhesion (Soncin and Ward, 2011). Recombinant E-cadherin, commercially available under the name of StemAdhere was used as an alternative candidate substrate. Adhesion complex enrichment was carried out with iPSCs plated on vitronectin and Stem Adhere-coated non-tissue cultured dishes (Figure 4.2C). iPSCs primarily recruited e-cadherin to bind StemAdhere adhesion complexes. Furthermore, significant αV-enrichment were observed on vitronectin-associated IACs compared to E-

cadherin (Figure 4.2C). These data suggest that IPSCs primarily use E-cadherin to engage StemAdhere and therefore this substrate was determined to be an appropriate negative control for subsequent IAC enrichment experiments.

To increase the amount of IAC components extracted during adhesion complex enrichment experiments, the concentration of the DTBP crosslinker was assessed. Previous IAC enrichment experiments performed by Joanna Thomas and Heather Swift, PhD students in the lab used a DTBP concentration of 3mM for 30 minutes. Cross-linking of IACs by increasing DTBP concentration demonstrated that the crosslinking time can be reduced (Ng, 2013). Crosslinking with DTBP for 3 minutes at 6mM concentration showed a 2-fold increase in recovery of talin, vinculin and paxillin (Ng, 2013). However, crosslinking with DTBP at 9mM concentration limited IAC recovery because of reduced sonication-mediated cell lysis (Ng, 2013). These results suggested that incubation of 3 minutes at 6mM DTBP concentration was optimal for the maximal recovery of IAC components (Ng, 2013). Based on this observation, IAC enrichment was performed on iPSCs using 3mM and 6mM DTBP concentration for 30 minutes and 3 minutes respectively. Results showed that there was an increased recovery of integrin αV subunit and vinculin, without a substantial increase in cytoplasmic BAK protein (Figure 4.2D). Although it was expected to obtain significantly enriched αV-subunit on vitronectin compared to the other substrates as observed in previous blots, the reduced enrichment maybe because of experimental variability. Further repetition optimisation experiments were carried out to ensure experimental consistency was achieved before running samples through mass spectrometer. Thus, optimisation of IAC enrichment identified StemAdhere as an appropriate negative control and crosslinking with 6mM DTBP for 3 minutes optimal.

IAC enrichment was performed using StemAdhere as a negative control and optimal DTBP concentration of iPSCs plated on vitronectin, fibronectin, ZTFN and ZT910. IACs enrichment revealed enrichment of α5 subunit only in fibronectin and ZT910-associated IACs (Figure 4.3). Vitronectin-associated IACs revealed substantial enrichment of integrin αV and β5 subunits (Figure 4.3). Vinculin, a canonical focal adhesion protein was enriched on all substrates (Figure 4.3). Although it appears that the α5 subunit was enriched on StemAdhere, further examination of the blots showed non-specific background staining for the StemAdhere on this membrane.

Following this, large-scale adhesion complex enrichment experiments were performed for the isolation of IACs for proteomic analysis.

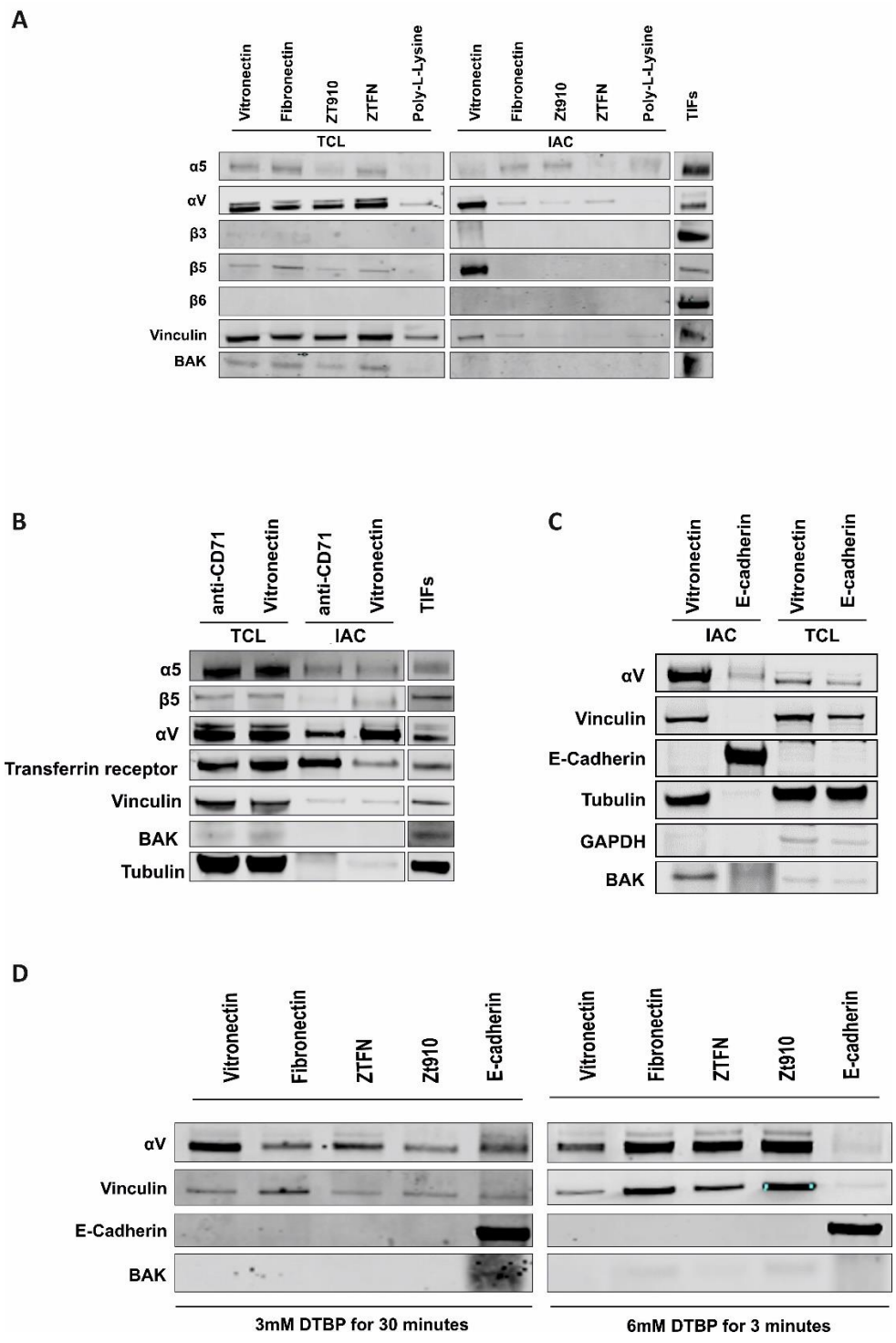

Figure 4.2: Identification of e-cadherin as an appropriate negative control of integrin-associated complex enrichment in iPSCs. iPSCs were plated on vitronectin (5µg/mL), fibronectin (10µg/mL), ZTFN (10µg/mL), ZT910 (10µg/mL) and a negative control substrate. Immunoblotting in total cell lysate (TCL) and isolated integrin-associated complexes (IAC) for the adhesome components integrin alpha subunits, beta subunits, vinculin, negative control protein BAK from other subcellular compartments. Positive control of TIF total cell lysate. N=1. (A) Poly-L-Lysine as a negative control, (B) CD71 receptor, (C) E-cadherin (StemAdhere) (D) Optimising DTBP concentration

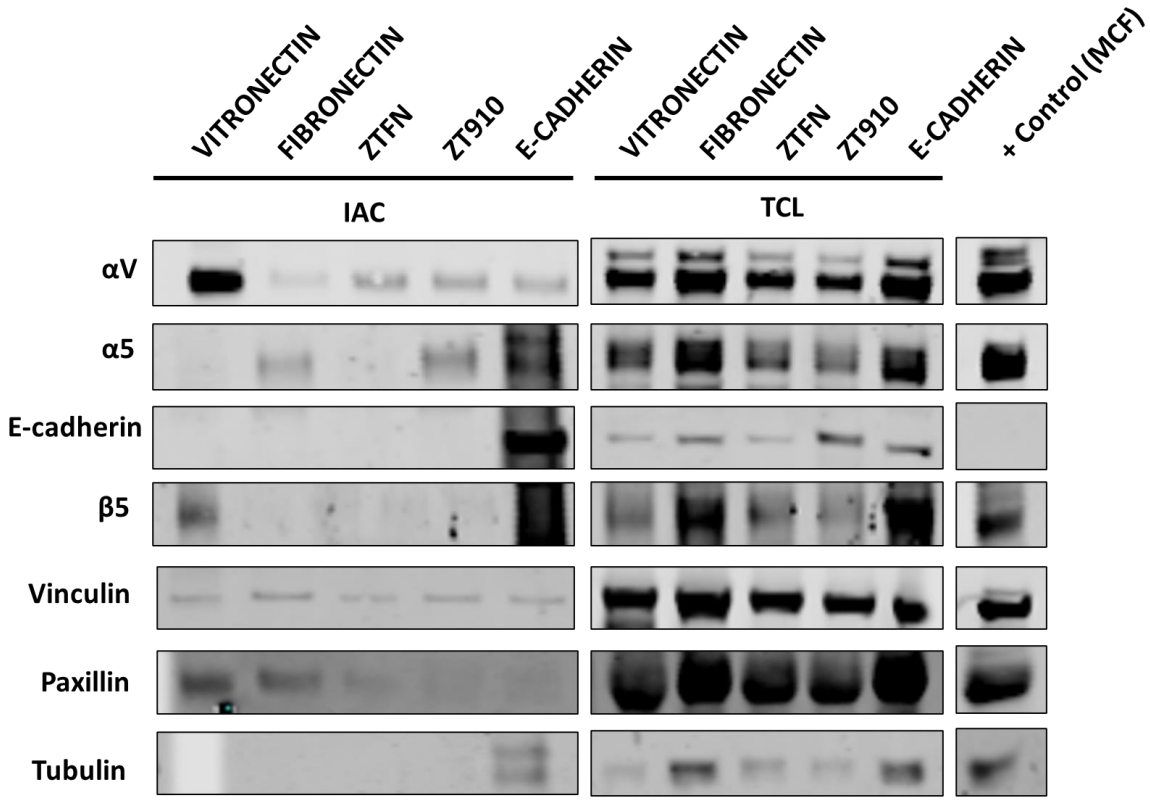

Figure 4.3: IAC enrichment in iPSCs show integrin-specific enrichment on defined substrates. iPSCs were plated on vitronectin (5µg/mL) and StemAdhere (E-cadherin) for 4 hours. immunoblotting in total cell lysate (TCL) and isolated IACs for the adhesome components integrin α5, αV, β5, e-cadherin, paxillin, vinculin and negative control protein tubulin from other subcellular compartments. Positive control of MCF7 total cell lysate. Representative blot of two independent experiments.

4.2.2. Proteomic analysis of IACs

4.2.2.1. Mass Spectrometry dataset quality

IAC samples were processed and analysed by mass spectrometry to characterise substrate-specific integrin-associated networks in an unbiased manner. To assess the quality of the IACs isolated from each integrin adhesion complex enrichment experiment, the reproducibility of the datasets across the 5 substrates and between the three biological replicated was assessed using a correlation matrix (Figure 4.4). Uncharacterised and bait proteins were not included in the correlation analysis. Pearson correlation coefficient values were determined for normalized spectral abundance factor (NSAF) values and were all above 0.8 for substrates fibronectin, ZTFN and e-cadherin; and above 0.69 for substrates vitronectin and ZT910, demonstrating good reproducibility between the replicates (Figure 4.4). Mass spectrometry of IACs across all five substrates identified a total of 710 proteins. Following the removal of uncharacterised, bait and unreviewed proteins, threshold for protein identification were applied to the dataset. Peptide threshold was set to >4 peptides counts and/or identified in ≥ 2 separate experiments.

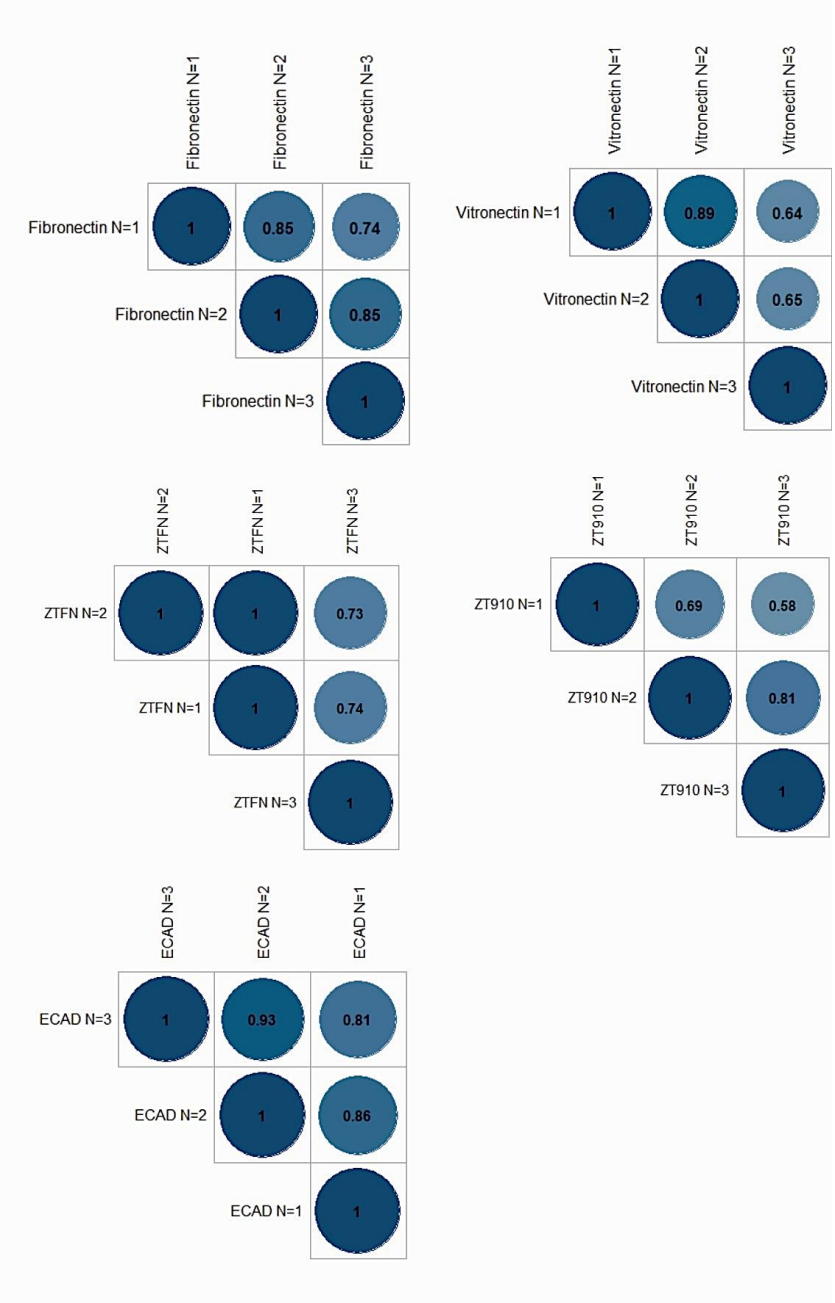

Figure 4.4: IACs isolated from iPSCs showed good reproducibility for the five ligands. Pairwise comparison of normalized spectral abundance factor (NSAF) values between replicates for Vitronectin, Fibronectin, ZTFN, ZT910 and E-cadherin. Pearson correlation coefficient value is indicated within each circle.

4.2.3. Characterisation of the adhesomes

To characterise IACs enriched on vitronectin. fibronectin, ZTFN and ZT910, the thresholded dataset was compared to the consensus, meta and non-adhesome proteins. A total of 19 (32%) and 349 (14.5%) proteins were identified to belong to the consensus and meta-adhesome respectively. To characterise compositional changes of enriched IAC-associated proteins identified on vitronectin, fibronectin, ZTFN and ZT910, mean enrichment of identified proteins was compared to the negative control substrate, E-cadherin. Protein-protein interaction networks were constructed in Cytoscape (version 3.9.0) and protein interactions were mapped using Protein Interaction Network Analysis (PINA) database (version: 21/05/2014). Fourteen proteins could not be mapped (E9PAV3, P34932, P49368, P55265, P59998, P78385, Q2Q1W2, Q15758, Q6P2Q9, Q92841, Q96DA0, Q9H9Z2, Q9UBF2 and Q08431) as they were not present in the protein-protein interaction network.

Characterisation of 1.5-fold enriched statistically significant protein within the IACs showed differential enrichment of proteins identified in the αVβ5-VIT, α5β1-FN, αVβ1-ZTFN and α5β1-ZT910 adhesome. A total of 182, 56, 52 and 123 proteins were significantly enriched 1.5-fold on fibronectin, vitronectin, ZTFN and ZT910 respectively. Furthermore, there were large substrate-specific differences in enriched proteins within the consensus and meta-adhesome (Figure 4.5A). Comparing proteins identified within each adhesome to the canonical consensus adhesome showed ~3-9% consensus adhesome-related proteins, with 5 proteins identified within the α5β1-ZT910 and αVβ1-ZTFN adhesome, 6 proteins identified within the α5β1-FN, and 2 proteins identified within the αVβ5-VIT adhesome (Figure 4.5A). Canonical consensus adhesome proteins talin was enriched 1.5-fold on fibronectin, ZTFN and ZT910, whereas vinculin was only enriched 1.5-fold on vitronectin. There were large differences in

the number of proteins identified within the meta-adhesome between vitronectin (46), fibronectin (135), ZTFN (29) and ZT910 (89) (Figure 4.5A). A total of 4 proteins (AHNAK, FN1, SLC3A2 and YWHAQ) within the meta-adhesome was shared between all four substrates (Figure 4.5A). Integrative analysis comparing proteins enriched between two substrates show that the α5β1-adhesome on fibronectin and ZT910 share the most proteins (43%), while αVβ5 and αVβ1 adhesome on vitronectin and ZTFN respectively share the least proteins (5%) (Figure 4.5B). These results reveal the extent of the differences in the integrin heterodimer-specific adhesome formed by IPSCs on these four integrin-engaging substrates.

To characterise the αVβ5-VIT, α5β1-FN, αVβ1-ZTFN and α5β1-ZT910 adhesomes, functional enrichment analysis was performed on statistically significant proteins that were 1.5-fold enriched on each ligand in comparison to the negative control substrate E-cadherin. Gene Ontology (GO) analysis was performed to characterise the cellular location, molecular function and biological process of the proteins isolated from IACs. ClueGO analysis using Cytoscape was employed to analyse interrelation of gene ontology terms and functional groups in the identified biological networks. ClueGO analysis was mapped to the Reactome Pathway terms to classify families of proteins enriched on each ligand (Figure 4.6, 4.7, 4.8 and 4.9). The α5β1 (fibronectin)-associated adhesome enriched for proteins associated with Nervous System Development, Metabolism of RNA, Disease, Cell cycle, Immune system, L13a-mediated translational silencing of Ceruloplasmin expression, Metabolism of proteins, Innate immune system, Signal transduction, Adaptive Immune system, Post-translational protein modification, Infectious Disease, Signalling by Rho GTPases, Non-integrin membrane-ECM interactions and Metabolism (Figure 4.6, Supplementary figure 2 and Supplementary Table 1). αVβ5 (Vitronectin)-associated adhesome enriched for proteins associated with

Metabolism, Immune system and Metabolism of Proteins (Figure 4.7, Supplementary figure 3 and Supplementary Table 2). αVβ1 (ZTFN)-associated adhesome enriched for proteins associated with Signal Transduction, Metabolism, Metabolism of RNA and Metabolism of proteins (Figure 4.8 Supplementary figure 4 and Supplementary Table 3). α5β1 (ZT910)-associated adhesome enriched for proteins associated with Metabolism of RNA, Disease, Metabolism of proteins and Cytokine signalling in Immune system (Figure 4.9, Supplementary figure 5 and Supplementary Table 4).

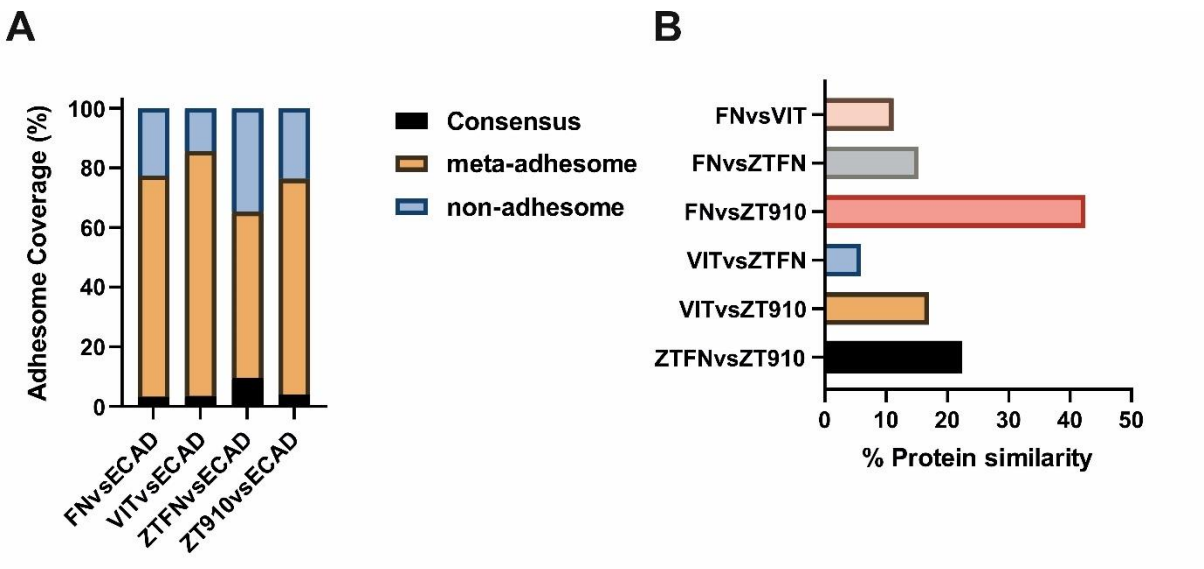

Figure 4.5: Proteome dataset classification. (A) Representation of 1.5-fold significantly enriched protein distribution within the consensus, meta adhesome and non-adhesome. (B) Percentage of proteins that are similar in pairwise substrate comparison of proteins enriched the 1.5-fold in FNvsVIT (11%), FNvsZTFN (15%), FNvsZT910 (43%), VITvsZTFN (6%), VITvsZT910 (17%) and ZTFNvsZT910 (22%).

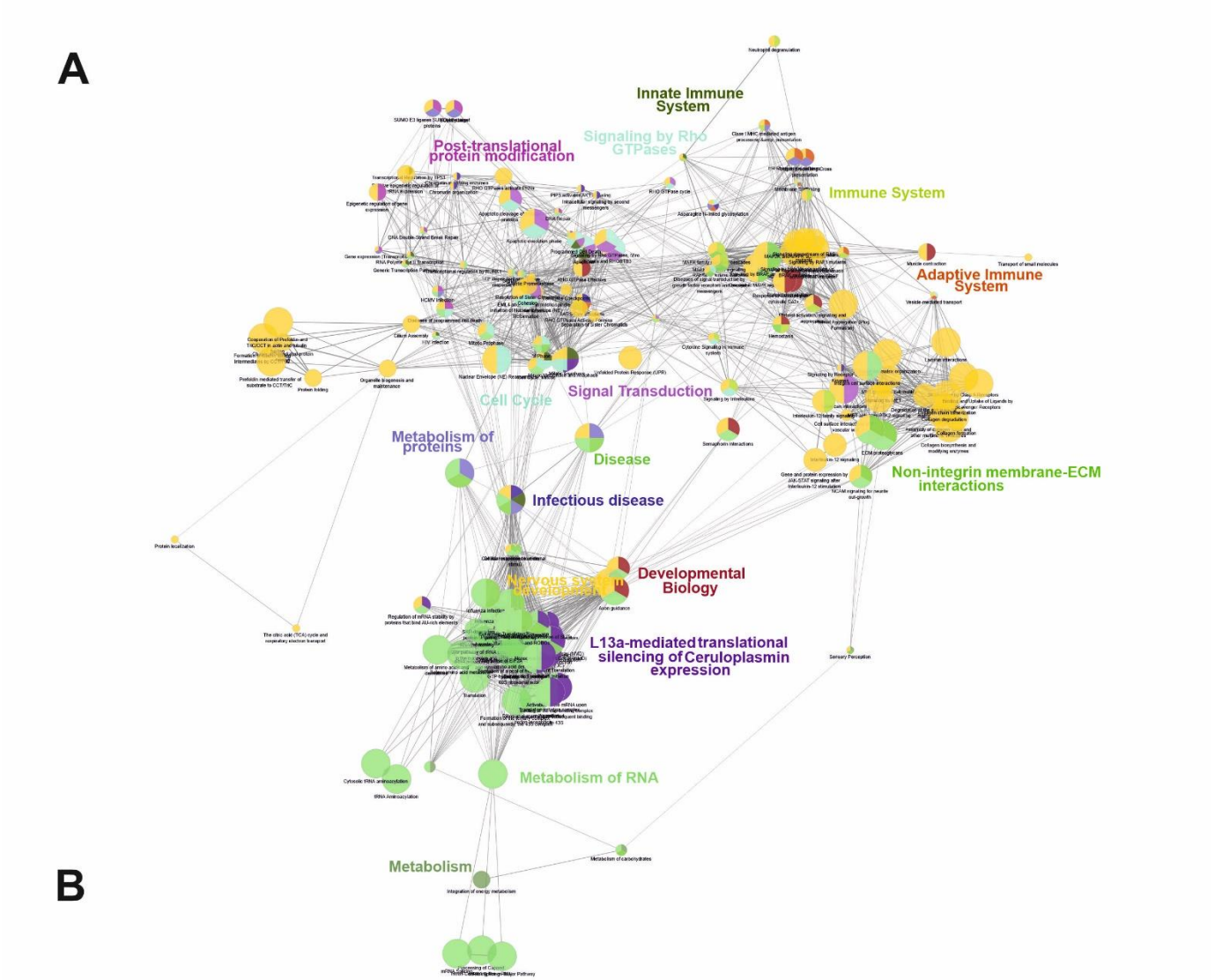
A
Innate Immune System
Post-translational protein modification
Signaling by Rho GTPases
Immune System
Adaptive Immune System
Cell Cycle
Signal Transduction
Metabolism of proteins
Disease
Infectious disease
Non-integrin membrane-ECM interactions
Developmental Biology
L13a-mediated translational silencing of Ceruloplasmin expression
Metabolism of RNA
Metabolism
B
Nervous system development 12.78% **
Metabolism of RNA 14.85% **
Disease 8.87% **
Cell Cycle 5.05% **
Immune System 6.39%
L13a-mediated translational silencing of Ceruloplasmin expression 2.47% **
Metabolism 4.43%
Non-integrin membrane-ECM interactions 2.06%
Signaling by Rho GTPases 4.12% **
Infectious disease 4.43% **
Post-translational protein modification 4.54%
Adaptive Immune System 4.64% .
Signal Transduction 4.74%
Developmental Biology 5.15% **
Innate Immune System 6.49% **
Metabolism of proteins 8.97% **

Figure 4.6: Reactome Pathway terms enriched on α5β1-Fibronectin. (A) Hierarchical layout of represented Reactome terms. Nodes with split colours belong to multiple groups. Nodes represent individual Reactome pathway terms. (B) Pie-chart organised by the % of genes per term. Analysis parameters: minimum 5 genes per cluster, GO term/pathway network connectivity (Kappa score) =0.2; Statistical test Enrichment/Depletion (Two-sided hypergeometric test), Benjamini-Hochberg p-value correction, GO term grouping based on kappa score, 50% of genes for group merge, 50% terms for group merge. Leading group term based on % gene/termvscluster.

A

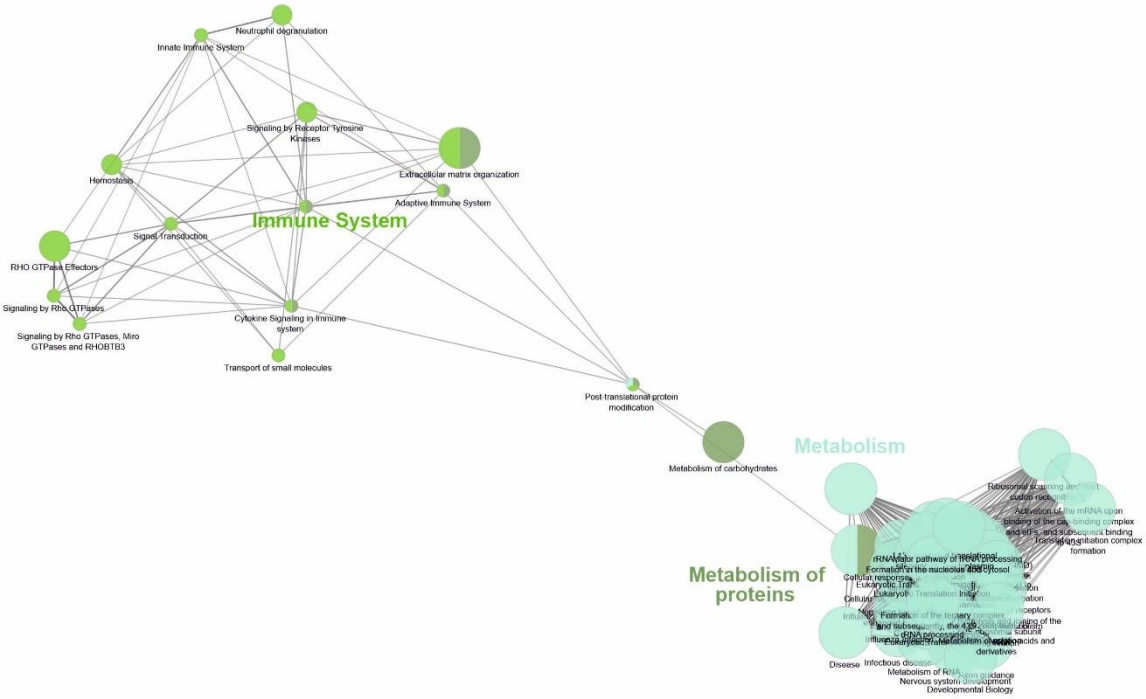
Neutrophil degranulation
Innate Immune System
Signaling by Receptor Tyrosine Kinases
Extracellular matrix organization
Hemostasis
Adaptive Immune System
Immune System
Signal Transduction
RHO GTPase Effectors
Signaling by Rho GTPases
Signaling by Rho GTPases, Miro GTPases and RHOBTB3
Cytokine Signaling in Immune system
Transport of small molecules
Post-translational protein modification
Metabolism of carbohydrates
Metabolism
Metabolism of proteins
Disease
Infectious disease
Metabolism of RNA
Nervous system development
Developmental Biology

B

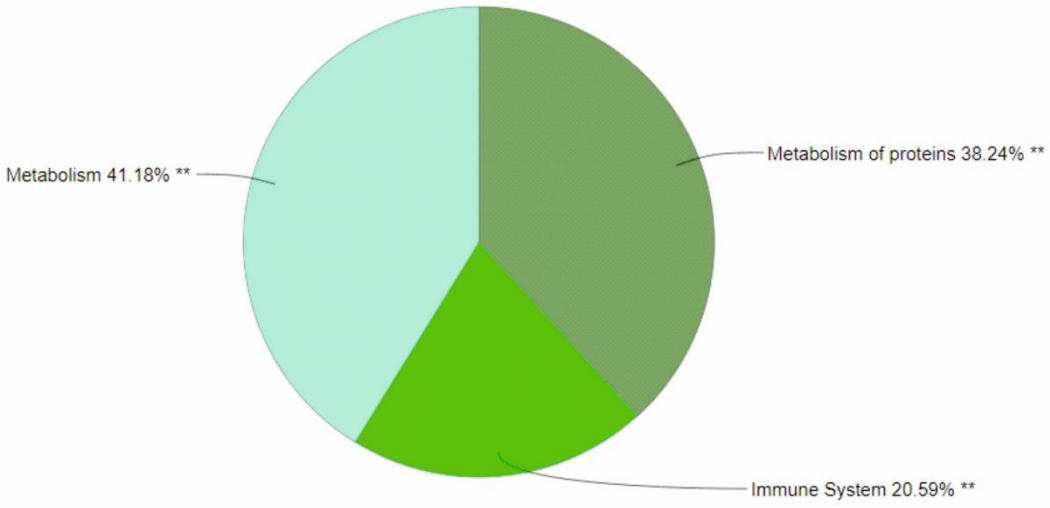
Metabolism 41.18% **
Metabolism of proteins 38.24% **
Immune System 20.59% **

Figure 4.7: Reactome Pathway terms enriched on αVβ5-Vitronectin. (A) Hierarchical layout of represented Reactome terms. Nodes with split colours belong to multiple groups. Nodes represent individual Reactome pathway terms. (B) Pie-chart organised by the % of genes per term. Analysis parameters: minimum 5 genes per cluster, GO term/pathway network connectivity (Kappa score) =0.2; Statistical test Enrichment/Depletion (Two-sided hypergeometric test), Benjamini-Hochberg p-value correction, GO term grouping based on kappa score, 50% of genes for group merge, 50% terms for group merge. Leading group term based on % gene/termvscluster.

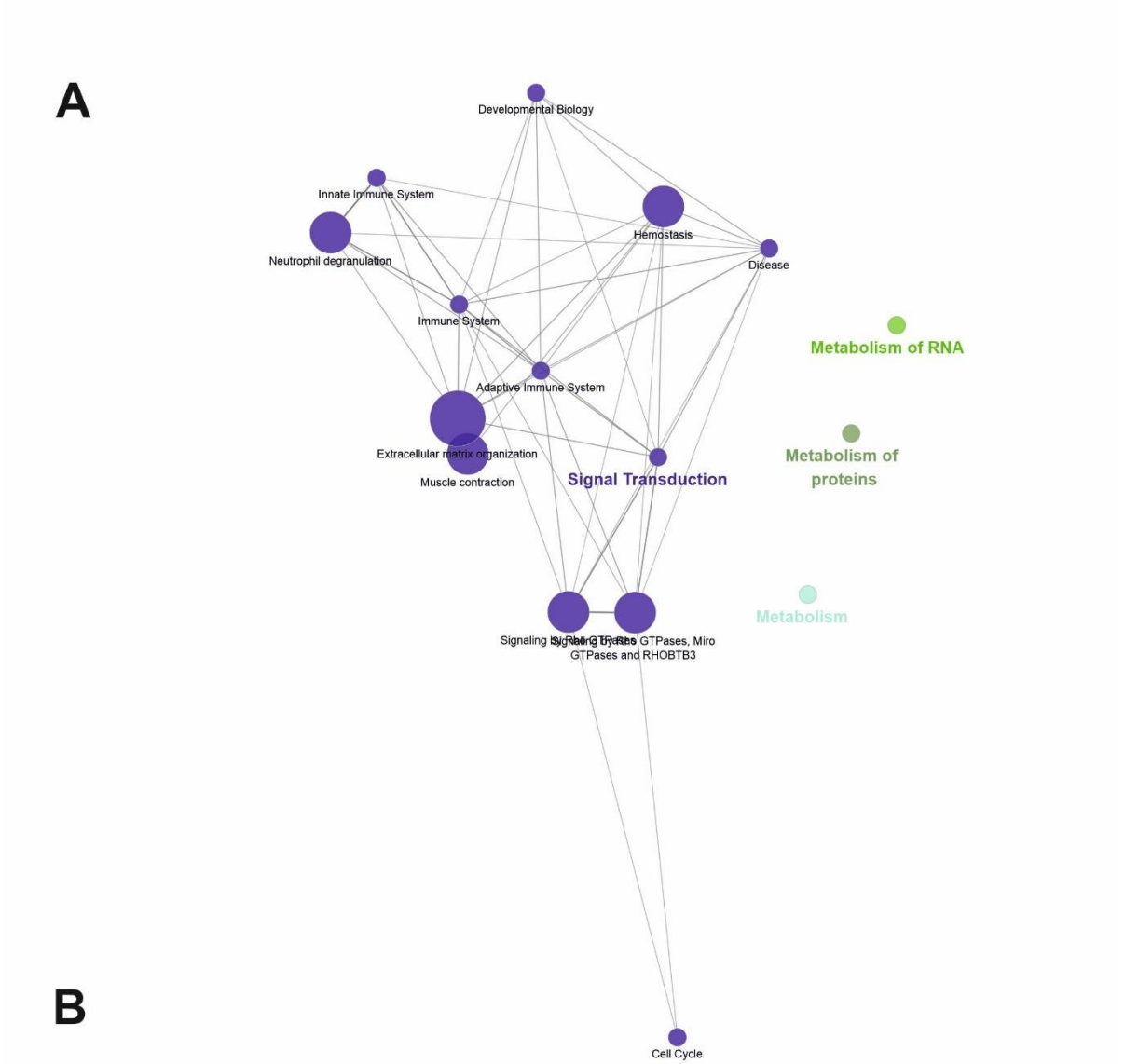
A
Developmental Biology
Innate Immune System
Neutrophil degranulation
Hemostasis
Disease
Immune System
Adaptive Immune System
Extracellular matrix organization
Muscle contraction
Signal Transduction
Metabolism of RNA
Metabolism of proteins
Metabolism
GTPases and RHOBTB3
Cell Cycle

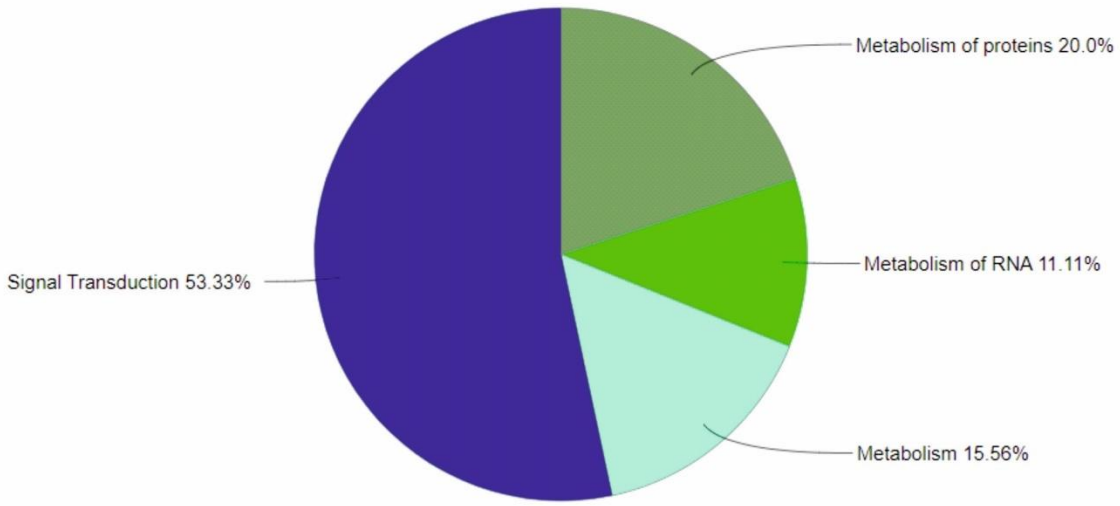
B
Metabolism of proteins 20.0%
Metabolism of RNA 11.11%
Metabolism 15.56%
Signal Transduction 53.33%

Figure 4.8: Reactome Pathway terms enriched on αVβ1-ZTFN. (A) Hierarchical layout of represented Reactome terms. Nodes with split colours belong to multiple groups. Nodes represent individual Reactome pathway terms. (B) Pie-chart organised by the % of genes per term. Analysis parameters: minimum 5 genes per cluster, GO term/pathway network connectivity (Kappa score) =0.2; Statistical test Enrichment/Depletion (Two-sided hypergeometric test), Benjamini-Hochberg p-value correction, GO term grouping based on kappa score, 50% of genes for group merge, 50% terms for group merge. Leading group term based on % gene/termvscluster.

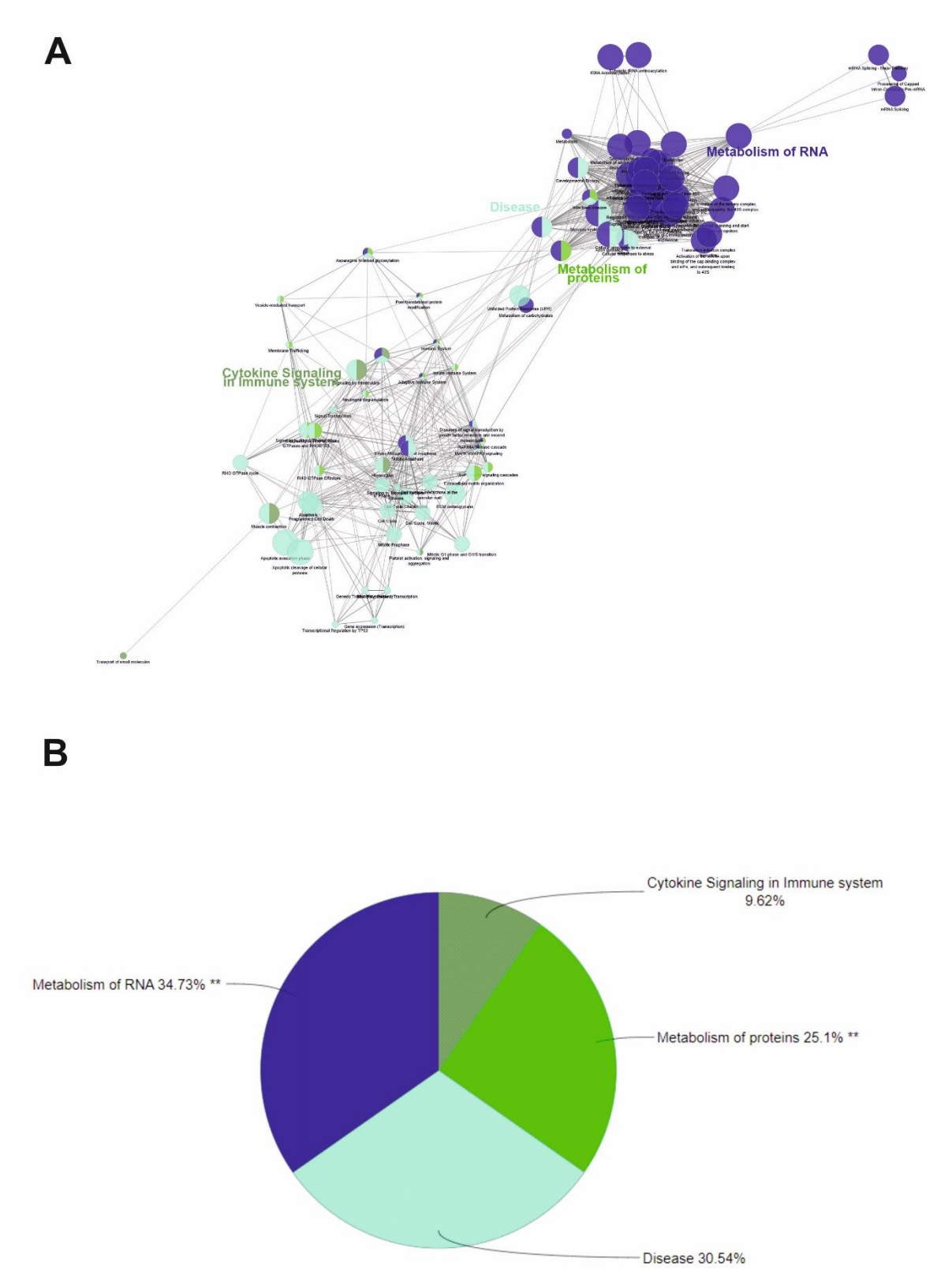
A
Metabolism of RNA
Disease
Metabolism of proteins
Cytokine Signaling in Immune system
B
Cytokine Signaling in Immune system 9.62%
Metabolism of RNA 34.73% **
Metabolism of proteins 25.1% **
Disease 30.54%

Figure 4.9: Reactome Pathway terms enriched on α5β1-ZT910. (A) Hierarchical layout of represented Reactome terms. Nodes with split colours belong to multiple groups. Nodes represent individual Reactome pathway terms. (B) Pie-chart organised by the % of genes per term. Analysis parameters: minimum 5 genes per cluster, GO term/pathway network connectivity (Kappa score) =0.2; Statistical test Enrichment/Depletion (Two-sided hypergeometric test), Benjamini-Hochberg p-value correction, GO term grouping based on kappa score, 50% of genes for group merge, 50% terms for group merge. Leading group term based on % gene/termvscluster.

4.2.4. Ontological and functional analysis of adhesomes

4.2.4.1. α5β1 vs αVβ5 adhesome

Following the characterisation of substrate-specific adhesome on vitronectin, fibronectin, ZTFN and ZT910, we sought to identify significant functionally relevant proteins. Although IAC proteomic datasets characterised on ZTFN and ZT910 contain valuable insights of IACs recruited on these self-assembling nanofiber substrates, due to the potential complexity of downstream candidate validation experiments, for this study we aimed to characterise functional protein clusters enriched on both αVβ5-VIT and α5β1-FN adhesome. To characterise functional similarities and differences of α5β1 and αVβ5 adhesome, GO term analysis was performed on statistically significant proteins that were enriched 1.5-fold on both fibronectin and vitronectin, to characterise the cellular location, molecular function and biological process of the proteins isolated from IACs. ClueGO analysis using Cytoscape was employed to analyse the interrelation of gene ontology terms and functional groups in the identified biological networks. ClueGO analysis was mapped to the Reactome Pathway terms to classify families of proteins enriched on each ligand. Reactome term analysis identified significant enrichment of proteins associated with Disease, Metabolism, Post-translational modification, Mitotic Metaphase and Anaphase, Metabolism of Proteins, Developmental Biology, Signalling of Rho GTPases, Extracellular matrix organisation and Metabolism of Carbohydrates (Figure 4.10A and 4.10B, Table 6).

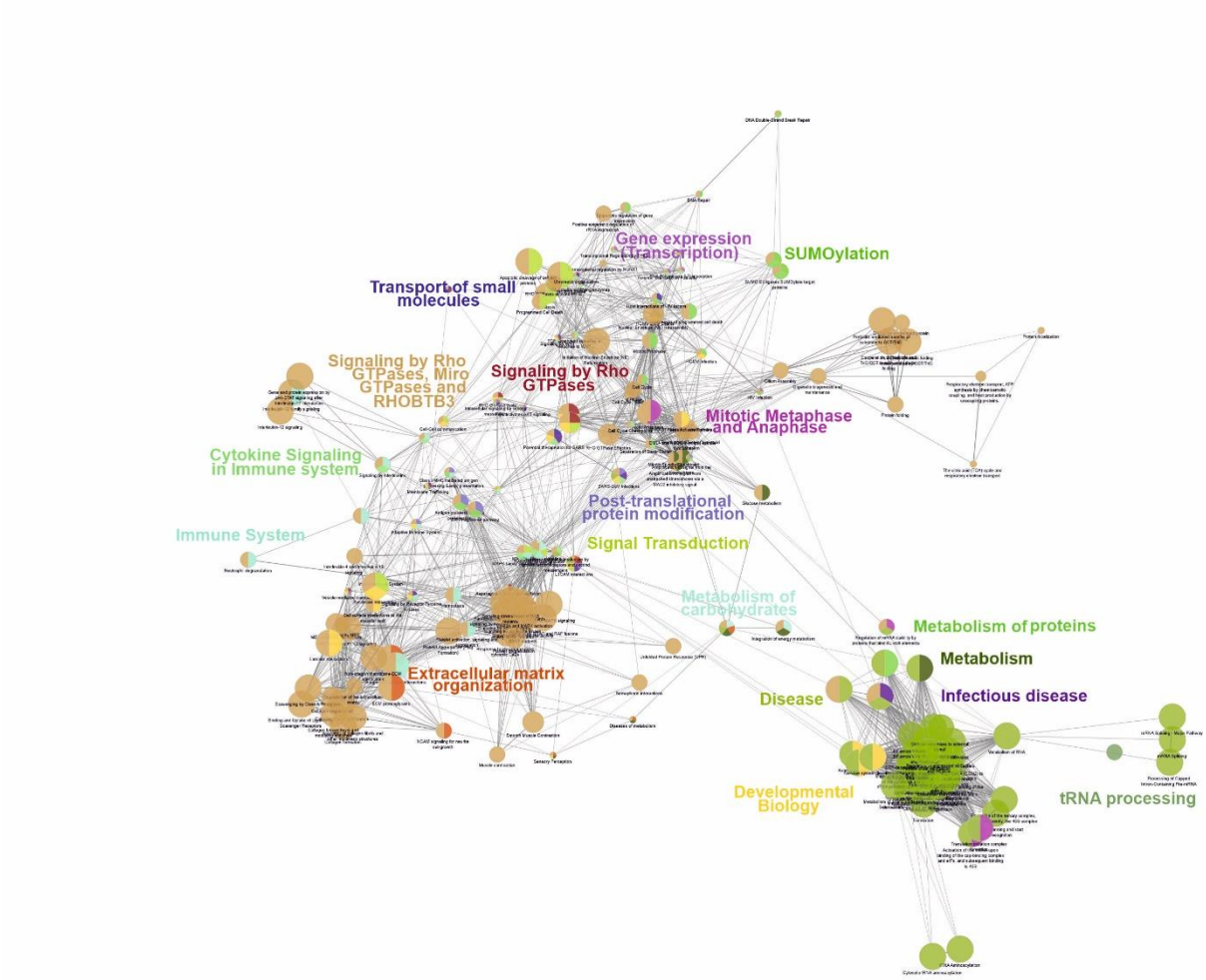
Gene expression (Transcription)
SUMOylation
Transport of small molecules
Signaling by Rho GTPases, Miro GTPases and RHOBTB3
Signaling by Rho GTPases
Mitotic Metaphase and Anaphase
Cytokine Signaling in Immune system
Post-translational protein modification
Immune System
Signal Transduction
Metabolism of carbohydrates
Metabolism of proteins
Metabolism
Infectious disease
Disease
Extracellular matrix organization
Developmental Biology
tRNA processing

B

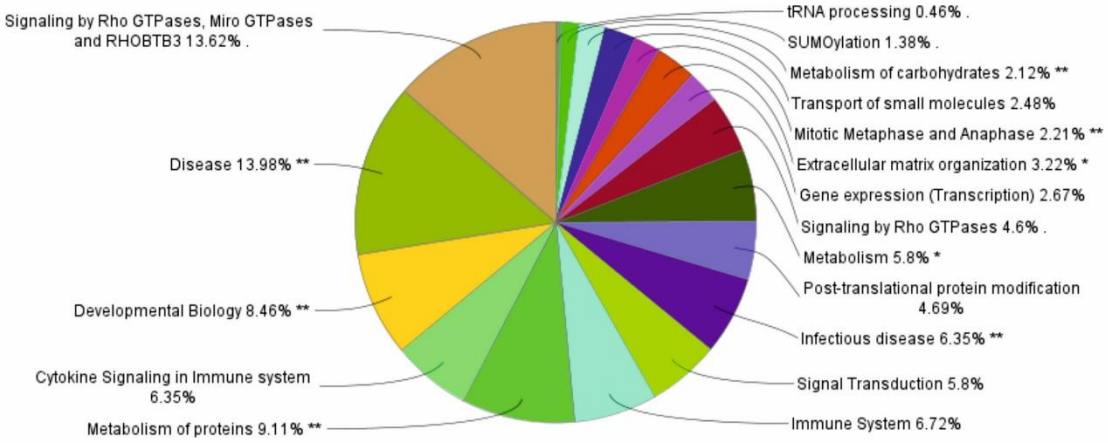
Signaling by Rho GTPases, Miro GTPases and RHOBTB3 13.62% .
Disease 13.98% **
Developmental Biology 8.46% **
Cytokine Signaling in Immune system 6.35%
Metabolism of proteins 9.11% **
tRNA processing 0.46% .
SUMOylation 1.38% .
Metabolism of carbohydrates 2.12% **
Transport of small molecules 2.48%
Mitotic Metaphase and Anaphase 2.21% **
Extracellular matrix organization 3.22% *
Gene expression (Transcription) 2.67%
Signaling by Rho GTPases 4.6% .
Metabolism 5.8% *
Post-translational protein modification 4.69%
Infectious disease 6.35% **
Signal Transduction 5.8%
Immune System 6.72%

Figure 4.10: **Reactome Pathway term enriched on both α5β1-Fibronectin and α5β1-Vitronectin.** (A) Hierarchical layout of represented Reactome terms. Nodes with split colours belong to multiple groups. Nodes represent individual Reactome pathway terms. (B) Pie-chart organised by the % of genes per term. Analysis parameters: minimum 5 genes per cluster, GO term/pathway network connectivity (Kappa score) =0.2; Statistical test Enrichment/Depletion (Two-sided hypergeometric test), Benjamini-Hochberg p-value correction, no p-value threshold applied; GO term grouping based on kappa score, 50% of genes for group merge, 50% terms for group merge. Leading group term based on % gene/term.

Table 6: **Reactome GO Term analysis of proteins enriched on both Fibronectin and Vitronectin.** The top group leading terms with their respective statistical p values, and the Benjamini-Hochberg corrected p-value. Associated Genes Found comprises the list of proteins identified with the MS dataset and within each GO term.

ID	Term	Group PValue	Group PValue Corrected with Benjamini-Hochberg	Associated Genes Found
R-HSA:1643685	Disease	3.84E-16	6.92E-15	[AGRN, AHCY, AP2B1, ATP1A1, CALR, CANX, CHD4, CLTC, DNMT3B, ENO1, FGB, FGF2, FGG, FN1, H2AC7, H4-16, HNRNPK, HSPG2, IPO5, IQGAP1, ITGB1, KDM1A, KPNA2, KPNB1, LMNA, LMNB1, MSH6, NPM1, PARP1, PPP1CC, PPP2R1A, PSMB3, RANBP2, RPL10, RPL13A, RPL15, RPL17, RPL23, RPL24, RPL26, RPL3, RPL32, RPL5, RPL6, RPL8, RPL9, RPN2, RPS11, RPS16, RPS17, RPS23, RPS3A, RPS4X, RPS7, SLC2A1, SLC3A2, SND1, SUPT16H, TALDO1, TLN1, TUBB4A, VCAN, VCL, XRCC5]
R-HSA:1430728	Metabolism	3.84E-16	6.92E-15	[AASS, AGRN, AHCY, ALDH18A1, ATP5F1A, ATP5F1B, ATP5PO, CAD, CYCS, ENO1, EPRS1, GMPS, HSD17B10, HSD17B4, HSPG2, IARS1, IQGAP1, KPNB1, LARS1, LRP1, MARCKS, MARS1, MDH2, PAICS, PPP1CC, PPP2R1A, PRPS1, PSAT1, PSMB3, RANBP2, RARS1, RPL10, RPL13A, RPL15, RPL17, RPL23, RPL24, RPL26, RPL3, RPL32, RPL5, RPL6, RPL8, RPL9, RPS11, RPS16, RPS17, RPS23, RPS3A, RPS4X, RPS7, SLC25A11, SLC2A1, SLC3A2, TALDO1, THRAP3, TKT, TRAP1, VCAN]
R-HSA:597592	Post-translational protein modification	3.84E-16	6.92E-15	[CALR, CAND1, CANX, DNMT3B, FGG, FN1, H2AC7, H4-16, HNRNPK, NOP58, NPM1, PARP1, PDIA3, PRKDC, PSMB3, RANBP2, RPN2, SEC16A, SPTAN1, TOP2A, TOP2B, TUBB4A, UCHL1, UGGT1, USP9X, VCAN]
R-HSA:2555396	Mitotic Metaphase and Anaphase	1.47E-09	1.32E-08	[CKAP5, KPNB1, LMNA, LMNB1, PPP1CC, PPP2R1A, PSMB3, RANBP2, RCC2, TMPO, TNPO1, TUBB4A]
R-HSA:392499	Metabolism of proteins	2.02E-07	1.21E-06	[AARS1, CALR, CAND1, CANX, CCT2, CCT5, CCT8, DNMT3B, EIF2S3, EIF3A, EIF4G1, EPRS1, FGG, FN1, GARS1, H2AC7, H4-16, HNRNPK, HSPA5, HSPG2, IARS1, INHBE, KHSRP, LARS1, LMNA, MARS1, NOP58, NPM1, PABPC1, PARP1, PDIA3, PRKDC, PSMB3, RANBP2, RARS1, RPL10, RPL13A, RPL15, RPL17, RPL23, RPL24, RPL26, RPL3, RPL32, RPL5, RPL6, RPL8, RPL9, RPN2, RPS11, RPS16, RPS17, RPS23, RPS3A, RPS4X, RPS7, SEC16A, SPTAN1, SRP54, TCP1, TLN1, TOP2A, TOP2B, TUBB4A, UCHL1, UGGT1, USP9X, VCAN]
R-HSA:1266738	Developmental Biology	6.70E-07	3.01E-06	[AGRN, AP2B1, CFL1, CLTC, COL2A1, COL4A1, COL4A2, DPYSL3, EIF4G1, ENAH, EZR, FGF2, H2AC7, H4-16, ITGAV, ITGB1, KRT18, KRT8, LIN28A, MYL12A, PABPC1, PSMB3, RPL10, RPL13A, RPL15, RPL17, RPL23, RPL24, RPL26, RPL3, RPL32, RPL5, RPL6, RPL8, RPL9, RPS11, RPS16, RPS17, RPS23, RPS3A, RPS4X, RPS7, SALL4, SMARCA4, SPTAN1, THRAP3, TLN1, TUBB4A]
R-HSA:194315	Signaling by Rho GTPases	6.70E-07	3.01E-06	[ACTN1, AKAP12, CCT2, CFL1, CKAP5, CLTC, H2AC7, H4-16, IQGAP1, ITGB1, KDM1A, LMNB1, MYL12A, PPP1CC, PPP2R1A, RANBP2, RBMX, RCC2, SPTAN1, TFRC, TMPO, TUBB4A, USP9X, VIM, YWHAQ]
R-HSA:1474244	Extracellular matrix organization	1.82E-05	5.45E-05	[ACTN1, AGRN, COL18A1, COL1A1, COL1A2, COL2A1, COL4A1, COL4A2, FGB, FGF2, FGG, FN1, HSPG2, ITGAV, ITGB1, PLEC, SERPINH1, VCAN, VTN]
R-HSA:71387	Metabolism of carbohydrates	9.16E-04	2.06E-03	[AGRN, ENO1, HSPG2, MDH2, PPP2R1A, PRPS1, RANBP2, SLC25A11, SLC2A1, TALDO1, TKT, VCAN]

4.2.5. Enriched GO terms

Having identified Reactome GO terms over-represented by proteins significantly enriched on both fibronectin and vitronectin, protein-protein interaction networks were constructed for protein associated with each Reactome GO term. Clustering of proteins within each GO term was performed to classify functionally related nodes using the Cytoscape plug-in 'clusterMaker 2' using the Community Clustering (GLay) algorithm. Due to overlap between represented groups, the Reactome GO terms Metabolism of Carbohydrates, Extracellular Organisation, Developmental Biology and Mitotic Metaphase and Anaphase were not analysed. Furthermore, functionally related nodes that overlap between GO terms and did not form edges with related proteins were not analysed to avoid repetition.

4.2.5.1. Disease

The Reactome GO term Disease was over-represented in the fibronectin and vitronectin enriched dataset. The first cluster within Disease contains the canonical adhesion proteins talin and vinculin (Figure 4.11). Cell adhesion, migration, and the generation of actomyosin-mediated forces involve the dynamic recruitment and turnover of focal adhesion molecules talin and vinculin (Atherton et al., 2015). Fibrinogen is a hexameric protein that is secreted as a zymogen that regulates multiple functions including platelet recruitment and aggregation, playing an important role in the coagulation cascade and consists of three genes: FGG, FGB and FGA (Naz et al., 2017). SLC3A2 has been shown to associate with integrin β1 constitutively and specifically, and there is increasing evidence SLC3A2 plays an important role in regulating integrin-mediated downstream signalling in cancer cells (Henderson et al., 2004) (Figure 4.11). NPM1 (Nucleophosmin 1) is a protein is found at high levels in the nucleus of

proliferating cells. The protein plays a critical role in mRNA transport, maintenance of genome stability, chromatin remodelling and apoptosis. α-enolase-1 is a multifunctional glycolytic enzyme that catalyses 2-phosphoglycerate (2-PGA) to phosphoenolpyruvic acid (PEP) in glycolysis (Didiasova et al., 2019) (Figure 4.11). In addition, α-enolase-1 localises to the plasma membrane where it serves as a receptor activating plasminogen to mediate cell migration and invasion (Didiasova et al., 2019).

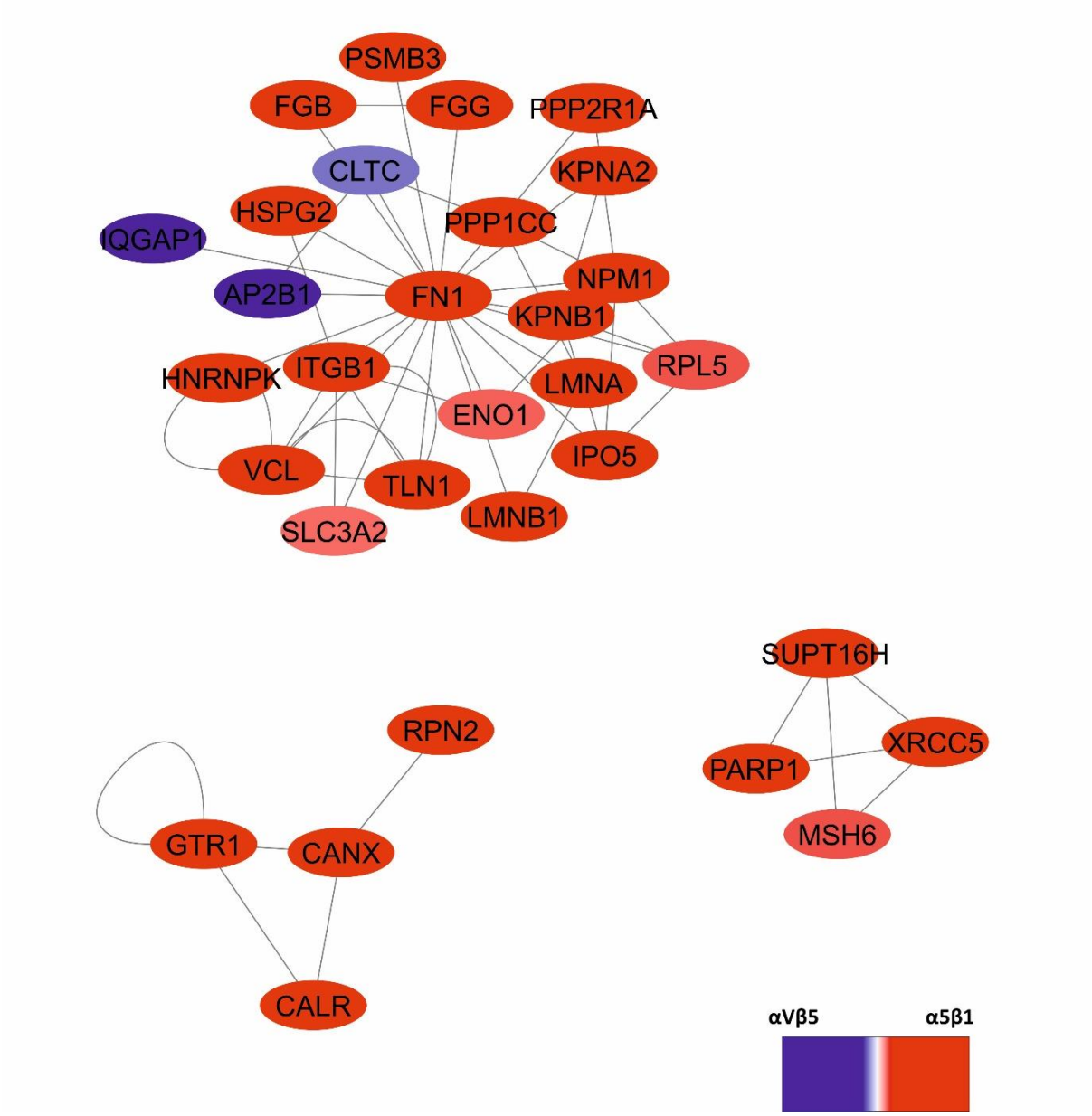

Figure 4.11: **Disease GO term subnetwork clusters.** (A) Selected key clusters from proteins associated with the Disease Reactome term group. Nodes represent proteins, and edges are known interactions. Node colour blue and red corresponds to >1.5-fold log_2 enrichment Fibronectin (red) and vitronectin (blue).

4.2.5.2. Post-translation protein modification and Signalling by Rho GTPases

The Reactome GO term post-translation protein modification was over-represented in the fibronectin and vitronectin enriched dataset (Figure 4.12A). PDIA3 (Protein disulfide-isomerase A3) are multifunctional chaperone proteins that are primarily involved in regulating the catalysis of protein disulphide bonds and modulating protein function through oxidation and reduction (Mahmood et al., 2021). Calnexin is a calcium-binding protein belonging to one of the four lectin chaperones in the endoplasmic reticulum, acts as a quality control apparatus by facilitating glycoprotein folding and retaining protein that has misfold within the endoplasmic reticulum (Kozlov and Gehring, 2020). Similarly, calreticulin is a calcium-binding protein that regulates intracellular Ca^{2+} levels. Although calreticulin is ubiquitously expressed within all cellular compartments, it localises within the endoplasmic reticulum to interact with newly synthesized glycoproteins and mRNA (Varricchio et al., 2017). NOP58 (Nucleolar Protein 58) is a protein that forms a core component of box C/D small nucleolar ribonucleoproteins, which play an important role in the processing and modification of ribosomal RNA in the nucleolus. When DNA is damaged, the repair of DNA is mediated by the recruitment of poly(ADP-ribose) polymerase 1 (PARP1), which mediates the repair of single-stranded and double-stranded DNA breaks (Ke et al., 2017).

The Reactome GO term Signalling by Rho GTPases was over-represented in the fibronectin and vitronectin enriched dataset (Figure 4.12B). IQGAP comprises multiple domains including the calponin homology which can interact with actin and GAP-related domain (GRD) of small GTPases that regulate actin dynamics to promote cell migration and cytokinesis (Wang et al., 2009). Furthermore, IQGAP binds mTOR and couples cell growth and cell cycle progression

through an IQGAP-CDC42 complex (Wang et al., 2009). RCC2 (Regulator of chromosome condensation 2) also known as Telophase Disc-60 (TD-60) is a protein that plays an essential role in regulating cell cycle progression during interphase (Wu et al., 2018). Vimentin is a type III intermediate filament that has been down to induce integrin clustering by directly binding to integrin β1 following engagement to fibronectin (Kim et al., 2016). Cofilin 1 belongs to a family of actin-binding proteins that play a key role in regulating actin dynamics (Bravo-Cordero et al., 2013).

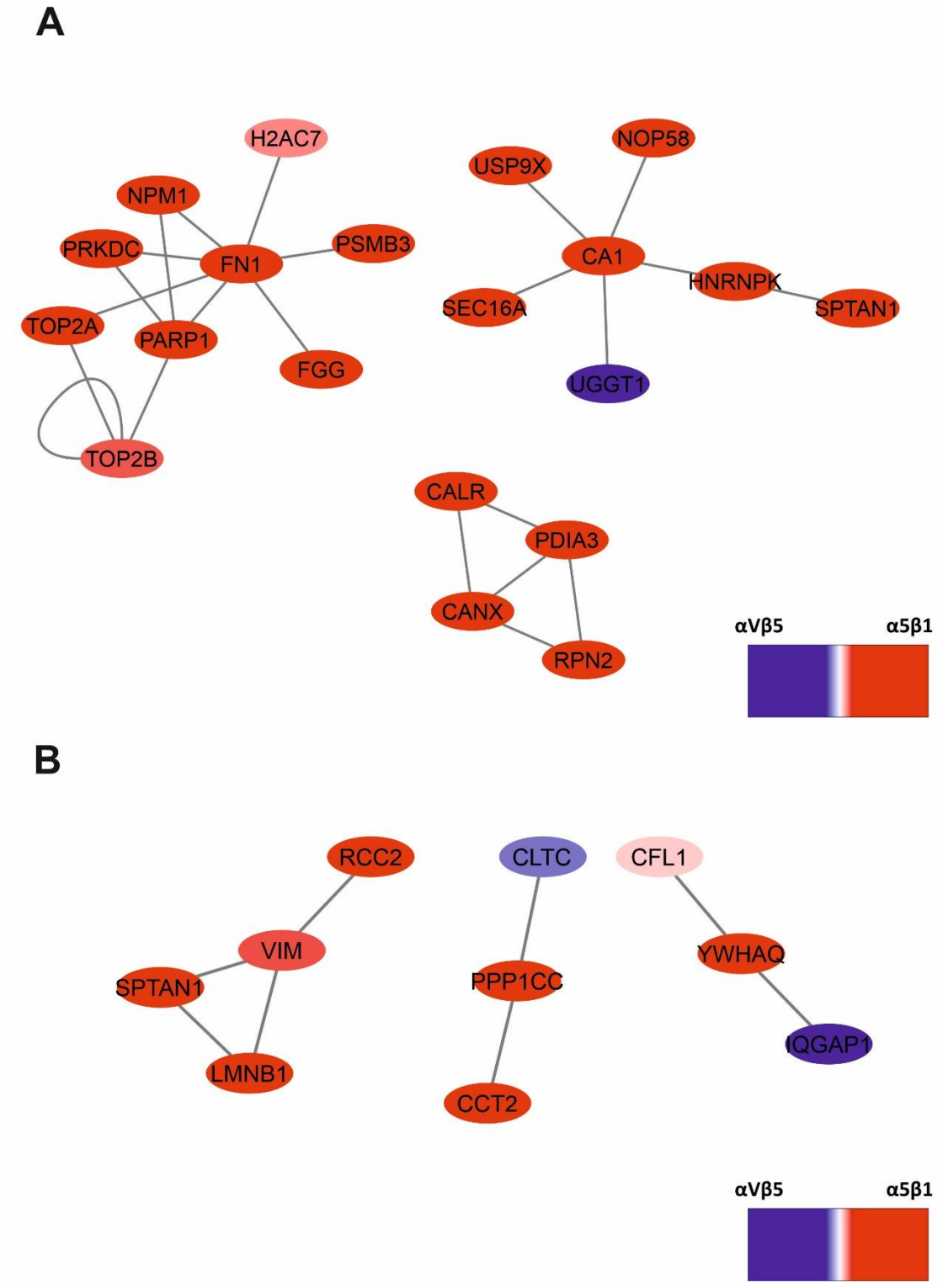

Figure 4.12: Post-translation protein modification and Signalling by Rho GTPases term subnetwork clusters. (A) Selected key clusters from proteins associated with the Post-translation protein modification pathway Reactome term group. (B) Selected key clusters from proteins associated with the Signalling by Rho GTPases term group. Nodes represent proteins, and edges are known interactions. Node colour blue and red corresponds to >1.5-fold $\log_2$ enrichment Fibronectin (red) and vitronectin (blue).

4.2.5.3. Metabolism and Metabolism of proteins

The Reactome GO terms Metabolism and Metabolism of Proteins were overrepresented in the fibronectin and vitronectin enriched dataset (Figure 4.13A and 4.13B). Phosphoserine aminotransferase 1 (PSAT1) is an enzyme that is involved in the synthesis of the amino acid Serine. Transaldolase 1 is an enzyme that plays an important role in the nonoxidative pentose phosphate pathway by mediating the generation of ribose-5-phosphate for nucleic acid synthesis and NADPH for lipid synthesis. Transketolase (TKT) is a thiamine-dependent enzyme that plays a role in transferring excess sugar phosphates into glycolysis.

CCTs (CCT2, CCT5 and CCT8) (chaperonin-containing tailless complex polypeptides) are a family of proteins that are involved in regulating the folding of newly synthesised cytoskeletal proteins (Vallin and Grantham, 2019). Spectrin (spectrin α1 and spectrin β1) is a cytoskeletal protein that forms a complex network that interacts with intercellular proteins such as actin, to maintain the shape and structure of the cell membrane (Zhang et al., 2013). PABPC1 (poly(A)-binding protein C1) is a basic protein that binds to the poly adenylate tail of mature eukaryotic mRNA and regulates their translation and metabolism (Sawazaki et al., 2018). KHSRP (KH-Type Splicing Regulatory Protein) is a single-stranded nucleic acid-binding protein that interacts with the promoter region of the oncogene c-myc (Briata et al., 2016). Aminoacyl-tRNA synthetases such as MARS1, RARS1, EPRS1 and LARS1 are a class of enzymes that catalyses the aminoacylation of amino acids (Cerini et al., 1991).

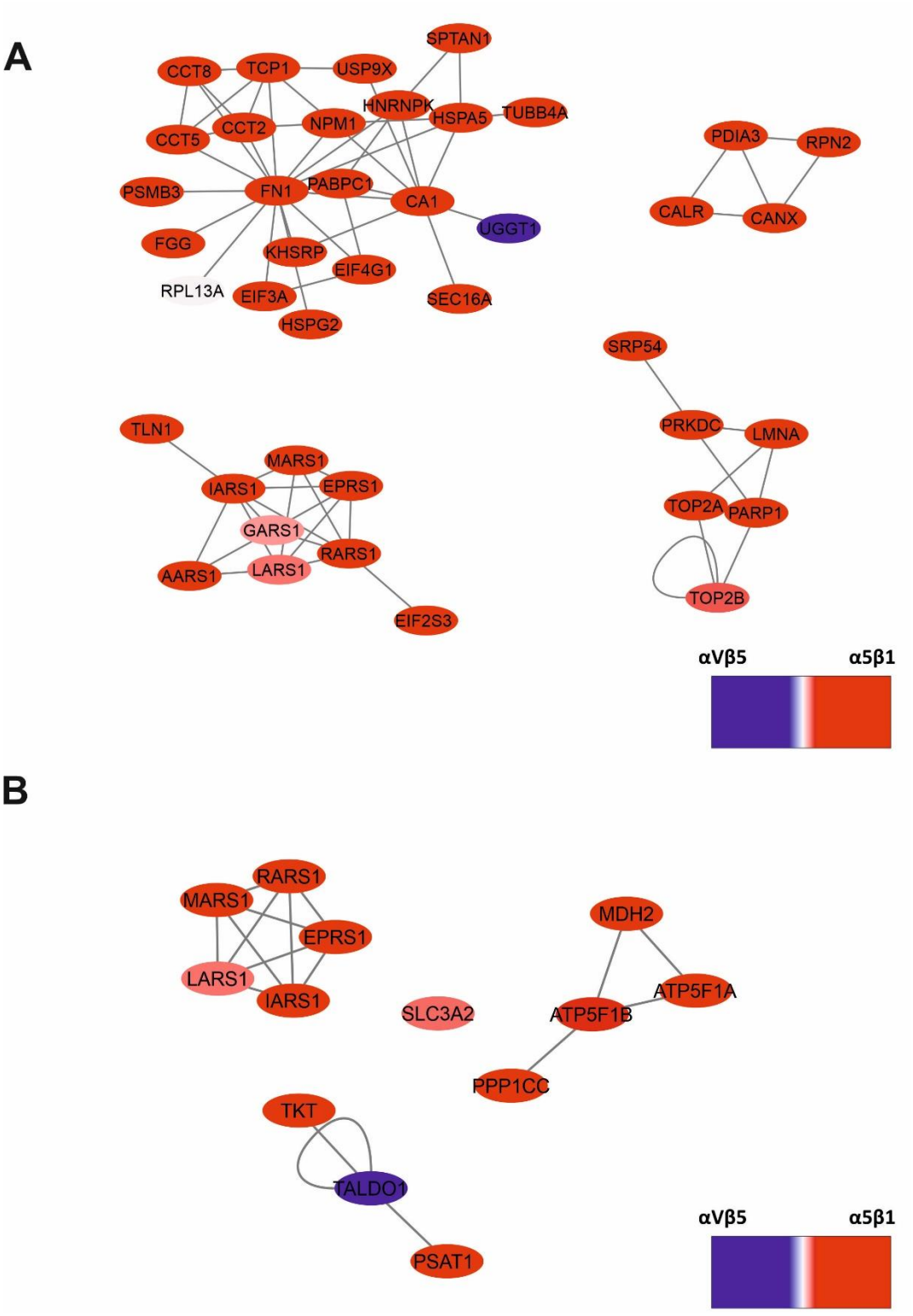

Figure 4.13: Metabolism and Metabolism of Proteins pathway term subnetwork clusters. (A) Selected key clusters from proteins associated with the Metabolism Reactome term group. (B) Selected key clusters from proteins associated with the Metabolism of Proteins term group. Nodes represent proteins, and edges are known interactions. Node colour blue and red corresponds to >1.5-fold log_2 enrichment Fibronectin (red) and vitronectin (blue).

4.2.5.4. SLC3A2

A review of GO terms significantly enriched to the α5β1 and αVβ5 adhesome revealed a surprising enrichment of proteins that regulate metabolism (GOterms: Metabolism, Metabolism of proteins and Metabolism of Carbohydrates). Furthermore, canonical focal adhesion proteins such as integrin β1, vinculin, talin and IQGAP were enriched within the GO term Disease, which also included numerous proteins that were represented in the GO terms related to metabolism (Table 6).

There is increasing evidence that integrins play an important role in the regulation of metabolism through several mechanisms, including the activation of specific signalling pathways and regulation of metabolite transport through its association with amino acid transporters (Ata and Antonescu, 2017). To identify a key node that may potentially integrate stem cell signalling and metabolism in an integrin-dependent manner, the proteins within the GO terms Disease and Metabolism were merged. The proteins were then filtered to select proteins that were significantly enriched two-fold, on either α5β1-FN and αVβ5-VIT adhesomes. A total of 71 proteins were identified (Figure 4.14). Following this, proteins that were enriched on both disease and metabolism GO terms and those that directly associate integrin subunit β1-FN and β5-VIT adhesomes were identified. SLC3A2 was identified as a key node that may potentially integrate stem cell signalling and metabolism in an integrin-dependent manner. One-hop and two-hop protein interaction networks were generated for SLC3A2 (Figure 4.15). This analysis revealed that SLC3A2 directly interacts with integrin β1, ARF6, PHB2, HNRNPD, ATP2A2, VCP and FN (Figure 4.15). The Integrin β5 (ITGB5) node was added *in silico* based on the evidence of αVβ5 enrichment in immunofluorescence and adhesion complex enrichment experiments (Figure 4.15). β1 has been shown to associate

with SLC3A2 constitutively and specifically, and there is increasing evidence SLC3A2 plays an important role in regulating integrin-mediated downstream signalling in cancer cells (Henderson et al., 2004).

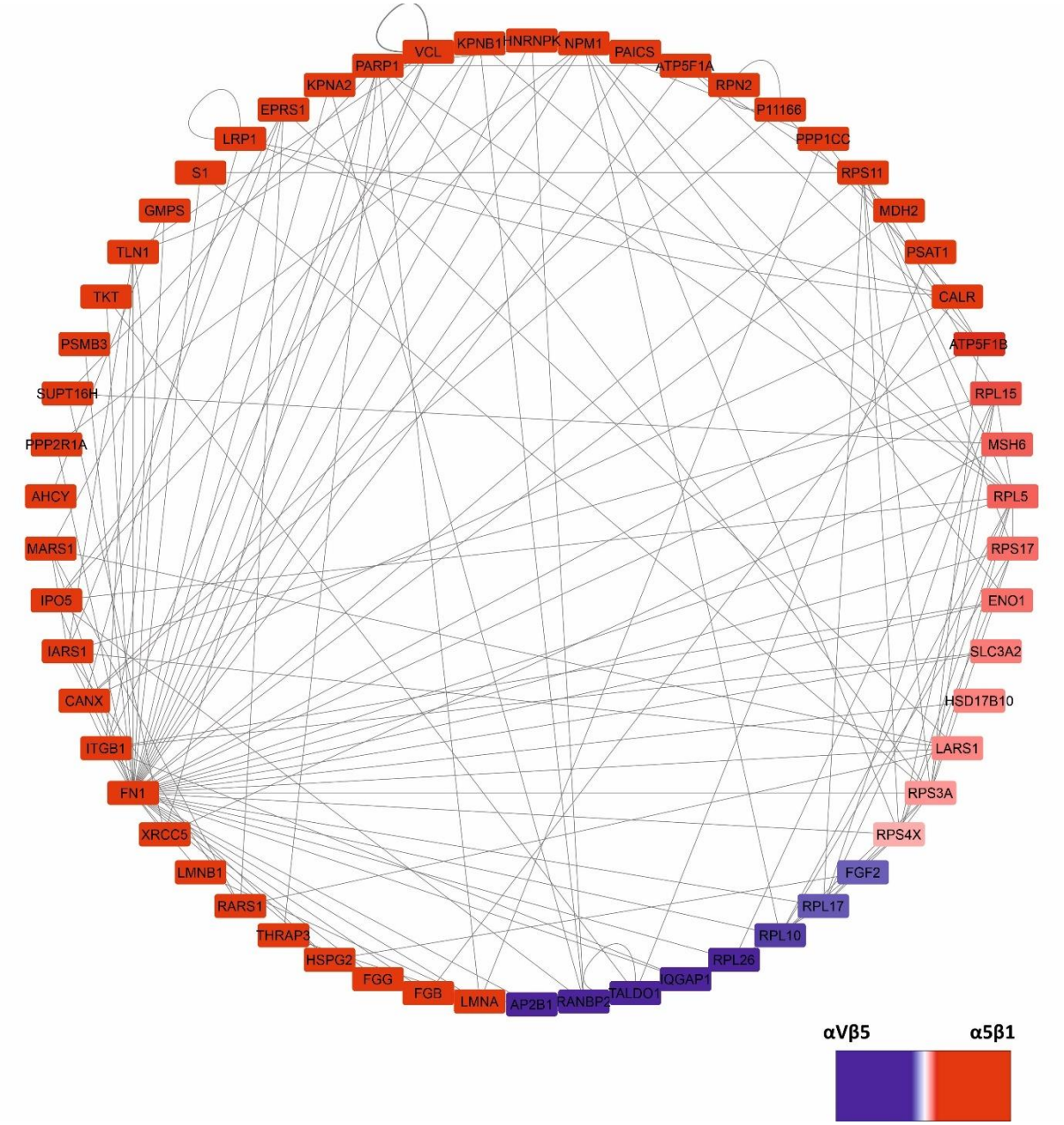

Figure 4.14: Disease and Metabolism GO term proteins that directly interact with ITGB1. Node colour blue and red correspond to >1.5-fold log_2 enrichment Fibronectin (red) and vitronectin (blue).

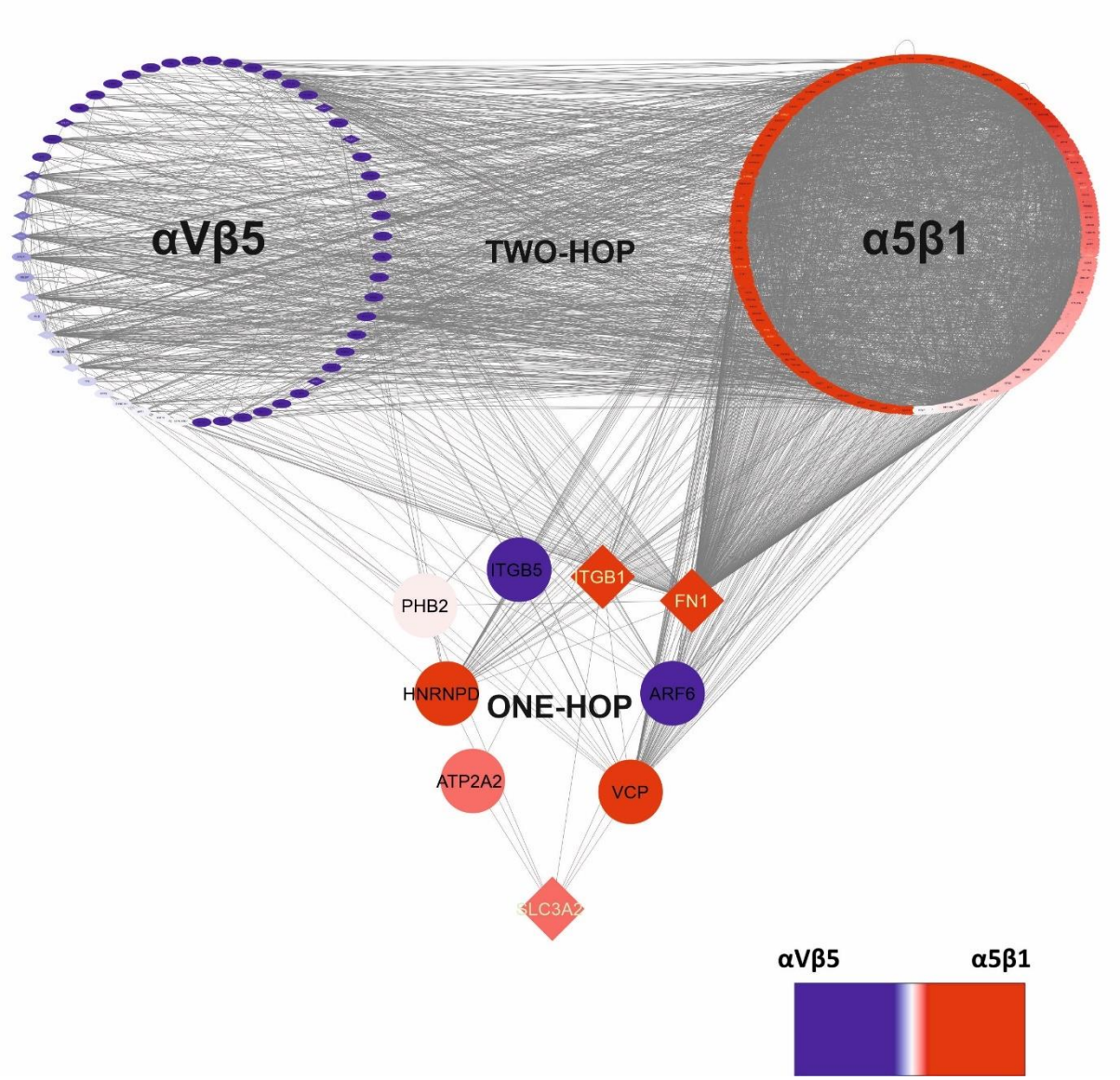

Figure 4.15: Network analysis of SLC3A2's one-hop and two-hop neighbours. The two-hop neighbours were classed into proteins that were enriched on the αVβ5 and α5β1 adhesome, with proteins identified with the GO terms Disease and Metabolism displayed within a diamond shape. Node colour blue and red correspond to >1.5-fold log2 enrichment Fibronectin (red) and vitronectin (blue).

4.3. Discussion

In this chapter, IAC isolated from iPSCs plated on vitronectin, fibronectin, ZTFN and ZT910 enabled the characterisation of the αVβ5, α5β1 and αVβ1 integrin adhesome in iPSCs. Functional enrichment analysis on proteins that were significantly enriched 1.5-fold provided insights into the nature of the integrin-specific stem cell adhesome compared to both the consensus and meta-adhesome. The consensus adhesome and meta-adhesome comprise a total of 60 and 2412 proteins respectively. Although the thresholded dataset identified 19 and 369 proteins belonging to the consensus and meta-adhesome respectively, the enrichment of these proteins varied between substrates. The characterisation of the consensus adhesome following the integration of proteomic analyses of isolated IACs from previous studies suggested that proteins within the consensus adhesome represented a core cell adhesion machinery that focused around four signalling axes, namely, 1) ILK–PINCH–kindlin, 2) FAK–paxillin, 3) talin–vinculin and 4) α-actinin–zyxin–VASP (Horton et al., 2015). Our dataset identified proteins that belonged to two of the four integrin downstream signalling axes; vinculin, talin, zyxin, VASP and α-actinin. This observation suggests that iPSCs are mediating downstream signalling through specific modules, however, since the four modules are interconnected, a comparative analysis of the different adhesome is required to determine their specificity within the stem cell adhesome.

Functional enrichment analysis showed that a total of 182, 56, 52 and 123 proteins were significantly enriched on fibronectin, vitronectin, ZTFN and ZT910 respectively. These data suggest the number of proteins differentially recruited to IACs is integrin-heterodimer specific, with α5β1-associated substrates fibronectin and ZT910 recruiting a greater number of proteins (182 and 123 respectively) compared to the αVβ5 and αVβ1-associated substrates

vitronectin and ZTFN (56 and 52 respectively). The α5β1-associated adhesome enriched on either fibronectin or ZT910 showed the highest level of protein similarity at 56%. This similarity suggests that the majority of proteins recruited to α5β1-associated adhesome are a consequence of α5β1 binding, irrespective of which RGD-containing substrate the receptor is engaging. However, the differences observed may be dependent on how the conformation of the RGD-motif on fibronectin vs ZT910 modulate the localisation and recruitment of downstream signalling proteins. Alternatively, the disparities may be due to differences in ligand structure, periodicity, or the presence/absence of other functional domains. For example, full-length fibronectin contains receptor-binding motifs for α4β1 integrin and heparan sulfate proteoglycans, such as syndecan-4, which are absent in ZT910 (Wolanska and Morgan, 2015).

Comparative analysis of enriched proteins reveals distinct differences in the adhesome composition between vitronectin, fibronectin, ZTFN and ZT910. The canonical consensus adhesome protein talin was enriched on α5β1 (fibronectin), αVβ1 (ZTFN) and α5β1 (ZT910). Talin interacts with the integrin β1 tail through the conserved membrane-proximal NPIY motif promoting integrin activation and linking the integrin to the actin cytoskeleton (Nieves et al., 2010). Although super-resolution of iPSC cornerstone adhesions has shown the presence of talin at high density (Stubb et al., 2019), we did not detect it as enriched on vitronectin, even though it was recruited in the integrin adhesion complex enrichment (Figure 4.3) (Stubb et al., 2019). Furthermore, vinculin was only enriched on α5β1-associated adhesome on fibronectin. This enrichment of α5β1-associated adhesome on fibronectin compared to the αVβ5-VIT, αVβ1-ZTFN and α5β1-ZT910 associated adhesome perhaps gives us an insight into the degree of vinculin-mediated bidirectional mechanotransduction. For example, traction

force and adhesion strength are enhanced upon vinculin binding to the talin tail (Dumbauld et al., 2013). These observations suggest that the greater force transmission observed on iPSCs plated on fibronectin (Figure 3.8C) may be a consequence of vinculin binding to talin. However, because vinculin is recruited to E-cadherin cell-cell contacts and αVβ5-VIT cell-matrix adhesions, the lack of enrichment of vinculin on vitronectin is likely a result of similar levels of vinculin enrichment on E-cadherin (Bays and DeMali, 2017b, Wayner et al., 1991).

4.3.1. Nuclear, Ribosomal and RNA binding proteins

A striking feature of the characterised adhesome is the presence of nuclear, ribosomal and RNA binding proteins in multiple GO terms including Post-translation Protein Modification, Metabolism of RNA and Metabolism of Proteins. Proteins identified within these GO terms are involved in the regulation of numerous aspects of gene expression including mRNA transcription, translation, transport, and processing. The characterisation of The Contaminant Repository for Affinity Purification (CRAPome) to classify proteins that represent genuine localised protein-protein interactions versus background contaminants, considered ribosomal proteins to be the most common family of contaminants (Mellacheruvu et al., 2013). However, there is increasing evidence that these nuclear, ribosomal and RNA binding proteins may possess a functional role localised at focal adhesion. The traditional view of ribosome function involves, either a ribosomal pool associated with the endoplasmic reticulum, where the localised translation of proteins occurs or the cytosol, where cytosolic proteins are synthesised (Willett et al., 2010). The localisation of ribosomes and mRNA at focal adhesions was first observed following the engagement of cells to ECM-coated microbeads (Chicurel et al., 1998). Paxillin, a focal adhesion protein interacts with PABPs during cell migration to facilitate the transport of mRNAs from the site of protein synthesis at the

endoplasmic reticulum to the lamellipodia (Woods et al., 2002). Furthermore, inhibiting this interaction perturbed cell spreading and migration on fibronectin (Woods et al., 2005). These results suggest that the recruitment of mRNA and RNA binding proteins convey a functional role in localising to IACs and regulating cell adhesion, spreading and migration (Humphries et al., 2015).

4.3.2. Metabolism

Another distinctive feature of the characterised adhesomes is the presence of proteins that regulate metabolism. Cells must coordinate numerous intercellular processes with their metabolism. When cells experience metabolic stress, which corresponds to low ATP levels because of inflammation, hypoxia, the availability of nutrients and increased energy demand, several sensors of metabolic sensors activate to ensure cell survival and homeostasis (Ata and Antonescu, 2017). These sensors include mTOR (mammalian target of rapamycin), AMPK (AMP-activated protein kinase) and HIF (hypoxia-inducible factor) which collectively integrate stimuli of dynamic changes in environmental conditions to coordinate responses to metabolic stress (Ata and Antonescu, 2017). Compared to normal somatic cells, cancer cells have a higher rate of proliferation, resulting in high demand for metabolites. As a result, cancer cells shift from oxidative phosphorylation to aerobic glycolysis for ATP production (Ata and Antonescu, 2017). This is accompanied by increased expression of glucose transporters and increased glucose consumption to meet the increased metabolic demand. Similarly, pluripotent stem cells utilize glycolysis despite sufficient oxygen (Tsogtbaatar et al., 2020). This process enables intermediates of glycolysis to rapidly synthesise lipids and nucleotides (Tsogtbaatar et al., 2020). These metabolic processes were traditionally thought to be primarily mediated within the cytoplasm and mitochondria, but our integrative proteomic

analysis of iPSCs on cultured substrates that engage distinct integrin heterodimers suggests the presence of important underappreciated protein clusters that regulate metabolism within the adhesome in an integrin-dependent manner. Interestingly, BioID proximity labelling of mTOR components combined with proteomics suggests that in nutrient-replete conditions mTORC1 localises near focal adhesion components such as talin, paxillin and VASP (Rabanal-Ruiz et al., 2021). Furthermore, increased mTORC1 activity was observed at the cell edge in response to amino acid or growth factor stimulation (Rabanal-Ruiz et al., 2021). Disruption of focal adhesion formation through talin knockdown suppressed mTORC1 activation, growth factor signalling and amino acid uptake (Rabanal-Ruiz et al., 2021). These results suggest that focal adhesion components modulate amino acid uptake and growth factor signalling to co-ordinate downstream mTORC1 signalling responses. SLC3A2 has been shown to act as an important regulator of metabolic processes and amino acid uptake (Nicklin et al., 2009). These data, when considered in the context of the present study, raise the intriguing possibility that integrin-mediated regulation of SLC3A2 may contribute to metabolic programming.

4.3.3. One and two-hop neighbours of SLC3A2

To understand the potential involvement of SLC3A2 in integrin-mediated functions, a one-hop and two-hop SLC3A2 network was generated. A total of 8 and 343 proteins were identified to be enriched as one-hop and two-hop neighbours of SLC3A2, respectively. The one-hop neighbours of SLC3A2 were integrin β1, ARF6, PHB2, HNRNPD, ATP2A2, VCP and FN. ARF6 (ADP-ribosylation factor 6) is a small GTPase that following activation modulates membrane trafficking (Donaldson and Jackson, 2011) (Figure 4.15). ARF6 has been shown to associate with endosomal membranes and mediates their recycling to the plasma membrane (Donaldson and Jackson, 2011). This enables re-localisation and recruitment of proteins such

as integrin β1 that regulate cell adhesion and migration to the plasma membrane (Donaldson and Jackson, 2011). In several cell systems, modulation of ARF6 activity enables co-ordinated delivery of αVβ3 and α5β1 to the cell-matrix interface to regulate adhesion dynamics and migration (Morgan et al., 2013). Transitional endoplasmic reticulum ATPase (TER ATPase) or Valosin-containing protein (VCP) belongs to the ATPases Associated with diverse cellular Activities (AAA) proteins that are involved in the regulation of several cellular processes including protein degradation, vesicle transport and mitochondria quality control (Bastola et al., 2016). Loss of VCP is associated with induction of endoplasmic reticulum stress, that in a sustained state, leads to cell death (Bastola et al., 2016).

Post-translational regulation and stability of mRNAs by RNA binding proteins modulate gene expression. HNRNPD is an adenylate-uridylate (AU)-rich element [ARE]-binding protein which plays an important role in regulating the mRNA stability of several genes that regulate cell proliferation, cell cycle and cell survival. HNRNPs have been shown to bind to genes and regulate the expression of integrin/extracellular genes (Li et al., 2021). Furthermore, integrin α6β1 interacts with HNRNP-K during oligodendrocyte differentiation and myelination (Laursen et al., 2011). In the absence of HNRNPs, stem cells have been shown to detach from the dermis as a result of reduced integrin/ECM expression (Li et al., 2021). Prohibitin 2 (PHB2) is a multifunctional protein that is involved in the regulation of various cellular processes including signal transduction, gene expression and metabolism, which is mediated by its localisation to the nucleus, the endoplasmic reticulum and the plasma membrane. (Wu et al., 2021). In the mitochondria, PHB2 formed complexes with PHB1 to maintain the structure of mitochondria. Furthermore, PHBs guard newly synthesised proteins from degradation alongside VCP and promote mitochondrial protein synthesis (Thuaud et al., 2013). At the

plasma membrane. PHB2 has been shown to interact with focal adhesion protein Ras Suppressor 1 (RSU1) to play a role in inhibiting ERK signalling following cell-extracellular matrix detachment (Wang et al., 2021b). ATPA2 also known as SERCA2 belongs to a family of ATPase enzymes that mediate the transport of Ca^{2+} ions from the cytosol to the endoplasmic reticulum (Li et al., 2017). Mutation of ATP2A2 leads to the development of Darier's disease that is characterised by the loss of epidermal cell-cell adhesions and abnormal keratinization (Li et al., 2017).

In the present study, combinatorial analysis of protein-protein interaction networks of proteins enriched within metabolism and disease identified SLC3A2 as a putative node that may integrate stem cell signalling and metabolism in an integrin-dependent manner. This bifunctional role of SLC3A2 is hypothesised based on the ability of the SLC3A2 heavy chain to bind integrin β1 and the light chain comprising an amino acid transporter. In the next chapter, further investigations were carried out to determine the role SLC3A2 plays in integrating stem cell signalling and metabolism in an integrin-dependent manner.

5. THE ROLE OF SLC3A2 IN INTEGRIN SIGNALLING AND METABOLISM

5.1. Introduction

Solute Carrier Family 3 Member 2 (SLC3A2, also known as CD98hc and 4F2hc) is a bifunctional type II transmembrane protein that was originally identified in T-cells (Haynes et al., 1981). SLC3A2 is covalently linked to L-type amino acid transporters (such as LAT1) which mediates the transport of large neutral amino acids, hormones, and drugs across the plasma membrane in a sodium-independent manner (Chiduza et al., 2019). Expression of the SLC3A2-LAT1 complex is critical in foetal development, where it plays an essential role in regulating the uptake of amino acids and hormones (Aiko et al., 2014). In cancer, the transport activity of the SLC3A2-LAT1 complex is pro-tumorigenic and is abnormally detected in an increasing number of tumours. SLC3A2 knockout restricted the formation of teratocarcinoma in mouse embryonic stem cells (Feral et al., 2005).

SLC3A2 possesses two distinct functions: firstly, SLC3A2 regulate the expression and localization of the light chain counterpart to regulate amino acid transport, and secondly, SLC3A2 can associate and regulate the function of specific integrin heterodimers (Feral et al., 2005). For example, SLC3A2 interacts with integrins β1 and β3 to mediate integrin activation (Sun et al., 2014). Furthermore, in invasive trophoblast, SLC3A2 displayed an association with αVβ3 and αVβ3-associated IAC proteins paxillin, vinculin, and focal adhesion kinase (FAK) (Kabir-Salmani et al., 2008). Each aspect of the SLC3A2 function is dependent on distinct domains within SLC3A2 (Feral et al., 2005).

Cryo-electron microscopy has provided insights into the heterodimeric architecture of the SLC3A2-LAT1 complex (Lee et al., 2019b). The SLC3A2 heavy chain comprises a large extracellular domain, a transmembrane, and a cytoplasmic domain. The large extracellular

domain is positioned above the transmembrane domain of LAT1 and interacts through a short disulfide bond (Lee et al., 2019b). Furthermore, electrostatic interactions between the positively charged SLC3A2 and negatively charged LAT1 have been proposed to further stabilize the interaction between both subunits (Lee et al., 2019b). The generation of SLC3A2 chimaeras that inhibit the function of the extracellular, transmembrane, and cytoplasmic domains individually were employed to study the effect of distinct SLC3A2 domains on amino acid transport and integrin function (Fenczik et al., 2001). These studies revealed that the transmembrane and cytoplasmic domains were required for regulating integrin function, and the extracellular domain is required for regulating amino acid transport (Fenczik et al., 2001).

The evidence of the bifunctional nature of SLC3A2 in conjunction with the proteomic IAC analyses in the previous chapter (Figure 4.15) suggests that SLC3A2 may play an essential role in integrating cell metabolism and integrin function. SLC3A2 regulates tumorigenesis by modulating integrin-mediated mechanotransduction (Estrach et al., 2014). For example, a stiffer and more organised microenvironment promotes tumour formation and invasiveness. However, SLC3A2-deleted skin displayed low Pa values indicating a softer tissue (Estrach et al., 2014). Furthermore, knockdown of the SLC3A2 heavy chain has been shown to protect against Ras-driven skin carcinogenesis by modulating the rigidity of the tumour microenvironment (Estrach et al., 2014). For example, SLC3A2 heavy chain knockdown decreased epidermal tissue stiffness, which was associated with the disorganised collagen-rich dermis and abnormal fibronectin deposition (Estrach et al., 2014). These results suggest that SLC3A2 regulate integrin mechanosensing to drive tumorigenesis.

Fibroblasts with SLC3A2 knockdown failed to spread on fibronectin-coated gels with stiffness of 3.5kPa. However, normal spreading was partially restored following adhesion of fibroblasts

to stiffer substrates, and then fully restored following expression of the full-length SLC3A2 heavy chain (Estrach et al., 2014, Boulter et al., 2018). This lack of cell spreading was accompanied by a reduction in the expression of total AKT, phosphorylated FAK, and proteins that are active promoters of cell proliferation, survival, and invasion. Furthermore, SLC3A2 knockdown *in vivo* is associated with reduced RhoA/ROCK signalling and transcription of genes regulated by YAP/TAZ (Estrach et al., 2014). These results suggest that SLC3A2 regulates integrin signalling to modulate cell behaviour.

The SLC3A2/LAT1 complex regulates the bi-directional transport of amino acids to modulate autophagy and mTOR activation. Cells within an amino acid-rich environment mediate the activation of mTOR, which promotes translation and inhibits autophagy (Mizushima et al., 2008). However, when the availability of amino acids is a limiting factor, mTOR is inhibited and autophagy recycles intracellular molecules to provide an alternative source of amino acids (Mizushima et al., 2008). Consequently, the SLC3A2/LAT1 complex directly regulates mTOR activity. For example, the transport of L-glutamine by another transporter SLC1A5 (ASCT2) mediates the bidirectional extracellular efflux of L-glutamine and the intracellular influx of L-Leucine through the SLC3A2/LAT1 complex (Nicklin et al., 2009). This influx of leucine was associated with phosphorylation of ribosomal S6 protein and mTOR activation (Nicklin et al., 2009). Knockdown of either SLC1A5, SLC7A5 or SLC3A2 inhibits phosphorylation of ribosomal S6 protein, which was similar upon mTOR inhibition (Nicklin et al., 2009). These results suggest that SLC3A2/LAT1 complex indirectly regulates mTOR activation.

SLC3A2 regulates the availability of amino acids and nucleotides for cell cycle progression (Cano-Crespo et al., 2019). Ablation of SLC3A2 induced a significant reduction in the intracellular nucleotide pool resulting in increased replicative cell stress and a reduced rate

of mitosis (Cano-Crespo et al., 2019). These results suggest an important role of the SLC3A2/LAT1 complex in mediating amino transport and modulating mTOR activity to regulate various cellular processes including cell cycle progression. Furthermore, SLC3A2 has been shown to associate with Glucose transporter 1 (GLUT1) at the plasma membrane (Ohno et al., 2011). Overexpression of SLC3A2 increased intracellular GLUT1 protein and was associated with increased glucose uptake, while SLC3A2 knockdown was associated with a marked reduction in GLUT1 and glucose uptake (Ohno et al., 2011). These results suggest that SLC3A2 has an additional role in regulating glucose metabolism.

Metabolomic profiling of SLC3A2 mutants and SLC3A2 null cells re-expressing SLC3A2 revealed that the total expression of 238 metabolites was significantly altered (Boulter et al., 2018). These metabolites primarily belonged to the amino acid and sphingolipid metabolism family. Subsequent downstream analysis revealed that SLC3A2 knockdown decreased the availability of sphingolipid at the plasma membrane, which inhibited normal membrane recruitment and activation of proteins that play an important role in force transduction such as Src kinases and GEF-H1 (Boulter et al., 2018). Furthermore, integrin recycling to the plasma membrane was slower than SLC3A2 null cells (Boulter et al., 2018). These results suggested a novel mechanism of SLC3A2 regulating integrin mechanosensing and cell metabolism via a sphingolipid biosynthesis pathway.

In the previous chapter, proteomic analysis of IAC proteins that were statistically enriched 1.5-fold on αVβ5-VIT and α5β1-FN adhesome identified SLC3A2 as a putative node that may potentially integrate stem cell signalling and metabolism in an integrin-dependent manner. To assess the bifunctional role of SLC3A2 in integrin mechanosensing and cell metabolism, downstream analysis aimed to determine if SLC3A2 associates with αVβ5-VIT and α5β1-FN in

an integrin-specific manner. Following this, traction force microscopy was employed to assess the effect of SLC3A2 on mechanotransduction. To assess the effect of SLC3A2 on metabolism, expression of metabolic proteins, oxygen consumption rate, extracellular acidification rate and the total levels of ATP were assessed of iPSC plated on vitronectin and fibronectin.

5.2. Results

5.2.1. SLC3A2 localizes to α5 integrin focal adhesions

SLC3A2 associates with specific integrin heterodimers (Boulter et al., 2018, Fenczik et al., 2001, Sun et al., 2014, Veettil Mohanan et al., 2008). To determine if SLC3A2 regulates integrin mechano-signalling and metabolism in an integrin-dependent manner, immunofluorescence of SLC3A2 and integrin α5 and αV subunit was assessed on iPSC plated on fibronectin and vitronectin respectively. The immunofluorescence data showed that SLC3A2 localised with integrin α5 (corresponding to the recruitment of α5β1) at IACs (Figure 5.1). Whereas SLC3A2 did not co-localize with integrin αV (corresponding to the recruitment of αVβ5) at IACs (Figure 5.1). This co-localization was confirmed with the plot profile that quantified the integrin α5 and SLC3A2, and integrin αV and SLC3A2 gray values in fibronectin and vitronectin respectively (Figure 5.1). These data suggest that SLC3A2 is enriched in integrin α5β1-mediated fibronectin adhesions, but not integrin αV-mediated adhesion on vitronectin.

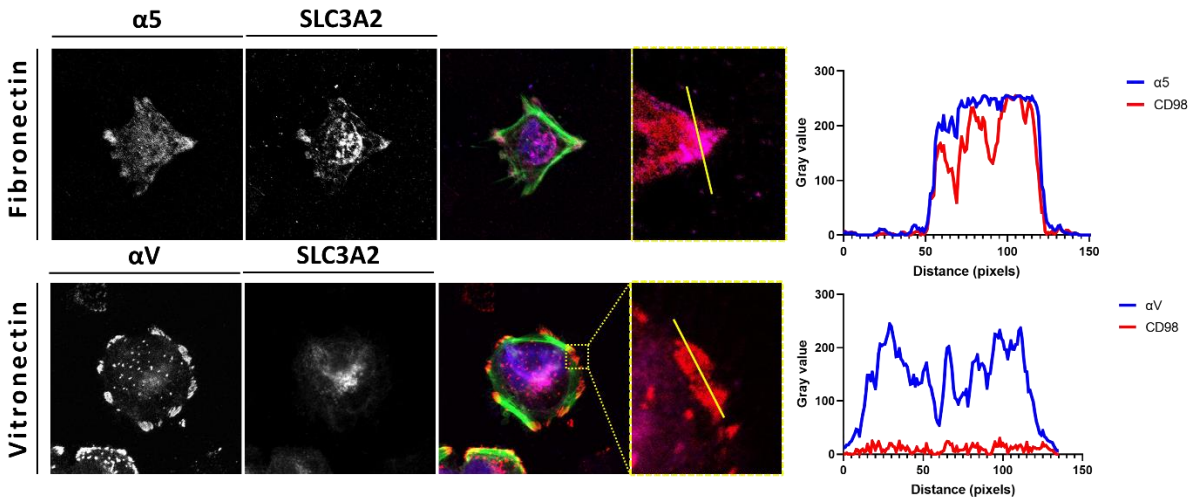

Figure 5.1: **SLC3A2 localises to integrin α5 but not integrin αV.** Representative immunofluorescence and intensity profile plots of iPSC plated on fibronectin and vitronectin, and probed for SLC3A2 and integrins α5, αV. Intensity plot profiles were generated and measured across a line of 133 pixels that span across focal adhesion structure labelled by integrin subunit α5 and αV (red) and SLC3A2 (magenta).N=1 and n=10.

5.2.2. Traction force microscopy and YAP localization

SLC3A2 has been linked to the regulation of integrin mechano-signalling (Boulter et al., 2018). Based on this observation, the role of SLC3A2 in regulating mechanotransduction in αVβ5-mediated adhesions (vitronectin) and α5β1-mediated adhesions (fibronectin) was assessed using traction force microscopy. To determine the effect of SLC3A2 in regulating integrin mechanotransduction, force magnitude of siRNA control knockdown and SLC3A2 siRNA-depleted iPSCs (~92% reduction in SLC3A2 expression following knockdown (Supplementary Figure 6)) was assessed following plating on 5kPa hydrogels coated with vitronectin and fibronectin (Figure 5.2). No significant difference was observed between vitronectin siRNA CTRL vs vitronectin SLC3A2 siRNA, and fibronectin SiRNA CTRL vs fibronectin SLC3A2 siRNA (Figure 5.2A). These results suggest that SLC3A2 does not modulate force transmission in an integrin-dependent manner. Additionally, to determine if SLC3A2 plays a role in regulating downstream mechano-signalling of transcriptional activator in αVβ5-mediated adhesions (vitronectin) and α5β1-mediated adhesions (fibronectin), the nuclear/cytoplasmic localization of YAP was assessed on siRNA control and SLC3A2 siRNA iPSCs following plating on 5kPa polyacrylamide gels coated with vitronectin and fibronectin (Figure 5.2B). No significant difference was observed between vitronectin siRNA CTRL vs vitronectin SLC3A2 siRNA, and fibronectin siRNA CTRL vs fibronectin SLC3A2 siRNA (Figure 5.2B). These results suggest that SLC3A2 does not modulate integrin-mediated mechanotransduction or mechano-signalling in an integrin-dependent manner.

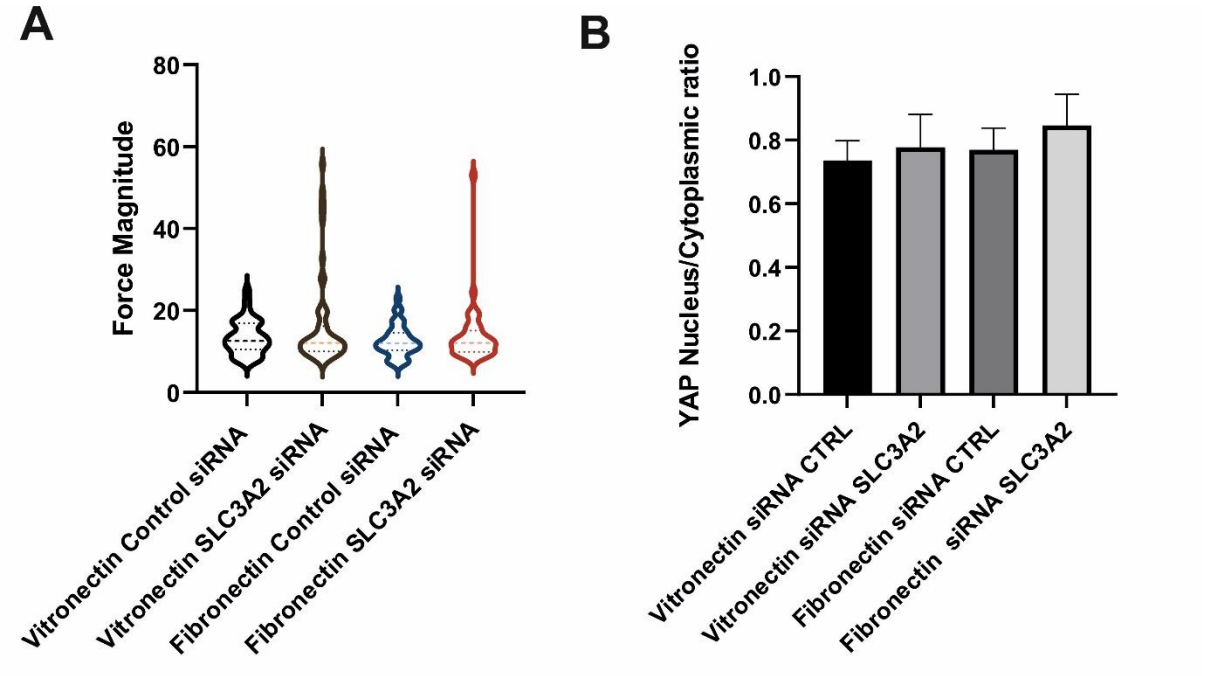

Figure 5.2: SLC3A2 knockdown displays no difference in force transmission and nuclear YAP localisation. Traction Force Microscopy and YAP localization of iPSCs on 5kPa rigidity. iPSCs plated on vitronectin (5µg/mL) and fibronectin (10µg/mL) for 4 hours. The cells were plated on the rigidity of 5kPa. (A) Quantitative representation of force magnitude of iPSCs at 5kPa on vitronectin and fibronectin. n=30-62 cells per condition. (B) Quantitative representation comparing YAP localization of iPSCs plated on vitronectin and fibronectin at 5kPa. n=40-50 cells per condition Kruskal-Wallis with Dunn's post-hoc test employed, and data shown are representative of three independent experiments.

5.2.3. The effect of SLC3A2 on the expression of metabolic proteins

SLC3A2 regulates the bi-directional transport of amino acids to modulate mTOR activation. To assess the effect of substrate/integrin heterodimer-specificity on mTOR signalling, total cell lysates of iPSCs grown on vitronectin and fibronectin were obtained to quantify the basal expression of mTOR and, proteins upstream (AKT, and pAKT) and downstream of mTOR (S6 and pS6). While the data did not reach statistical significance across three biological replicate experiments, there was a trend toward an elevated expression of total mTOR and S6 in iPSCs plated on fibronectin, when compared with vitronectin (Figure 5.3). Whereas no change in total AKT expression was noted between the two ligands (Figure 5.3). Despite the apparent change in S6 expression, the proportion of S6 that was phosphorylated was unchanged between the two conditions (Figure 5.3). Likewise, no reproducible changes in AKT phosphorylation were detected (Figure 5.3).

Secondly, to determine the role of SLC3A2 in regulating mTOR signalling, total cell lysates of iPSC siRNA control and siRNA SLC3A2 grown on vitronectin and fibronectin were obtained to quantify the expression of mTOR and, proteins upstream (AKT, and pAKT) and downstream of mTOR (S6 and pS6). No change in total AKT and S6 expression was noted between the two ligands (Figure 5.4). Despite no change in AKT expression, the proportion of AKT that was phosphorylated, was elevated in siRNA control knockdown cells on fibronectin compared to the other conditions (Figure 5.4). However, elevated S6 phosphorylation was detected in all conditions except siRNA control knockdown cells on vitronectin (Figure 5.4). While the data did not reach statistical significance across three biological replicate experiments again, there was a trend toward the reduced expression of total mTOR in the siRNA control knockdown and siRNA SLC3A2-depleted cells plated on fibronectin compared to vitronectin (Figure 5.4).

Interestingly, the trend observed in the expression of total mTOR, S6, and AKT expression on vitronectin and fibronectin is not translated to the siRNA control iPSC plated on vitronectin and fibronectin (Figure 5.4). This may be due to the inherent variability of these experiments and the need to perform further independent biological replicates. These results suggest that the process of nucleofection of iPSCs is perturbing protein expression on top of the effects of siRNA oligonucleotides that are introduced.

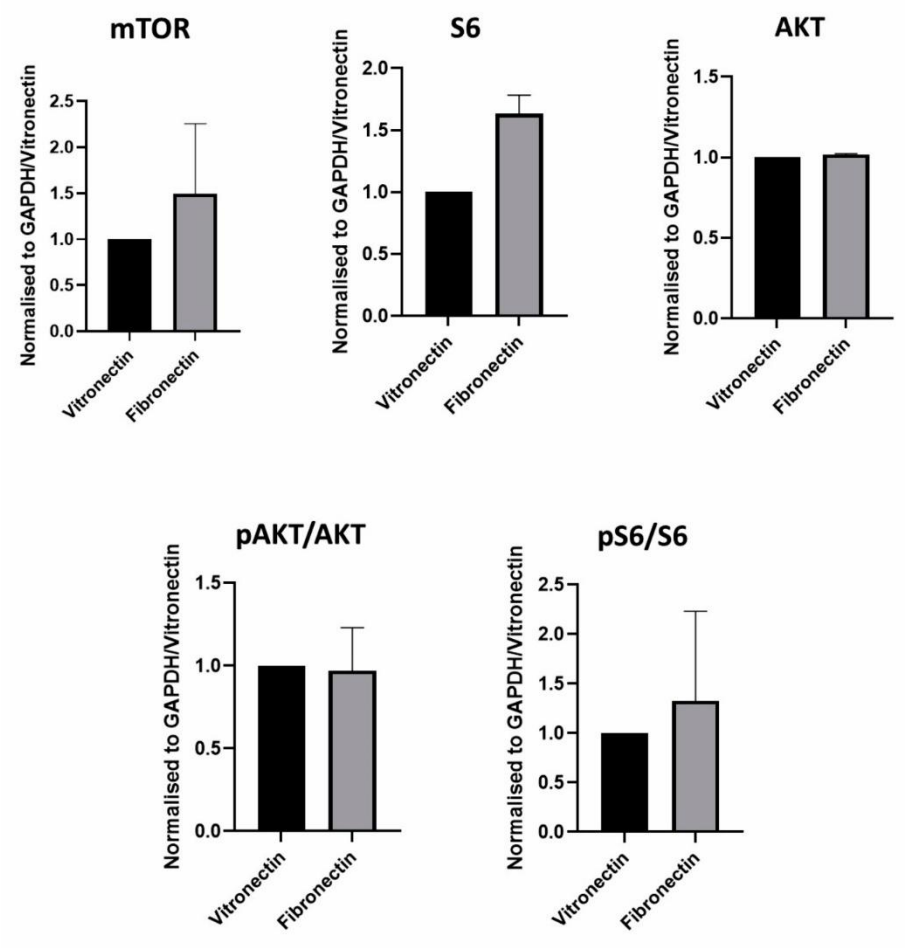

Figure 5.3: iPSCs show no difference in the expression of metabolic proteins mTOR, S6, pS6, AKT, and pAKT on vitronectin and fibronectin. Immunoblotting of iPSCs plated on vitronectin and fibronectin for 4 hours. Protein expression was normalized to GAPDH and then vitronectin protein expression. Data are shown as mean ± SEM of three independent experiments, unpaired t-test with a Welch's correction.

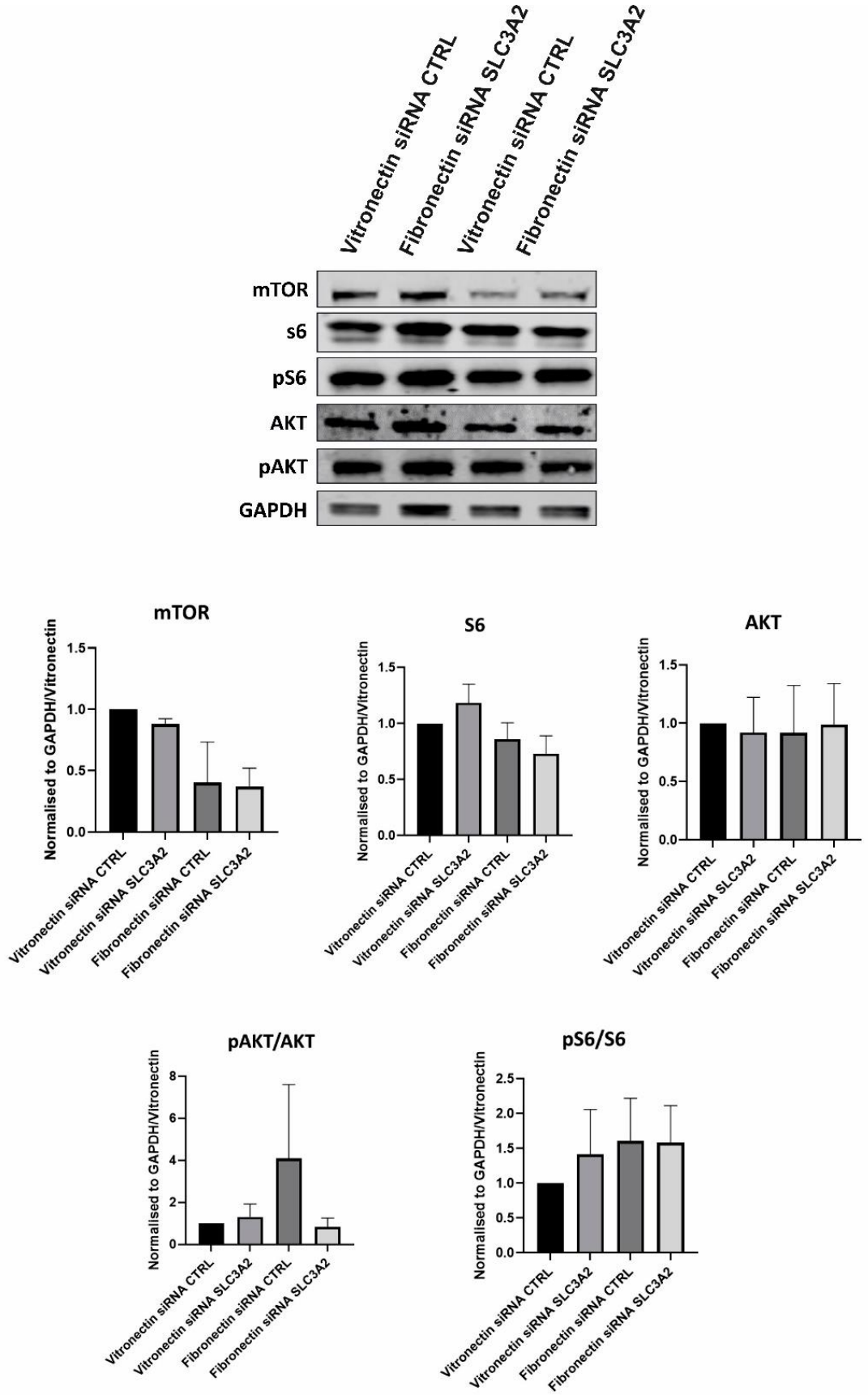
Vitronectin siRNA CTRL
Fibronectin siRNA SLC3A2
Vitronectin siRNA CTRL
Fibronectin siRNA SLC3A2
mTOR
s6
pS6
AKT
pAKT
GAPDH
mTOR
S6
AKT
pAKT/AKT
pS6/S6
Normalised to GAPDH/Vitronectin
Vitronectin siRNA CTRL
Vitronectin siRNA SLC3A2
Fibronectin siRNA CTRL
Fibronectin siRNA SLC3A2

Figure 5.4: iPSCs show no difference in the expression of metabolic proteins mTOR, S6, pS6, AKT, and pAKT upon SLC3A2 knockdown on vitronectin and fibronectin. Expression of metabolic proteins mTOR, S6, pS6, AKT and pAKT on iPSC siRNA control and siRNA SLC3A2. Immunoblotting of metabolic protein mTOR, S6, pS6, AKT and pAKT expression of single iPSC siRNA control and siRNA SLC3A2 plated on vitronectin and fibronectin for 4 hours. Protein expression was normalized to GAPDH and then vitronectin protein expression. Kruskal-Wallis with Dunn's post-hoc test was employed, and data are shown as mean ± SEM of three independent experiments.

5.2.4. Effect of SLC3A2 on glycolysis and mitochondrial respiration

Cells primarily use either glycolysis or OXPHOS to generate ATP to drive various intracellular processes. Therefore, a seahorse assay was employed to assess cellular oxygen consumption rate (OCR) and proton excretion (ECAR), which indicate mitochondrial respiration and glycolysis respectively. Control siRNA and SLC3A2-targeting siRNA expressing iPSCs were plated on fibronectin and vitronectin for 4 hours and treated sequentially with oligomycin, Carbonyl cyanide-p-trifluoromethoxyphenylhydrazone (FCCP) and rotenone to modulate different aspects of glycolysis and mitochondrial oxidative phosphorylation. While the data was a single experiment, substrate-dependent modulation of OCR and ECAR was observed in iPSCs siRNA control and SLC3A2-targeting siRNA cells. Furthermore, no effect was observed on OCR and ECAR activity on vitronectin (Figure 5.5). However, iPSCs siRNA control and SLC3A2-targeting siRNA in the presence of LAT1 inhibitor displayed a substantial reduction in OCR and ECAR activity on fibronectin (Figure 5.5). These data suggest that both SLC3A2 and LAT1 may influence mitochondrial respiration and glycolysis in a substrate/integrin-dependent manner. iPSCs siRNA control on fibronectin and SLC3A2-targeting siRNA on vitronectin showed comparable OCR and ECAR activity, however, SLC3A2-targeting siRNA on iPSCs on fibronectin displayed a substantial reduction in OCR and ECAR activity compared to iPSCs siRNA control on fibronectin (Figure 5.5). These data suggest that knockdown of SLC3A2 in iPSCs on fibronectin which recruits α5β1 has a greater effect in modulating OCR and ECAR activity compared to iPSCs on αVβ5-engaging vitronectin (Figure 5.5). SLC3A2-targeting siRNA on iPSCs that were treated with LAT1 inhibitor on fibronectin displayed a reduction in OCR activity compared to the other conditions, however, iPSC siRNA control treated with LAT1 inhibitor showed a substantial reduction in OCR and ECAR activity on vitronectin and fibronectin compared to iPSC siRNA control with no LAT1 treatment (Figure 5.5). These data

suggest that the effect of LAT1 inhibition may be more sensitive to modulation in glycolysis compared to mitochondrial respiration independent of substrate/integrin recruitment. Lastly, SLC3A2-targeting siRNA in iPSCs that were treated with LAT1 inhibitor showed a substantial reduction in OCR and ECAR activity on fibronectin compared to the other conditions (Figure 5.5). Taken together, these results suggest that SLC3A2 and LAT1 influence mitochondrial respiration and glycolysis in an integrin-dependent manner.

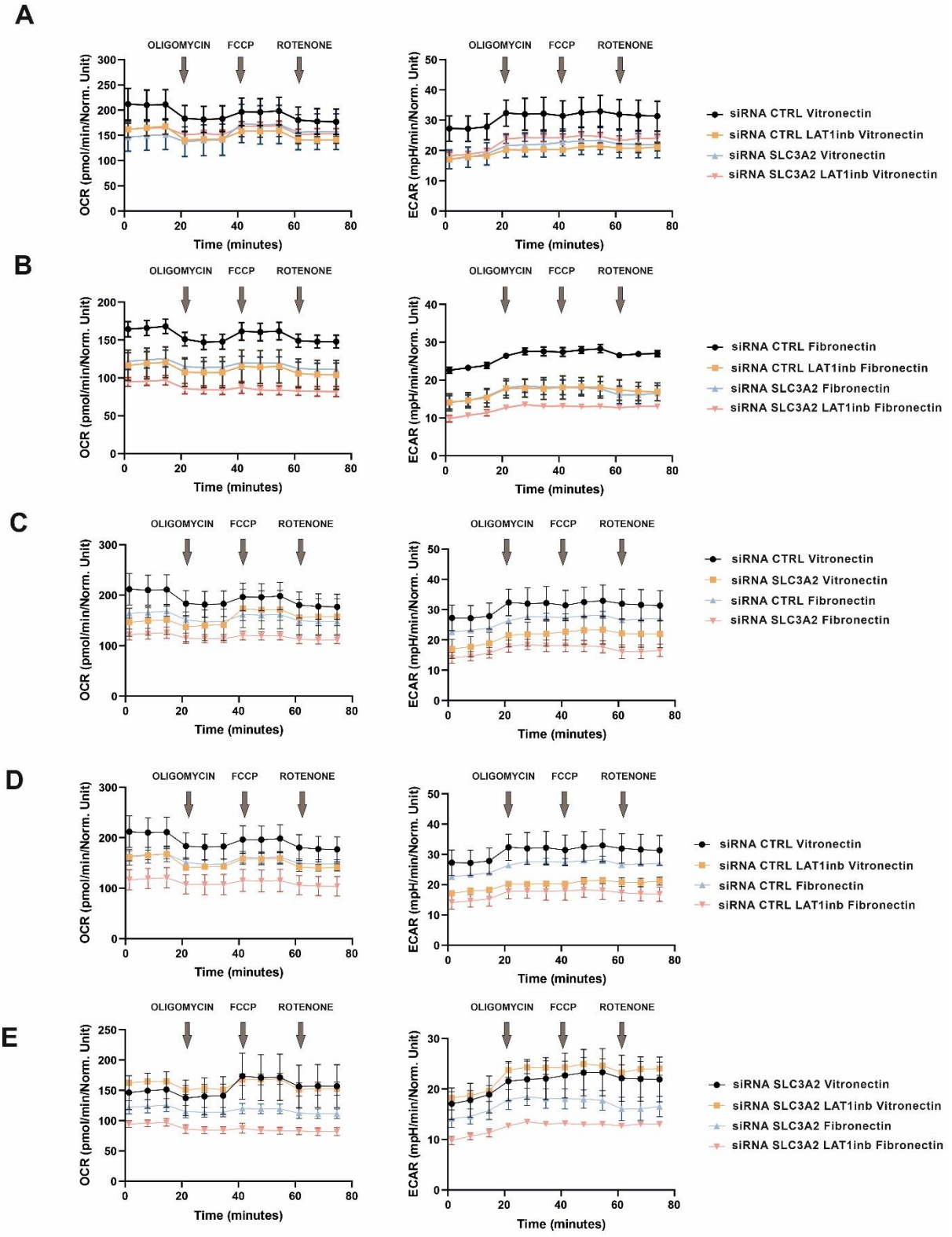

Figure 5.5: Seahorse assay: iPSCs display substrate/integrin heterodimer-specific difference in intracellular ATP upon perturbation of SLC3A2 and LAT1. Seahorse assay of iPSC siRNA control and siRNA SLC3A2 plated on vitronectin and fibronectin for 4 hours. Data are shown as mean ± SEM of technical replicates from a single experiment.

5.2.5. Effect of SLC3A2 on intracellular ATP

The primary output of glycolysis and oxidative phosphorylation is the production of ATP. Therefore, quantification of ATP levels conveys the degree of cellular metabolic activity. To assess the effect of SLC3A2 and LAT1 on the overall metabolic state, CellTitre-Glo cell viability ATP assay was employed to determine the level of ATP thereby assessing the overall metabolic state of iPSCs. siRNA control and siRNA SLC3A2 iPSCs were plated on fibronectin and vitronectin for 4 hours.

The analysis of the data showed no significant difference in ATP levels between iPSC siRNA control and iPSC siRNA SLC3A2 plated on fibronectin or vitronectin siRNA control and siRNA SLC3A2 (Figure 5.6). The ATP levels of siRNA SLC3A2 with LAT1 treatment plated on fibronectin were significantly reduced compared to iPSC siRNA control on fibronectin, however, there was no significant difference in ATP levels of iPSCs siRNA control with LAT1 treatment on fibronectin compared to iPSC siRNA control on fibronectin (Figure 5.6). The ATP levels of iPSCs siRNA control and siRNA SLC3A2 treated with LAT1 on fibronectin and, iPSCs siRNA SLC3A2 treated with LAT1 were significantly reduced compared to iPSCs siRNA control plated on vitronectin (Figure 5.6). Furthermore, ATP levels of iPSC siRNA SLC3A2 treated with LAT1 plated on vitronectin were significantly reduced on iPSC siRNA control plated on vitronectin. These results suggest that on fibronectin, a combinatorial knockdown/inhibition of SLC3A2/LAT1, and LAT1 inhibition alone significantly reduces ATP levels compared to iPSCs siRNA control on both fibronectin and vitronectin. However, on vitronectin the combinatorial knockdown of SLC3A2 and inhibition of LAT1 is required to reduce ATP levels compared to iPSCs siRNA control on vitronectin.

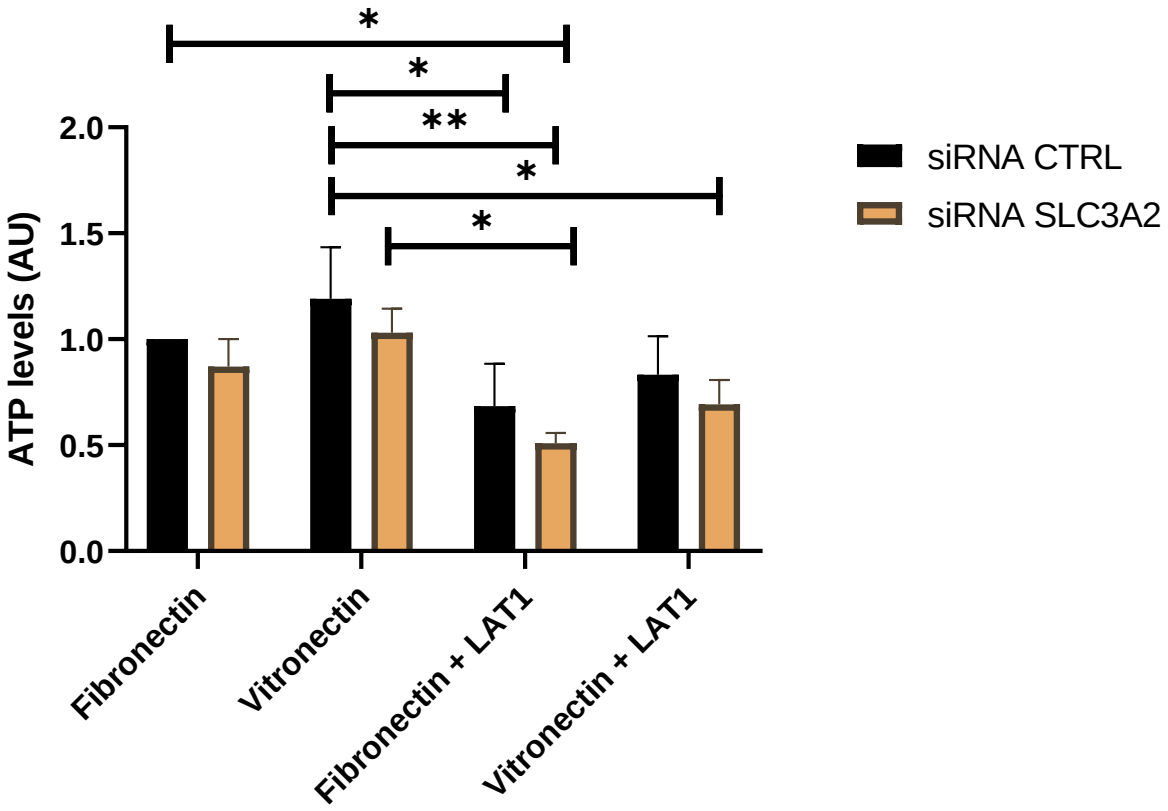

Figure 5.6: iPSCs display substrate/integrin heterodimer-specific difference in intracellular ATP upon perturbation of SLC3A2 and LAT1. Cell-titre Glo ATP assay of iPSC siRNA control and siRNA SLC3A2 plated on vitronectin and fibronectin for 4 hours. Luminescence was normalized to fibronectin siRNA control luminescence following subtraction of basal ATP luminescence induced by 10µM oligomycin treatment. Data are shown as mean ± SEM of three independent experiments. Two-way ANOVA with Tukey's post-hoc test *$p<0.05$ and **$p<0.01$.

5.3. Discussion

SLC3A2 has been identified as a potential novel mediator of metabolic regulation in an integrin heterodimer-dependent manner. In our study, the immunofluorescence dataset revealed that SLC3A2 localizes to α5β1-mediated adhesion on fibronectin, but not αVβ5-mediated adhesions on vitronectin. Reciprocal immunoprecipitation experiments demonstrated that SLC3A2 constitutively and specifically associates with β1 integrins (Kolesnikova et al., 2001). These experiments showed specific SLC3A2 co-localisation with integrins α2β1, α3β1, α5β1 and α6β1, but not α4β1 (Kolesnikova et al., 2001). To determine if the integrin α chain determined integrin-SLC3A2 association, immunoprecipitation experiments were carried out with wild-type α3 and α3-deficient cells (Kolesnikova et al., 2001). However, SLC3A2 was shown to associate with β1 integrins equally well in both conditions. Within the extracellular domain, SLC3A2 possesses two cysteines (C109S and C330S) (Kolesnikova et al., 2001). Mutational immunoprecipitation assays of cysteine to serine at position 109 (C109S) and cysteine to serine at position 330 (C330S) showed that mutation of C109S alone, or in combination with C330S inhibited the formation of stable heterodimers and translated to reduced amino acid transport (Kolesnikova et al., 2001). However, these mutations showed no significant observable changes in the ability of SLC3A2 to associate with β1 integrins (Kolesnikova et al., 2001). Although mutation of C109S and C330S leads to the covalent dissociation of the heavy chain and light chain, these chains can still interact through non-covalent interactions (Pfeiffer et al., 1998). For example, mutation of C109S mediated surface expression of the light chain and displayed amino transport across the plasma membrane, although at a reduced rate (Pfeiffer et al., 1998). This observation suggests that the association between the SLC3A2 heavy and light chain is not necessary for the interaction of the SLC3A2 heavy chain with β1 integrins. However, more work is needed

in light of the work in this thesis, to understand the intrinsic characteristics of both β1 and β5 integrins that mediate integrin SLC3A2 co-localization specificity, which may ultimately provide insights into SLC3A2 integrin-dependent function.

Previous studies have shown the role of SLC3A2 in regulating mechanotransduction and metabolism. To this end, traction force microscopy, YAP localization, and expression of metabolic proteins were assessed. However, no significant differences were observed in force transduction, the localization of YAP and expression of metabolic proteins in both iPSC siRNA control and siRNA SLC3A2 However, the same trends observed when assessing traction force and expression of metabolic proteins between wild type iPSCs were not observed on iPSC control siRNA control when plated on fibronectin and vitronectin. These results suggested that the process of nucleofection of iPSC which introduced both siRNA control and siRNA SLC3A2 may have negatively influenced iPSC function independent of the effects of the siRNA alone. Interestingly, the luminescence dataset of un-transfected iPSC and iPSC siRNA control showed an increase in raw luminescence of iPSC siRNA control plated on both fibronectin and vitronectin compared to the untransfected iPSCs (Supplementary Figure 7). These results also suggest that the process of nucleofection mediates significant intracellular metabolic changes that may influence a range of cellular processes. Nucleofection of cells is used widely in many research laboratories to introduce molecules that do not normally pass through the plasma membrane including RNA and fluorescent dyes (Grys et al., 2017). However, difficulties have been observed in obtaining reproducible results. The lack of reproducibility can be attributed to the effects of nucleofection, which include temperature changes mediated by the flow of current in the solution, changes in the pH associated with transfection reagent, and the formation of substances that are toxic to the cells (Grys et al., 2017). These cell changes can

mediate abnormal lipid peroxidation, mitochondrial disruption, ATP depletion, and damage membrane-embedded proteins (Batista Napotnik et al., 2021).

CellTitre-Glo cell viability ATP assay was employed to determine the levels of ATP to get a picture of the overall metabolic state of iPSCs. These results showed that when comparing fibronectin and vitronectin, knockdown of SLC3A2 and inhibition of LAT1 (SLC3A2 heavy and light chain) reduced cellular ATP production compared to siRNA control. However, on fibronectin LAT1 inhibition alone is sufficiently reduced cellular ATP production. These results suggest that LAT1 activity in addition to SLC3A2 may be integrin heterodimer-specific in regulating overall cellular ATP levels. Furthermore, the seahorse assay was employed to assess cellular oxygen consumption rate (OCR) and proton excretion (ECAR), which indicate mitochondrial respiration and glycolysis respectively. While the data was a single experiment, substrate-dependent modulation of OCR and ECAR of iPSCs siRNA control and siRNA SLC3A2 cells suggests SLC3A2 and LAT1 influence mitochondrial respiration and glycolysis in an integrin-dependent manner. Interestingly, the immunofluorescence dataset showed that SLC3A2 did not localise with integrin αV when iPSCs were plated on vitronectin but was instead found within the cytoplasm. The question remains; why is this case? LAT1 inhibition resulted in the reduction of ATP levels between iPSC siRNA control and iPSC siRNA SLC3A2 when plated on vitronectin, while SLC3A2 is internalised. Since SLC3A2 has been shown to associate with multiple LATs, it is important to assess if SLC3A2 heavy chain associates with another light chain transporter in an integrin-specific manner upon iPSC engagement on vitronectin. Clearly, further work is needed to deconstruct the mechanisms of SLC3A2- and LAT1- regulation of integrin function, and integrin heterodimer-specific modulation of SLC3A2- and LAT1-dependent metabolic programming.

6. DISCUSSION

This study aimed to define the stem cell adhesome by deciphering the role of distinct integrin signalling networks recruited on defined substrates in regulating stem cell behaviour. To this end, iPSCs were employed as the primary cell model to study the integrin heterodimers that were recruited upon engagement on vitronectin, fibronectin, ZTFN and ZT910. Immunofluorescent imaging, in addition to integrin inhibitory attachment assays, revealed that iPSCs primarily recruit integrin heterodimers αVβ5, α5β1, αVβ1 and α5β1 on vitronectin, fibronectin, ZTFN and ZT910 respectively.

6.1. Integrin heterodimer-specific mechanotransduction

Traction force microscopy suggested that the different integrin heterodimers recruited on vitronectin, fibronectin, ZTFN and ZT910 possessed distinct mechanical properties. These data support the observation that regulating the expression of different integrin heterodimers at the cell-matrix interface can tune force generation (Elosegui-Artola et al., 2014a, Roca-Cusachs et al., 2009). The ability of integrins to sense and adapt to ECM rigidity is essential to several integrin-dependent cellular processes, including cell polarization, contractility and spreading, maturation of IACs and regulation of stem cell proliferation and differentiation (Engler et al., 2006, Ingber and Folkman, 1989, Pelham and Wang, 1997, Riveline et al., 2001). However, precise mechanisms that mediate distinct integrin-heterodimer specific mechanotransduction has not been evaluated. It is likely that the precise mechanisms that modulate these differences are due to dynamic force-dependent changes in the IACs composition of integrins and integrin-dependent signalling proteins. Total internal fluorescent imaging coupled with fluorescent speckle microscopy revealed that structural and regulatory IAC components displayed different mechanics within integrin αVβ3-mediated

IACs (Hu et al., 2007). For example, IAC proteins that possessed no known actin-binding properties such as zyxin, paxillin and FAK moved slowly and at random. Integrin αVβ3 moved the slowest due to its interaction with the ECM (Hu et al., 2007). In contrast, core focal adhesion proteins such as talin, vinculin and α-actinin displayed greater motility and persistence (Hu et al., 2007). Single-protein tracking coupled with super-resolution imaging revealed distinct IACs dynamics of different integrin heterodimers (Rossier et al., 2012). For example, β3 integrin-mediated IACs displayed a two-fold IAC enrichment compared to β1 integrin-mediated IACs (Rossier et al., 2012). Furthermore, this difference in integrin heterodimer-specific IAC composition and dynamics was revealed to be determined by the extracellular domains for integrins β3 and β1. These dynamic integrin heterodimer-specific differences in IACs composition and mechanics are likely to influence changes in force transmission. For example, mature IACs displayed increased fluctuation in internal mechanics and exhibited a pattern of constant centripetal tugging of the ECM (Plotnikov et al., 2012). It was determined that activation of the FAK/phospho-paxillin/vinculin pathway was essential for cells to transmit a traction force over a broad range of ECM rigidities (Plotnikov et al., 2012). Therefore, careful deconstruction of the integrin heterodimer-specific composition of the dynamic IACs using a combination of super resolution interferometric photo-activated localisation microscopy and fluorescent speckle microscopy, will shed light on the precise mechanisms that modulate integrin heterodimer-specific mechanotransduction.

6.2. Effect of integrin heterodimer-specific on YAP localisation

To study the downstream effects of distinct biophysical properties of integrin heterodimers recruited on cell behaviour; the localisation of YAP, nuclear morphology and chromatin organisation were assessed. These experiments showed that the different integrin

mechanical properties significantly modulated chromatin organisation. However, there was no significant differences in YAP localisation and nuclear morphology. Mechanical cues at the cell-matrix interface can lead to the establishment and bidirectional transmission of force between the nucleus and the cytoskeleton (Elosegui-Artola et al., 2017a, Crisp et al., 2006, Guilluy et al., 2014, Rothballer et al., 2013, Tajik et al., 2016). Dynamic changes in this force transmission can modulate nuclear morphology, chromatin organisation and nuclear translocation of transcriptional activators (Elosegui-Artola et al., 2017b). YAP is a mechanosensitive transcriptional activator, a member of the Hippo signalling pathway that plays a critical role in cancer and regeneration. In this study, there was no change in nuclear YAP localisation between soft and stiff ECM rigidities. This is contrary to previous studies which showed a clear YAP nuclear translocation at a stiff ECM rigidity (Elosegui-Artola et al., 2017a, Nukuda et al., 2015). The lack of nuclear YAP localisation in response to ECM rigidity is likely due to the complex integrative effects of growth factor-mediated activation of YAP (present in the growth medium) as a member of the Hippo-signalling pathway and ECM rigidity that is difficult to dissect. Do biochemical or mechanical inputs assert regulatory dominance over each other or are their downstream signalling regulation integrative? Mechanical forces take less than a millisecond to reach the nucleus, while mechanical cues at the cell-matrix interface can be transmitted to the nucleus through a biochemical pathway mediated by changes in conformational changes in mechanosensitive such as talin, vinculin, FAK and paxillin (Wang et al., 2009a). These data suggest in the context of the iPSC model in this study, both complex biochemical and mechanical signalling regulate YAP activation and localisation.

6.3. Effect of integrin heterodimer-specific on nuclear and chromatin organisation

Next, the effect of different biophysical properties of integrin heterodimers recruited on nuclear morphology and chromatin organisation was assessed. Changes in chromatin organisation are associated with variations in histone modifications such as methylation and acetylation (Mattout and Meshorer, 2010). Application of varying shear stress on integrins using magnetic beads mediated a 70-100% increase in transgene transcription (Tajik et al., 2016). Furthermore, the application of mechanical force led to an increase in H3K27me3, which is indicative of chromatin condensation, restricted differentiation lineage-commitment of multipotent stem cells of the human epidermis (Le et al., 2016). For example, a sustained mechanical stimulus-induced chromatin condensation upon differentiation of mesenchymal stem cells (Heo et al., 2016). In our study, only a short-term effect of distinct integrin biophysical properties on chromatin organisation was studied. However, the integrin-mediated changes in chromatin organisation may influence the differentiation potential of pluripotent stem cells. For example, ESCs plated on stiffer substrates demonstrated enhanced osteogenic differentiation (Evans et al., 2009, Engler et al., 2006, Smith et al., 2018, Swift et al., 2013). A long-term differentiation study of pluripotent stem cells on vitronectin, fibronectin, ZTFN and ZT910 will provide essential insights into how small changes in integrin-mediated force application and/or signalling modulate chromatin organisation to co-ordinate stem cell differentiation.

6.4. Role of SLC3A2 in integrating cell metabolism and integrin mechanosignalling

For the first time, integrin adhesion complex enrichment was employed to characterise the stem cell adhesome established upon engagement of distinct integrin heterodimers on vitronectin, fibronectin, ZTFN and ZT910. This novel approach aimed to derive new insights into how integrin-associated signalling networks may differentially modulate different aspects of stem cell behaviour. Using e-cadherin as a negative control, the pluripotent stem cell αVβ5-VIT, α5β1-FN, αVβ1-ZTFN and α5β1-ZT910 enriched adhesomes were obtained. A comparison of these adhesomes revealed clusters of substrate-specific functional clusters that are similar and distinct to each other. The GO term enrichment profiles of each integrin heterodimer adhesome revealed the enrichment of specific signalling pathways that are both distinct and common between all four substrates. Although IAC proteomic datasets characterised on ZTFN and ZT910 contain valuable insights of IACs recruited on these self-assembling nanofiber substrates, due to vitronectin and fibronectin being more biologically relevant substrates *in vivo* and the potential complexity of downstream candidate validation experiments, further combinatorial and integrative analysis of these substrates were not performed. Nonetheless, the ZT datasets will offer a resource for analysis, candidate identification and hypothesis generation in the future.

Combinatorial and Integrative network analysis of the αVβ5-VIT and α5β1-FN adhesome suggested that SLC3A2 possessed a role in potentially linking both integrin signalling and cell metabolism. Downstream analyses aimed to determine whether SLC3A2 regulates integrin-dependent mechano-signalling and metabolism.

Traction force microscopy and immunofluorescence imaging were employed to study whether SLC3A2 regulated mechanotransduction and YAP localisation respectively, in an integrin-dependent manner on vitronectin and fibronectin by generating iPSCs expressing control and SLC3A2-targeting siRNA. Furthermore, to assess the effect of SLC3A2 on mTOR activation, total cell lysates of iPSC grown on vitronectin and fibronectin were obtained to quantify the basal expression of mTOR and, proteins upstream (AKT, and pAKT) and downstream of mTOR (S6 and pS6). Although in both cases no significant differences were observed, there were interesting trends that require further follow-up investigation.

Cellular ATP assays were employed to determine the total levels of ATP thereby obtaining an overall picture of the metabolic state of iPSCs. Quantification of ATP levels suggested that a combination of SLC3A2 knockdown and LAT1 inhibition, or LAT1 inhibition alone mediated substrate-specific changes in overall intracellular ATP level. These results suggest that LAT1 activity in addition to SLC3A2 may be integrin heterodimer specific in regulating overall cellular ATP levels. However, the results of these experiments were complicated by the variability introduced following nucleofection of iPSCs. Although nucleofection did not affect overall cell survival, it increased the overall luminescence in siRNA control cells compared to untransfected cells, suggesting that the process of nucleofection aberrantly influences intracellular metabolism. This unfortunate side effect of siRNA nucleofection can be resolved by the generation of stable SLC3A2 knockout cell lines which will enable a more consistent and reliable study of SLC3A2 integrin-mediated influence on mechanosignalling and metabolism.

The data in this thesis highlights a potentially novel role of SLC3A2 in regulating metabolism in an integrin-dependent manner. However further work is needed to deconstruct the mechanisms of both SLC3A2 and LAT1-mediated bidirectional regulation of integrin function.

6.5. Future of SLC3A2 research

The generation of SLC3A2 chimaeras to investigate distinct domains of SLC3A2 revealed that the transmembrane and cytoplasmic domains were required for regulating integrin function, and the extracellular domain is required for regulating amino acid transport (Fenczik et al., 2001). However, a thorough analysis of how integrins directly associate with SLC3A2 is required. Acquisition of the three-dimensional cryo-EM structure of the SLC3A2-LAT1 complex will enable researchers to look at the integrative role of SLC3A2, LAT1 and integrin in greater detail. Interestingly, the SLC3A2-LAT1 complex comprises an RGE motif in the SLC3A2 extracellular domain that possesses a residue availability probability of 1, which makes the residue accessible to binding from complementary molecules such as integrins (Figures 6.1A and 6.1B) (Yan et al., 2019). Integrin heterodimers engage to RGD motif on extracellular matrix ligands such as fibronectin and vitronectin to mediate cell adhesion (Benito-Jardón et al., 2020). Although substituting an aspartate to glutamate from RGD to RGE has been shown to eliminate integrin α5-mediated integrin binding, however FN^{RGE} has been shown to preserve the binding of αV integrin and promote fibrillogenesis (Benito-Jardón et al., 2020, Takahashi et al., 2007b). However, other studies have shown that the introduction of RGD to RGE mutation in vitronectin eliminated cell adhesion (Cherny et al., 1993). Together, these studies suggest that ligand properties such as ligand domain and RGD motif flanking sequences may influence the specificity of αV-binding of FN^{RGE} (Benito-Jardón et al., 2020). This raises the following questions; Does the RGE motif present in the

extracellular domain of SLC3A2 bind and regulate integrin function? And, do different integrin heterodimers associate with SLC3A2 with differing affinities and/or through different mechanisms?

LAT1 displays an inward open conformation that interacts with SLC3A2 on the extracellular side, within the transmembrane and on the intracellular side (Chiduza et al., 2019, Lee et al., 2019b, Yan et al., 2019) (Figure 6.2). Of particular note is a lipid-like density that is observed on the intracellular side of the membrane that is aligned with a transmembrane segment of SLC3A2 (Yan et al., 2019) (Figure 6.2). SLC3A2 transmembrane residue Arginine 183 (R183) interacts with this lipid-like density of LAT1 (Figure 6.2). Mutational analysis of R183 displayed a substantial reduction in LAT1 transporter activity (Yan et al., 2019). Each aspect of the SLC3A2 function is dependent on distinct domains within SLC3A2, where the extracellular domain of SLC3A2 is essential in regulating amino acid transport activity of LAT1, and the transmembrane and the cytoplasmic domain of SLC3A2 is essential for integrin β1 association, therefore, mutational analysis of R183 will answer if an additional integrin-dependent mechanism of SLC3A2 regulation of LAT1 activity is present. During the final months of my PhD, I generated mutated constructs R183L, RGE -> RGD and RGE -> GGG to examine this mechanism, however, due to lack of time and experimental issues these analyses could not be completed.

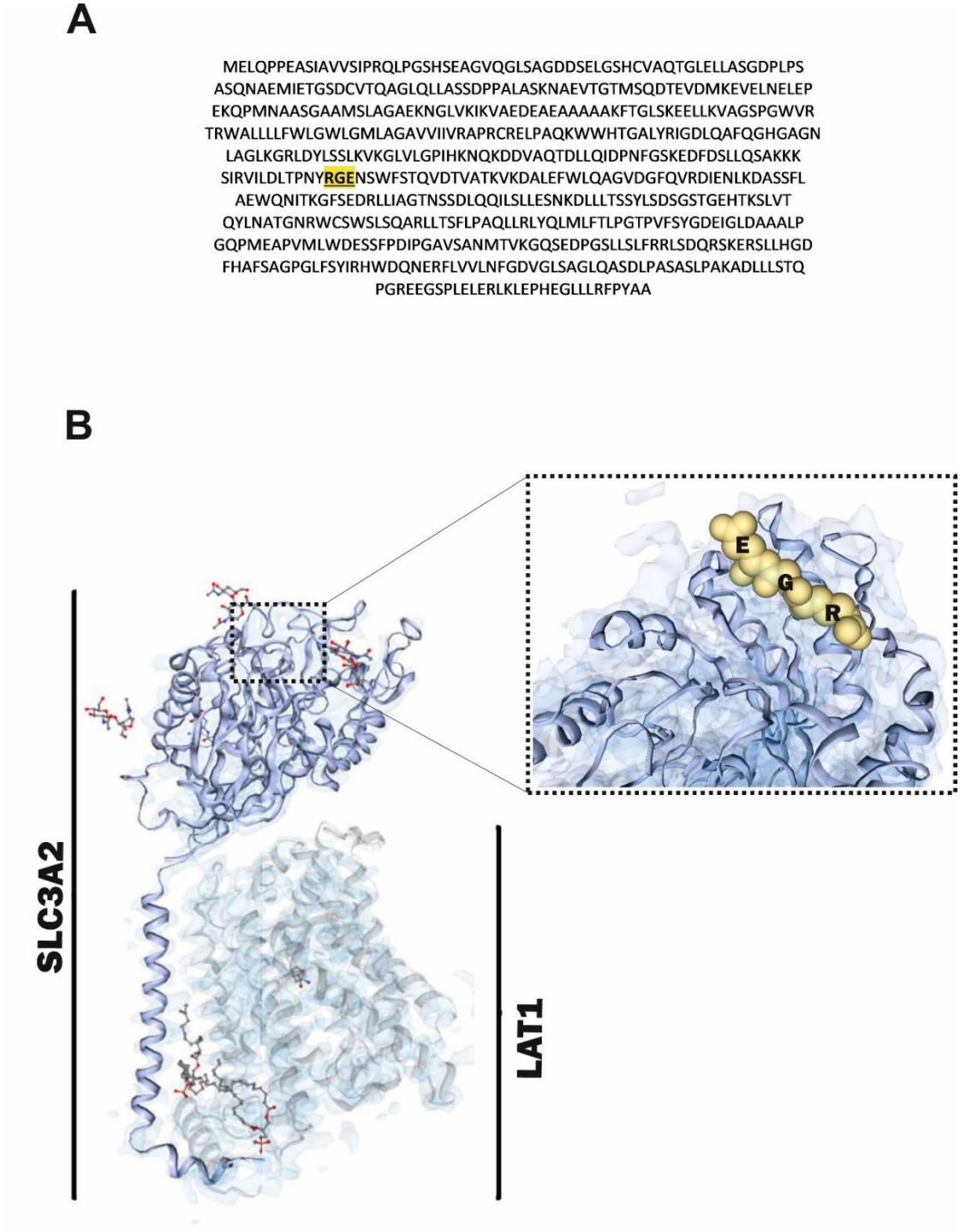

Figure 6.1: RGE motif on SLC3A2. (A) amino acid sequence of SLC3A2 present at position 314-316 with the RGE residue highlighted (yellow). (B) Structure of the human LAT1-SLC3A2 heteromeric amino acid transporter complex, with the SLC3A2 emphasized in colour. Region of RGE motif is highlighted by zoom profile with RGE residues labelled. Cyro-EM structure obtained from: http://3dbionotes.cnb.csic.es/?queryId=EMD-9722 (Yan et al., 2019), but modified to include the RGE residues.

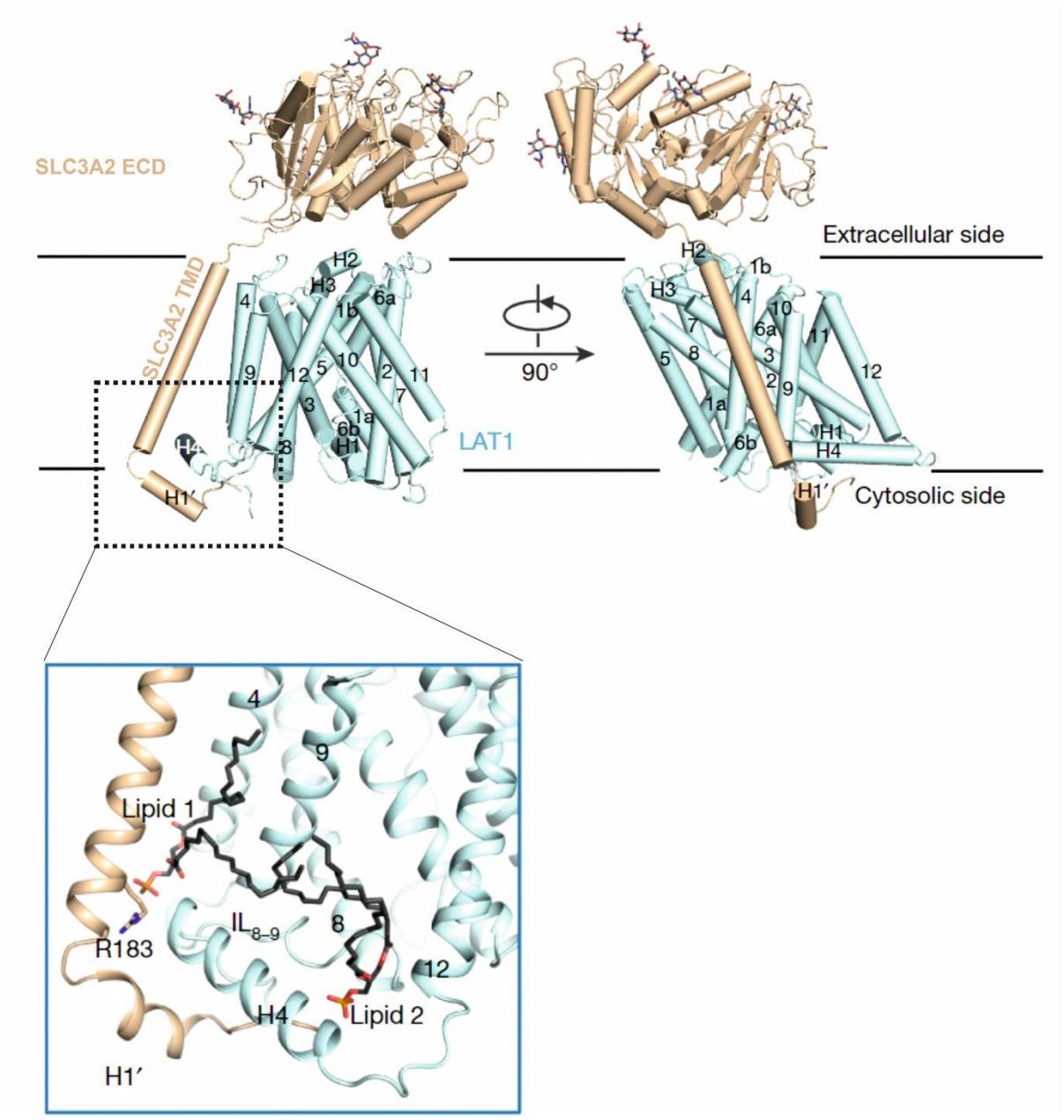

Figure 6.2: Transmembrane interaction between SLC3A2 and LAT1. The SLC3A2-LAT1 complex comprises an extracellular domain, a transmembrane domain and a cytoplasmic domain. Zoomed inset of two lipid-like densities observed on the intracellular side of the membrane. Arginine 183 is present in the first lipid pocket and appears to interact with the polar head of the first lipid molecule. Modified from source: (Yan et al., 2019)

Ultimately, the investigations carried out in this study have shed light on the role of SLC3A2 in the reciprocal regulation of cell metabolism and integrin function. This reciprocal regulation of metabolism and integrin function is an emerging area of research that can modulate cell growth, survival, and metastasis in cancer cells, and potentially modulate the maintenance and differentiation of pluripotent stem cells. Answers to the questions highlighted in this chapter and further follow-up investigations will provide structural insights into the interaction between integrins and SLC3A2 that will enable a better understanding of the mechanisms that regulate integrin mechano-signalling and metabolism to provide new avenues for the identification of novel drug targets to treat cancer.

Bibliography

AIKO, Y., ASKEW, D. J., ARAMAKI, S., MYOGA, M., TOMONAGA, C., HACHISUGA, T., SUGA, R., KAWAMOTO, T., TSUJI, M. & SHIBATA, E. 2014. Differential levels of amino acid transporters System L and ASCT2, and the mTOR protein in placenta of preeclampsia and IUGR. *BMC pregnancy and childbirth,* 14**,** 181-181.

ALY, R. M. 2020. Current state of stem cell-based therapies: an overview. *Stem cell investigation,* 7**,** 8-8.

AOTA, S., NOMIZU, M. & YAMADA, K. M. 1994. The short amino acid sequence Pro-His-Ser-Arg-Asn in human fibronectin enhances cell-adhesive function. *Journal of Biological Chemistry,* 269**,** 24756-24761.

ARJONEN, A., ALANKO, J., VELTEL, S. & IVASKA, J. 2012. Distinct recycling of active and inactive β1 integrins. *Traffic (Copenhagen, Denmark),* 13**,** 610-625.

ATA, R. & ANTONESCU, C. N. 2017. Integrins and Cell Metabolism: An Intimate Relationship Impacting Cancer. *International journal of molecular sciences,* 18**,** 189.

ATHERTON, P., STUTCHBURY, B., JETHWA, D. & BALLESTREM, C. 2016. Mechanosensitive components of integrin adhesions: Role of vinculin. *Exp Cell Res,* 343**,** 21-27.

ATHERTON, P., STUTCHBURY, B., WANG, D.-Y., JETHWA, D., TSANG, R., MEILER-RODRIGUEZ, E., WANG, P., BATE, N., ZENT, R., BARSUKOV, I. L., GOULT, B. T., CRITCHLEY, D. R. & BALLESTREM, C. 2015. Vinculin controls talin engagement with the actomyosin machinery. *Nature Communications,* 6**,** 10038.

BACHMANN, M., KUKKURAINEN, S., HYTÖNEN, V. P. & WEHRLE-HALLER, B. 2019. Cell Adhesion by Integrins. *Physiological Reviews,* 99**,** 1655-1699.

BANERJEE, I., ZHANG, J., MOORE-MORRIS, T., PFEIFFER, E., BUCHHOLZ, K. S., LIU, A., OUYANG, K., STROUD, M. J., GERACE, L., EVANS, S. M., MCCULLOCH, A. & CHEN, J. 2014. Targeted ablation of nesprin 1 and nesprin 2 from murine myocardium results in cardiomyopathy, altered nuclear morphology and inhibition of the biomechanical gene response. *PLoS Genet,* 10**,** e1004114.

BARCZYK, M., CARRACEDO, S. & GULLBERG, D. 2010. Integrins. *Cell Tissue Res,* 339**,** 269-80.

BÁRTOVÁ, E., GALIOVÁ, G., KREJCÍ, J., HARNICAROVÁ, A., STRASÁK, L. & KOZUBEK, S. 2008. Epigenome and chromatin structure in human embryonic stem cells undergoing differentiation. *Dev Dyn,* 237**,** 3690-702.

BASTOLA, P., NEUMS, L., SCHOENEN, F. J. & CHIEN, J. 2016. VCP inhibitors induce endoplasmic reticulum stress, cause cell cycle arrest, trigger caspase-mediated cell death and synergistically kill ovarian cancer cells in combination with Salubrinal. *Molecular oncology,* 10**,** 1559-1574.

BATISTA NAPOTNIK, T., POLAJŽER, T. & MIKLAVČIČ, D. 2021. Cell death due to electroporation – A review. *Bioelectrochemistry,* 141**,** 107871.

BAYS, J. L. & DEMALI, K. A. 2017a. Vinculin in cell-cell and cell-matrix adhesions. *Cell Mol Life Sci,* 74**,** 2999-3009.

BAYS, J. L. & DEMALI, K. A. 2017b. Vinculin in cell-cell and cell-matrix adhesions. *Cellular and molecular life sciences : CMLS,* 74**,** 2999-3009.

BENITO-JARDÓN, M., STROHMEYER, N., ORTEGA-SANCHÍS, S., BHARADWAJ, M., MOSER, M., MÜLLER, D. J., FÄSSLER, R. & COSTELL, M. 2020. αv-Class integrin binding to fibronectin is solely mediated by RGD and unaffected by an RGE mutation. *Journal of Cell Biology,* 219.

BERK, J. M., TIFFT, K. E. & WILSON, K. L. 2013. The nuclear envelope LEM-domain protein emerin. *Nucleus,* 4**,** 298-314.

BÖTTCHER, R. T., VEELDERS, M., ROMBAUT, P., FAIX, J., THEODOSIOU, M., STRADAL, T. E., ROTTNER, K., ZENT, R., HERZOG, F. & FÄSSLER, R. 2017. Kindlin-2 recruits paxillin and Arp2/3 to promote membrane protrusions during initial cell spreading. *J Cell Biol,* 216**,** 3785-3798.

BOULTER, E., ESTRACH, S., TISSOT, F. S., HENNRICH, M. L., TOSELLO, L., CAILLETEAU, L., DE LA BALLINA, L. R., PISANO, S., GAVIN, A.-C. & FÉRAL, C. C. 2018. Cell metabolism regulates integrin mechanosensing via an SLC3A2-dependent sphingolipid biosynthesis pathway. *Nature Communications,* 9**,** 4862.

BRAVO-CORDERO, J. J., MAGALHAES, M. A. O., EDDY, R. J., HODGSON, L. & CONDEELIS, J. 2013. Functions of cofilin in cell locomotion and invasion. *Nature Reviews Molecular Cell Biology,* 14**,** 405-415.

BRIATA, P., BORDO, D., PUPPO, M., GORLERO, F., ROSSI, M., PERRONE-BIZZOZERO, N. & GHERZI, R. 2016. Diverse roles of the nucleic acid-binding protein KHSRP in cell differentiation and disease. *Wiley interdisciplinary reviews. RNA,* 7**,** 227-240.

BRIDGEWATER, R. E., NORMAN, J. C. & CASWELL, P. T. 2012. Integrin trafficking at a glance. *Journal of cell science,* 125**,** 3695-3701.

BURGESS, R. J., AGATHOCLEOUS, M. & MORRISON, S. J. 2014. Metabolic regulation of stem cell function. *Journal of internal medicine,* 276**,** 12-24.

BYRON, A., HUMPHRIES, J. D., BASS, M. D., KNIGHT, D. & HUMPHRIES, M. J. 2011. Proteomic analysis of integrin adhesion complexes. *Sci Signal,* 4**,** pt2.

BYRON, A., MORGAN, M. R. & HUMPHRIES, M. J. 2010. Adhesion signalling complexes. *Curr Biol,* 20**,** R1063-r1067.

CAMPBELL, I. D. & HUMPHRIES, M. J. 2011. Integrin structure, activation, and interactions. *Cold Spring Harbor perspectives in biology,* 3**,** a004994.

CANO-CRESPO, S., CHILLARÓN, J., JUNZA, A., FERNÁNDEZ-MIRANDA, G., GARCÍA, J., POLTE, C., R. DE LA BALLINA, L., IGNATOVA, Z., YANES, Ó., ZORZANO, A., STEPHAN-OTTO ATTOLINI, C. & PALACÍN, M. 2019. CD98hc (SLC3A2) sustains amino acid and nucleotide availability for cell cycle progression. *Scientific Reports,* 9**,** 14065.

CARISEY, A. & BALLESTREM, C. 2011. Vinculin, an adapter protein in control of cell adhesion signalling. *Eur J Cell Biol,* 90**,** 157-63.

CARISEY, A., TSANG, R., GREINER, A. M., NIJENHUIS, N., HEATH, N., NAZGIEWICZ, A., KEMKEMER, R., DERBY, B., SPATZ, J. & BALLESTREM, C. 2013. Vinculin regulates the recruitment and release of core focal adhesion proteins in a force-dependent manner. *Curr Biol,* 23**,** 271-81.

CASWELL, P. T., VADREVU, S. & NORMAN, J. C. 2009. Integrins: masters and slaves of endocytic transport. *Nature Reviews Molecular Cell Biology,* 10**,** 843-853.

CERINI, C., KERJAN, P., ASTIER, M., GRATECOS, D., MIRANDE, M. & SÉMÉRIVA, M. 1991. A component of the multisynthetase complex is a multifunctional aminoacyl-tRNA synthetase. *Embo j,* 10**,** 4267-77.

CHAN, C. E. & ODDE, D. J. 2008. Traction dynamics of filopodia on compliant substrates. *Science,* 322**,** 1687-91.

CHASTNEY, M. R., CONWAY, J. R. W. & IVASKA, J. 2021. Integrin adhesion complexes. *Current Biology,* 31**,** R536-R542.

CHEN, C., MANSO, A. M. & ROSS, R. S. 2019. Talin and Kindlin as Integrin-Activating Proteins: Focus on the Heart. *Pediatric cardiology,* 40**,** 1401-1409.

CHEN, J., OU, Y., LUO, R., WANG, J., WANG, D., GUAN, J., LI, Y., XIA, P., CHEN, P. R. & LIU, Y. 2021. SAR1B senses leucine levels to regulate mTORC1 signalling. *Nature,* 596**,** 281-284.

CHERNY, R. C., HONAN, M. A. & THIAGARAJAN, P. 1993. Site-directed mutagenesis of the arginine-glycine-aspartic acid in vitronectin abolishes cell adhesion. *J Biol Chem,* 268**,** 9725-9.

CHICUREL, M. E., SINGER, R. H., MEYER, C. J. & INGBER, D. E. 1998. Integrin binding and mechanical tension induce movement of mRNA and ribosomes to focal adhesions. *Nature,* 392**,** 730-3.

CHIDUZA, G. N., JOHNSON, R. M., WRIGHT, G. S. A., ANTONYUK, S. V., MUENCH, S. P. & HASNAIN, S. S. 2019. LAT1 (SLC7A5) and CD98hc (SLC3A2) complex dynamics revealed by single-particle cryo-EM. *Acta Crystallogr D Struct Biol,* 75**,** 660-669.

CHO, S., IRIANTO, J. & DISCHER, D. E. 2017. Mechanosensing by the nucleus: From pathways to scaling relationships. *J Cell Biol,* 216**,** 305-315.

CHRZANOWSKA-WODNICKA, M. & BURRIDGE, K. 1996. Rho-stimulated contractility drives the formation of stress fibers and focal adhesions. *J Cell Biol,* 133**,** 1403-15.

CORLEY, K. M., TAYLOR, C. J. & LILLY, B. 2005. Hypoxia-inducible factor 1alpha modulates adhesion, migration, and FAK phosphorylation in vascular smooth muscle cells. *J Cell Biochem,* 96**,** 971-85.

CORONADO, D., GODET, M., BOURILLOT, P.-Y., TAPPONNIER, Y., BERNAT, A., PETIT, M., AFANASSIEFF, M., MARKOSSIAN, S., MALASHICHEVA, A., IACONE, R., ANASTASSIADIS, K. & SAVATIER, P. 2013. A short G1 phase is an intrinsic determinant of naïve embryonic stem cell pluripotency. *Stem Cell Research,* 10**,** 118-131.

CRISP, M., LIU, Q., ROUX, K., RATTNER, J. B., SHANAHAN, C., BURKE, B., STAHL, P. D. & HODZIC, D. 2006. Coupling of the nucleus and cytoplasm: role of the LINC complex. *J Cell Biol,* 172**,** 41-53.

CRITCHLEY, D. R. & GINGRAS, A. R. 2008. Talin at a glance. *J Cell Sci,* 121**,** 1345-7.

DANEN, E. H., SONNEVELD, P., BRAKEBUSCH, C., FASSLER, R. & SONNENBERG, A. 2002. The fibronectin-binding integrins alpha5beta1 and alphavbeta3 differentially modulate RhoA-GTP loading, organization of cell matrix adhesions, and fibronectin fibrillogenesis. *J Cell Biol,* 159**,** 1071-86.

DANEN, E. H., SONNEVELD, P., SONNENBERG, A. & YAMADA, K. M. 2000. Dual stimulation of Ras/mitogen-activated protein kinase and RhoA by cell adhesion to fibronectin supports growth factor-stimulated cell cycle progression. *The Journal of cell biology,* 151**,** 1413-1422.

DAS, M., ITHYCHANDA, S., QIN, J. & PLOW, E. F. 2014. Mechanisms of talin-dependent integrin signaling and crosstalk. *Biochim Biophys Acta,* 1838**,** 579-88.

DEL RIO, A., PEREZ-JIMENEZ, R., LIU, R., ROCA-CUSACHS, P., FERNANDEZ, J. M. & SHEETZ, M. P. 2009. Stretching single talin rod molecules activates vinculin binding. *Science,* 323**,** 638-41.

DI BLASIO, L., DROETTO, S., NORMAN, J., BUSSOLINO, F. & PRIMO, L. 2010. Protein kinase D1 regulates VEGF-A-induced alphavbeta3 integrin trafficking and endothelial cell migration. *Traffic,* 11**,** 1107-18.

DIDIASOVA, M., SCHAEFER, L. & WYGRECKA, M. 2019. When Place Matters: Shuttling of Enolase-1 Across Cellular Compartments. *Frontiers in cell and developmental biology,* 7**,** 61-61.

DIXON, J. R., JUNG, I., SELVARAJ, S., SHEN, Y., ANTOSIEWICZ-BOURGET, J. E., LEE, A. Y., YE, Z., KIM, A., RAJAGOPAL, N., XIE, W., DIAO, Y., LIANG, J., ZHAO, H., LOBANENKOV, V. V., ECKER, J. R., THOMSON, J. A. & REN, B. 2015. Chromatin architecture reorganization during stem cell differentiation. *Nature,* 518**,** 331-6.

DONALDSON, J. G. & JACKSON, C. L. 2011. ARF family G proteins and their regulators: roles in membrane transport, development and disease. *Nature Reviews Molecular Cell Biology,* 12**,** 362-375.

DONATO, D. M., RYZHOVA, L. M., MEENDERINK, L. M., KAVERINA, I. & HANKS, S. K. 2010. Dynamics and mechanism of p130Cas localization to focal adhesions. *J Biol Chem,* 285**,** 20769-79.

DORNER, D., GOTZMANN, J. & FOISNER, R. 2007. Nucleoplasmic lamins and their interaction partners, LAP2alpha, Rb, and BAF, in transcriptional regulation. *Febs j,* 274**,** 1362-73.

DOSS, B. L., PAN, M., GUPTA, M., GRENCI, G., MÈGE, R. M., LIM, C. T., SHEETZ, M. P., VOITURIEZ, R. & LADOUX, B. 2020. Cell response to substrate rigidity is regulated by active and passive cytoskeletal stress. *Proc Natl Acad Sci U S A,* 117**,** 12817-12825.

DREES, B. E., ANDREWS, K. M. & BECKERLE, M. C. 1999. Molecular dissection of zyxin function reveals its involvement in cell motility. *J Cell Biol,* 147**,** 1549-60.

DUBAND-GOULET, I. & COURVALIN, J. C. 2000. Inner nuclear membrane protein LBR preferentially interacts with DNA secondary structures and nucleosomal linker. *Biochemistry,* 39**,** 6483-8.

DUMBAULD, D. W., LEE, T. T., SINGH, A., SCRIMGEOUR, J., GERSBACH, C. A., ZAMIR, E. A., FU, J., CHEN, C. S., CURTIS, J. E., CRAIG, S. W. & GARCÍA, A. J. 2013. How vinculin regulates force transmission. *Proc Natl Acad Sci U S A,* 110**,** 9788-93.

DUPONT, S. 2016. Role of YAP/TAZ in cell-matrix adhesion-mediated signalling and mechanotransduction. *Exp Cell Res,* 343**,** 42-53.
DUPONT, S., MORSUT, L., ARAGONA, M., ENZO, E., GIULITTI, S., CORDENONSI, M., ZANCONATO, F., LE DIGABEL, J., FORCATO, M., BICCIATO, S., ELVASSORE, N. & PICCOLO, S. 2011. Role of YAP/TAZ in mechanotransduction. *Nature,* 474**,** 179-183.
EDMONDSON, R., BROGLIE, J. J., ADCOCK, A. F. & YANG, L. 2014. Three-dimensional cell culture systems and their applications in drug discovery and cell-based biosensors. *Assay Drug Dev Technol,* 12**,** 207-18.
ELLIS, S. J. & TANENTZAPF, G. 2010. Integrin-mediated adhesion and stem-cell-niche interactions. *Cell Tissue Res,* 339**,** 121-30.
ELOSEGUI-ARTOLA, A., ANDREU, I., BEEDLE, A. E. M., LEZAMIZ, A., UROZ, M., KOSMALSKA, A. J., ORIA, R., KECHAGIA, J. Z., RICO-LASTRES, P., LE ROUX, A.-L., SHANAHAN, C. M., TREPAT, X., NAVAJAS, D., GARCIA-MANYES, S. & ROCA-CUSACHS, P. 2017a. Force Triggers YAP Nuclear Entry by Regulating Transport across Nuclear Pores. *Cell,* 171**,** 1397-1410.e14.
ELOSEGUI-ARTOLA, A., ANDREU, I., BEEDLE, A. E. M., LEZAMIZ, A., UROZ, M., KOSMALSKA, A. J., ORIA, R., KECHAGIA, J. Z., RICO-LASTRES, P., LE ROUX, A. L., SHANAHAN, C. M., TREPAT, X., NAVAJAS, D., GARCIA-MANYES, S. & ROCA-CUSACHS, P. 2017b. Force Triggers YAP Nuclear Entry by Regulating Transport across Nuclear Pores. *Cell,* 171**,** 1397-1410.e14.
ELOSEGUI-ARTOLA, A., BAZELLIÈRES, E., ALLEN, M. D., ANDREU, I., ORIA, R., SUNYER, R., GOMM, J. J., MARSHALL, J. F., JONES, J. L., TREPAT, X. & ROCA-CUSACHS, P. 2014a. Rigidity sensing and adaptation through regulation of integrin types. *Nature Materials,* 13**,** 631-637.
ELOSEGUI-ARTOLA, A., BAZELLIÈRES, E., ALLEN, M. D., ANDREU, I., ORIA, R., SUNYER, R., GOMM, J. J., MARSHALL, J. F., JONES, J. L., TREPAT, X. & ROCA-CUSACHS, P. 2014b. Rigidity sensing and adaptation through regulation of integrin types. *Nat Mater,* 13**,** 631-7.
ELOSEGUI-ARTOLA, A., ORIA, R., CHEN, Y., KOSMALSKA, A., PÉREZ-GONZÁLEZ, C., CASTRO, N., ZHU, C., TREPAT, X. & ROCA-CUSACHS, P. 2016. Mechanical regulation of a molecular clutch defines force transmission and transduction in response to matrix rigidity. *Nat Cell Biol,* 18**,** 540-8.
ELOSEGUI-ARTOLA, A., TREPAT, X. & ROCA-CUSACHS, P. 2018. Control of Mechanotransduction by Molecular Clutch Dynamics. *Trends Cell Biol,* 28**,** 356-367.
ENGLER, A. J., SEN, S., SWEENEY, H. L. & DISCHER, D. E. 2006. Matrix elasticity directs stem cell lineage specification. *Cell,* 126**,** 677-89.
EROSHENKO, N., RAMACHANDRAN, R., YADAVALLI, V. K. & RAO, R. R. 2013. Effect of substrate stiffness on early human embryonic stem cell differentiation. *J Biol Eng,* 7**,** 7.
ESKELAND, R., EBERHARTER, A. & IMHOF, A. 2007. HP1 binding to chromatin methylated at H3K9 is enhanced by auxiliary factors. *Mol Cell Biol,* 27**,** 453-65.
ESTRACH, S., LEE, S.-A., BOULTER, E., PISANO, S., ERRANTE, A., TISSOT, F. S., CAILLETEAU, L., PONS, C., GINSBERG, M. H. & FÉRAL, C. C. 2014. CD98hc (SLC3A2) loss protects against ras-driven tumorigenesis by modulating integrin-mediated mechanotransduction. *Cancer research,* 74**,** 6878-6889.
EVANS, M. J. & KAUFMAN, M. H. 1981. Establishment in culture of pluripotential cells from mouse embryos. *Nature,* 292**,** 154-6.
EVANS, N. D., MINELLI, C., GENTLEMAN, E., LAPOINTE, V., PATANKAR, S. N., KALLIVRETAKI, M., CHEN, X., ROBERTS, C. J. & STEVENS, M. M. 2009. Substrate stiffness affects early differentiation events in embryonic stem cells. *Eur Cell Mater,* 18**,** 1-13; discussion 13-4.
EYCKMANS, J., BOUDOU, T., YU, X. & CHEN, C. S. 2011. A hitchhiker's guide to mechanobiology. *Dev Cell,* 21**,** 35-47.
FEDORCHAK, G. R., KAMINSKI, A. & LAMMERDING, J. 2014. Cellular mechanosensing: getting to the nucleus of it all. *Prog Biophys Mol Biol,* 115**,** 76-92.

FENCZIK, C. A., ZENT, R., DELLOS, M., CALDERWOOD, D. A., SATRIANO, J., KELLY, C. & GINSBERG, M. H. 2001. Distinct domains of CD98hc regulate integrins and amino acid transport. *J Biol Chem,* 276**,** 8746-52.

FERAL, C. C., NISHIYA, N., FENCZIK, C. A., STUHLMANN, H., SLEPAK, M. & GINSBERG, M. H. 2005. CD98hc (SLC3A2) mediates integrin signaling. *Proceedings of the National Academy of Sciences of the United States of America,* 102**,** 355-360.

FORTIER, L. A. 2005. Stem cells: classifications, controversies, and clinical applications. *Vet Surg,* 34**,** 415-23.

FRANTZ, C., STEWART, K. M. & WEAVER, V. M. 2010. The extracellular matrix at a glance. *J Cell Sci,* 123**,** 4195-200.

FRANZ, C. M. & MÜLLER, D. J. 2005. Analyzing focal adhesion structure by atomic force microscopy. *Journal of Cell Science,* 118**,** 5315-5323.

GALLAGHER, S. M., CASTORINO, J. J. & PHILP, N. J. 2009. Interaction of monocarboxylate transporter 4 with beta1-integrin and its role in cell migration. *Am J Physiol Cell Physiol,* 296**,** C414-21.

GASPAR-MAIA, A., ALAJEM, A., MESHORER, E. & RAMALHO-SANTOS, M. 2011. Open chromatin in pluripotency and reprogramming. *Nat Rev Mol Cell Biol,* 12**,** 36-47.

GATTAZZO, F., URCIUOLO, A. & BONALDO, P. 2014. Extracellular matrix: a dynamic microenvironment for stem cell niche. *Biochim Biophys Acta,* 1840**,** 2506-19.

GEIGER, B. & YAMADA, K. M. 2011. Molecular architecture and function of matrix adhesions. *Cold Spring Harb Perspect Biol,* 3.

GEIGER, T. & ZAIDEL-BAR, R. 2012. Opening the floodgates: proteomics and the integrin adhesome. *Curr Opin Cell Biol,* 24**,** 562-8.

GEORGIADOU, M. & IVASKA, J. 2017a. Tensins: Bridging AMP-Activated Protein Kinase with Integrin Activation. *Trends in Cell Biology,* 27**,** 703-711.

GEORGIADOU, M. & IVASKA, J. 2017b. Tensins: Bridging AMP-Activated Protein Kinase with Integrin Activation. *Trends Cell Biol,* 27**,** 703-711.

GEORGIADOU, M., LILJA, J., JACQUEMET, G., GUZMÁN, C., RAFAEVA, M., ALIBERT, C., YAN, Y., SAHGAL, P., LERCHE, M., MANNEVILLE, J.-B., MÄKELÄ, T. P. & IVASKA, J. 2017. AMPK negatively regulates tensin-dependent integrin activity. *The Journal of cell biology,* 216**,** 1107-1121.

GRUENBAUM, Y., MARGALIT, A., GOLDMAN, R. D., SHUMAKER, D. K. & WILSON, K. L. 2005. The nuclear lamina comes of age. *Nat Rev Mol Cell Biol,* 6**,** 21-31.

GRYS, M., MADEJA, Z. & KOROHODA, W. 2017. Avoiding the side effects of electric current pulse application to electroporated cells in disposable small volume cuvettes assures good cell survival. *Cellular & Molecular Biology Letters,* 22**,** 1.

GU, Z., NOSS, E. H., HSU, V. W. & BRENNER, M. B. 2011. Integrins traffic rapidly via circular dorsal ruffles and macropinocytosis during stimulated cell migration. *Journal of Cell Biology,* 193**,** 61-70.

GUILLUY, C., OSBORNE, L. D., VAN LANDEGHEM, L., SHAREK, L., SUPERFINE, R., GARCIA-MATA, R. & BURRIDGE, K. 2014. Isolated nuclei adapt to force and reveal a mechanotransduction pathway in the nucleus. *Nat Cell Biol,* 16**,** 376-81.

GUO, X. & ZHAO, B. 2013a. Integration of mechanical and chemical signals by YAP and TAZ transcription coactivators. *Cell & Bioscience,* 3**,** 33.

GUO, X. & ZHAO, B. 2013b. Integration of mechanical and chemical signalsby YAP and TAZ transcription coactivators. *Cell & Bioscience*.

GUPTA, M., SARANGI, B. R., DESCHAMPS, J., NEMATBAKHSH, Y., CALLAN-JONES, A., MARGADANT, F., MÈGE, R. M., LIM, C. T., VOITURIEZ, R. & LADOUX, B. 2015. Adaptive rheology and ordering of cell cytoskeleton govern matrix rigidity sensing. *Nat Commun,* 6**,** 7525.

HAHN, S. S., TANG, Q., ZHENG, F., ZHAO, S., WU, J. & CHEN, J. 2014. Repression of integrin-linked kinase by antidiabetes drugs through cross-talk of PPARγ- and AMPKα-dependent signaling: role of AP-2α and Sp1. *Cell Signal,* 26**,** 639-47.

HALDER, G., DUPONT, S. & PICCOLO, S. 2012. Transduction of mechanical and cytoskeletal cues by YAP and TAZ. *Nat Rev Mol Cell Biol,* 13**,** 591-600.
HANDORF, A. M., ZHOU, Y., HALANSKI, M. A. & LI, W. J. 2015. Tissue stiffness dictates development, homeostasis, and disease progression. *Organogenesis,* 11**,** 1-15.
HARBURGER, D. S. & CALDERWOOD, D. A. 2009. Integrin signalling at a glance. *J Cell Sci,* 122**,** 159-63.
HAYNES, B. F., HEMLER, M. E., MANN, D. L., EISENBARTH, G. S., SHELHAMER, J., MOSTOWSKI, H. S., THOMAS, C. A., STROMINGER, J. L. & FAUCI, A. S. 1981. Characterization of a monoclonal antibody (4F2) that binds to human monocytes and to a subset of activated lymphocytes. *J Immunol,* 126**,** 1409-14.
HENDERSON, N. C., COLLIS, E. A., MACKINNON, A. C., SIMPSON, K. J., HASLETT, C., ZENT, R., GINSBERG, M. & SETHI, T. 2004. CD98hc (SLC3A2) Interaction with β1 Integrins Is Required for Transformation*. *Journal of Biological Chemistry,* 279**,** 54731-54741.
HEO, S. J., HAN, W. M., SZCZESNY, S. E., COSGROVE, B. D., ELLIOTT, D. M., LEE, D. A., DUNCAN, R. L. & MAUCK, R. L. 2016. Mechanically Induced Chromatin Condensation Requires Cellular Contractility in Mesenchymal Stem Cells. *Biophys J,* 111**,** 864-874.
HILL, C. J., FLEMING, J. R., MOUSAVINEJAD, M., NICHOLSON, R., TZOKOV, S. B., BULLOUGH, P. A., BOGOMOLOVAS, J., MORGAN, M. R., MAYANS, O. & MURRAY, P. 2019. Self-Assembling Proteins as High-Performance Substrates for Embryonic Stem Cell Self-Renewal. *Advanced Materials,* 31**,** 1807521.
HOFFMANN, K., DREGER, C. K., OLINS, A. L., OLINS, D. E., SHULTZ, L. D., LUCKE, B., KARL, H., KAPS, R., MÜLLER, D., VAYÁ, A., AZNAR, J., WARE, R. E., SOTELO CRUZ, N., LINDNER, T. H., HERRMANN, H., REIS, A. & SPERLING, K. 2002. Mutations in the gene encoding the lamin B receptor produce an altered nuclear morphology in granulocytes (Pelger-Huët anomaly). *Nat Genet,* 31**,** 410-4.
HORTON, E. R., BYRON, A., ASKARI, J. A., NG, D. H. J., MILLON-FRÉMILLON, A., ROBERTSON, J., KOPER, E. J., PAUL, N. R., WARWOOD, S., KNIGHT, D., HUMPHRIES, J. D. & HUMPHRIES, M. J. 2015. Definition of a consensus integrin adhesome and its dynamics during adhesion complex assembly and disassembly. *Nat Cell Biol,* 17**,** 1577-1587.
HORTON, E. R., HUMPHRIES, J. D., JAMES, J., JONES, M. C., ASKARI, J. A. & HUMPHRIES, M. J. 2016. The integrin adhesome network at a glance. *J Cell Sci,* 129**,** 4159-4163.
HU, K., JI, L., APPLEGATE, K. T., DANUSER, G. & WATERMAN-STORER, C. M. 2007. Differential transmission of actin motion within focal adhesions. *Science,* 315**,** 111-5.
HU, P. & LUO, B. H. 2013. Integrin bi-directional signaling across the plasma membrane. *J Cell Physiol,* 228**,** 306-12.
HU, X., MARGADANT, F. M., YAO, M. & SHEETZ, M. P. 2017. Molecular stretching modulates mechanosensing pathways. *Protein Sci,* 26**,** 1337-1351.
HUMPHRIES, J. D., BYRON, A., BASS, M. D., CRAIG, S. E., PINNEY, J. W., KNIGHT, D. & HUMPHRIES, M. J. 2009. Proteomic analysis of integrin-associated complexes identifies RCC2 as a dual regulator of Rac1 and Arf6. *Sci Signal,* 2**,** ra51.
HUMPHRIES, J. D., BYRON, A. & HUMPHRIES, M. J. 2006. Integrin ligands at a glance. *J Cell Sci,* 119**,** 3901-3.
HUMPHRIES, J. D., PAUL, N. R., HUMPHRIES, M. J. & MORGAN, M. R. 2015. Emerging properties of adhesion complexes: what are they and what do they do? *Trends Cell Biol,* 25**,** 388-97.
HUMPHRIES, J. D., WANG, P., STREULI, C., GEIGER, B., HUMPHRIES, M. J. & BALLESTREM, C. 2007. Vinculin controls focal adhesion formation by direct interactions with talin and actin. *J Cell Biol,* 179**,** 1043-57.
HYNES, R. O. & NABA, A. 2012. Overview of the matrisome--an inventory of extracellular matrix constituents and functions. *Cold Spring Harb Perspect Biol,* 4**,** a004903.
INGBER, D. E. 2003. Mechanosensation through integrins: cells act locally but think globally. *Proc Natl Acad Sci U S A,* 100**,** 1472-4.

INGBER, D. E. & FOLKMAN, J. 1989. How does extracellular matrix control capillary morphogenesis? *Cell,* 58**,** 803-5.

IOZZO, R. V. & SCHAEFER, L. 2015. Proteoglycan form and function: A comprehensive nomenclature of proteoglycans. *Matrix biology : journal of the International Society for Matrix Biology,* 42**,** 11-55.

JANOŠTIAK, R., BRÁBEK, J., AUERNHEIMER, V., TATÁROVÁ, Z., LAUTSCHAM, L. A., DEY, T., GEMPERLE, J., MERKEL, R., GOLDMANN, W. H., FABRY, B. & RÖSEL, D. 2014a. CAS directly interacts with vinculin to control mechanosensing and focal adhesion dynamics. *Cell Mol Life Sci,* 71**,** 727-44.

JANOŠTIAK, R., PATAKI, A. C., BRÁBEK, J. & RÖSEL, D. 2014b. Mechanosensors in integrin signaling: the emerging role of p130Cas. *Eur J Cell Biol,* 93**,** 445-54.

JANOŠTIAK, R., TOLDE, O., BRŮHOVÁ, Z., NOVOTNÝ, M., HANKS, S. K., RÖSEL, D. & BRÁBEK, J. 2011. Tyrosine phosphorylation within the SH3 domain regulates CAS subcellular localization, cell migration, and invasiveness. *Mol Biol Cell,* 22**,** 4256-67.

JONES, M. C., HUMPHRIES, J. D., BYRON, A., MILLON-FRÉMILLON, A., ROBERTSON, J., PAUL, N. R., NG, D. H. J., ASKARI, J. A. & HUMPHRIES, M. J. 2015. Isolation of integrin-based adhesion complexes. *Curr Protoc Cell Biol,* 66**,** 9.8.1-9.8.15.

KABIR-SALMANI, M., FUKUDA, M. N., KANAI-AZUMA, M., AHMED, N., SHIOKAWA, S., AKIMOTO, Y., SAKAI, K., NAGAMORI, S., KANAI, Y., SUGIHARA, K. & IWASHITA, M. 2008. The membrane-spanning domain of CD98 heavy chain promotes alpha(v)beta3 integrin signals in human extravillous trophoblasts. *Molecular endocrinology (Baltimore, Md.),* 22**,** 707-715.

KALASKAR, D. M., DOWNES, J. E., MURRAY, P., EDGAR, D. H. & WILLIAMS, R. L. 2013. Characterization of the interface between adsorbed fibronectin and human embryonic stem cells. *Journal of the Royal Society, Interface,* 10**,** 20130139-20130139.

KALVERDA, B., RÖLING, M. D. & FORNEROD, M. 2008. Chromatin organization in relation to the nuclear periphery. *FEBS Lett,* 582**,** 2017-22.

KANCHANAWONG, P., SHTENGEL, G., PASAPERA, A. M., RAMKO, E. B., DAVIDSON, M. W., HESS, H. F. & WATERMAN, C. M. 2010. Nanoscale architecture of integrin-based cell adhesions. *Nature,* 468**,** 580-4.

KE, Y., HAN, Y., GUO, X., WEN, J., WANG, K., JIANG, X., TIAN, X., BA, X., BOLDOGH, I. & ZENG, X. 2017. PARP1 promotes gene expression at the post-transcriptional level by modulating the RNA-binding protein HuR. *Nature Communications,* 8**,** 14632.

KECHAGIA, J. Z., IVASKA, J. & ROCA-CUSACHS, P. 2019. Integrins as biomechanical sensors of the microenvironment. *Nature Reviews Molecular Cell Biology,* 20**,** 457-473.

KIM, J., JANG, J., YANG, C., KIM, E. J., JUNG, H. & KIM, C. 2016. Vimentin filament controls integrin α5β1-mediated cell adhesion by binding to integrin through its Ser38 residue. *FEBS Letters,* 590**,** 3517-3525.

KIM, S. H., TURNBULL, J. & GUIMOND, S. 2011. Extracellular matrix and cell signalling: the dynamic cooperation of integrin, proteoglycan and growth factor receptor. *J Endocrinol,* 209**,** 139-51.

KINNUNEN, J., KOKKONEN, H. T., KOVANEN, V., HAUTA-KASARI, M., VAHIMAA, P. & JURVELIN, J. S. 2012. Changes in collagen cross-linking of articular cartilage are revealed by spectral reflectance imaging. *2012 25th IEEE International Symposium on Computer-Based Medical Systems (CBMS)***,** 1-4.

KOIKE, T., KIMURA, N., MIYAZAKI, K., YABUTA, T., KUMAMOTO, K., TAKENOSHITA, S., CHEN, J., KOBAYASHI, M., HOSOKAWA, M., TANIGUCHI, A., KOJIMA, T., ISHIDA, N., KAWAKITA, M., YAMAMOTO, H., TAKEMATSU, H., SUZUKI, A., KOZUTSUMI, Y. & KANNAGI, R. 2004. Hypoxia induces adhesion molecules on cancer cells: A missing link between Warburg effect and induction of selectin-ligand carbohydrates. *Proceedings of the National Academy of Sciences of the United States of America,* 101**,** 8132-8137.

KOLESNIKOVA, T. V., MANNION, B. A., BERDITCHEVSKI, F. & HEMLER, M. E. 2001. Beta1 integrins show specific association with CD98 protein in low density membranes. *BMC biochemistry,* 2**,** 10-10.

KOZLOV, G. & GEHRING, K. 2020. Calnexin cycle – structural features of the ER chaperone system. *The FEBS Journal,* 287**,** 4322-4340.

KREJCÍ, J., UHLÍROVÁ, R., GALIOVÁ, G., KOZUBEK, S., SMIGOVÁ, J. & BÁRTOVÁ, E. 2009. Genome-wide reduction in H3K9 acetylation during human embryonic stem cell differentiation. *J Cell Physiol,* 219**,** 677-87.

KURIYAN, A. E., ALBINI, T. A., TOWNSEND, J. H., RODRIGUEZ, M., PANDYA, H. K., LEONARD, R. E., 2ND, PARROTT, M. B., ROSENFELD, P. J., FLYNN, H. W., JR. & GOLDBERG, J. L. 2017. Vision Loss after Intravitreal Injection of Autologous "Stem Cells" for AMD. *N Engl J Med,* 376**,** 1047-1053.

LAMMERDING, J., HSIAO, J., SCHULZE, P. C., KOZLOV, S., STEWART, C. L. & LEE, R. T. 2005. Abnormal nuclear shape and impaired mechanotransduction in emerin-deficient cells. *J Cell Biol,* 170**,** 781-91.

LAMMERDING, J., SCHULZE, P. C., TAKAHASHI, T., KOZLOV, S., SULLIVAN, T., KAMM, R. D., STEWART, C. L. & LEE, R. T. 2004. Lamin A/C deficiency causes defective nuclear mechanics and mechanotransduction. *J Clin Invest,* 113**,** 370-8.

LAURSEN, L. S., CHAN, C. W. & FFRENCH-CONSTANT, C. 2011. Translation of myelin basic protein mRNA in oligodendrocytes is regulated by integrin activation and hnRNP-K. *J Cell Biol,* 192**,** 797-811.

LE, H. Q., GHATAK, S., YEUNG, C.-Y. C., TELLKAMP, F., GÜNSCHMANN, C., DIETERICH, C., YEROSLAVIZ, A., HABERMANN, B., POMBO, A., NIESSEN, C. M. & WICKSTRÖM, S. A. 2016. Mechanical regulation of transcription controls Polycomb-mediated gene silencing during lineage commitment. *Nature Cell Biology,* 18**,** 864-875.

LEE, J. H., HART, S. R. & SKALNIK, D. G. 2004. Histone deacetylase activity is required for embryonic stem cell differentiation. *Genesis,* 38**,** 32-8.

LEE, J. Y., DOMINGUEZ, A. A., NAM, S., STOWERS, R. S., QI, L. S. & CHAUDHURI, O. 2019a. Identification of cell context-dependent YAP-associated proteins reveals beta1 and beta4 integrin mediate YAP translocation independently of cell spreading. *Sci Rep,* 9**,** 17188.

LEE, Y., WIRIYASERMKUL, P., JIN, C., QUAN, L., OHGAKI, R., OKUDA, S., KUSAKIZAKO, T., NISHIZAWA, T., ODA, K., ISHITANI, R., YOKOYAMA, T., NAKANE, T., SHIROUZU, M., ENDOU, H., NAGAMORI, S., KANAI, Y. & NUREKI, O. 2019b. Cryo-EM structure of the human L-type amino acid transporter 1 in complex with glycoprotein CD98hc. *Nat Struct Mol Biol,* 26**,** 510-517.

LELE, T. P., PENDSE, J., KUMAR, S., SALANGA, M., KARAVITIS, J. & INGBER, D. E. 2006. Mechanical forces alter zyxin unbinding kinetics within focal adhesions of living cells. *J Cell Physiol,* 207**,** 187-94.

LI, J., CHEN, Y., TIWARI, M., BANSAL, V. & SEN, G. L. 2021. Regulation of integrin and extracellular matrix genes by HNRNPL is necessary for epidermal renewal. *PLoS Biol,* 19**,** e3001378.

LI, J., SONG, W., PAN, G. & ZHOU, J. 2014. Advances in understanding the cell types and approaches used for generating induced pluripotent stem cells. *Journal of Hematology & Oncology,* 7**,** 50.

LI, W. Q., ZHONG, N. Z., HE, J., LI, Y. M., HOU, L. J., LIU, H. M., XIA, C. Y., WANG, L. Z. & LU, Y. C. 2017. High ATP2A2 expression correlates with better prognosis of diffuse astrocytic tumor patients. *Oncol Rep,* 37**,** 2865-2874.

LIN, C. H. & FORSCHER, P. 1995. Growth cone advance is inversely proportional to retrograde F-actin flow. *Neuron,* 14**,** 763-71.

LOBERT, V. H., BRECH, A., PEDERSEN, N. M., WESCHE, J., OPPELT, A., MALERØD, L. & STENMARK, H. 2010. Ubiquitination of α5β1 Integrin Controls Fibroblast Migration through Lysosomal Degradation of Fibronectin-Integrin Complexes. *Developmental Cell,* 19**,** 148-159.

LOW, B. C., PAN, C. Q., SHIVASHANKAR, G. V., BERSHADSKY, A., SUDOL, M. & SHEETZ, M. 2014. YAP/TAZ as mechanosensors and mechanotransducers in regulating organ size and tumor growth. *FEBS Lett,* 588**,** 2663-70.

LU, C., WU, F., QIU, W. & LIU, R. 2013. P130Cas substrate domain is intrinsically disordered as characterized by single-molecule force measurements. *Biophys Chem,* 180-181**,** 37-43.

LUO, B. H. & SPRINGER, T. A. 2006. Integrin structures and conformational signaling. *Curr Opin Cell Biol,* 18**,** 579-86.

MAHMOOD, F., XU, R., AWAN, M. U. N., SONG, Y., HAN, Q., XIA, X. & ZHANG, J. 2021. PDIA3: Structure, functions and its potential role in viral infections. *Biomedicine & Pharmacotherapy,* 143**,** 112110.

MAI, A., VELTEL, S., PELLINEN, T., PADZIK, A., COFFEY, E., MARJOMÄKI, V. & IVASKA, J. 2011. Competitive binding of Rab21 and p120RasGAP to integrins regulates receptor traffic and migration. *J Cell Biol,* 194**,** 291-306.

MANDAI, M., WATANABE, A., KURIMOTO, Y., HIRAMI, Y., MORINAGA, C., DAIMON, T., FUJIHARA, M., AKIMARU, H., SAKAI, N., SHIBATA, Y., TERADA, M., NOMIYA, Y., TANISHIMA, S., NAKAMURA, M., KAMAO, H., SUGITA, S., ONISHI, A., ITO, T., FUJITA, K., KAWAMATA, S., GO, M. J., SHINOHARA, C., HATA, K. I., SAWADA, M., YAMAMOTO, M., OHTA, S., OHARA, Y., YOSHIDA, K., KUWAHARA, J., KITANO, Y., AMANO, N., UMEKAGE, M., KITAOKA, F., TANAKA, A., OKADA, C., TAKASU, N., OGAWA, S., YAMANAKA, S. & TAKAHASHI, M. 2017. Autologous Induced Stem-Cell-Derived Retinal Cells for Macular Degeneration. *N Engl J Med,* 376**,** 1038-1046.

MANIOTIS, A. J., CHEN, C. S. & INGBER, D. E. 1997. Demonstration of mechanical connections between integrins, cytoskeletal filaments, and nucleoplasm that stabilize nuclear structure. *Proc Natl Acad Sci U S A,* 94**,** 849-54.

MARGADANT, F., CHEW, L. L., HU, X., YU, H., BATE, N., ZHANG, X. & SHEETZ, M. 2011. Mechanotransduction in vivo by repeated talin stretch-relaxation events depends upon vinculin. *PLoS Biol,* 9**,** e1001223.

MARTIEL, J. L., LEAL, A., KURZAWA, L., BALLAND, M., WANG, I., VIGNAUD, T., TSENG, Q. & THÉRY, M. 2015. Measurement of cell traction forces with ImageJ. *Methods Cell Biol,* 125**,** 269-87.

MARTIN, G. R. 1981. Isolation of a pluripotent cell line from early mouse embryos cultured in medium conditioned by teratocarcinoma stem cells. *Proc Natl Acad Sci U S A,* 78**,** 7634-8.

MARTINO, F., PERESTRELO, A. R., VINARSKÝ, V., PAGLIARI, S. & FORTE, G. 2018. Cellular Mechanotransduction: From Tension to Function. *Frontiers in Physiology,* 9.

MATTOUT, A. & MESHORER, E. 2010. Chromatin plasticity and genome organization in pluripotent embryonic stem cells. *Curr Opin Cell Biol,* 22**,** 334-41.

MELLACHERUVU, D., WRIGHT, Z., COUZENS, A. L., LAMBERT, J.-P., ST-DENIS, N. A., LI, T., MITEVA, Y. V., HAURI, S., SARDIU, M. E., LOW, T. Y., HALIM, V. A., BAGSHAW, R. D., HUBNER, N. C., AL-HAKIM, A., BOUCHARD, A., FAUBERT, D., FERMIN, D., DUNHAM, W. H., GOUDREAULT, M., LIN, Z.-Y., BADILLO, B. G., PAWSON, T., DUROCHER, D., COULOMBE, B., AEBERSOLD, R., SUPERTI-FURGA, G., COLINGE, J., HECK, A. J. R., CHOI, H., GSTAIGER, M., MOHAMMED, S., CRISTEA, I. M., BENNETT, K. L., WASHBURN, M. P., RAUGHT, B., EWING, R. M., GINGRAS, A.-C. & NESVIZHSKII, A. I. 2013. The CRAPome: a contaminant repository for affinity purification–mass spectrometry data. *Nature Methods,* 10**,** 730-736.

MESHORER, E. & MISTELI, T. 2006. Chromatin in pluripotent embryonic stem cells and differentiation. *Nat Rev Mol Cell Biol,* 7**,** 540-6.

MIROSHNIKOVA, Y. A., NAVA, M. M. & WICKSTRÖM, S. A. 2017. Emerging roles of mechanical forces in chromatin regulation. *J Cell Sci,* 130**,** 2243-2250.

MITCHISON, T. & KIRSCHNER, M. 1988. Cytoskeletal dynamics and nerve growth. *Neuron,* 1**,** 761-772.

MIZUSHIMA, N., LEVINE, B., CUERVO, A. M. & KLIONSKY, D. J. 2008. Autophagy fights disease through cellular self-digestion. *Nature,* 451**,** 1069-75.

MOHRI, Z., DEL RIO HERNANDEZ, A. & KRAMS, R. 2017. The emerging role of YAP/TAZ in mechanotransduction. *J Thorac Dis,* 9**,** E507-e509.

MONTEIRO, A. I., KOLLMETZ, T. & MALMSTRÖM, J. 2018. Engineered systems to study the synergistic signaling between integrin-mediated mechanotransduction and growth factors (Review). *Biointerphases,* 13**,** 06d302.

MOORE, S. W., ROCA-CUSACHS, P. & SHEETZ, M. P. 2010. Stretchy proteins on stretchy substrates: the important elements of integrin-mediated rigidity sensing. *Dev Cell,* 19**,** 194-206.

MORGAN, M. R., HAMIDI, H., BASS, M. D., WARWOOD, S., BALLESTREM, C. & HUMPHRIES, M. J. 2013. Syndecan-4 phosphorylation is a control point for integrin recycling. *Dev Cell,* 24**,** 472-85.

NABA, A., CLAUSER, K. R., HOERSCH, S., LIU, H., CARR, S. A. & HYNES, R. O. 2012. The matrisome: in silico definition and in vivo characterization by proteomics of normal and tumor extracellular matrices. *Mol Cell Proteomics,* 11**,** M111.014647.

NAVA, M. M., MIROSHNIKOVA, Y. A., BIGGS, L. C., WHITEFIELD, D. B., METGE, F., BOUCAS, J., VIHINEN, H., JOKITALO, E., LI, X., GARCÍA ARCOS, J. M., HOFFMANN, B., MERKEL, R., NIESSEN, C. M., DAHL, K. N. & WICKSTRÖM, S. A. 2020. Heterochromatin-Driven Nuclear Softening Protects the Genome against Mechanical Stress-Induced Damage. *Cell,* 181**,** 800-817.e22.

NAZ, A., BISWAS, A., KHAN, T. N., GOODEVE, A., AHMED, N., SAQLAIN, N., AHMED, S., UJJAN, I. D., SHAMSI, T. S. & OLDENBURG, J. 2017. Identification of novel mutations in congenital afibrinogenemia patients and molecular modeling of missense mutations in Pakistani population. *Thrombosis Journal,* 15**,** 24.

NG, D. 2013. *Investigating the dynamics of adhesion complex turnover by mass spectrometry based proteomics.* PhD Thesis, University of Manchester.

NG, T., SHIMA, D., SQUIRE, A., BASTIAENS, P. I., GSCHMEISSNER, S., HUMPHRIES, M. J. & PARKER, P. J. 1999. PKCalpha regulates beta1 integrin-dependent cell motility through association and control of integrin traffic. *Embo j,* 18**,** 3909-23.

NICKLIN, P., BERGMAN, P., ZHANG, B., TRIANTAFELLOW, E., WANG, H., NYFELER, B., YANG, H., HILD, M., KUNG, C., WILSON, C., MYER, V. E., MACKEIGAN, J. P., PORTER, J. A., WANG, Y. K., CANTLEY, L. C., FINAN, P. M. & MURPHY, L. O. 2009. Bidirectional transport of amino acids regulates mTOR and autophagy. *Cell,* 136**,** 521-534.

NIEVES, B., JONES, C. W., WARD, R., OHTA, Y., REVERTE, C. G. & LAFLAMME, S. E. 2010. The NPIY motif in the integrin beta1 tail dictates the requirement for talin-1 in outside-in signaling. *J Cell Sci,* 123**,** 1216-26.

NISHIDA, N., XIE, C., SHIMAOKA, M., CHENG, Y., WALZ, T. & SPRINGER, T. A. 2006. Activation of Leukocyte β2 Integrins by Conversion from Bent to Extended Conformations. *Immunity,* 25**,** 583-594.

NUKUDA, A., SASAKI, C., ISHIHARA, S., MIZUTANI, T., NAKAMURA, K., AYABE, T., KAWABATA, K. & HAGA, H. 2015. Stiff substrates increase YAP-signaling-mediated matrix metalloproteinase-7 expression. *Oncogenesis,* 4**,** e165-e165.

OHNO, H., NAKATSU, Y., SAKODA, H., KUSHIYAMA, A., ONO, H., FUJISHIRO, M., OTANI, Y., OKUBO, H., YONEDA, M., FUKUSHIMA, T., TSUCHIYA, Y., KAMATA, H., NISHIMURA, F., KURIHARA, H., KATAGIRI, H., OKA, Y. & ASANO, T. 2011. 4F2hc stabilizes GLUT1 protein and increases glucose transport activity. *Am J Physiol Cell Physiol,* 300**,** C1047-54.

OXLEY, C. L., ANTHIS, N. J., LOWE, E. D., VAKONAKIS, I., CAMPBELL, I. D. & WEGENER, K. L. 2008. An integrin phosphorylation switch: the effect of beta3 integrin tail phosphorylation on Dok1 and talin binding. *J Biol Chem,* 283**,** 5420-6.

PAJEROWSKI, J. D., DAHL, K. N., ZHONG, F. L., SAMMAK, P. J. & DISCHER, D. E. 2007. Physical plasticity of the nucleus in stem cell differentiation. *Proc Natl Acad Sci U S A,* 104**,** 15619-24.

PANKOV, R., CUKIERMAN, E., KATZ, B. Z., MATSUMOTO, K., LIN, D. C., LIN, S., HAHN, C. & YAMADA, K. M. 2000. Integrin dynamics and matrix assembly: tensin-dependent translocation of alpha(5)beta(1) integrins promotes early fibronectin fibrillogenesis. *J Cell Biol,* 148**,** 1075-90.

PARK, S. H., PARK, S. H., KOOK, M. C., KIM, E. Y., PARK, S. & LIM, J. H. 2004. Ultrastructure of human embryonic stem cells and spontaneous and retinoic acid-induced differentiating cells. *Ultrastruct Pathol,* 28**,** 229-38.

PELHAM, R. J., JR. & WANG, Y. 1997. Cell locomotion and focal adhesions are regulated by substrate flexibility. *Proc Natl Acad Sci U S A,* 94**,** 13661-5.

PENAGOS-PUIG, A. & FURLAN-MAGARIL, M. 2020. Heterochromatin as an Important Driver of Genome Organization. *Front Cell Dev Biol,* 8**,** 579137.

PFEIFFER, R., SPINDLER, B., LOFFING, J., SKELLY, P. J., SHOEMAKER, C. B. & VERREY, F. 1998. Functional heterodimeric amino acid transporters lacking cysteine residues involved in disulfide bond. *FEBS Lett,* 439**,** 157-62.

PICCOLO, S., DUPONT, S. & CORDENONSI, M. 2014. The biology of YAP/TAZ: hippo signaling and beyond. *Physiol Rev,* 94**,** 1287-312.

PINHEIRO, C., LONGATTO-FILHO, A., AZEVEDO-SILVA, J., CASAL, M., SCHMITT, F. C. & BALTAZAR, F. 2012. Role of monocarboxylate transporters in human cancers: state of the art. *J Bioenerg Biomembr,* 44**,** 127-39.

PLOTNIKOV, S. V., PASAPERA, A. M., SABASS, B. & WATERMAN, C. M. 2012. Force fluctuations within focal adhesions mediate ECM-rigidity sensing to guide directed cell migration. *Cell,* 151**,** 1513-27.

POULET, A., ARGANDA-CARRERAS, I., LEGLAND, D., PROBST, A. V., ANDREY, P. & TATOUT, C. 2015. NucleusJ: an ImageJ plugin for quantifying 3D images of interphase nuclei. *Bioinformatics,* 31**,** 1144-6.

POWELKA, A. M., SUN, J., LI, J., GAO, M., SHAW, L. M., SONNENBERG, A. & HSU, V. W. 2004. Stimulation-dependent recycling of integrin beta1 regulated by ARF6 and Rab11. *Traffic,* 5**,** 20-36.

PRADHAN, R., RANADE, D. & SENGUPTA, K. 2018. Emerin modulates spatial organization of chromosome territories in cells on softer matrices. *Nucleic Acids Res,* 46**,** 5561-5586.

PRIGIONE, A., FAULER, B., LURZ, R., LEHRACH, H. & ADJAYE, J. 2010. The senescence-related mitochondrial/oxidative stress pathway is repressed in human induced pluripotent stem cells. *Stem Cells,* 28**,** 721-33.

PROWSE, A. B., CHONG, F., GRAY, P. P. & MUNRO, T. P. 2011. Stem cell integrins: implications for ex-vivo culture and cellular therapies. *Stem Cell Res,* 6**,** 1-12.

RABANAL-RUIZ, Y., BYRON, A., WIRTH, A., MADSEN, R., SEDLACKOVA, L., HEWITT, G., NELSON, G., STINGELE, J., WILLS, J. C., ZHANG, T., ZEUG, A., FÄSSLER, R., VANHAESEBROECK, B., MADDOCKS, O. D. K., PONIMASKIN, E., CARROLL, B. & KOROLCHUK, V. I. 2021. mTORC1 activity is supported by spatial association with focal adhesions. *Journal of Cell Biology,* 220.

RAINERO, E., HOWE, J. D., CASWELL, P. T., JAMIESON, N. B., ANDERSON, K., CRITCHLEY, D. R., MACHESKY, L. & NORMAN, J. C. 2015. Ligand-Occupied Integrin Internalization Links Nutrient Signaling to Invasive Migration. *Cell Rep,* 10**,** 398-413.

RANTALA, J. K., POUWELS, J., PELLINEN, T., VELTEL, S., LAASOLA, P., MATTILA, E., POTTER, C. S., DUFFY, T., SUNDBERG, J. P., KALLIONIEMI, O., ASKARI, J. A., HUMPHRIES, M. J., PARSONS, M., SALMI, M. & IVASKA, J. 2011. SHARPIN is an endogenous inhibitor of β1-integrin activation. *Nat Cell Biol,* 13**,** 1315-24.

REILLY, G. C. & ENGLER, A. J. 2010. Intrinsic extracellular matrix properties regulate stem cell differentiation. *J Biomech,* 43**,** 55-62.

RIVELINE, D., ZAMIR, E., BALABAN, N. Q., SCHWARZ, U. S., ISHIZAKI, T., NARUMIYA, S., KAM, Z., GEIGER, B. & BERSHADSKY, A. D. 2001. Focal contacts as mechanosensors: externally applied local mechanical force induces growth of focal contacts by an mDia1-dependent and ROCK-independent mechanism. *J Cell Biol,* 153**,** 1175-86.

ROBERTS, G. C. & CRITCHLEY, D. R. 2009. Structural and biophysical properties of the integrin-associated cytoskeletal protein talin. *Biophys Rev,* 1**,** 61-69.

ROCA-CUSACHS, P., GAUTHIER, N. C., DEL RIO, A. & SHEETZ, M. P. 2009. Clustering of alpha(5)beta(1) integrins determines adhesion strength whereas alpha(v)beta(3) and talin enable mechanotransduction. *Proc Natl Acad Sci U S A,* 106**,** 16245-50.

ROSS, E., ATA, R., THAVARAJAH, T., MEDVEDEV, S., BOWDEN, P., MARSHALL, J. G. & ANTONESCU, C. N. 2015. AMP-Activated Protein Kinase Regulates the Cell Surface Proteome and Integrin Membrane Traffic. *PLOS ONE,* 10**,** e0128013.

ROSSIER, O., OCTEAU, V., SIBARITA, J.-B., LEDUC, C., TESSIER, B., NAIR, D., GATTERDAM, V., DESTAING, O., ALBIGÈS-RIZO, C., TAMPÉ, R., COGNET, L., CHOQUET, D., LOUNIS, B. & GIANNONE, G. 2012. Integrins β1 and β3 exhibit distinct dynamic nanoscale organizations inside focal adhesions. *Nature Cell Biology,* 14**,** 1057-1067.

ROTHBALLER, A., SCHWARTZ, T. U. & KUTAY, U. 2013. LINCing complex functions at the nuclear envelope: what the molecular architecture of the LINC complex can reveal about its function. *Nucleus,* 4**,** 29-36.

ROWLAND, T. J., MILLER, L. M., BLASCHKE, A. J., DOSS, E. L., BONHAM, A. J., HIKITA, S. T., JOHNSON, L. V. & CLEGG, D. O. 2010. Roles of Integrins in Human Induced Pluripotent Stem Cell Growth on Matrigel and Vitronectin. *Stem Cells and Development,* 19**,** 1231-1240.

ROZARIO, T. & DESIMONE, D. W. 2010. The extracellular matrix in development and morphogenesis: a dynamic view. *Dev Biol,* 341**,** 126-40.

SALTI, A., ETEMAD, S., CUBERO, M. S., ALBERTINI, E., KOVACS-SZALKA, B., HOLZKNECHT, M., CAPPUCCIO, E., CAVINATO, M., EDENHOFER, F. & JANSEN DÜRR, P. 2021. High Glycolytic Activity Enhances Stem Cell Reprogramming of Fahd1-KO Mouse Embryonic Fibroblasts. *Cells,* 10**,** 2040.

SAWADA, Y., TAMADA, M., DUBIN-THALER, B. J., CHERNIAVSKAYA, O., SAKAI, R., TANAKA, S. & SHEETZ, M. P. 2006. Force sensing by mechanical extension of the Src family kinase substrate p130Cas. *Cell,* 127**,** 1015-26.

SAWAZAKI, R., IMAI, S., YOKOGAWA, M., HOSODA, N., HOSHINO, S.-I., MIO, M., MIO, K., SHIMADA, I. & OSAWA, M. 2018. Characterization of the multimeric structure of poly(A)-binding protein on a poly(A) tail. *Scientific Reports,* 8**,** 1455.

SCHAEFER, L. & SCHAEFER, R. M. 2010. Proteoglycans: from structural compounds to signaling molecules. *Cell Tissue Res,* 339**,** 237-46.

SCHAFER, Z. T., GRASSIAN, A. R., SONG, L., JIANG, Z., GERHART-HINES, Z., IRIE, H. Y., GAO, S., PUIGSERVER, P. & BRUGGE, J. S. 2009. Antioxidant and oncogene rescue of metabolic defects caused by loss of matrix attachment. *Nature,* 461**,** 109-113.

SCHILLER, H. B., HERMANN, M. R., POLLEUX, J., VIGNAUD, T., ZANIVAN, S., FRIEDEL, C. C., SUN, Z., RADUCANU, A., GOTTSCHALK, K. E., THÉRY, M., MANN, M. & FÄSSLER, R. 2013. β1- and αv-class integrins cooperate to regulate myosin II during rigidity sensing of fibronectin-based microenvironments. *Nat Cell Biol,* 15**,** 625-36.

SCHULTZ, G. S. & WYSOCKI, A. 2009. Interactions between extracellular matrix and growth factors in wound healing. *Wound Repair Regen,* 17**,** 153-62.

SCHWARTZ, L., DA VEIGA MOREIRA, J. & JOLICOEUR, M. 2018. Physical forces modulate cell differentiation and proliferation processes. *J Cell Mol Med,* 22**,** 738-745.

SHI, F. & SOTTILE, J. 2008. Caveolin-1-dependent beta1 integrin endocytosis is a critical regulator of fibronectin turnover. *J Cell Sci,* 121**,** 2360-71.

SHINDERMAN-MAMAN, E., COHEN, K., WEINGARTEN, C., NABRISKI, D., TWITO, O., BARAF, L., HERCBERGS, A., DAVIS, P. J., WERNER, H., ELLIS, M. & ASHUR-FABIAN, O. 2016. The thyroid hormone-αvβ3 integrin axis in ovarian cancer: regulation of gene transcription and MAPK-dependent proliferation. *Oncogene,* 35**,** 1977-87.

SMITH, L. R., CHO, S. & DISCHER, D. E. 2018. Stem Cell Differentiation is Regulated by Extracellular Matrix Mechanics. *Physiology (Bethesda),* 33**,** 16-25.

SONCIN, F. & WARD, C. M. 2011. The function of e-cadherin in stem cell pluripotency and self-renewal. *Genes,* 2**,** 229-259.

SPRINGER, T. A. & DUSTIN, M. L. 2012. Integrin inside-out signaling and the immunological synapse. *Curr Opin Cell Biol,* 24**,** 107-15.

STEPHENS, A. D., LIU, P. Z., BANIGAN, E. J., ALMASSALHA, L. M., BACKMAN, V., ADAM, S. A., GOLDMAN, R. D. & MARKO, J. F. 2018. Chromatin histone modifications and rigidity affect nuclear morphology independent of lamins. *Mol Biol Cell,* 29**,** 220-233.

STUBB, A., GUZMÁN, C., NÄRVÄ, E., AARON, J., CHEW, T.-L., SAARI, M., MIIHKINEN, M., JACQUEMET, G. & IVASKA, J. 2019. Superresolution architecture of cornerstone focal adhesions in human pluripotent stem cells. *Nature Communications,* 10**,** 4756.

SUN, C., ZARGHAM, R., SHAO, Q., GUI, X., MARCUS, V., LAZARIS, A., SALMAN, A., METRAKOS, P., QU, X. & GAO, Z. 2014. Association of CD98, integrin β1, integrin β3 and Fak with the progression and liver metastases of colorectal cancer. *Pathology - Research and Practice,* 210**,** 668-674.

SUN, Z., COSTELL, M. & FÄSSLER, R. 2019. Integrin activation by talin, kindlin and mechanical forces. *Nature Cell Biology,* 21**,** 25-31.

SWIFT, J., IVANOVSKA, I. L., BUXBOIM, A., HARADA, T., DINGAL, P. C., PINTER, J., PAJEROWSKI, J. D., SPINLER, K. R., SHIN, J. W., TEWARI, M., REHFELDT, F., SPEICHER, D. W. & DISCHER, D. E. 2013. Nuclear lamin-A scales with tissue stiffness and enhances matrix-directed differentiation. *Science,* 341**,** 1240104.

TAJIK, A., ZHANG, Y., WEI, F., SUN, J., JIA, Q., ZHOU, W., SINGH, R., KHANNA, N., BELMONT, A. S. & WANG, N. 2016. Transcription upregulation via force-induced direct stretching of chromatin. *Nat Mater,* 15**,** 1287-1296.

TAKAHASHI, K., TANABE, K., OHNUKI, M., NARITA, M., ICHISAKA, T., TOMODA, K. & YAMANAKA, S. 2007a. Induction of pluripotent stem cells from adult human fibroblasts by defined factors. *Cell,* 131**,** 861-72.

TAKAHASHI, K. & YAMANAKA, S. 2006. Induction of pluripotent stem cells from mouse embryonic and adult fibroblast cultures by defined factors. *Cell,* 126**,** 663-76.

TAKAHASHI, S., LEISS, M., MOSER, M., OHASHI, T., KITAO, T., HECKMANN, D., PFEIFER, A., KESSLER, H., TAKAGI, J., ERICKSON, H. P. & FÄSSLER, R. 2007b. The RGD motif in fibronectin is essential for development but dispensable for fibril assembly. *The Journal of cell biology,* 178**,** 167-178.

TANOSAKI, S., TOHYAMA, S., KISHINO, Y., FUJITA, J. & FUKUDA, K. 2021. Metabolism of human pluripotent stem cells and differentiated cells for regenerative therapy: a focus on cardiomyocytes. *Inflammation and Regeneration,* 41**,** 5.

TEE, S. Y., FU, J., CHEN, C. S. & JANMEY, P. A. 2011. Cell shape and substrate rigidity both regulate cell stiffness. *Biophys J,* 100**,** L25-7.

THEODOSIOU, M., WIDMAIER, M., BÖTTCHER, R. T., ROGNONI, E., VEELDERS, M., BHARADWAJ, M., LAMBACHER, A., AUSTEN, K., MÜLLER, D. J., ZENT, R. & FÄSSLER, R. 2016. Kindlin-2 cooperates with talin to activate integrins and induces cell spreading by directly binding paxillin. *Elife,* 5**,** e10130.

THERIOT, J. A. & MITCHISON, T. J. 1991. Actin microfilament dynamics in locomoting cells. *Nature,* 352**,** 126-31.

THIEVESSEN, I., FAKHRI, N., STEINWACHS, J., KRAUS, V., MCISAAC, R. S., GAO, L., CHEN, B. C., BAIRD, M. A., DAVIDSON, M. W., BETZIG, E., OLDENBOURG, R., WATERMAN, C. M. & FABRY, B. 2015. Vinculin is required for cell polarization, migration, and extracellular matrix remodeling in 3D collagen. *Faseb j,* 29**,** 4555-67.

THOMSON, J. A., ITSKOVITZ-ELDOR, J., SHAPIRO, S. S., WAKNITZ, M. A., SWIERGIEL, J. J., MARSHALL, V. S. & JONES, J. M. 1998. Embryonic stem cell lines derived from human blastocysts. *Science,* 282**,** 1145-7.

THOMSON, M., LIU, S. J., ZOU, L. N., SMITH, Z., MEISSNER, A. & RAMANATHAN, S. 2011. Pluripotency factors in embryonic stem cells regulate differentiation into germ layers. *Cell,* 145**,** 875-89.

THUAUD, F., RIBEIRO, N., NEBIGIL, C. G. & DÉSAUBRY, L. 2013. Prohibitin ligands in cell death and survival: mode of action and therapeutic potential. *Chemistry & biology,* 20**,** 316-331.

TOTARO, A., CASTELLAN, M., BATTILANA, G., ZANCONATO, F., AZZOLIN, L., GIULITTI, S., CORDENONSI, M. & PICCOLO, S. 2017. YAP/TAZ link cell mechanics to Notch signalling to control epidermal stem cell fate. *Nat Commun,* 8**,** 15206.

TRUONG, T., SHAMS, H. & MOFRAD, M. R. K. 2015. Mechanisms of integrin and filamin binding and their interplay with talin during early focal adhesion formation. *Integrative Biology,* 7**,** 1285-1296.

TSOGTBAATAR, E., LANDIN, C., MINTER-DYKHOUSE, K. & FOLMES, C. D. L. 2020. Energy Metabolism Regulates Stem Cell Pluripotency. *Frontiers in cell and developmental biology,* 8**,** 87-87.

TULOUP-MINGUEZ, V., HAMAÏ, A., GREFFARD, A., NICOLAS, V., CODOGNO, P. & BOTTI, J. 2013. Autophagy modulates cell migration and β1 integrin membrane recycling. *Cell Cycle,* 12**,** 3317-28.

TURGAY, Y., EIBAUER, M., GOLDMAN, A. E., SHIMI, T., KHAYAT, M., BEN-HARUSH, K., DUBROVSKY-GAUPP, A., SAPRA, K. T., GOLDMAN, R. D. & MEDALIA, O. 2017. The molecular architecture of lamins in somatic cells. *Nature,* 543**,** 261-264.

VALLIN, J. & GRANTHAM, J. 2019. The role of the molecular chaperone CCT in protein folding and mediation of cytoskeleton-associated processes: implications for cancer cell biology. *Cell Stress and Chaperones,* 24**,** 17-27.

VANDER HEIDEN, M. G., CANTLEY, L. C. & THOMPSON, C. B. 2009. Understanding the Warburg effect: the metabolic requirements of cell proliferation. *Science (New York, N.Y.),* 324**,** 1029-1033.

VARRICCHIO, L., FALCHI, M., DALL'ORA, M., DE BENEDITTIS, C., RUGGERI, A., UVERSKY, V. N. & MIGLIACCIO, A. R. 2017. Calreticulin: Challenges Posed by the Intrinsically Disordered Nature of Calreticulin to the Study of Its Function. *Front Cell Dev Biol,* 5**,** 96.

VEETTIL MOHANAN, V., SADAGOPAN, S., SHARMA-WALIA, N., WANG, F.-Z., RAGHU, H., VARGA, L. & CHANDRAN, B. 2008. Kaposi's Sarcoma-Associated Herpesvirus Forms a Multimolecular Complex of Integrins (αVβ5, αVβ3, and α3β1) and CD98-xCT during Infection of Human Dermal Microvascular Endothelial Cells, and CD98-xCT Is Essential for the Postentry Stage of Infection. *Journal of Virology,* 82**,** 12126-12144.

VICENTE-MANZANARES, M. & HORWITZ, A. R. 2011. Adhesion dynamics at a glance. *Journal of cell science,* 124**,** 3923-3927.

VITORINO, P., YEUNG, S., CROW, A., BAKKE, J., SMYCZEK, T., WEST, K., MCNAMARA, E., EASTHAM-ANDERSON, J., GOULD, S., HARRIS, S. F., NDUBAKU, C. & YE, W. 2015. MAP4K4 regulates integrin-FERM binding to control endothelial cell motility. *Nature,* 519**,** 425-30.

VLCEK, S., JUST, H., DECHAT, T. & FOISNER, R. 1999. Functional diversity of LAP2alpha and LAP2beta in postmitotic chromosome association is caused by an alpha-specific nuclear targeting domain. *Embo j,* 18**,** 6370-84.

WANG, D. Y., MELERO, C., ALBARAKY, A., ATHERTON, P., JANSEN, K. A., DIMITRACOPOULOS, A., DAJAS-BAILADOR, F., REID, A., FRANZE, K. & BALLESTREM, C. 2021a. Vinculin is required for neuronal mechanosensing but not for axon outgrowth. *Exp Cell Res,* 407**,** 112805.

WANG, H., LUO, X. & LEIGHTON, J. 2015. Extracellular Matrix and Integrins in Embryonic Stem Cell Differentiation. *Biochem Insights,* 8**,** 15-21.

WANG, M., LIU, J., TU, Y., ZHAO, Z., QU, J., CHEN, K., CHEN, Y., SUN, Y., ZHAO, H., DENG, Y. & WU, C. 2021b. RSU-1 interaction with prohibitin-2 links cell–extracellular matrix detachment to downregulation of ERK signaling. *Journal of Biological Chemistry,* 296**,** 100109.

WANG, N., TYTELL, J. D. & INGBER, D. E. 2009a. Mechanotransduction at a distance: mechanically coupling the extracellular matrix with the nucleus. *Nat Rev Mol Cell Biol,* 10**,** 75-82.

WANG, X., LIN, G., MARTINS-TAYLOR, K., ZENG, H. & XU, R. H. 2009b. Inhibition of caspase-mediated anoikis is critical for basic fibroblast growth factor-sustained culture of human pluripotent stem cells. *J Biol Chem,* 284**,** 34054-64.

WATT, F. M. & HUCK, W. T. 2013. Role of the extracellular matrix in regulating stem cell fate. *Nat Rev Mol Cell Biol,* 14**,** 467-73.

WAYNER, E. A., ORLANDO, R. A. & CHERESH, D. A. 1991. Integrins alpha v beta 3 and alpha v beta 5 contribute to cell attachment to vitronectin but differentially distribute on the cell surface. *The Journal of cell biology,* 113**,** 919-929.

WIBLIN, A. E., CUI, W., CLARK, A. J. & BICKMORE, W. A. 2005. Distinctive nuclear organisation of centromeres and regions involved in pluripotency in human embryonic stem cells. *J Cell Sci,* 118**,** 3861-8.

WILLETT, M., POLLARD, H. J., VLASAK, M. & MORLEY, S. J. 2010. Localization of ribosomes and translation initiation factors to talin/beta3-integrin-enriched adhesion complexes in spreading and migrating mammalian cells. *Biol Cell,* 102**,** 265-76.

WINOGRAD-KATZ, S. E., FÄSSLER, R., GEIGER, B. & LEGATE, K. R. 2014. The integrin adhesome: from genes and proteins to human disease. *Nature Reviews Molecular Cell Biology,* 15**,** 273-288.

WINOGRAD-KATZ, S. E., ITZKOVITZ, S., KAM, Z. & GEIGER, B. 2009. Multiparametric analysis of focal adhesion formation by RNAi-mediated gene knockdown. *J Cell Biol,* 186**,** 423-36.

WOLANSKA, K. I. & MORGAN, M. R. 2015. Fibronectin remodelling: cell-mediated regulation of the microenvironment. *Biochem Soc Trans,* 43**,** 122-8.

WOLFENSON, H., LAVELIN, I. & GEIGER, B. 2013. Dynamic regulation of the structure and functions of integrin adhesions. *Dev Cell,* 24**,** 447-58.

WOODS, A. J., KANTIDAKIS, T., SABE, H., CRITCHLEY, D. R. & NORMAN, J. C. 2005. Interaction of paxillin with poly(A)-binding protein 1 and its role in focal adhesion turnover and cell migration. *Mol Cell Biol,* 25**,** 3763-73.

WOODS, A. J., ROBERTS, M. S., CHOUDHARY, J., BARRY, S. T., MAZAKI, Y., SABE, H., MORLEY, S. J., CRITCHLEY, D. R. & NORMAN, J. C. 2002. Paxillin associates with poly(A)-binding protein 1 at the dense endoplasmic reticulum and the leading edge of migrating cells. *J Biol Chem,* 277**,** 6428-37.

WU, B., CHANG, N., XI, H., XIONG, J., ZHOU, Y., WU, Y., WU, S., WANG, N., YI, H., SONG, Y., CHEN, L. & ZHANG, J. 2021. PHB2 promotes tumorigenesis via RACK1 in non-small cell lung cancer. *Theranostics,* 11**,** 3150-3166.

WU, N., REN, D., LI, S., MA, W., HU, S., JIN, Y. & XIAO, S. 2018. RCC2 over-expression in tumor cells alters apoptosis and drug sensitivity by regulating Rac1 activation. *BMC Cancer,* 18**,** 67.

XIAO, T., TAKAGI, J., COLLER, B. S., WANG, J. H. & SPRINGER, T. A. 2004. Structural basis for allostery in integrins and binding to fibrinogen-mimetic therapeutics. *Nature,* 432**,** 59-67.

YAN, R., ZHAO, X., LEI, J. & ZHOU, Q. 2019. Structure of the human LAT1-4F2hc heteromeric amino acid transporter complex. *Nature,* 568**,** 127-130.

YASHIRO, K., SHIRATORI, H. & HAMADA, H. 2007. Haemodynamics determined by a genetic programme govern asymmetric development of the aortic arch. *Nature,* 450**,** 285-8.

YE, Q. & WORMAN, H. J. 1996. Interaction between an integral protein of the nuclear envelope inner membrane and human chromodomain proteins homologous to Drosophila HP1. *J Biol Chem,* 271**,** 14653-6.

YUE, B. 2014. Biology of the extracellular matrix: an overview. *J Glaucoma,* 23**,** S20-3.

ZHANG, J., NOU, X. A., KIM, H. & SCARCELLI, G. 2017. Brillouin flow cytometry for label-free mechanical phenotyping of the nucleus. *Lab Chip,* 17**,** 663-670.

ZHANG, R., ZHANG, C., ZHAO, Q. & LI, D. 2013. Spectrin: structure, function and disease. *Sci China Life Sci,* 56**,** 1076-85.

ZHENG, J. 2012. Energy metabolism of cancer: Glycolysis versus oxidative phosphorylation (Review). *Oncology letters,* 4**,** 1151-1157.

ZHENG, R., GHIRLANDO, R., LEE, M. S., MIZUUCHI, K., KRAUSE, M. & CRAIGIE, R. 2000. Barrier-to-autointegration factor (BAF) bridges DNA in a discrete, higher-order nucleoprotein complex. *Proc Natl Acad Sci U S A,* 97**,** 8997-9002.

ZHOU, H. & KRAMER, R. H. 2005. Integrin engagement differentially modulates epithelial cell motility by RhoA/ROCK and PAK1. *J Biol Chem,* 280**,** 10624-35.

Appendix

A

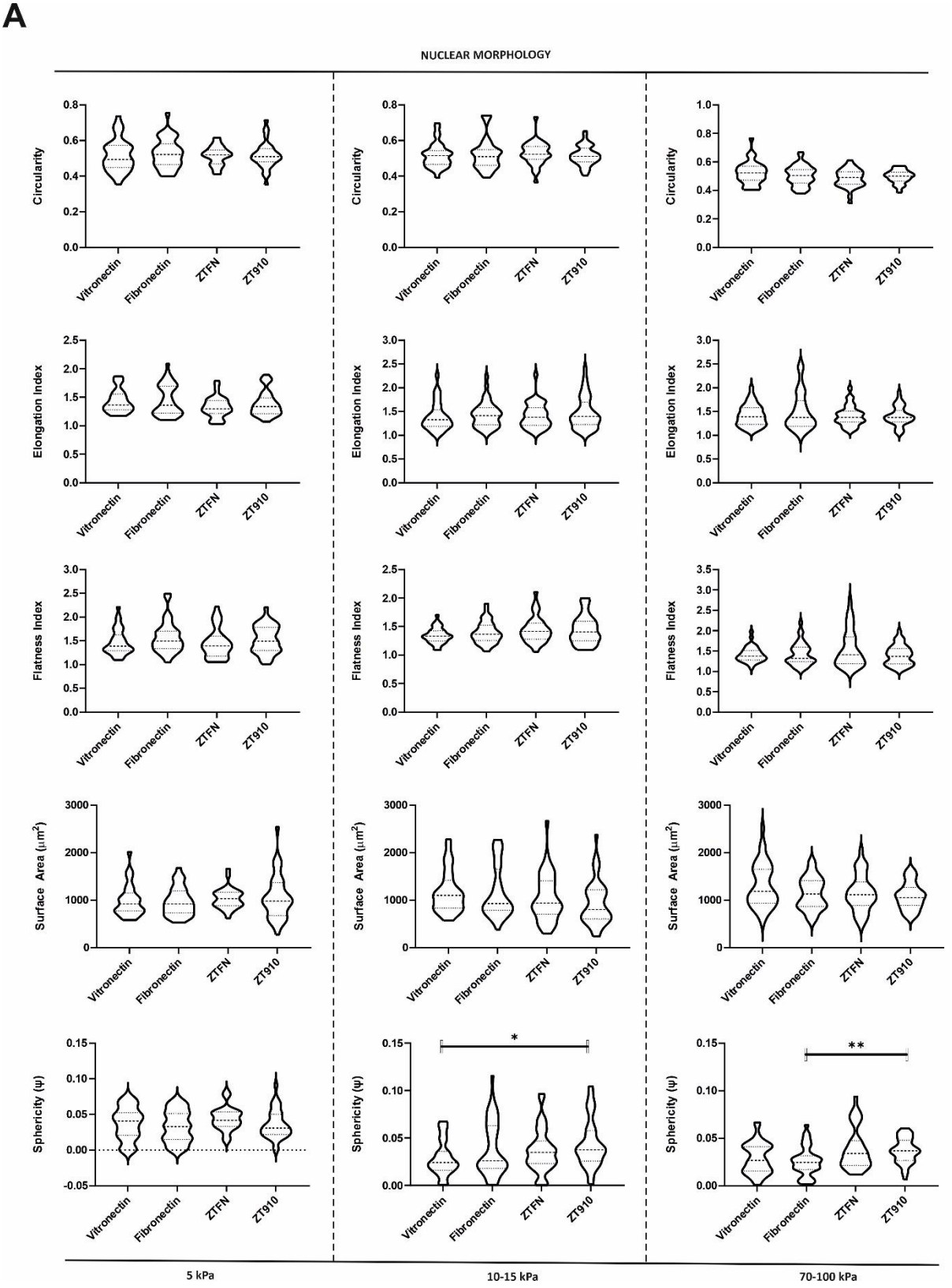
NUCLEAR MORPHOLOGY
Circularity
Elongation Index
Flatness Index
Surface Area (μm²)
Sphericity (ψ)
Vitronectin
Fibronectin
ZTFN
ZT910
*
**
5 kPa
10-15 kPa
70-100 kPa

B

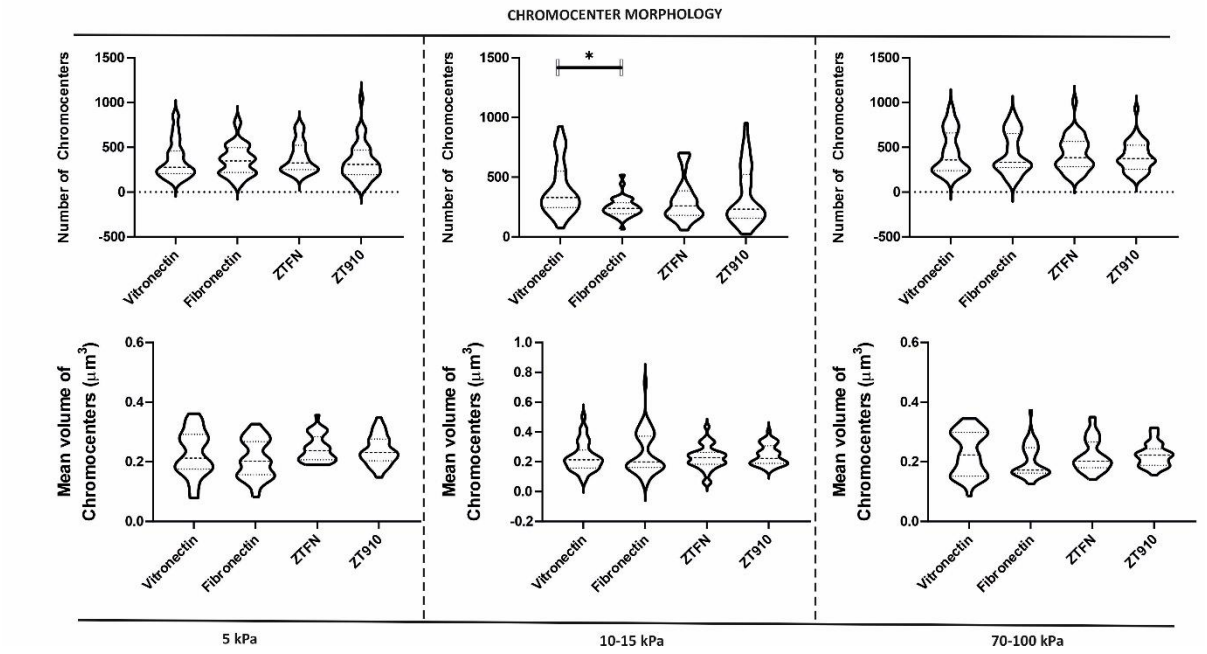

Supplementary Figure 1: Nuclear and chromocentre morphology of iPSCs on different rigidities. iPSCs plated on vitronectin (5µg/mL), fibronectin (10µg/mL), ZTFN (10µg/mL) and ZT910 (10µg/mL) for 4 hours. The cells were plated on three different rigidities ranging from soft to stiff rigidity; 5kPa, 10-15 kPa and 70-100 kPa respectively. (A) Quantitative profile of nuclear morphology including circularity, elongation index, flatness index, sphericity and surface area. (B) Quantitative profile of chromocentre morphology including the number of chromocenter, mean volume of chromocentres, distance from barycentre to border and distance from barycentre border to border. Nuclear and chromocentre morphology were determined by imageJ plugin NucleusJ. Data shown are representative of three independent experiments. Violin plots represent median, upper and lower quartiles. Kruskal-Wallis with Dunn's post-hoc test: * $p<0.05$.

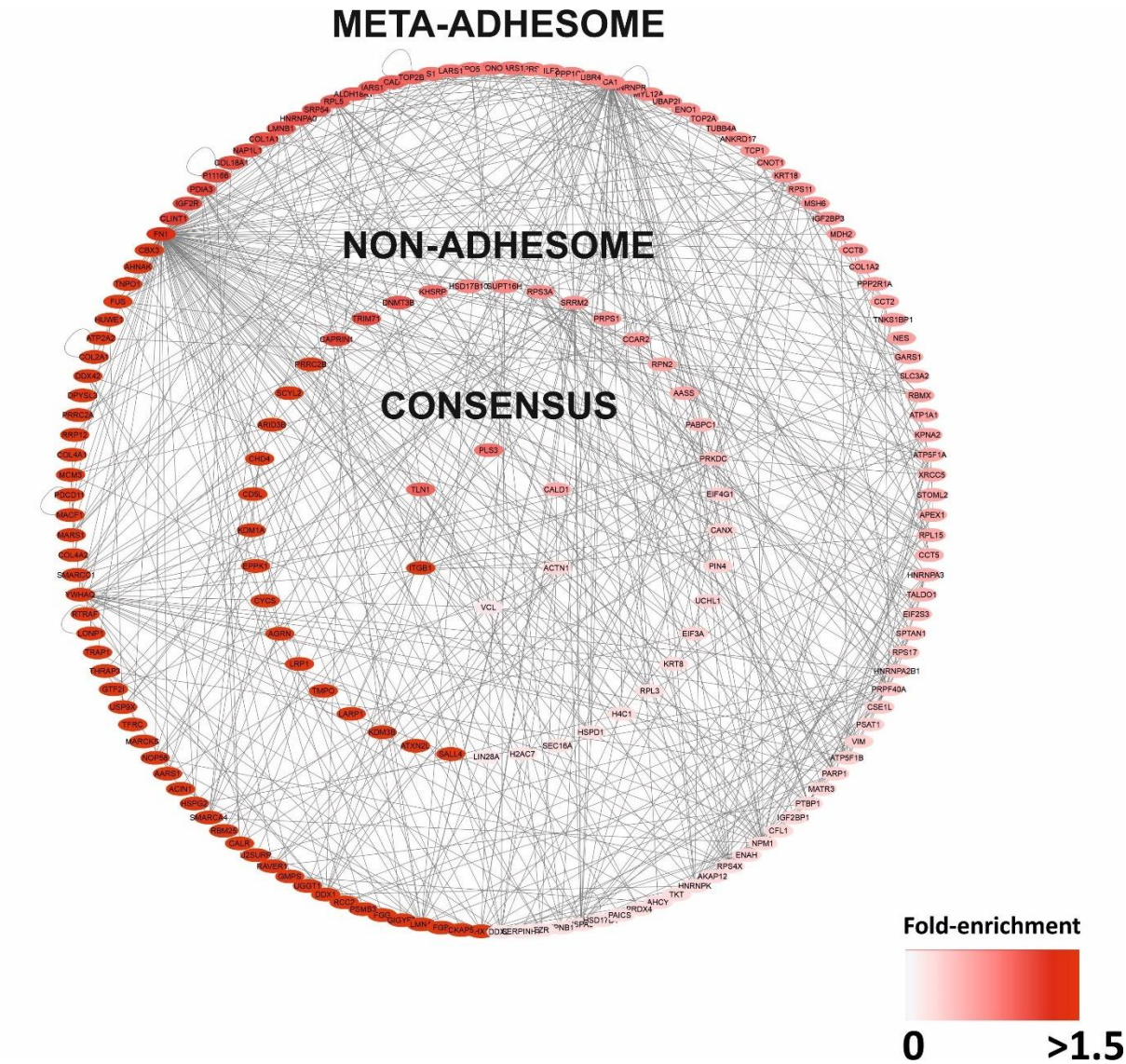

Supplementary Figure 2: **α5β1-associated adhesome (Fibronectin).** >1.5-fold enriched proteins on fibronectin versus E-cadherin. Total number of proteins = 182. Node colour red to blue gradient = log2 fold enrichment Fibronectin versus E-cadherin. Protein nodes are organised into the consensus, meta-adhesome and non-adhesome.

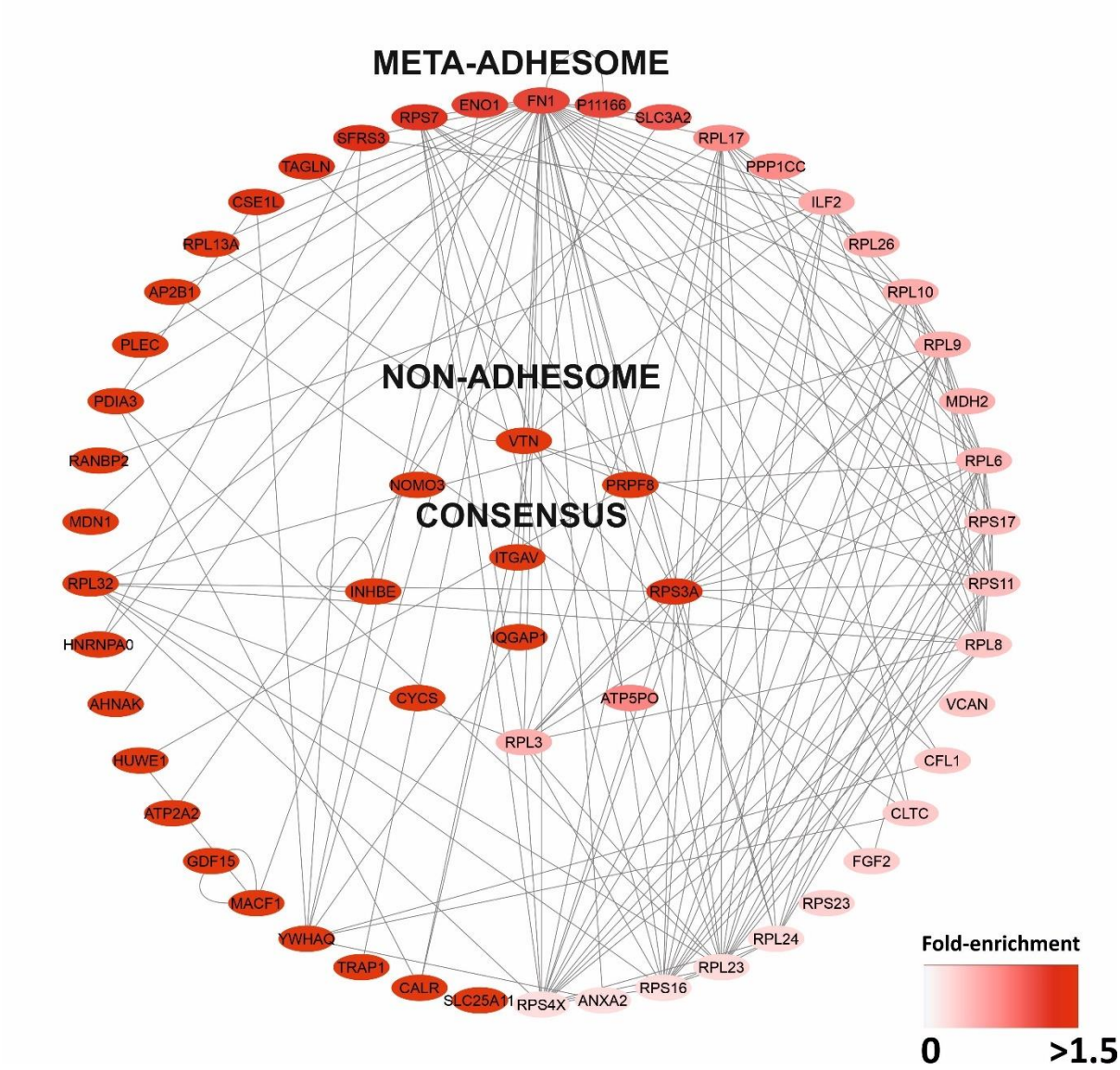

Supplementary Figure 3: αVβ5-associated adhesome (Vitronectin). >1.5-fold enriched proteins on vitronectin versus E-cadherin. Total number of proteins = 56. Node colour red to blue gradient = log2 fold enrichment vitronectin versus E-cadherin. Protein nodes are organised into the consensus, meta-adhesome and non-adhesome.

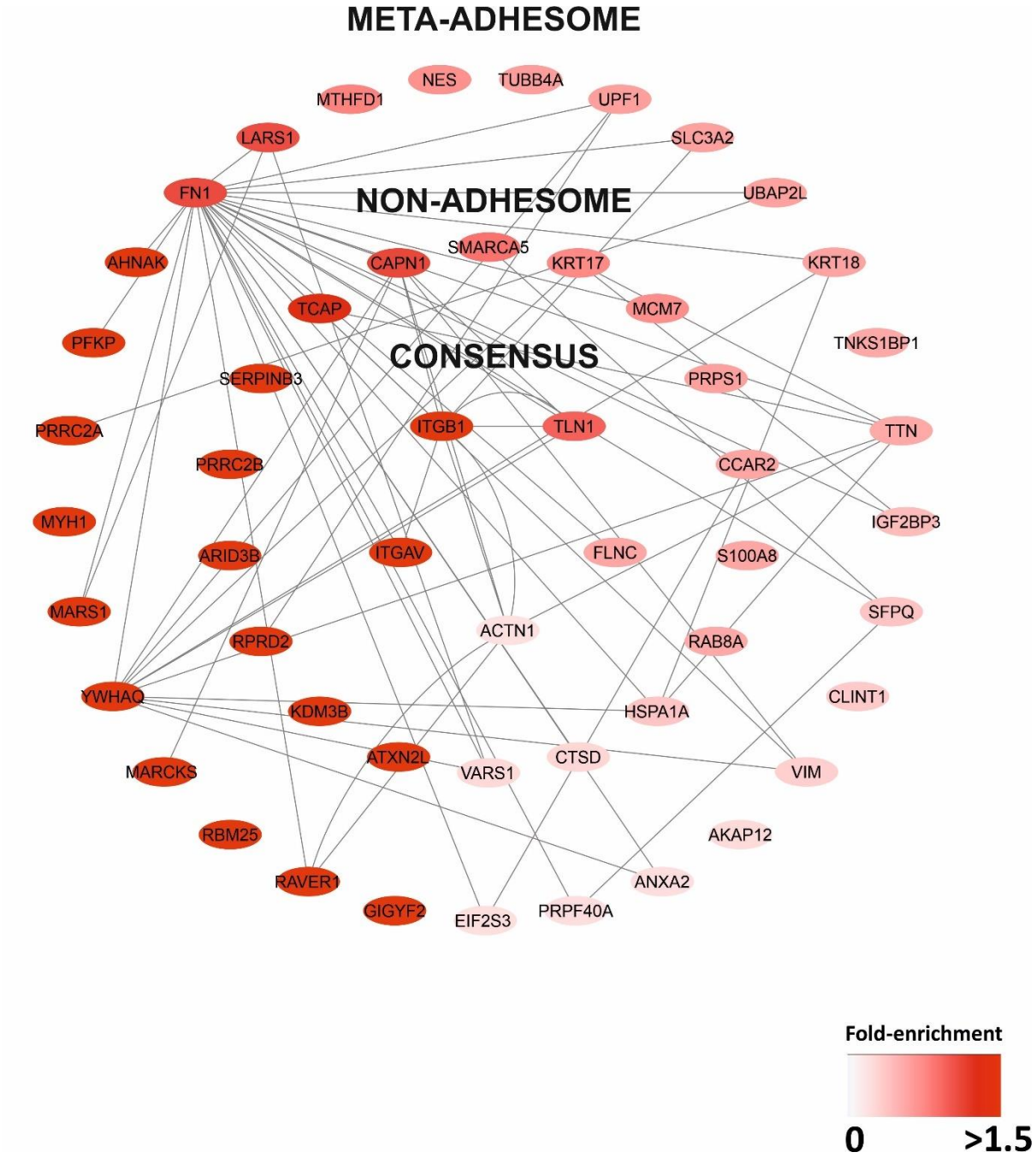

Supplementary Figure 4: αVβ1-associated adhesome (ZTFN). >1.5-fold enriched proteins on ZTFN versus E-cadherin. Total number of proteins = 52. Node colour red to blue gradient = log2 fold enrichment ZTFN versus E-cadherin. Protein nodes are organised into the consensus, meta-adhesome and non-adhesome.

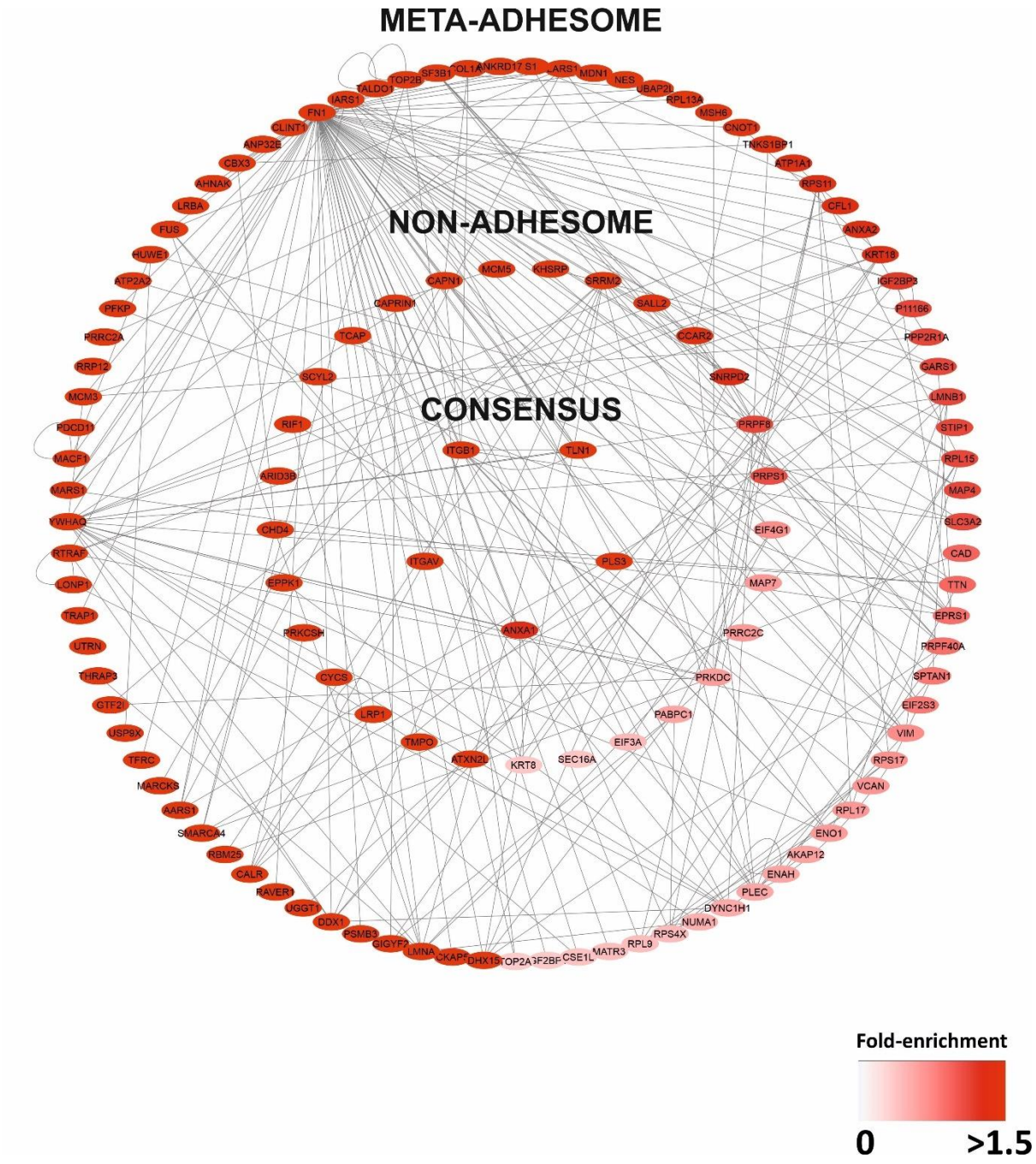

Supplementary Figure 5: α5β1-associated adhesome (ZT910). >1.5-fold enriched proteins on ZT910 versus E-cadherin. Total number of proteins = 123. Node colour red to blue gradient = log2 fold enrichment ZT910 versus E-cadherin. Protein nodes are organised into the consensus, meta-adhesome and non-adhesome.

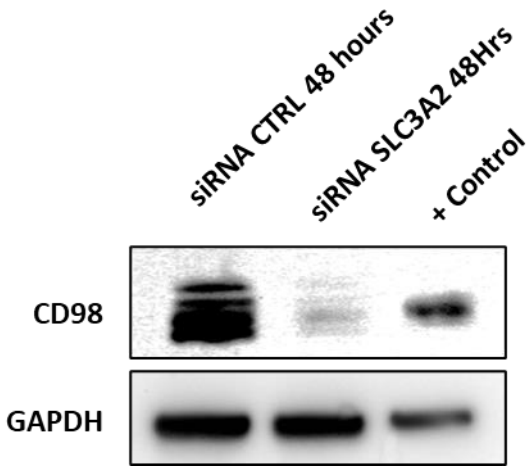

Supplementary Figure 6: Expression of SLC3A2 following siRNA silencing 48 hours after knockdown. Immunoblotting of SLC3A2 of single iPSC plated on vitronectin and fibronectin for 4 hours. 92% of SLC3A2 knockdown was achieved. Representative immunoblot is shown of two independent experiments.

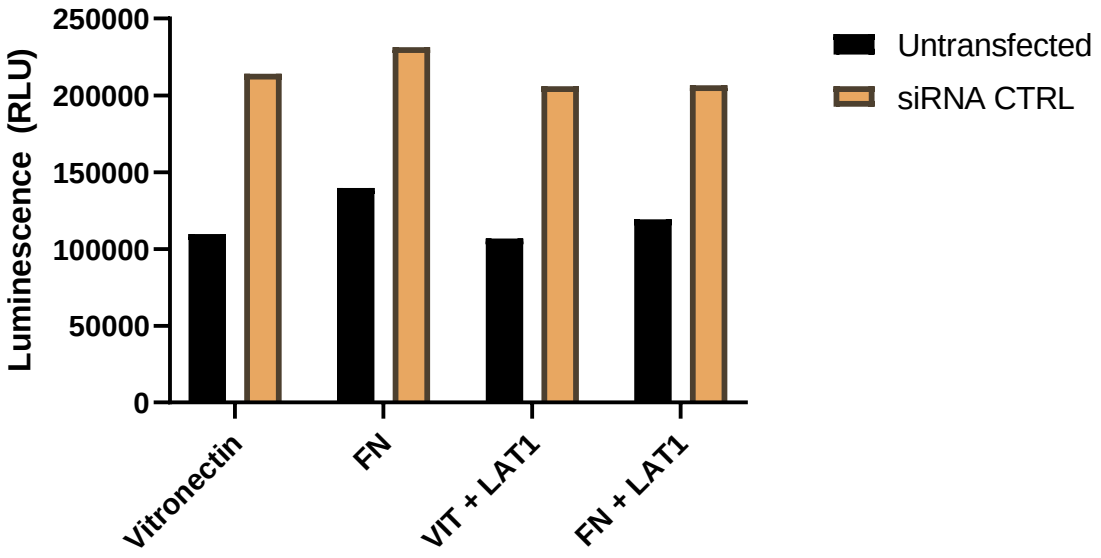

Supplementary Figure 7: Cell-titre Glo ATP assay of iPSC siRNA control and siRNA and SLC3A2. Cell-titre Glo ATP assay of iPSC siRNA control and siRNA SLC3A2 plated on vitronectin and fibronectin for 4 hours. Luminescence represents raw luminescence Data are shown as mean ± SEM of three independent experiments.

Supplementary table 1: Reactome GO Term analysis of protein enriched on Fibronectin compared to the negative control E-cadherin. Top group leading terms with their respective statistical p values, and the Benjamini-Hochberg corrected p value. Associated Genes Found comprises the list of proteins identified with the MS dataset and within each GO term.

ID	Term	Group PValue	Group PValue Corrected with Benjamini-Hochberg	Associated Genes Found
R-HSA:9675108	Nervous system development	2.84E-01	3.49E-01	[AGRN, CFL1, COL2A1, COL4A1, COL4A2, DPYSL3, EIF4G1, ENAH, EZR, ITGB1, MYL12A, PABPC1, PSMB3, RPL15, RPL3, RPL5, RPS11, RPS17, RPS3A, RPS4X, SMARCA4, SPTAN1, TLN1, TUBB4A]
R-HSA:8953854	Metabolism of RNA	9.69E-09	1.55E-07	[CNOT1, DDX1, DDX21, DDX42, DHX15, EIF4G1, EPRS1, FUS, HNRNPA0, HNRNPA2B1, HNRNPA3, HNRNPK, HNRNPR, HSD17B10, IGF2BP1, IGF2BP3, KHSRP, NOP58, PABPC1, PDCD11, PPP2R1A, PRPF40A, PSMB3, PTBP1, RBMX, RPL15, RPL3, RPL5, RPS11, RPS17, RPS3A, RPS4X, RTRAF, SRRM2, TNKS1BP1, TNPO1, U2SURP]
R-HSA:1643685	Disease	9.69E-09	1.55E-07	[AGRN, AHCY, ATP1A1, CALR, CANX, CHD4, DNMT3B, ENO1, FGB, FGG, FN1, H2AC7, H4-16, HNRNPK, HSPG2, IPO5, ITGB1, KDM1A, KPNA2, KPNB1, LMNA, LMNB1, MSH6, NPM1, PARP1, PPP1CC, PPP2R1A, PSMB3, RPL15, RPL3, RPL5, RPN2, RPS11, RPS17, RPS3A, RPS4X, SLC2A1, SLC3A2, SND1, SUPT16H, TALDO1, TLN1, TUBB4A, VCL, XRCC5]
R-HSA:1640170	Cell Cycle	9.69E-09	1.55E-07	[CKAP5, H2AC7, H4-16, KPNB1, LMNA, LMNB1, MCM3, NPM1, PPP1CC, PPP2R1A, PSMB3, RCC2, TMPO, TNPO1, TOP2A, TUBB4A,
R-HSA:168256	Immune System	2.84E-01	3.49E-01	[CALR, CAND1, CANX, CCT2, CCT8, CFL1, COL1A1, COL1A2, COL2A1, EIF4G1, ENAH, FGB, FGG, FN1, HNRNPA2B1, HSPA5, HUWE1, IGF2R, ILF2, ITGB1, KPNA2, KPNB1, LMNB1, PDIA3, PPP2R1A, PRDX4, PRKDC, PSMB3, SMARCA4, SPTAN1, TALDO1, TCP1, TRIM71,
R-HSA:156827	L13a-mediated translational silencing of Ceruloplasmin expression	6.79E-08	5.43E-07	[EIF2S3, EIF3A, EIF4G1, PABPC1, RPL15, RPL3, RPL5, RPS11, RPS17, RPS3A, RPS4X]
R-HSA:392499	Metabolism of proteins	1.36E-05	5.42E-05	[AARS1, CALR, CAND1, CANX, CCT2, CCT5, CCT8, DNMT3B, EIF2S3, EIF3A, EIF4G1, EPRS1, FGG, FN1, GARS1, H2AC7, H4-16, HNRNPK, HSPA5, HSPG2, IARS1, KHSRP, LARS1, LMNA, MARS1, NOP58, NPM1, PABPC1, PARP1, PDIA3, PRKDC, PSMB3, RARS1, RPL15, RPL3, RPL5, RPN2, RPS11, RPS17, RPS3A, RPS4X, SEC16A, SPTAN1, SRP54, TCP1, TLN1, TOP2A, TOP2B, TUBB4A, UCHL1,
R-HSA:168249	Innate Immune System	4.52E-03	9.05E-03	[CAND1, CCT2, CCT8, CFL1, FGB, FGG, HUWE1, IGF2R, ILF2, KPNB1, PPP2R1A, PRDX4, PRKDC, PSMB3, SPTAN1, UBR4, VCL,
R-HSA:1266738	Developmental Biology	1.90E-05	6.07E-05	[AGRN, CFL1, COL2A1, COL4A1, COL4A2, DPYSL3, EIF4G1, ENAH, EZR, H2AC7, H4-16, ITGB1, KRT18, KRT8, LIN28A, MYL12A, PABPC1, PSMB3, RPL15, RPL3, RPL5, RPS11, RPS17, RPS3A, RPS4X, SALL4, SMARCA4, SPTAN1, THRAP3, TLN1, TUBB4A]
R-HSA:162582	Signal Transduction	1.60E-01	2.13E-01	[ACTN1, AKAP12, ATP2A2, CCT2, CFL1, CHD4, CKAP5, COL1A1, COL1A2, COL2A1, COL4A1, COL4A2, EIF4G1, FGB, FGG, FN1, H2AC7, H4-16, IGF2BP1, ITGB1, KDM1A, KPNA2, LMNB1, MYL12A, PARP1, PPP1CC, PPP2R1A, PSMB3, PTBP1, RBMX, RCC2, SALL4, SMARCA4, SPTAN1, TFRC, TLN1, TMPO, TUBB4A, USP9X, VCL, VIM, YWHAQ]
R-HSA:1280218	Adaptive Immune System	5.11E-02	8.17E-02	[CALR, CANX, COL1A1, COL1A2, COL2A1, ENAH, FGB, FGG, HSPA5, HUWE1, ITGB1, PDIA3, PPP2R1A, PSMB3, TRIM71, TUBB4A,
R-HSA:597592	Post-translational protein modification	5.83E-01	6.22E-01	[CALR, CAND1, CANX, DNMT3B, FGG, FN1, H2AC7, H4-16, HNRNPK, NOP58, NPM1, PARP1, PDIA3, PRKDC, PSMB3, RPN2, SEC16A, SPTAN1, TOP2A, TOP2B, TUBB4A, UCHL1, UGGT1, USP9X]
R-HSA:5663205	Infectious disease	4.32E-04	9.88E-04	[ATP1A1, CALR, CANX, CHD4, ENO1, H2AC7, H4-16, HNRNPK, IPO5, ITGB1, KDM1A, KPNA2, KPNB1, NPM1, PARP1, PSMB3, RPL15, RPL3, RPL5, RPN2, RPS11, RPS17, RPS3A, RPS4X, SUPT16H, TUBB4A, XRCC5]
R-HSA:194315	Signaling by Rho GTPases	3.36E-04	8.96E-04	[ACTN1, AKAP12, CCT2, CFL1, CKAP5, H2AC7, H4-16, ITGB1, KDM1A, LMNB1, MYL12A, PPP1CC, PPP2R1A, RBMX, RCC2, SPTAN1, TFRC, TMPO, TUBB4A, USP9X, VIM, YWHAQ]
R-HSA:3000171	Non-integrin membrane-ECM interactions	9.14E-02	1.33E-01	[ACTN1, AGRN, COL1A1, COL1A2, COL2A1, COL4A1, COL4A2, FN1, HSPG2, ITGB1]
R-HSA:1430728	Metabolism	3.46E-01	3.96E-01	[AASS, AGRN, AHCY, ALDH18A1, ATP5F1A, ATP5F1B, CAD, CYCS, ENO1, EPRS1, GMPS, HSD17B10, HSD17B4, HSPG2, IARS1, KPNB1, LARS1, LRP1, MARCKS, MARS1, MDH2, PAICS, PPP1CC, PPP2R1A, PRPS1, PSAT1, PSMB3, RARS1, RPL15, RPL3, RPL5, RPS11, RPS17, RPS3A, RPS4X, SLC2A1, SLC3A2, TALDO1, THRAP3, TKT, TRAP1]

Supplementary table 2: Reactome GO Term analysis of protein enriched on Vitronectin compared to the negative control E-cadherin. Top group leading terms with their respective statistical p values, and the Benjamini-Hochberg corrected p value. Associated Genes Found comprises the list of proteins identified with the MS dataset and within each GO term.

ID	Term	Group PValue	Group PValue Corrected with Benjamini-Hochberg	Associated Genes Found
R-HSA:1430728	Metabolism	4.16E-06	6.23E-06	[ATP5PO, CYCS, ENO1, IQGAP1, MDH2, PPP1CC, RANBP2, RPL10, RPL13A, RPL17, RPL23, RPL24, RPL26, RPL3, RPL32, RPL6, RPL8, RPL9, RPS11, RPS16, RPS17, RPS23, RPS3A, RPS4X, RPS7, SLC25A11, SLC2A1, SLC3A2, TRAP1, VCAN]
R-HSA:168256	Immune System	1.00E-09	3.01E-09	[ANXA2, AP2B1, CALR, CFL1, CLTC, FGF2, FN1, HUWE1, ILF2, IQGAP1, ITGAV, PDIA3, RANBP2, VTN]
R-HSA:392499	Metabolism of proteins	1.00E-09	3.01E-09	[CALR, FN1, INHBE, PDIA3, RANBP2, RPL10, RPL13A, RPL17, RPL23, RPL24, RPL26, RPL3, RPL32, RPL6, RPL8, RPL9, RPS11, RPS16, RPS17, RPS23, RPS3A, RPS4X, RPS7, VCAN]

Supplementary table 3: Reactome GO Term analysis of protein enriched on ZTFN compared to the negative control E-cadherin. Top group leading terms with their respective statistical p values, and the Benjamini-Hochberg corrected p value. Associated Genes Found comprises the list of proteins identified with the MS dataset and within each GO term.

ID	Term	Group PValue	Group PValue Corrected with Benjamini-Hochberg	Associated Genes Found
R-HSA:162582	Signal Transduction	6.39E-01	8.52E-01	[ACTN1, AKAP12, CTSD, FN1, ITGAV, ITGB1, S100A8, SFPQ, TLN1, TUBB4A, VIM, YWHAQ]
R-HSA:1430728	Metabolism	8.44E-01	8.44E-01	[LARS1, MARCKS, MARS1, MTHFD1, PFKP, PRPS1, SLC3A2]
R-HSA:8953854	Metabolism of RNA	1.08E-01	4.30E-01	[HSPA1A, IGF2BP3, PRPF40A, TNKS1BP1, UPF1]
R-HSA:392499	Metabolism of proteins	5.51E-01	1.00E+00	[CTSD, EIF2S3, FN1, LARS1, MARS1, RAB8A, TLN1, TUBB4A, VARS1]

Supplementary table 4: Reactome GO Term analysis of protein enriched on ZT910 compared to the negative control E-cadherin. Top group leading terms with their respective statistical p values, and the Benjamini-Hochberg corrected p value. Associated Genes Found comprises the list of proteins identified with the MS dataset and within each GO term.

ID	Term	Group PValue	Group PValue Corrected with Benjamini-Hochberg	Associated Genes Found
R-HSA:1643685	Disease	2.62E-01	2.62E-01	[ATP1A1, CALR, CAPN1, CHD4, DYNC1H1, ENO1, FN1, ITGB1, LMNA, LMNB1, MSH6, PPP2R1A, PRKCSH, PSMB3, RPL13A, RPL15, RPL17, RPL9, RPS11, RPS17, RPS4X, SLC2A1, SLC3A2, SND1, TALDO1, TLN1, VCAN]
R-HSA:8953854	Metabolism of RNA	2.55E-06	1.02E-05	[CNOT1, DDX1, DHX15, EIF4G1, EPRS1, FUS, IGF2BP1, IGF2BP3, KHSRP, PABPC1, PDCD11, PPP2R1A, PRPF40A, PRPF8, PSMB3, RPL13A, RPL15, RPL17, RPL9, RPS11, RPS17, RPS4X, RTRAF, SF3B1, SNRPD2, SRRM2, TNKS1BP1]
R-HSA:392499	Metabolism of proteins	8.84E-04	1.77E-03	[AARS1, CALR, DYNC1H1, EIF2S3, EIF3A, EIF4G1, EPRS1, FN1, GARS1, IARS1, KHSRP, LARS1, LMNA, MARS1, PABPC1, PRKCSH, PRKDC, PSMB3, RPL13A, RPL15, RPL17, RPL9, RPS11, RPS17, RPS4X, SEC16A, SPTAN1, TLN1, TOP2A, TOP2B, UGGT1, USP9X, VCAN]
R-HSA:1280215	Cytokine Signaling in Immune system	1.43E-01	1.91E-01	[ANXA1, ANXA2, CFL1, EIF4G1, FN1, ITGB1, LMNB1, PPP2R1A, PSMB3, SMARCA4, TALDO1, VIM]